Modelling Cu, Zn, Cd and Pb Adsorption by Iron Oxyhydroxides in SO_4-rich Systems Simulating Acid Mine Drainage.

Peter Swedlund

February 2004

A thesis submitted in fulfilment of the requirements for the degree of Doctor of Philosophy.

For the cygnets and the swan.

"Such great happiness I never dreamed of,

When I was but the ugly duckling."

(Anderson, 1844)

ABSTRACT

Acid mine drainage (AMD) typically involves waters with low pH (pH 2-4) and high concentrations of Fe, SO_4 and potentially toxic trace metals. Adsorption onto iron oxyhydroxides is the dominant mechanism controlling the transport and toxicity of trace metals in water bodies impacted by AMD. The purpose of this study was to apply the Diffuse Layer Model (DLM) to describe the adsorption of trace metals by iron oxyhydroxides from these systems, using synthetic iron oxyhydroxide minerals, ferrihydrite, pure acicular goethite, SO_4-rich goethite prepared from $FeSO_4$ oxidation and a synthetic schwertmannite.

The ferrihydrite adsorption of the trace metals Cu, Zn, Cd and Co from single sorbate systems was accurately described using the DLM with two surface site types (type-1 and type-2) having site densities of 0.005 and 0.2 mol (mol Fe)$^{-1}$ respectively. The ferrihydrite adsorption of SO_4 from single sorbate systems was accurately described using the DLM with adsorption on the type-2 sites. However, the enhanced adsorption of Cu, Zn, Cd and Co in the presence of SO_4 was not predicted using adsorption constants derived from single sorbate systems. By including a neutral ternary complex with stoichiometry $\equiv Fe_{(2)}OHMeSO_4$ (where $\equiv Fe_{(2)}OH$ is a type-2 surface site and Me is the trace metal) the effect of SO_4 on metal adsorption was accurately described for the range of Me, Fe and SO_4 concentrations studied. The adsorption of Cu and Zn onto schwertmannite at total metal to iron ratios (Me_T:Fe) up to 8×10^{-3} was almost identical to that predicted for ferrihydrite in the presence of 0.01 mol kg^{-1} SO_4. To model the ferrihydrite adsorption of Pb from single sorbate systems a third higher affinity site (type-0) with a site density of 0.00035 mol (mol Fe)$^{-1}$ was required. The effect of SO_4 on Pb adsorption could only be modelled by including a neutral ternary complex on both the type 1 and type 2 sites in the case of Pb.

Metal adsorption onto a pure acicular goethite could be accurately described by the DLM with two surface site types. The type 2 site density that provided the best fit to the goethite adsorption data was 0.027 mol (mol Fe)$^{-1}$ corresponding to 2.3 nm^{-2}. The type-1 site density that provided the best fit to goethite adsorption of Cu, Pb and Cd was 0.00028 mol (mol Fe)$^{-1}$ corresponding to 0.024 nm^{-2}. For Zn adsorption on goethite the type-1 site density was significantly larger at 0.0015 mol (mol Fe)$^{-1}$ corresponding to 0.13 nm^{-2}. In all cases studied the presence of SO_4 caused an increase in the extent of metal adsorption by goethite. This increased adsorption of metals in the presence of SO_4 was accurately predicted by including ternary complex formation at both the high and low affinity adsorption sites.

For both ferrihydrite and goethite the values of adsorption constants for ternary complex formation ($\log K_{xMe}^{TC}$) were related to the adsorption constant for metal adsorption in the absence of SO_4 ($\log K_{xMe}^{INT}$). This was evident from a plot of $\log K_{xMe}^{TC}$ as a function of $\log K_{xMe}^{INT}$ for all metals, which showed a linear relationship with slope of 0.69 and intercept of 8.03. This relationship suggests that the enhancement of metal adsorption on both oxyhydroxides due to SO_4 occurs by the same process.

When comparing Cu, Zn and Cd adsorption onto ferrihydrite and acicular goethite the effect of the larger goethite adsorption constants are approximately compensated for by the lower goethite site densities. Therefore the Cu, Cd and Zn adsorption isotherms on ferrihydrite and acicular goethite are fairly similar at low adsorption densities. In the case of Pb, the site densities and adsorption constants are both larger on ferrihydrite and there is a large difference between the ferrihydrite and acicular goethite adsorption isotherms.

Sulfate-rich goethite had considerably higher site densities, per mol of oxide, than the pure acicular goethite. Adsorption onto the sulfate-rich goethite could be modelled reasonably accurately using the parameters developed to model adsorption onto the pure acicular goethite but with a higher surface area and a higher ratio of type-1 to type 2 sites. In general, therefore, the parameters developed for pure goethite are apparently similar to those for the sulfate-rich goethite, but are not directly transferable. The difficulty in measuring the surface area of the highly aggregated sulfate-rich goethite makes comparisons between the two goethites more difficult.

The adsorption of Cu, Zn and Cd onto the SO_4-rich goethite exceeds that of ferrihydrite because the higher adsorption constants of goethite are combined with the considerably higher site densities of the SO_4-rich goethite compared to the acicular goethite. In contrast the higher site densities of the SO_4-rich goethite does not completely compensate for the low $\log K^{INT}$ values of Pb adsorption on goethite. Therefore SO_4-rich goethite adsorption of Pb is lower than that of ferrihydrite.

When applied to literature data from AMD oxides the parameters derived in this thesis have significantly improved the ability of the DLM to predict trace metal adsorption in AMD systems, compared to using ferrihydrite as a proxy for all iron oxyhydroxides and adsorption data derived only from single sorbate systems.

Acknowledgements

There are many people who have contributed to this work. Firstly I must express my great gratitude to my primary supervisor, J.G. Webster, for her unstinting support and enthusiasm. Jenny is one of the rare people with insight into the somewhat parallel almost impenetrable complexities of both environmental systems and bureaucracies. This has made her an excellent supervisor. G.M. Miskelly was an invaluable 2IC, always happy to be accosted with numerous and diverse questions and was highly skilled at finding my deliberate mistakes. And lastly Jim Metson. Thanks for showing me some of the trickier tricks of trade, could be useful one day. However, next time you look a prospective student in the eye and declare your "great interest in the project" you should, in all fairness, explain that this "great interest" is purely pecuniary.

This brings me to those people who have helped me survive. Christina Clapp suffered my interminable ranting for nigh on three years. I'll take your secret to the grave; well no one I tell believes it anyway. Geoff Waterhouse and I had to consume chemical substances to alleviate the symptoms and spent many a happy hour discussing creative solutions to the problem. Damien, Baek, Chen and Nicole were all "brothers in arms" and Friday afternoons at OGH were very enjoyable times. Glenn Boyes, Vincent Lane, Paul Butler, Noel Renner, Peter Buchanan, Jeff Boyle, Shane Crump, Catherine Hobbis, "Briney" James, Prof. O'Connor, Assoc. Prof. Wright, Ritchie Simms and may others helped in various capacities along the way. Thanks.

Finally the family. Dad assisted every Saturday night with the always-appreciated Chinese takeaways and beer and refrained from the vengeful refrain "Are you there yet? Are you there yet?". Jane is to me as the periodic table is to chemistry, bringing understanding and structure to an otherwise dizzyingly incomprehensible confusion. Our children, Hannah and Ruskin, bring the dizzyingly incomprehensible confusion without which life would be dull. The elusive perfect balance. I am, in my opinion, the luckiest man in the world.

TABLE OF CONTENTS

LIST OF FIGURES

LIST OF TABLES

List of Abbreviations

σ	Surface charge (C m^{-2})
Ψ	Surface potential (V)
γ_x	Activity coefficient for species x
A^{2-}	Divalent anion
AAS	Atomic adsorption spectroscopy
AMD	Acid mine drainage
ARD	Acid rock drainage
ATR-IR	Attenuated total reflectance infrared spectroscopy
DLM	Diffuse layer model
EDL	Electric double layer theory
$\equiv Fe_{(x)}OH$	A type x surface hydroxyl group
GFAAS	Graphite furnace atomic adsorption spectroscopy
IC	Ion chromatography
ICPMS	Inductively coupled mass spectrometry
LFER	Linear free energy relationship
$logK_{A1}^{INT}$	First acidity constant of a surface hydroxyl group
$logK_{A2}^{INT}$	Second acidity constant of a surface hydroxyl group
$logK_{xMe}^{TC}$	Log of the formation constant for $\equiv Fe_{(x)}OHMeSO_4$
$logK_{xMe}^{INT}$	Log of the formation constant for $\equiv Fe_{(x)}OMe^{+}$
Me	A divalent trace metal
Me_{ads}	Adsorbed metal
Me_{aq}	Dissolved metal
Me_T	Total metal concentration i.e. dissolved plus adsorbed
N_s	Total site density
N_{sx}	Site density of type x sites
PPZC	Pristine point of zero charge
SEM	Scanning electron microscopy
s_T	Estimated error in total component concentration
s_X	Estimated error in species concentration
TLM	Triple layer model
TOTH	Total proton concentration
WSOS/DF	Weighted sum of squares divided by the degrees of freedom
XRD	X-ray diffraction
Y_X	The difference between the calculated and measured value of x

CHAPTER ONE
INTRODUCTION

1.1 ACID MINE DRAINAGE SYTEMS

The atmospheric oxidation of the metal sulfides occurring in metallic ore and coal deposits can produce the phenomenon known as acid rock drainage (ARD) or, where exposure is due to mining, acid mine drainage (AMD). The latter is "the most serious environmental problem caused by mining" (Doyle, 1996). Acid is produced from the oxidation of the iron sulfides, especially pyrite (Evangelou and Zhang, 1995), by the sequence of reactions presented in Equations 1.1 to 1.4 (Kleinmann et al., 1981). In addition to the products of pyrite oxidation, potentially toxic trace metals can be released into AMD systems from the oxidation of trace metal sulfides such as chalcopyrite, sphalerite and galena (Martycak et al., 1994). Therefore AMD systems typically involve waters with low pH (pH 2-4) and high concentrations of Fe, SO_4 and potentially toxic trace metals (Nordstrom and Alpers, 1997). As an extreme example Nordstrom et al. (1991) describe a drainage system from Iron Mountain California with a pH of –0.7, 80 gL^{-1} of Fe^{II}, 360 gL^{-1} of SO_4 and 2.3 gL^{-1} of Cu.

$$FeS_{2(s)} + 3.5O_2 + H_2O \Leftrightarrow Fe^{2+} + 2H^+ + 2SO_4^{2-} \quad \text{Eq. 1.1}$$

$$Fe^{2+} + 0.25O_2 + H^+ \Leftrightarrow Fe^{3+} + 0.5H_2O \quad \text{Eq. 1.2}$$

$$FeS_{2(s)} + 14Fe^{3+} + 8H_2O \Leftrightarrow 15Fe^{2+} + 2SO_4^{2-} + 16H^+ \quad \text{Eq. 1.3}$$

$$Fe^{2+} + 1.5H_2O + 0.25O_2 \Leftrightarrow FeOOH_{(s)} + 2H^+ \quad \text{Eq. 1.4}$$

A variety of iron oxyhydroxide minerals are formed from the oxidation of Fe^{II}, followed by hydrolysis (Equation 1.4, shown for goethite). This typically occurs "off-site" (Bigham et al., 1990) when the waters are exposed to O_2 and there is insufficient sulfide present to reduce the Fe^{III} back to Fe^{II}. Adsorption onto these iron oxyhydroxides is often the dominant mechanism controlling trace metal transport and toxicity in water bodies impacted by AMD (e.g. Paulson and Balistrieri, 1999), providing a fortuitous *in situ* mitigation mechanism for AMD systems. The purpose of this study was to be able to understand the mechanisms of and to model the adsorption of the trace metals Cu, Zn, Cd and Pb onto the iron oxyhydroxide minerals that typically precipitate in these AMD systems.

1.2 THE IRON OXYHYDROXIDES IN AMD SYSTEMS

The Fe^{III} oxides and oxyhydroxides found in AMD can be synthesized in the laboratory by precipitation from Fe^{II} solutions by oxidation followed by hydrolysis (Cornell and Schwertmann, 1996). Factors such as pH, rate of oxidation, and [Fe^{II}] determine which oxide is formed. For example the abiotic oxidation of $FeSO_4$ at pH 3 produces goethite and, if K^+ is present, jarosite. While jarosite is thermodynamically more stable, goethite is favoured kinetically (Stahl et al., 1993). In contrast, schwertmannite rather than goethite is produced by the oxidation of $FeSO_4$ at pH 3 if the bacteria *Thiobacillus ferroxidans* is present to catalyse the reaction (Bigham et al., 1990). Two-line ferrihydrite (hereafter called ferrihydrite) can be formed from AMD waters at pH > 4 from the rapid hydrolysis of Fe^{III} (Lee et al., 2002). The nature of the anion is also important in determining the mineralogy of the precipitate. For example lepidocrocite is formed by the abiotic oxidation of $FeCl_2$ at pH 3 (Taylor, 1984).

Table 1.1 Some iron oxyhydroxides that may be found in AMD systems.

	formula	colour[a]	structural analogue	principal habit
goethite	α-FeOOH	yellow-brown	diaspore	acicular
schwertmannite	$Fe_{16}O_{16}(OH)_y(SO_4)_z.nH_2O$	yellow-brown	hollandite	"hedge-hog" aggregates
ferrihydrite	$Fe_5HO_8.4H_2O$ [b]	red-brown	[b]	spheres
jarosite	$KFe_3(SO_4)_2(OH)_6$	yellow-brown	alunite	tabular to flattened rhombohedral
lepidocrocite	γ-FeOOH	orange	boehmite	laths

[a] color can change significantly with crystal form
[b] not fully established

Goethite, schwertmannite and ferrihydrite have all been found in the drainage below the tailings dam from the former Tui Pb-Zn mine at Te Aroha, New Zealand (Webster et al., 2000). At the time of sample collection (1997) the anoxic tailings seepage, with pH ≈ 3.5 and high Fe^{II} and sulfate concentrations, bubbled up as a spring through the sandy bottom of a small pool below the tailings dam. Schwertmannite was the solid phase here, whereas goethite was found approximately 40 m downstream from this spring, where the water was fully oxygenated and had a slightly lower pH of 2.9 (due to Fe^{III} hydrolysis) and lower iron concentration (Lane, 2000). Ferrihydrite has also been found in this region, precipitated from adit and surface drainage with pH > 4. The findings from a survey of secondary minerals in AMD systems on the West Coast of the South Island, New Zealand, (Webster and Brown, 2002) were consistent with the relationship between aqueous geochemistry and mineralogy

observed at the Tui mine, i.e. only goethite and schwertmannite precipitates were found in waters of pH < 4 and only ferrihydrite was found at pH > 4.

Figure 1.1 Drainage below the tailings dam from the former Tui Pb-Zn mine at Te Aroha, New Zealand. (a) region of spring of tailings water and schwertmannite precipitation (b) region of goethite precipitation. Note ferrihydrite precipitation occurred where a small tributary joined the tailings drainage just downstream of this photo.

Numerous studies of AMD aqueous geochemistry have revealed the importance of the secondary minerals, especially the iron oxyhydroxides, in controlling the speciation, concentration and transport of trace metals in these systems. For example Johnson (1986) studied the particulate/dissolved partitioning of Cu and Zn in Camon River system, England; a system impacted by acid mine drainage. There was no clear relationship between particulate and dissolved metal ($[Me_{ads}]/[Me_{aq}]$) when log ($[Me_{ads}]/[Me_{aq}]$) was plotted versus pH (Figure 1.2). However, when normalized for the particulate Fe concentration i.e. log ($[Me_{ads}]/[Me_{aq}][Fe_{part}]$), the data showed a clear positive slope. Ball et al. (2001) modelled the downstream transport of Cu in an AMD system. Copper was non-conservative and adsorption onto iron oxyhydroxides was indicated as the mechanism controlling Cu concentration. Because adsorption onto iron oxyhydroxides is important in controlling trace metal concentrations, a mechanistic understanding and accurate modelling of these reactions is required to predict trace metal speciation and transport in AMD systems. This, in turn, is

necessary to provide a scientific basis for environmental and regulatory decisions concerning mining activities.

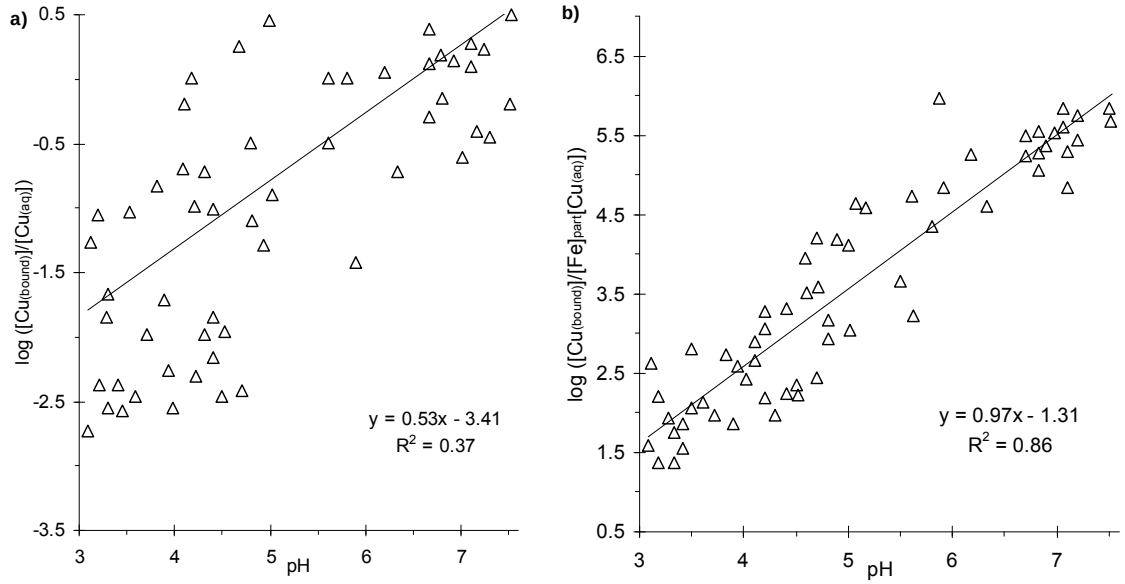

Figure 1.2 The particulate/dissolved partitioning of Cu as a function of pH (reproduced from Johnson, 1986).

1.3 MODELLING ADSORPTION

A model is a "simplified representation of a complex system, especially one designed to facilitate calculations and predictions" (Collins, 1990). There are several theoretical models to describe solute adsorption at an oxide water interface. Most models are based on the concept of a "surface complex" in which adsorption is considered to occur at surface hydroxyl sites (e.g. ≡FeOH) and is analogous to solution complex formation. Unlike models of solution complex formation however, adsorption models include a term in the adsorption mass action equations to modify the activity of sorbing ions by the work necessary for the ions to penetrate the surface electrostatic potential. Prediction of adsorption behaviour over a range of conditions, for example pH or ionic strength, requires that the model include these surface charge effects.

The different adsorption models vary in the treatment of the electrostatics of the interface and in considering surface hydroxyl groups as being either diprotic, called 2 pK_A models (Equations 1.5 and 1.6), or monoprotic, called 1 pK_A models (Equation 1.7). In these equations ≡FeOH refers to a surface hydroxyl group and the -½ charge on the surface species in Equation 1.7 arises by distributing the Fe^{3+} charge equally between the Fe ion's 6 oxygen ligands.

2 pK_A model	$\equiv FeOH^0 + H^+$	$\Leftrightarrow$	$\equiv FeOH_2^+$	Eq. 1.5
	$\equiv FeOH^0$	$\Leftrightarrow$	$\equiv FeO^- + H^+$	Eq. 1.6
1 pK_A model	$\equiv FeOH^{-½} + H^+$	$\Leftrightarrow$	$\equiv FeOH_2^{+½}$	Eq. 1.7

The three adsorption models described below can be considered to exist on a continuum between applicability to real environmental systems and scientific rigor, and have been compared in more detail in Hayes et al (1990), Dzombak and Morel (1990), Venema et al. (1996a) and Robertson and Leckie (1998). Venema et al. (1996b) describes the most commonly used 1 pK_A model; the charge distribution multi-site complexation model (CD-MUSIC). This model has been applied to oxyhydroxides with well-defined crystal morphology and enclosing forms, such as acicular goethite, and attempts to reconcile crystallographic, spectroscopic, surface chemistry and chemical data from adsorption experiments. While there are clearly many advantages to the rigorous approach of the CD-MUSIC model the disadvantages are that it is not readily incorporated into existing geochemistry speciation programs, such as MINTEQA2 (Allison et al., 1991), and would not be directly applicable to poorly defined minerals such as ferrihydrite.

The most widely used 2 pK_A models are the diffuse layer (DLM) and triple layer (TLM) models (Robertson and Leckie, 1998), which differ in their representation of the distribution of surface charge. In addition the constant capacitance model is a special case of the DLM for conditions of low surface potential or high ionic strength, where the surface potential is approximated as a linear function of surface charge. The constant capacitance model is not considered here because it is a simplified version of the DLM.

1.3.1 The Diffuse Layer Model

The DLM is used in this work. The main principles of the diffuse layer model are:

1. Adsorption reactions are considered as complexation reactions between surface hydroxyl groups and the sorbing species
2. These reactions can be described quantitatively by mass action equations
3. The charge on the oxide surface is the result of proton transfer and the coordination of cations and anions
4. The surface charge is considered to reside in one plane
5. A Gouy-Chapman distribution of ions is assumed for the solution side of the interface

6. The relationship between surface charge and potential is set by the electric double layer (EDL) theory
7. Mass action equations for sorption reactions include a coulombic term to modify the activity of sorbing ions approaching a charged surface.

With the DLM many of the features of cation and anion adsorption data can be accurately predicted, such as the effect of pH, ionic strength, adsorption density (Robertson and Leckie, 1998) and competition for adsorption sites (e.g. Swedlund and Webster, 1999). Because of the DLM's simplicity and the absence of fitting parameters it has been widely utilized for modelling both laboratory and field systems. Another advantage of the DLM is the existence of a database of surface complex equilibrium constants for the adsorption of many cations and anions onto ferrihydrite. Dzombak and Morel (1990) compiled this database from experimental data available in the literature, and used the DLM primarily for its simplicity and its ability to model experimental results over a wide range of solution conditions. For these reasons the DLM was used in this study. The equations used by the DLM to describe adsorption are discussed in Section 2.2d.

There are, however, deficiencies inherent in the DLM. These include the poor fitting to acid-base titration data, an underestimation of surface potentials at high surface charge, and an inability to consider the so called "outer sphere" electrostatic ion pair formation. Robertson and Leckie (1998) demonstrated that DLM fits to acid-base titration data were poor, and that site densities optimized from titration data were significantly lower than the maximum adsorption density of Cu. These deficiencies were not experienced with the TLM. The main difference in the models is that the DLM considers electrolyte ions as point charges whereas the TLM implicitly accounts for a finite electrolyte ion size by including weak electrostatic complexes between electrolyte ions and charged surface sites. Therefore at high charge densities, such as those involved in extrapolating to site saturation, the DLM will have unrealistic surface potentials. Lastly, attenuated total reflectance infrared (ATR-IR) spectroscopy studies (Peak et al., 1999, Elzinga et al., 2001) of sulfate adsorption at pH > 6, where SO_4 adsorption densities were low, supported a weak ion-pair (e.g. $\equiv FeOH_2^+$---SO_4^{2-}) as the principal mode of association. While this sort of "outer sphere" ion pair species is an integral part of the TLM it is not possible to include it in the DLM, where all charge resides on a single plane. Therefore when using the DLM these deficiencies must be considered.

1.4 RESEARCH OBJECTIVES AND APPROACH

Objectives

Over the last two decades there have been substantial advances in modelling the adsorption of trace metals onto mineral surfaces and surface complexation models have become a fundamental tool in this endeavour. Adsorption studies are moving to systems of greater complexity, from well-characterized pure mineral phases with a single adsorbing species to systems with many adsorbing species and diverse solid phases. In this way the gap between laboratory studies and field studies is being narrowed. The aim of this thesis is to contribute to this process by providing a detailed description of adsorption processes pertinent to metal adsorption in AMD systems. This will be achieved by incrementally increasing the complexity of the systems studied.

Approach

Chapter 2 describes the methods and materials used in this study. The synthesis and characterization of the iron oxyhydroxides used in this work are presented. These include ferrihydrite, schwertmannite, pure acicular goethite and sulfate-rich goethite. The experimental design and instruments used to measure adsorption onto the iron oxyhydroxides are described. In addition the methods used to model the adsorption data are described here.

Chapter 3 describes the effect of SO_4 on the adsorption of Cu and Zn onto ferrihydrite, by studying adsorption initially in the absence of SO_4 and then in the presence of SO_4. Ferrihydrite was chosen as the first mineral to study because parameters for modelling adsorption to this mineral are already available, compiled by Dzombak and Morel (1990). In addition ferrihydrite is often considered a proxy for natural iron oxyhydroxides in aquatic systems. A comparison of Cu and Zn adsorption onto schwertmannite, with that onto ferrihydrite in the presence of SO_4, was also made. The content of this chapter was published in Applied Geochemistry (Swedlund and Webster, 2001).

Chapter 4 describes the effect of SO_4 on the adsorption of Co, Pb and Cd onto ferrihydrite, again by studying adsorption initially in the absence of SO_4 and then in the presence of SO_4. This involved an increase in the level of complexity because Pb adsorption was not well described by the 2-site model of Dzombak and Morel (1990). Therefore additional site heterogeneity needed to be included to model the Pb data in the presence and absence of SO_4. The content of this chapter was published in Applied Geochemistry (Swedlund et al., 2003).

Chapter 5 describes the effect of SO_4 on the adsorption of Cu, Zn, Cd and Pb onto a well-characterized acicular goethite, by studying adsorption in the absence of SO_4 and then in the presence of SO_4. Because there are no generally accepted parameters to model adsorption onto goethite, data are presented to support the choice of site densities, acidity constants and cation and anion adsorption constants for goethite. While a complete survey of goethite adsorption data in the literature is beyond the scope of this work relevant comparisons with other studies are made.

In Chapter 6 adsorption onto the poorly ordered sulfate-rich goethite, typical of AMD systems, (synthesized by the abiotic oxidation of $FeSO_4$ at pH 3) is compared to that on the acicular pure goethite from Chapter 5. Goethite synthesized from abiotic $FeSO_4$ oxidation at pH 3 has been found to have very similar adsorption properties to the goethite sample collected from the base of the Tui tailings dam (Webster et al., 1999). By first considering complexity in the solution phase, namely the presence of SO_4, and then complexity in the solid phase, namely different crystal morphologies and the presence of solid phase SO_4, a better understanding of the process of trace metal adsorption onto this AMD goethite is gained.

Chapter 7 reviews the implications of these experiments and theoretical data determinations to modelling metal adsorption in AMD systems.

CHAPTER TWO
MATERIALS, METHODS AND MODELLING

2.1 MATERIALS

2.1a. Reagents

All reagents used were analytical grade. Unless otherwise stated, the water used was 18.2 MΩ grade water and experiments were carried out under an Ar atmosphere to exclude CO_2. Water was acidified to pH 3 with HNO_3 and bubbled with Ar for 2-3 hours to remove CO_2. Sodium hydroxide solutions were prepared by diluting the clear supernatant of a 50 % (w/w) NaOH solution with the CO_2 free water.

2.1b Solid Phase Characterization

Powder X-ray Diffraction

X-ray diffraction spectra (XRD) of randomly orientated powder samples were measured to positively identify the mineral phases studied. Spectra were measured on the University of Auckland Geology Dept. diffractometer (Phillips PW 1140 goniometer) using a CuKα (λ=1.5418 Å) source. The step size was 0.02 ° 2θ and a count time of 2 s. Data shown are the average for steps of 0.2 ° 2θ.

Specific Surface Area

The specific surface areas of the iron oxyhydroxides were measured by nitrogen adsorption and BET analysis. Ferrihydrite, schwertmannite and the sulfate-rich goethite surface areas were measured with one point BET on the University of New South Wales' Phlosorb instrument. Pure and sulfate-rich goethite samples were measured by three point BET on the University of Auckland Quantasorb Junior, after outgassing for 30 min at 110 °C.

Scanning Electron Microscopy (SEM)

Images were recorded on the University of Auckland Chemical and Materials Engineering Dept. Phillips SFEG XL30 Scanning Electron Microscope. Samples were collected by filtering onto a 0.45 μm membrane, attaching this to a sample stub and coating with platinum. Images were obtained at between 18,000 and 40,000 magnification.

Total Iron and Sulfate Content

The total Fe content of the oxides was measured using conc. HCl digestion followed by Atomic Adsorption Spectrophotometry as discussed in Section 2.3. The total sulfate content was determined by conc. HCl digest followed by the addition of 1 M NaOH to raise the pH to between 10 and 11. The addition of NaOH was rapid in order to avoid SO_4 adsorption and entrapment in the Fe oxide phase. The sample was centrifuged (2000 rpm) and SO_4 measured in the supernatant by ion chromatography as discussed in Section 2.3. Addition of known amounts of SO_4 to the digests of pure (i.e. SO_4-free) goethites demonstrated the validity of the method.

Oxalate Solubility

Oxalate solubility was used to test for the presence of ferrihydrite or schwertmannite in the goethite samples (Cornell and Schwertmann, 1996). A 40 mg sample of iron oxyhydroxide was mixed in the dark on an end-over-end mixer with 40 mL of 0.2 mol kg^{-1} ammonium oxalate/oxalic acid buffer at pH 3. Samples were taken at 15 min and then at 2, 4 and 6 hours. Samples were filtered through a 0.22 μm filter membrane and acidified with approximately 50 μL conc. HNO_3 per 10 mL sample and analyzed by AAS as discussed in Section 2.3.

2.1c The Iron Oxyhydroxides

Ferrihydrite

Ferrihydrite was synthesized from a starting solution prepared from $Fe(NO_3)_3.9H_2O$ in 0.1 mol kg^{-1} $NaNO_3$. The pH was rapidly raised from < 2.0 to 8.0 ± 0.5 with NaOH, based on the method of Schwertmann and Cornell (1991). The total [Fe] ranged from 0.9 to 15 mmol kg^{-1}. The oxide formed as a red/brown, loose gelatinous precipitate and was aged for 18-24 hours in the electrolyte solution before adsorption experiments were undertaken. The freeze-dried product had the two broad XRD peaks characteristic of 2-line ferrihydrite (Figure 2.1). An SEM image of the freeze-dried product, Webster et al. (1998), shows no visible morphology. The specific surface area of the freeze-dried product was 205 m^2g^{-1}, which is within the range of previously reported values (Dzombak and Morel, 1990). The product could be completely dissolved after 15 min. in 0.2 mol kg^{-1} ammonium oxalate/oxalic acid buffer at pH 3 after 15 min mixing.

Ferrihydrite is a poorly ordered iron oxyhydroxide. The two broad peaks in the X-ray diffraction (Figure 2.1) are indicative of some crystalline character but the bulk structure and chemical

composition of ferrihydrite is uncertain (Cornell and Schwertmann, 1996). Ferrihydrite is formed by rapid hydrolysis of ferric solutions at 20-30 °C (Dzombak and Morel, 1990). The first stages of hydrolysis are equivalent to the acid dissociation of the pale purple hexaquo ferric ion, $Fe(H_2O)_6^{3+}$, which is the predominant ferric species at a pH of 1. At a pH of 2 the deprotonated dimer $[Fe_2(OH)_2(H_2O)_8]^{4+}$ is the predominant ferric species. As the pH is raised above 2-3, further deprotonation and condensation occurs until ferrihydrite precipitates (Cotton and Wilkinson, 1980). Freshly precipitated ferrihydrite particles increase in size, from 1 to 10 nm spheres directly after precipitation, to highly porous micrometer-sized aggregates resembling swollen gels after several hours (Avontis, 1975; Murphy et al., 1976). A theoretical surface area of 840 $m^2\ g^{-1}$ has been calculated for ferrihydrite assuming 2 nm diameter spheres and a density of 3.57 g cm^{-3} (Davis, 1977). Experimental techniques using dried samples, such as BET, tend to underestimate the surface area and give results from 200-300 m^2g^{-1} for ferrihydrite. An estimate of 600 m^2g^{-1} was used by Dzombak and Morel (1990) as recommended by Davis and Leckie (1978).

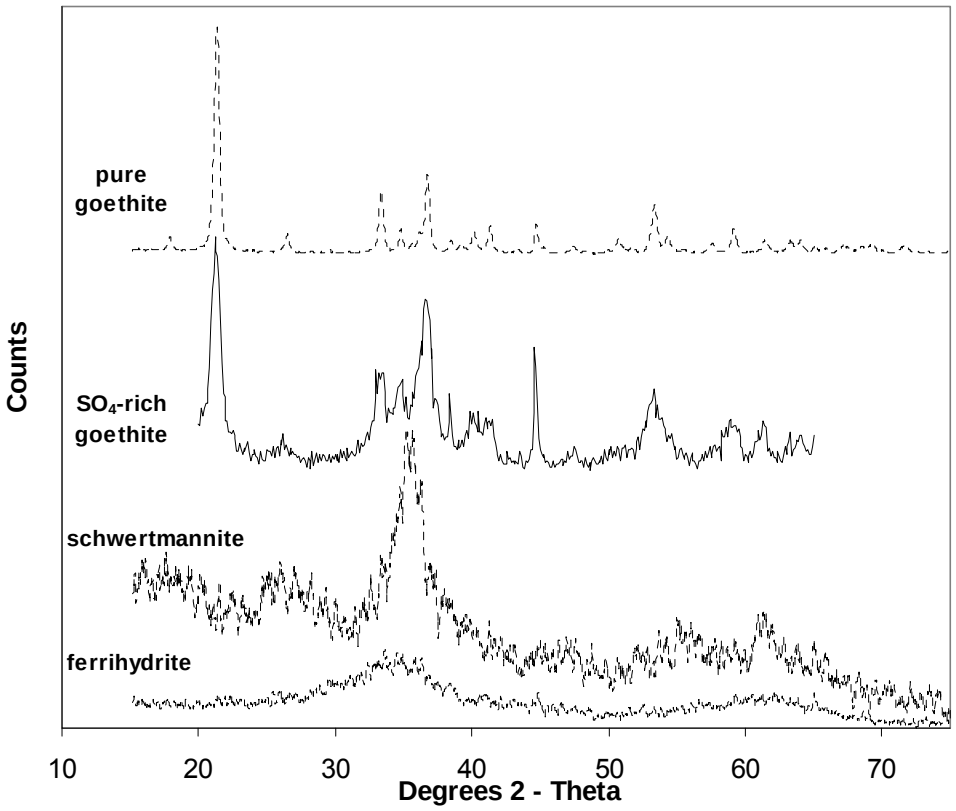

Figure 2.1. Powder X-ray diffraction of ferrihydrite, schwertmannite, pure goethite and sulfate-rich goethite.

a)

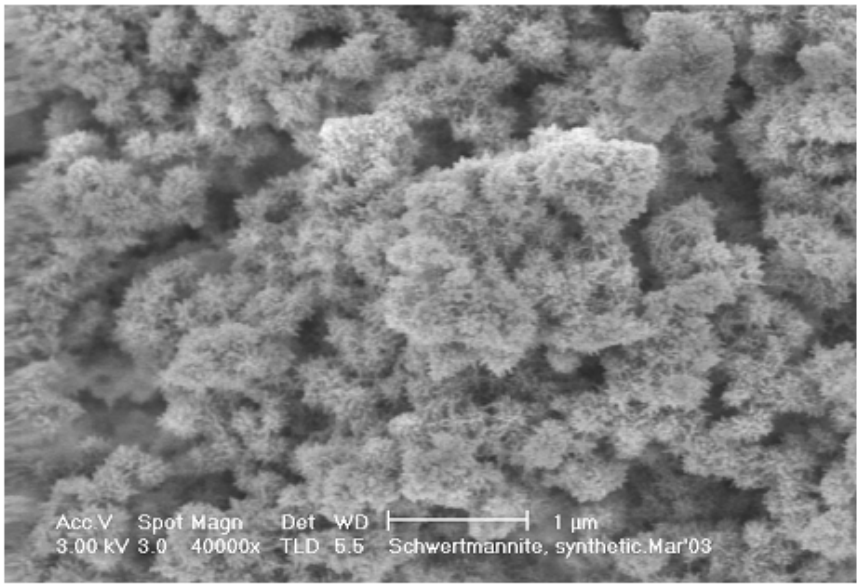

b)

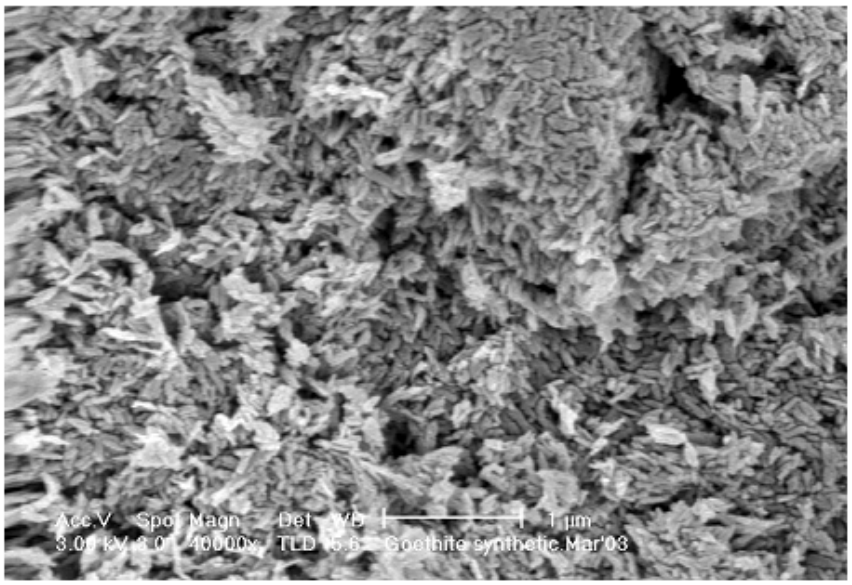

c)

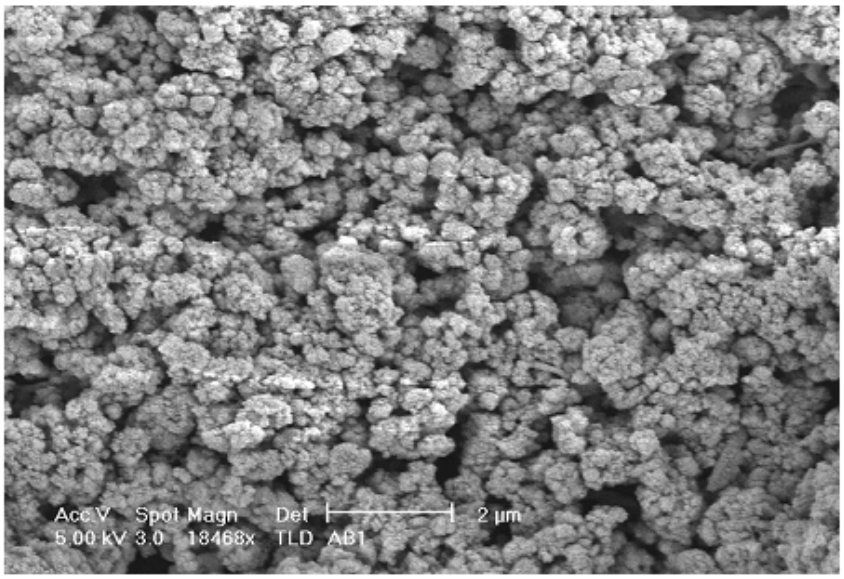

Figure 2.2 SEM images of synthetic schwertmannite (a), pure acicular goethite (b) and sulfate-rich goethite (c) as prepared for this study.

Schwertmannite

Schwertmannite was precipitated from a starting solution of $Fe(NO_3)_3.9H_2O$ in 0.1 mol kg^{-1} $NaNO_3$ and 0.02 mol kg^{-1} Na_2SO_4. A peristaltic pump was used to slowly transfer 5 mmol kg^{-1} NaOH into the stirred solution, gradually raising the pH from 2.0 to 5.0 ($\pm$0.5) over a period of 30 hrs. The precipitate was aged in the SO_4-rich solution at pH 3.0 for 24 hr, then the supernatant was removed from above the settled schwertmannite and replaced with 0.1 mol kg^{-1} $NaNO_3$ prior to adsorption experiments. Precipitates formed in this way were ochreous yellow/brown in color, adhered to the vessel wall, and had an average SO_4 content of 11 wt% (Webster et al., 1998). X-ray diffraction of the freeze-dried product showed only the broad peaks characteristic of schwertmannite (Figure 2.1). The specific surface area of the freeze-dried product was 55 m^2g^{-1} which is somewhat lower than the range of 100-200 m^2g^{-1} specified for schwertmannite when it was first recognized as a mineral (Bigham et al., 1994). The lower surface area presumably reflects the higher pH at the end of the synthesis, compared to the thermal hydrolysis method of Bigham et al. (1994), and therefore a greater degree of aggregation. SEM of the freeze-dried product is shown in Figure 2.2a and shows the "hedge-hog" aggregates typical of schwertmannite (Cornell and Schwertmann, 1996).

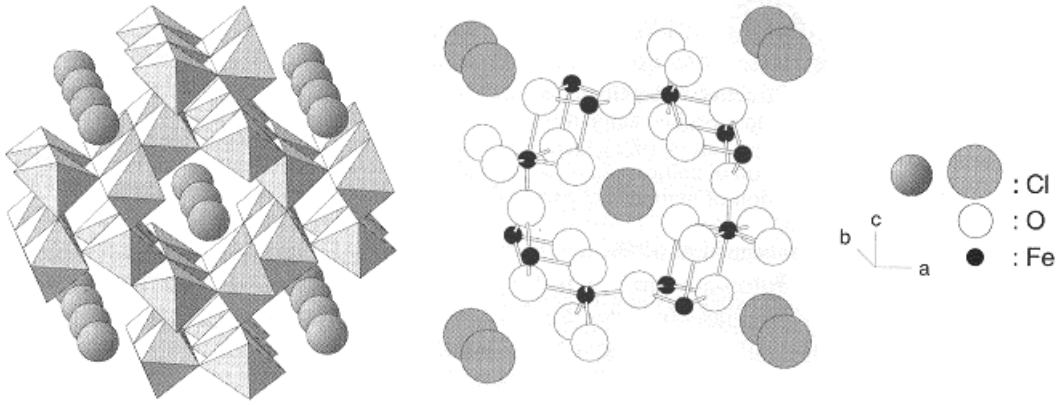

Figure 2.3. Akaganeite arrangement of octahedral chains with H atoms also shown. Schwertmannite is the sulfate analogue of akaganeite. Cornell and Schwertmann (1996)

Schwertmannite is the sulfate analogue of akaganeite. The structure (Figure 2.3) consists of double chains of edge sharing octahedra running parallel to the fourfold symmetrical *b*-axis. The double chains share corners with adjacent chains to give a three dimensional structure containing tunnels (Cornell and Schwertmann, 1996). The tunnels are stabilized by SO_4 anions which are considered to share oxygen atoms with the Fe octahedra of the tunnel wall thereby leading to some distortion. As a consequence the XRD lines of schwertmannite are broadened compared to those of akaganeite.

Goethite

Goethite can be synthesized from Fe^{II} oxidation followed by hydrolysis, or directly from Fe^{III} at high pH and elevated temperature (e.g. Goodman and Lewis, 1981; Atkinson et al., 1968). Both methods were used in this work. A pure, well-characterized acicular goethite was prepared at high pH and temperature, and then a SO_4-rich goethite was prepared by Fe^{II} oxidation and hydrolysis at pH 3 in a method simulating AMD conditions.

Pure acicular goethite was synthesized from ferrihydrite by a dissolution/reprecipitation process promoted by high temperature and pH (Atkinson et al., 1968). Solutions (in 100 mL batches) of 0.45 M ferric nitrate ($Fe(NO_3)_3.9H_2O$) and 0.34 M NaOH were prepared in HDPE vessels by first dissolving the ferric nitrate then adding the NaOH. These were aged at room temperature for 50 hours and then titrated to pH 12.0 by the drop-wise addition of 2.5 M NaOH under an Ar atmosphere. This resulted in the precipitation of ferrihydrite. This suspension was kept at 60 (± 1) °C for 4 days during which time the red-brown voluminous ferrihydrite was converted to a compact, yellow-brown goethite. Sodium nitrate was removed from the goethite by three cycles of centrifugation, decanting and resuspension in MilliQ water, then the goethite was freeze-dried.

The XRD (Figure 2.1) showed the only crystalline product present to be goethite. The product was insoluble in pH 3 ammonium oxalate/oxalic acid which demonstrates the absence of non-crystalline phases. The SEM (Figure 2.2 b) shows the presence of small uniform acicular crystals as is expected from the method used (Atkinson et al., 1968). Maintaining the $Fe(NO_3)_3$ solution for 50 hours at room temperature and low pH is a nucleation step, followed by a 4 day crystal growth step at pH 12 and 60 °C. The specific surface area of the freeze-dried product, determined by BET N_2 adsorption, was 80 ± 1 m^2g^{-1}. Ali and Dzombak (1996 a and b) used the same method to prepare goethite (although they dried their product at 40 °C) and the specific surface area of their goethite was 79.4 m^2g^{-1}.

Goethite has the diaspore structure (Figure 2.4), which consists of an hexagonal close packed array of anions (O^{2-} and OH^-) stacked along the [100] direction. The Fe^{III} ions occupy half the octahedral sites and are arranged in double rows which alternate with double rows of vacancies. The structure can also be described as double chains of edge sharing $FeO_3(OH)_3$ octahedra that run parallel to the [001] direction which are linked by corner sharing to adjacent double chains offset by c/2. Although goethite can display a multitude of shapes and

sizes there is essentially one basic morphology i.e. acicular with elongation in the [001] direction. The enclosing forms are predominantly {110} with {021} at the ends of the crystal (Figure 2.5).

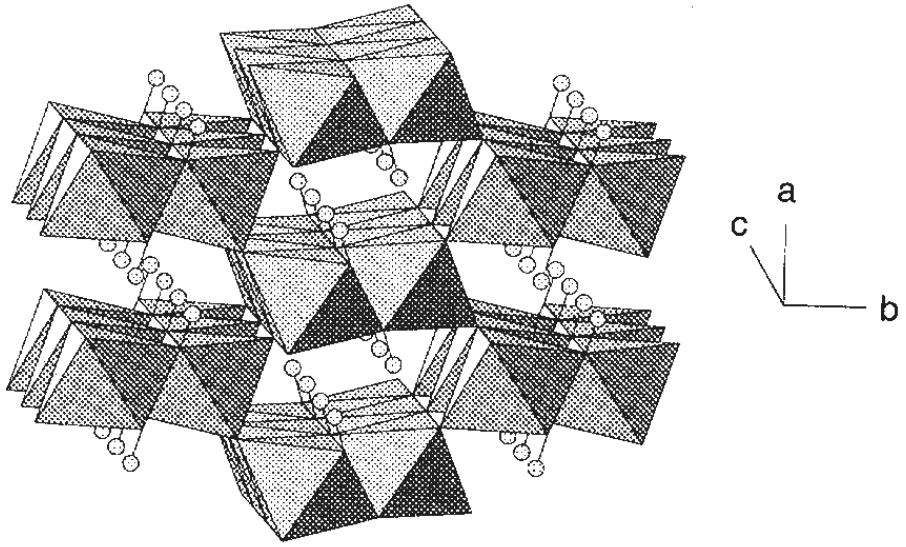

Figure 2.4. Goethite arrangement of octahedral chains with H atoms also shown (Cornell and Schwertmann, 1996).

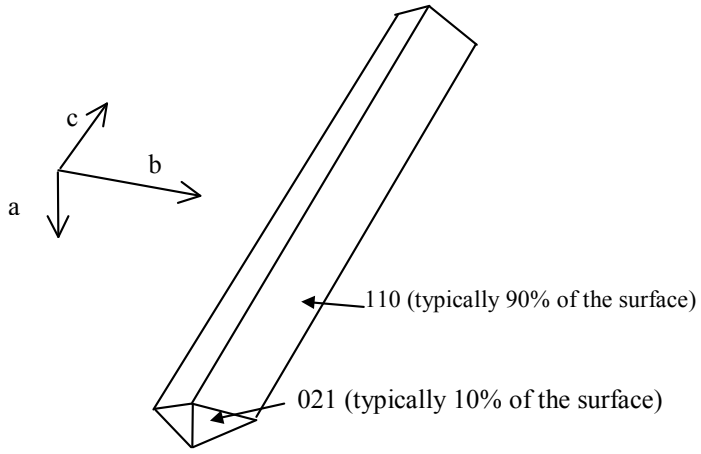

Figure 2.5. Schematic crystal morphology of acicular goethite (Venema et al, 1996).

Sulfate-rich goethite

Sulfate-rich goethite was synthesized by the abiotic atmospheric oxidation of $FeSO_4$ at pH 3.0. Because Fe^{II} oxidizing bacteria can affect the mineralogy of the product of $FeSO_4$ oxidation, steps were taken to ensure the reaction was abiotic. The starting solution was prepared in an autoclaved 1 L reaction vessel by filtering 100 mL of 1.0 mol kg^{-1} $FeSO_4$ solution at pH 2 (with H_2SO_4) through a sterile 0.2 μm filter membrane and then diluting to 1 L with 0.2 μm filtered MilliQ water. The solution was mixed on a magnetic stirrer and raised to pH 3 with a Metrohm Model 719 autotitater using autoclaved 1 mol kg^{-1} NaOH. The dispensing unit and pH electrode were sterilized with 70 % ethanol. Air was pumped through a sintered glass filter into the top of

the reaction vessel. The solution was initially clear and pale green/blue and slowly turned cloudy and yellow-brown as goethite precipitated. A temporary green precipitate, presumably $Fe(OH)_2$, formed in the mixing regions when NaOH was added but dissolved after approximately 5 minutes. The concentration of Fe^{III} in the suspension increased slowly and in a linear fashion so that after 46 days approximately 42 % of the Fe was present as Fe^{III}. The reaction was stopped after approximately 60 days and the supernatant decanted off the settled goethite. This product was rinsed in three cycles of centrifugation, decanting and resuspension in MilliQ water, and then freeze dried. Samples of the suspension at the end of the reaction were sent to Landcare Research to test for the presence of iron oxidizing bacteria by plating on FeTSBo agar plates for iron oxidizers (Johnson, 1995). No iron oxidizing bacteria were detected.

The XRD of the product is shown in Figure 2.1 and demonstrates that the only crystalline phase is goethite. The peaks are generally broader than those of the pure acicular goethite indicating a smaller crystal size. The sample dissolved slowly in pH 3 ammonium oxalate/oxalic acid, with solution Fe concentrations increasing in a linear fashion over 6 hours by which time 12 % of the sample had dissolved. SEM (Figure 2.2c) shows the goethite to be composed of aggregated rounded particles, as observed for the goethite present in the Tui AMD system by Webster et al. (1998). The BET specific surface area of the sample was 47 m^2g^{-1}, which appears to be inconsistent with the SEM images, which suggest a smaller particle size for the sulfate-rich goethite than for the acicular goethite. Presumably the high degree of aggregation in the SO_4-rich goethite causes the measured specific surface area to be low.

2.2 METHODS

2.2a Adsorption Experiments

Suspensions of the iron oxyhydroxides were prepared in 500 ml HDPE vessels, on a magnetic stirrer. Ferrihydrite and schwertmannite were used 18-24 h after precipitation and without drying. Pure and sulfate-rich goethite suspensions were prepared from a stock suspension of freeze-dried oxide in 0.1 M $NaNO_3$. In the case of the pure acicular goethite, the stock suspension pH was raised to 11, held for 30 minutes and the supernatant replaced twice by centrifugation, decanting and resuspension in 0.1 mol kg^{-1} $NaNO_3$ at pH 11. This was done to remove any CO_2 adsorbed onto the solid. However this was not done for the SO_4-rich goethite suspension, which was kept at pH 3, as replacing the supernatant with a pH 11 solution would also remove the SO_4. Given the high concentration of adsorbed SO_4 in this sample it is

probable (but not tested) that CO_2 adsorption on the solid would be less significant than on a pure goethite sample.

All adsorption experiments were carried out with a 0.1 mol kg^{-1} $NaNO_3$ electrolyte. For adsorption experiments with added SO_4, a portion of the 0.1 mol kg^{-1} $NaNO_3$ supernatant was removed from above the settled oxyhydroxide and replaced with water so that the ionic strength would remain at 0.1 mol kg^{-1} after Na_2SO_4 addition. For schwertmannite experiments the entire supernatant in which the oxyhydroxide was precipitated was replaced with 0.1 mol kg^{-1} $NaNO_3$ prior to adsorption experiments.

For metal adsorption edges the suspension pH was initially adjusted to 3.0 and the required concentration of Cu, Zn Pb, Cd, or Co was added from 1,000 mg kg^{-1} stock solutions at pH 3 of $Cu(NO_3)_2$, $Zn(NO_3)_2$, $Pb(NO_3)_2$, $Cd(NO_3)_2$, or $Co(NO_3)_2$. If required, Na_2SO_4 was also added at this time. The pH was then increased incrementally and 20-30 ml aliquots were retrieved at regular pH intervals. These aliquots were then equilibrated for 24-48 h in polypropylene centrifuge tubes on an end-over-end mixer at 25°C. After this time, the final pH of each sample was measured and phase separation achieved by filtration through 0.1 μm or 0.45 μm membranes. A portion of the filtrate was acidified to pH ≤ 2 with HNO_3 and analyzed for Cu, Zn, Pb, Cd or Co, while (for representative samples) the remainder was retained without acidification for SO_4 analysis. Adsorption isotherms were measured in a similar manner but the total metal concentration of the suspension was varied, while pH was held constant with any changes minimized by manual adjustment.

All raw experimental data has been included as an appendix of this thesis.

2.2b Acid-Base Titrations

Acid-base titrations were performed for the goethite samples to optimize the total site density and acidity constant parameters needed for modelling adsorption. For ferrihydrite the values for these parameters were taken from Dzombak and Morel (1990) and the schwertmannite adsorption of Cu and Zn was also modelled with the ferrihydrite parameters, as discussed in Chapter 3. Sulfate was removed from the SO_4-rich goethite prior to titrations by raising the pH to 10 for 30 minutes and then replacing the supernatant twice by centrifugation, decanting and resuspension in 0.1 mol kg^{-1} $NaNO_3$ at pH 10. Ion chromatography of the solutions showed that, within experimental error, all the SO_4 had desorbed after 30 min at pH 10. After

the final decanting the supernatant was replaced with MilliQ water and the ionic strength (I) adjusted to the lowest of the desired I to be used (0.004 mol kg^{-1}). Suspensions were titratated with a Metrohm model 716 DMS Titrino autotitrater using standardized 0.1 mol L^{-1} NaOH and HNO_3 under an Ar atmosphere to exclude CO_2. The rate of titration was set by using the lowest possible drift value of 0.5 mV min^{-1}.

To determine the pristine point of zero charge (PPZC) the pH of the suspension with I = 0.004 mol kg^{-1} was adjusted to pH ≈ 9 and the suspension left to equilibrate for 24 h. After this time the suspension was divided into three vessels and $NaNO_3$ added to raise the ionic strength of two suspensions to 0.020 and 0.10. Ionic strength was checked by comparing the supernatant conductivity to standard $NaNO_3$ solutions. The suspensions were left for another 24 h to equilibrate at the adjusted ionic strengths before titrations were begun. The addition of $NaNO_3$ shifts the pH of the suspension towards the PPZC. For example without added acid or base (TOTH=0) the pH's at I =0.004, 0.02 and 0.10 mol kg^{-1} were 9.29, 9.08 and 9.05 respectively. Furthermore, the higher the ionic strength the lower the change in pH as acid or base is added. Therefore the TOTH versus pH curves intercept and the point of intercept is where pH is independent of ionic strength and is therefore the PPZC.

Titrations were conducted at the three ionic strengths from pH ≈ 4 to 11. The titrations at I = 0.02 and 0.1 mol kg^{-1} were also back titrated to pH ≈ 4 with HNO_3. The titrations had some hysteresis such that between 10 and 20 % less HNO_3 was required to return the pH to the starting value compared to the amount of NaOH used for the base leg. Hysteresis in titration data for oxides is not always observed, e.g. Hayes et al. (1990), but is also not uncommon, e.g. Ali (1994) and Parks (1965). There was no significant difference between the degree of hysteresis with the pure goethite compared to the sulfate-rich goethite.

2.2c Analytical Methods

The pH was measured using a Ross "Sureflow" electrode (Orion). Concentrations of Cu, Zn, Co, Pb and Cd were measured by a combination of flame atomic adsorption spectrophotometry (AAS), graphite furnace atomic adsorption spectrophotometry (GFAAS) or inductively coupled plasma mass spectrometry (ICPMS) depending on the metal concentration. Tables 2.1 and 2.2 give the conditions and analytical ranges for AAS and GFAAS respectively. ICPMS was used

for samples with metal concentrations below the detection limit for GFAAS (Table 2.2) and the analyses were performed by Hill Laboratories Ltd. in Hamilton (N.Z.).

Iron oxyhydroxide concentrations were determined by measuring [Fe] in an unfiltered, acidified aliquot of the parent suspension. Ferrihydrite was rapidly soluble in HNO_3 and [Fe] was measured either by molecular absorption spectroscopy, from the adsorption at 450 nm after addition of KSCN (Vogel, 1981) or by AAS. Goethite required the addition of HCl to achieve dissolution and therefore [Fe] was measured by AAS, because Cl is a ligand for Fe and interfered with the KSCN method. The concentration of SO_4 in solution was measured by ion chromatography (IC) in samples without acidification using a Dionex AG4A guard and AS4A separation columns, H_2SO_4 suppression and conductivity detector.

Metal	λ (nm)	Flame	Bandpass (nm)	Limit of quantification (μmol kg^{-1})
Cu	324.7	oxidizing	0.2	1
Zn	213.9	oxidizing	0.2	0.2
Co	240.7	oxidizing	0.1	2
Cd	228.8	oxidizing	0.5	0.5
Pb	217.0	oxidizing	1.0	4
Fe	386.0	oxidizing	0.2	100

Table 2.1. Conditions for AAS analyses.

Metal	λ (nm)	Slit (nm)	Pretreatment ° C	Atomization	Limit of quantification (μmol kg^{-1})
Cu	324.7	0.7	1,200	2,300	0.1
Zn	213.9	0.7	700	1,800	0.02
Co	240.7	0.2	1,400	2,500	0.2
Cd	228.8	0.7	700	1,600	0.05
Pb	217.0	0.7	850	1,800	0.2

Table 2.2. Conditions for GFAAS analyses.

2.3 MODELLING

Modelling adsorption reactions requires that all chemical species present be considered, including solution and surface species. A set of components is defined such that every chemical species present can be written as the product of a reaction involving only these components. The components in this work were the free metal ions (e.g. Cu^{2+} and Na^{+}), the deprotonated anions (e.g. SO_4^{2-} and NO_3^{-}), the proton (H^{+}) and the neutral surface hydroxyl groups (≡Fe_xOH). Adsorption data were modelled using the DLM, as described in Chapter 1 and below in Section 2.3b. Equilibrium constants for adsorption reactions were optimized using the FITEQL3.2 computer program (Herbilin and Westall, 1996) as described in Section 2.3c below.

2.3a Solution Species

The solution species include the free ions (such as Cu^{2+} or SO_4^{2-}), the metal hydroxide complexes (such as $CuOH^+$), ion pairs (such as $CuSO_{4(aq)}$) and the products of protonation or deprotonation (such as H^+, OH^- or HSO_4^-). The equilibrium constants for the solution reactions were taken from Alison et al. (1991) with the exception of Co equilibrium constants which, not being cited in Alison et al. (1991), were taken from Smith and Martel (1976). The solution speciation will be important in modelling adsorption reactions where the activities of adsorbing species are affected, for example by the formation of solution complexes such as $CuSO_4^0{}_{(aq)}$ or $NaSO_4^-{}_{(aq)}$.

2.3b Adsorbed Species and the DLM

The principles of the DLM were discussed in Chapter 1. The surface adsorbed chemical species involved in the DLM are formed either by protonation reactions or the adsorption of cations and anions. Table 2.3 gives the equilibrium expressions for the formation of the adsorbed species. Surface hydroxyl groups are considered to be amphoteric. The surface reactions for proton transfer are given in Equations 2.1 to 2.4, where $\equiv Fe_{(1)}OH$ and $\equiv Fe_{(2)}OH$ denote type 1 and type 2 surface sites respectively as discussed below.

Reaction type:			
Surface Acid-Base Reaction			
$[\equiv Fe_{(1)}OH_2^+]$	=	$[\equiv Fe_{(1)}OH^0][H^+]\exp(-F\Psi/RT)\,\gamma_H(K_{A1}^{INT})^{-1}$	Eq. 2.1
$[\equiv Fe_{(2)}OH_2^+]$	=	$[\equiv Fe_{(2)}OH^0][H^+]\exp(-F\Psi/RT)\,\gamma_H(K_{A1}^{INT})^{-1}$	Eq 2.2
$[\equiv Fe_{(1)}O^-]$	=	$[\equiv Fe_{(1)}OH^0][H^+]^{-1}\exp(F\Psi/RT)\,(\gamma_H)^{-1}K_{A2}^{INT}$	Eq. 2.3
$[\equiv Fe_{(2)}O^-]$	=	$[\equiv Fe_{(2)}OH^0][H^+]^{-1}\exp(F\Psi/RT)\,(\gamma_H)^{-1}K_{A2}^{INT}$	Eq. 2.4
Me^{2+} Adsorption			
$[\equiv Fe_{(1)}OMe^+]$	=	$[\equiv Fe_{(1)}OH^0][H^+]^{-1}[Me^{2+}]\exp(-F\Psi/RT)(\gamma_H)^{-1}\gamma_{Me}\,K_1^{INT}$	Eq. 2.5
$[\equiv Fe_{(2)}OMe^+]$	=	$[\equiv Fe_{(2)}OH^0][H^+]^{-1}[Me^{2+}]\exp(-F\Psi/RT)(\gamma_H)^{-1}\gamma_{Me}\,K_2^{INT}$	Eq. 2.6
A^{2-} Adsorption			
$[\equiv Fe_{(2)}HA^0]$	=	$[\equiv Fe_{(2)}OH^0][H^+]^2[A^{2-}](\gamma_H)^2\gamma_A K_1^{INT}$	Eq 2.7
$[\equiv Fe_{(2)}A^-]$	=	$[\equiv Fe_{(2)}OH^0][H^+][A^{2-}]\gamma_H\gamma_A\exp(F\Psi/RT)K_2^{INT}$	Eq 2.8
$[\equiv Fe_{(2)}OHA^{2-}]$	=	$[\equiv Fe_{(2)}OH^0][A^{2-}]\gamma_A\exp(2F\Psi/RT)K_3^{INT}$	Eq 2.9
$[\equiv Fe_{(2)}OA^{3-}]$	=	$[\equiv Fe_{(2)}OH^0]\,[H^+]^{-1}[A^{2-}]\gamma_H^{-1}\gamma_A\exp(3F\Psi/RT)K_4^{INT}$	Eq. 2.10

Table 2.3 Equilibrium equations for adsorbed species. K^{INT} refers to an intrinsic adsorption constant which is independent of pH and ionic strength. $\equiv Fe_{(1)}OH$ and $\equiv Fe_{(2)}OH$ denote type 1 and type 2 surface hydroxyl groups respectively. [X] denotes the molar concentration of X, γ_X refers to the activity coefficients for solution species X, and Ψ refers to the surface potential. F is Faraday's constant, R is the gas constant and T is the temperature.

Cation adsorption on both ferrihydrite (Dzombak and Morel, 1990) and goethite (Robertson and Leckie, 1998) is considered to involve a small number of high affinity surface sites and a larger number of low affinity surface sites. The surface reactions for the adsorption of divalent cations are given in Equations 2.5 and 2.6 where $\equiv Fe_1OH$ and $\equiv Fe_2OH$ refer to high affinity (type 1) and low affinity (type 2) surface hydroxyl groups respectively. Note that it is an assumption of the model that the pK_A values are the same for both the type-1 and type-2 adsorption sites (Dzombak and Morel, 1990). The goethite adsorption of cations has been shown to involve 2 or 3 adjacent surface hydroxyl groups (e.g. Elzinga et al., 2001). However, for consistency with the database of Dzombak and Morel (1990), a stoichiometry of one surface site per metal is used for ferrihydrite. This enables the model parameters developed in the work to be incorporated in the database of Dzombak and Morel (1990). The stoichiometry used for cation adsorption onto goethite is discussed in Chapter 5.

All surface sites are considered equivalent with respect to anion adsorption. Several surface species with varying degrees of protonation may be necessary to model anion adsorption which occurs over a wider pH range than that of metals. (Dzombak and Morel, 1990). The surface adsorption reactions for a divalent anion A^{2-}, such as SO_4^{2-}, are given in Equations 2.7 to 2.10. Not all species may be required. For example Dzombak and Morel (1990) used only the species $\equiv Fe_{(2)}SO_4^-$ and $\equiv Fe_{(2)}OHSO_4^{2-}$ to model SO_4^{2-} adsorption on ferrihydrite, whereas Ali and Dzombak (1996a) used the species $\equiv Fe_{(2)}HSO_4^0$, $\equiv Fe_{(2)}OHSO_4^{2-}$ and $\equiv Fe_{(2)}OSO_4^{3-}$ to model SO_4^{2-} adsorption onto goethite.

The extent of adsorption of charged species will be influenced by the coulombic forces involved in a charged ion approaching a charged surface. The surface charge (σ with units of Cm^{-2}) is calculated from the algebraic sum of all charged surface species and is given by Equation 2.13 where A is the specific surface area ($m^2\ g^{-1}$), S is the solid concentration ($g\ L^{-1}$), [≡FeX] is the concentration of adsorbed species with component X having valence of Z_X and adsorption density of Γ_X in mol m^{-2} (Dzombak and Morel, 1990).

$$\sigma = (F/AS)([\equiv FeOH_2^+]-[\equiv FeO^-] + \Sigma_M[\equiv FeM]\, Z_M - \Sigma_A[\equiv FeA]\, Z_A) \qquad \text{Eq. 2.11}$$

$$= F[\Gamma_H - \Gamma_{OH} + \Sigma_M(Z_M\Gamma_M) - \Sigma_A(Z_A\Gamma_A)]$$

The surface potential (Ψ in units of V) is the amount of work required to move a positive charge of one Coulomb from the bulk solution to the charged surface. If the surface charge is positive, the surface potential will be positive, as work is expended bringing like charges together. The

surface potential is related to surface charge by the electric double-layer (EDL) theory as a function of ionic strength and temperature. For a symmetrical electrolyte of valency Z, the relationship is given in Equation 2.14 where ε is the dielectric constant of water (no units), ε◦ is the permittivity of free space (C V^{-1} m^{-1}) and c is the molar electrolyte concentration. The equilibrium expressions in Table 2.3 which involve a change in the surface charge include a coulombic term to correct for the electrostatic effect on the position of the equilibrium.

$$\sigma = (8RT\varepsilon\varepsilon_0 c\times 10^3)^{1/2} \cdot \sinh(ZF\Psi/2RT) \qquad \text{Eq. 2.12}$$

2.3c Parameter Optimization

FITEQL3.2 (Herbelin and Westall, 1996) is an iterative, gradient-directed nonlinear least squares optimization program based on the Gauss method (Bard, 1974 and Gans 1976). The program is designed to determine the optimal values of equilibrium constants, or total component concentration, in an equilibrium model applied to a set of experimental data (Dzombak and Morel, 1990). The equilibrium model is input as a list of components and matrices of mass action equations, for all chemical species, and mass balance equations for all components (Herbelin and Westall, 1996). The concentrations of all known components and all known equilibrium constants are input data. Guesses for the unknown parameters are required. The equilibrium data are also input, typically for a component for which the species concentration and total concentration are known, termed a Group II component. For acid-base titration data, for example, a list of species concentration ($[H^+]$) and the total component concentration (C_A-C_B) are required.

FITEQL3.2 computes the equilibrium species concentrations based on the input parameters and then calculates the weighted sum of squares (WSOS) for the Group II components. The WSOS is calculated from the residuals (the difference between the calculated total component concentration and the input value) which are weighted according to the error estimated for that residual as a result of experimental error. The WSOS divided by the number of degrees of freedom (WSOS/DF) constitutes the "objective function" to be minimized. FITEQL3.2 computes improved estimates for the adjustable parameters and recalculates the WSOS/DF for the revised estimates and tests for minimization of the WSOS/DF. Based on the change in the value of the WSOS/DF for the revised estimate for the adjustable parameters, FITEQL3.2 decides if the problem has converged or computes a further revised estimate for the adjustable parameters.

The error for each residual is calculated from an input of the absolute and relative error for measured total component concentrations and species concentrations. The estimated errors for experimentally measured total concentrations (s_T) and species concentration (s_X) are given in Equations 2.13 and 2.14 respectively, where s_J(abs) and s_J(rel) are respectively the input absolute and relative uncertainties for either species (X) or total component (T) concentration.

$$s_T = s_T(abs) + s_T(rel) \times T \quad \text{Eq. 2.13}$$

$$s_X = s_X(abs) + s_X(rel) \times X \quad \text{Eq. 2.14}$$

The input error values used in this study were based on those used by Dzombak and Morel (1990). For total metal (T_M), total anion (T_A) and total H^+ (T_H) the relative uncertainty was taken as 0.01, while the absolute uncertainty was 0.01 × the minimum value. For the proton concentration the relative uncertainty was taken as 0.05, representing an uncertainty of +/- 0.02 pH units. For free metal concentrations, discussed below, the relative uncertainty was taken as between 0.01 and 0.05 depending on the method of analysis, the metal and the concentration range. For AAS the value was typically 0.01 while for GFAAS it was typically 0.05. Absolute uncertainty for species concentrations were set at zero.

For adsorption experiments the total solution concentration of sorbate was measured rather than the free ion concentration. Therefore the total solution and the total adsorbed metal concentrations are known, rather than the concentration of any species. Therefore one can use a "dummy" Group II component e.g. "Total Solution Metal" ($T_{Me(sol)}$) or "Total Adsorbed Metal" ($T_{Me(ads)}$). In these cases FITEQL3.2 will adjust parameters based on minimizing the difference (Y) between the experimental and calculated value for Me_{sol} or Me_{ads} (examples given in Equations 2.15 and 2.16) where C_x is the calculated concentration of species X. Herbelin and Westall (1996) use the Me_{ads} Group II dummy component. However, because in general Me_{sol} is measured, using a Me_{sol} type II dummy component should give a more realistic estimate of the errors. Both options were used in this work, as discussed in the relevant sections, and the differences between them were small.

$$Y_{Me(sol)} = C_{Me^{++}} + C_{MeOH^+} - T_{Me(sol)} \quad \text{Eq. 2.15}$$

$$Y_{Me(ads)} = C_{\equiv Fe1OMe^+} + C_{\equiv Fe2OMe^+} - T_{Me(ads)} \quad \text{Eq. 2.16}$$

FITEQL3.2 calculations used molar concentrations, with solution and adsorption equilibrium constants adjusted for the ionic strength using the activity coefficients of solution species

calculated from the Davies equation as cited in Dzombak and Morel (1990). In all cases the reported intrinsic adsorption constants in this study have been corrected to zero ionic strength and a surface potential of zero.

CHAPTER THREE

Ferrihydrite And Schwertmannite Adsorption Of Cu And Zn: Ternary Surface Complex Formation With So_4.

Content published in Applied Geochemistry (Swedlund and Webster, 2001).

3.1 INTRODUCTION

Experimental adsorption studies on single sorbate, and single (usually synthetic) iron oxide sorbents may not be applicable to natural aquatic systems. The adsorption of Cu and Zn onto ferrihydrite and goethite, for example, was enhanced by SO_4 (Balistrieri and Murray, 1982; Ali and Dzombak, 1996a; Webster et al., 1998) though this effect is not predicted by the DLM and adsorption constants derived from single sorbate systems. Understanding the effect of SO_4 on the ferrihydrite adsorption of metals is important in the prediction of trace metal speciation in SO_4-rich systems, such as acid mine drainage (AMD) and marine waters. Furthermore, schwertmannite (ideal formula $Fe_8O_8(OH)_6SO_4$) is also a potentially important adsorptive surface regulating trace metal concentrations in AMD systems (Bigham et al., 1990). Previously determined Cu and Zn adsorption onto schwertmannite found it to be indistinguishable from the ferrihydrite adsorption of these metals in the presence of high solution SO_4 concentrations (Webster et al., 1998). Consequently a better understanding of the factors affecting Cu and Zn adsorption in the SO_4-ferrihydrite system, could also be applicable to Cu and Zn adsorption onto schwertmannite.

Modelling studies have accurately reproduced the effect of SO_4 on the goethite adsorption of trace metals. By including a ternary complex with stoichiometry $\equiv FeOHMeSO_4$, the effect of SO_4 on metal adsorption was accurately described for a wide range of Me, Fe and SO_4 concentrations (Ali and Dzombak, 1996; Hoins et al., 1993). XAFS and ATR-IR studies of the goethite/SO_4/Pb system support ternary complex formation with a 1:1 Pb:SO_4 ratio though involving 2 or 3 surface hydroxyl groups (Elzinga et al., 2001). As there have been no modelling or spectroscopic studies, as yet, for ferrihydrite/SO_4/Me systems the purpose of this chapter was to ascertain whether ternary complexes appeared to be of similar importance in the Cu or Zn-SO_4-ferrihydrite systems, if so the aim was to derive their ternary complex formation constants. As discussed in Section 2.3b adsorption reactions were considered to occur on single surface sites despite spectroscopic evidence of edge and corner sharing surface complexes on goethite. This was done to be consistent with the database of Dzombk and Morel (1990). The effect of SO_4 on the ferrihydrite adsorption of Cu and Zn was experimentally determined, and the formation of ternary surface complexes investigated by using the DLM to attempt to duplicate the observed data. Adsorption of Cu and Zn onto schwertmannite was also measured and compared to adsorption onto ferrihydrite in the presence of SO_4.

3.2 RESULTS

3.2a Ferrihydrite Single Sorbate Adsorption Studies

The ferrihydrite adsorption of Cu, Zn and SO_4 in single sorbate systems was determined as a function of pH for total metal ($Me_{(T)}$) to Fe mole ratios (Me_T:Fe) ranging from 0.000317 to 0.0264 for Cu and Zn, or SO_4:Fe ratios from 0.217 to 1.90. Results are shown in Figure 3.1, with model fits as discussed below. The percentage of metal adsorbed increased with increasing pH and with decreasing Me_T:Fe. Sulfate adsorption increased with decreasing pH and decreasing total sulfate ($SO_{4(T)}$) to Fe ratios.

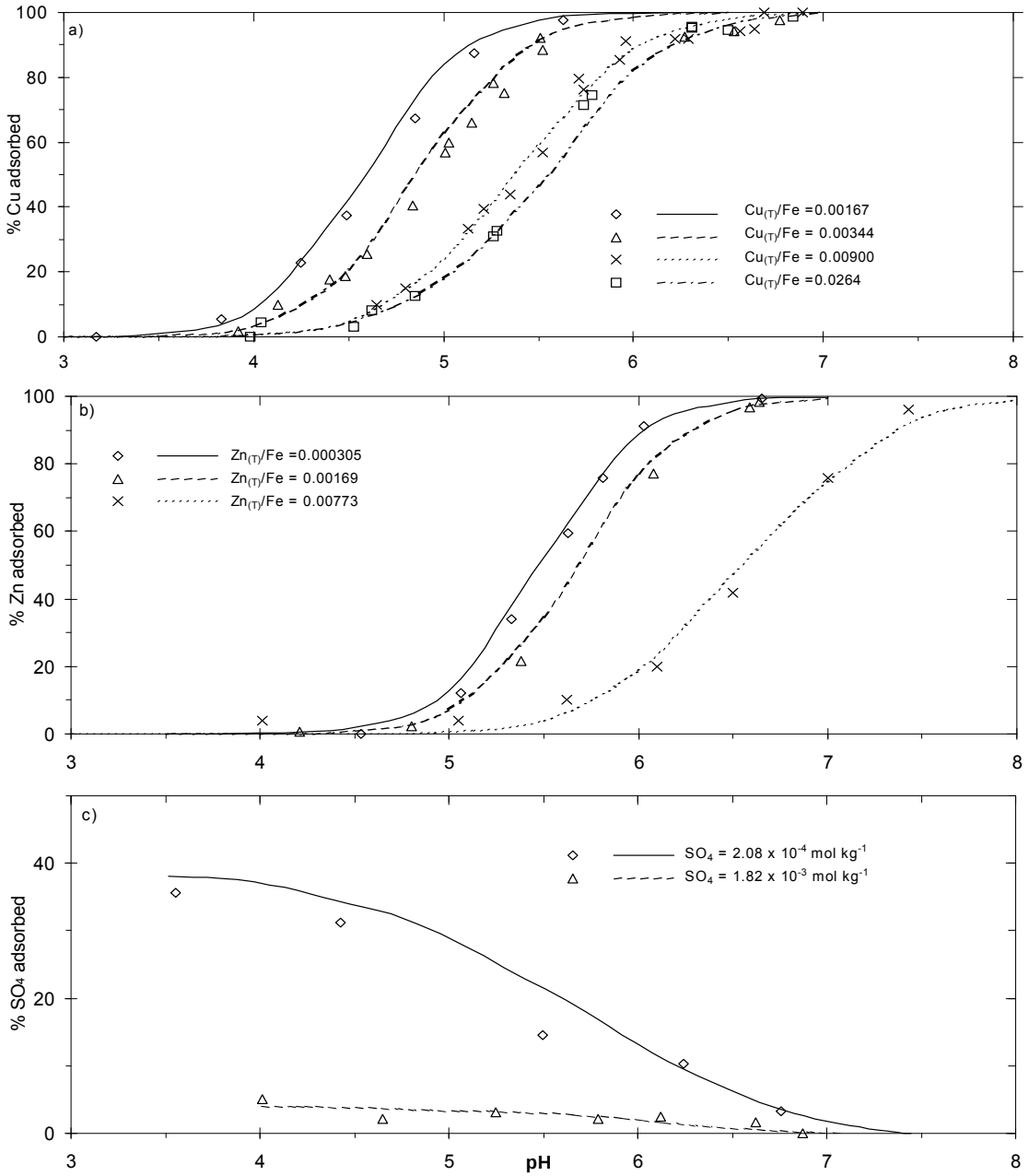

Figure 3.1. Experimental and modelled ferrihydrite adsorption of (a) Cu, (b) Zn and (c) SO_4 in single sorbate systems. Adsorption modelled using parameters of Dzombak and Morel (1990). Concentrations of Me and Fe for Figures 3.1 a) and b) are given in Table 3.1. The Fe concentration in Figure 3.1c was 9.6 x 10^{-4} mol kg^{-1}.

3.2b Ferrihydrite Adsorption of Cu or Zn in the Presence of SO_4.

The effect of SO_4 on the ferrihydrite adsorption of Cu or Zn is shown in Figures 3.2, 3.3 and 3.4. In general adsorption of Cu and Zn was increased in the presence of SO_4. The extent of this effect was largest for the systems with the lowest $Me_{(T)}$/Fe ratios. For example, the presence of SO_4 increased Cu adsorption up to 25% when the $Cu_{(T)}$/Fe ratio was 0.00167, but increased Cu adsorption by < 5%, when the $Cu_{(T)}$/Fe ratio was higher at 0.0264. Similarly for Zn, the presence of SO_4 increased Zn adsorption up to 40% when the $Zn_{(T)}$/Fe ratio was 0.000317, but increased Zn adsorption by < 5%, where the $Zn_{(T)}$/Fe ratio was higher at 0.00757. In addition, as SO_4 concentration increased, the effect of additional SO_4 on Cu or Zn adsorption decreased. Sulfate adsorption was not measurably affected by the concentration of Me, as might be expected given the much higher SO_4 concentration.

3.3 DISCUSSION

3.3a Ferrihydrite Single Sorbate Adsorption Studies

Adsorption data were modelled using the DLM and the values determined by Dzombak and Morel (1990) for surface area (600 m^2/g), adsorption site densities and intrinsic surface acidity constants. Cation adsorption (Equations 2.5 and 2.6) was considered to occur at both high affinity (type-1, $\equiv Fe_{(1)}OH$) and low affinity (type-2, $\equiv Fe_{(2)}OH$) sites, which have densities of 0.005 and 0.2 mol/mol Fe respectively. The surface acidity constants (Equations 2.1 to 2.4 in Table 2.3) used were –7.29 and –8.93 for $\log K_{A1}^{INT}$ and $\log K_{A2}^{INT}$ respectively. Sulfate adsorption was modelled using the monovalent and divalent surface species (Equations 2.8 and 2.9) with $\log K_2^{INT}$ and $\log K_3^{INT}$ of 7.78 and 0.79 as determined by Dzombak and Morel (1990).

Intrinsic adsorption constants were derived for each Cu or Zn data set (Table 3.1), and the weighted average values of these were within 0.07 log units of the values from Dzombak and Morel (1990). In particular the optimised $\log K_2^{INT}$ value for Cu was within 0.06 log units of the value estimated from a Linear Free Energy Relationship (LFER) between metal hydrolysis constants and metal adsorption constants (Dzombak and Morel, 1990). The modelled adsorption edges, using the intrinsic adsorption constants of Dzombak and Morel (1990), are shown with the results from this study in Figure 3.1. In general, Cu, Zn and SO_4 adsorption in single sorbate experiments was well predicted using these constants.

Table 3.1. Intrinsic adsorption constants (and standard deviations in parentheses) from experimental data for Cu and Zn adsorption on ferrihydrite in single sorbate systems. Weighted average intrinsic adsorption constants are also shown, with the 95% uncertainty level (in italics in parentheses). "nc" indicates values that were unable to be derived from the data.

Cu μmol kg^{-1}	Fe mmol kg^{-1}	$Cu_{(T)}$/Fe	$logK_1^{INT}$	$logK_2^{INT}$	WSOS/DF
24.4	14.7	0.00167	2.87 (0.028)	nc	1.59
16.5	4.80	0.00344	2.90 (0.019)	nc	3.87
8.37	0.930	0.00900	2.89 (0.057)	0.59 (0.046)	2.59
24.7	0.935	0.0264	2.74 (0.10)	0.71 (0.034)	1.55
	Weighted averages		**2.87**	**0.66**	
			(2.82, 2.92)	*(0.15,1.19)*	
	Dzombak and Morel (1990)		2.89	0.60[a]	

Zn μmol kg^{-1}	Fe mmol kg^{-1}	$Zn_{(T)}$/Fe	$logK_1^{INT}$	$logK_2^{INT}$	WSOS/DF
8.24	27.0	0.000305	0.929 (0.026)	nc	0.61
24.0	14.2	0.00169	0.902 (0.038)	nc	0.13
7.96	1.03	0.00773	0.99 [b]	-2.07 (0.10)	10.8
	Weighted average		**0.92**		
			(0.80, 1.04)		
	Dzombak and Morel (1990)		0.99	-1.99	

[a] Estimated from Linear Free Energy Relationship (Dzombak and Morel, 1990).

[b] No convergence of this value so it was fixed at this value for consistency between results.

3.3b Ferrihydrite adsorption of Cu and Zn in the Presence of SO_4

Sulfate had the greatest effect on Me adsorption in experiments with $Me_{(T)}$/Fe ratios < 0.005, when adsorption should occur predominantly at high affinity (type-1) adsorption sites (Dzombak & Morel, 1990). Adsorption modelled using the $logK^{INT}$ derived from single sorbate systems (Table 3.1) did not predict the degree of change in Me adsorption due to the presence of SO_4 and its effect on surface charge. Using the DLM and the $logK^{INT}$ from Table 1, adsorption of Me was predicted to change < 3% when SO_4 concentrations increased from 0 to 0.01 mol kg^{-1}. Experimental observation showed up to 40% increase in Me adsorption due to the presence of SO_4.

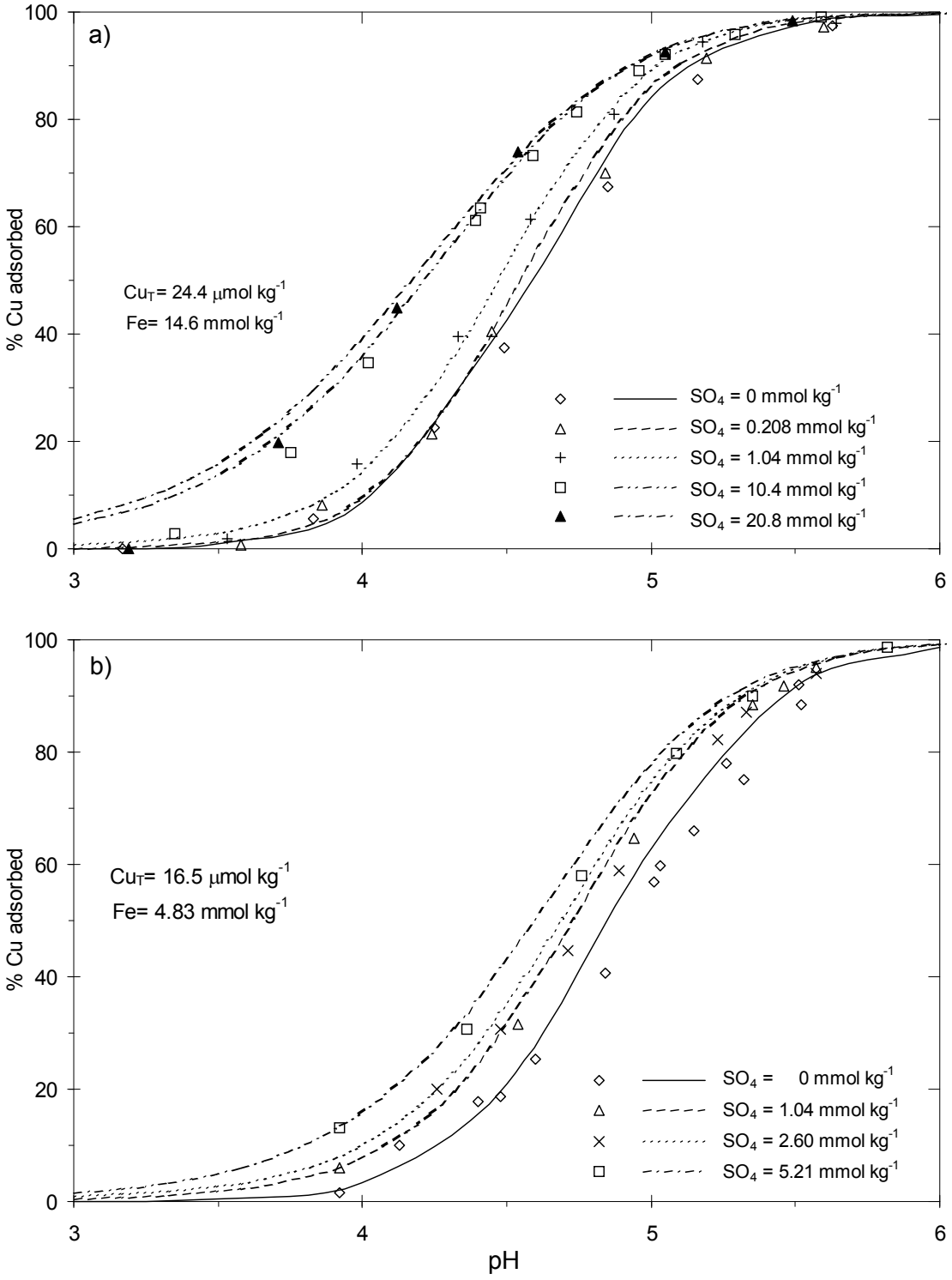

Figure 3.2. Experimental and modelled ferrihydrite adsorption for Cu in the presence of SO_4 for low $Cu_{(T)}$/Fe ratios. a) $Cu_{(T)}$ /Fe =0.00167, b) $Cu_{(T)}$ /Fe =0.00344. Modelled adsorption used all the adsorption parameters of Dzombak and Morel (1990) and the weighted average constant in Table 3.2

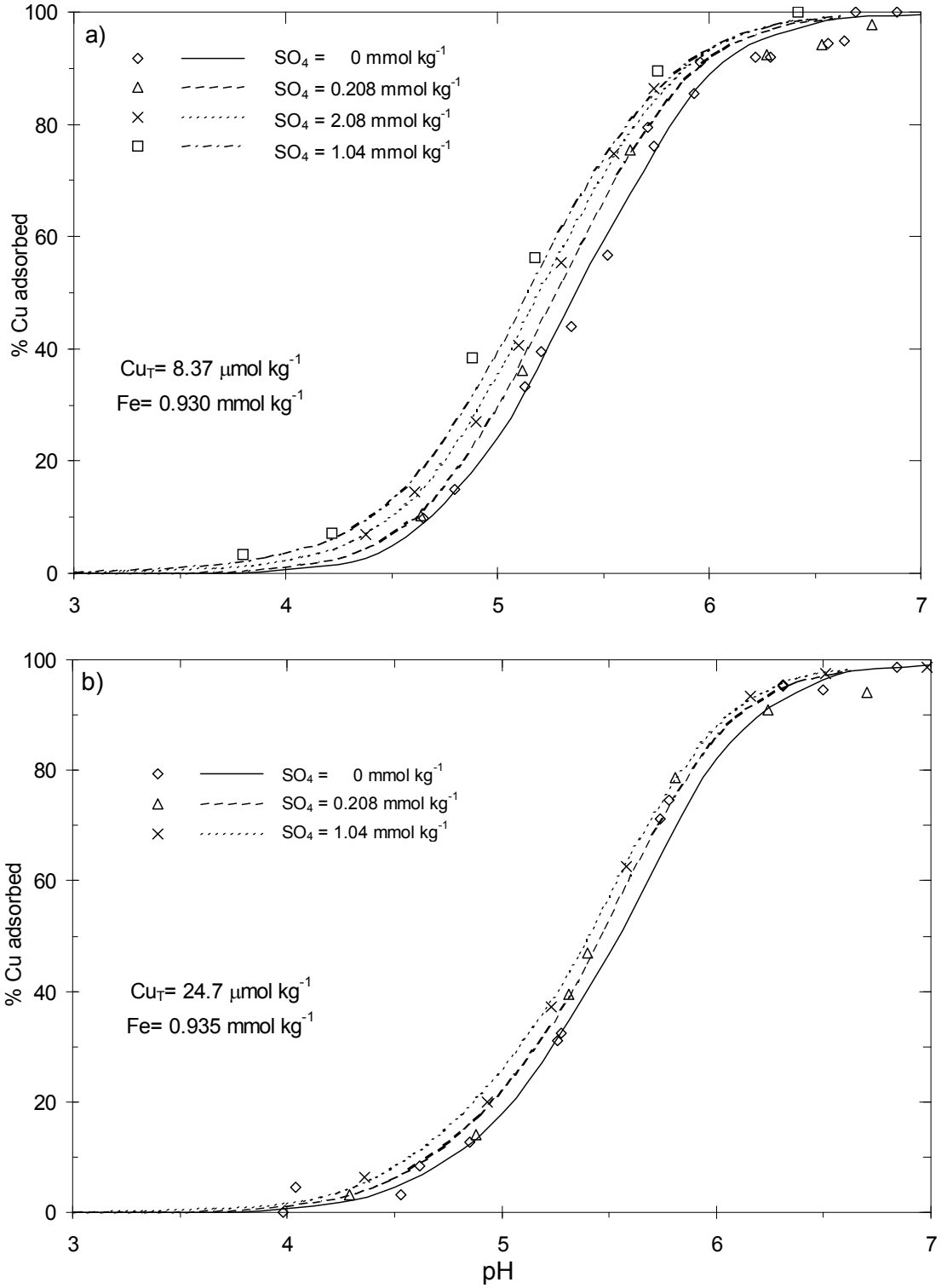

Figure 3.3 Experimental and modelled ferrihydrite adsorption for Cu in the presence of SO_4 for high $Cu_{(T)}$/Fe ratios. a) $Cu_{(T)}$ /Fe =0.00900, b) $Cu_{(T)}$ /Fe =0.0264. Modelled adsorption used all the adsorption parameters of Dzombak and Morel (1990) and the weighted average constant in Table 3.2.

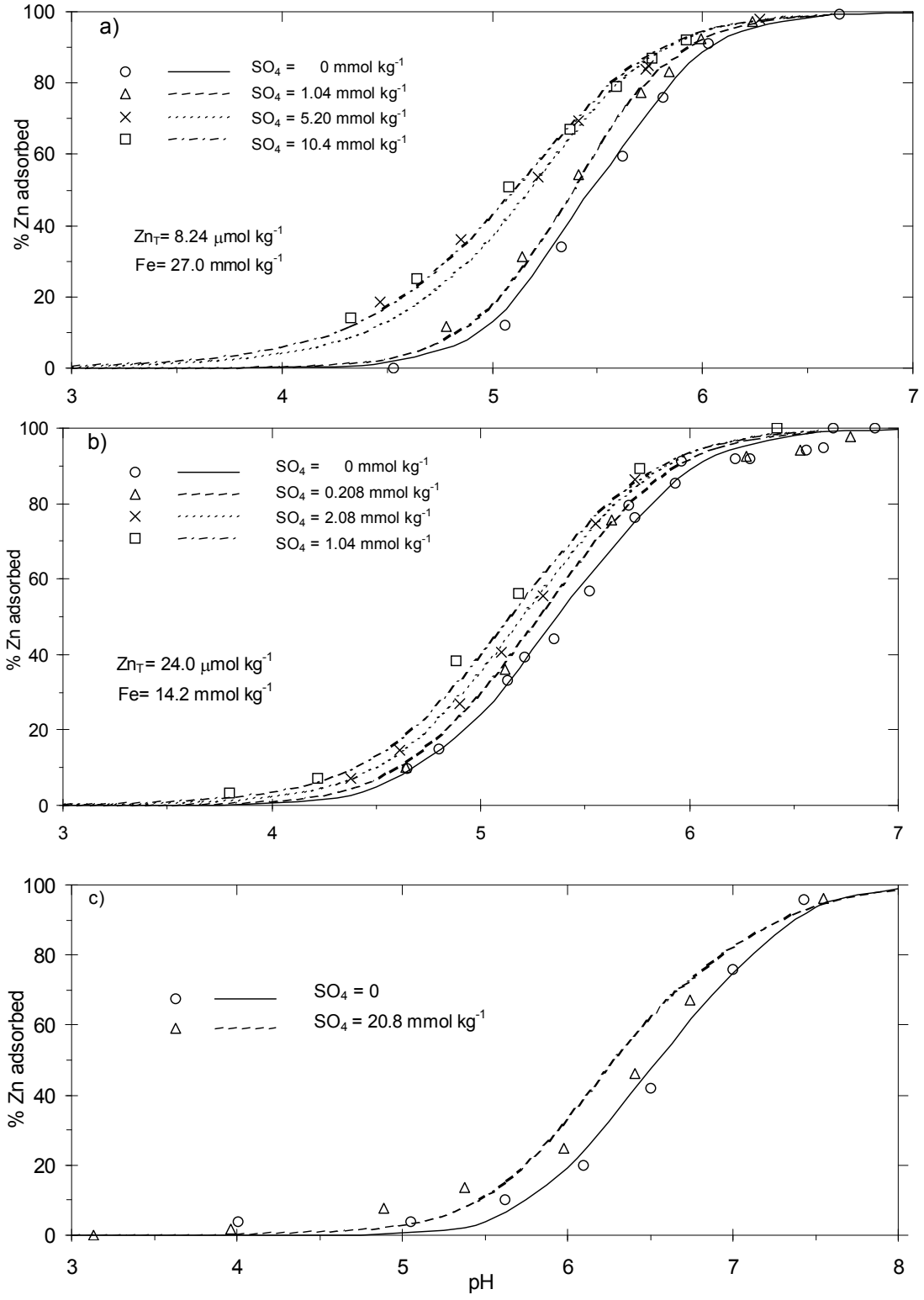

Figure 3.4. Experimental and modelled ferrihydrite adsorption for Zn in the presence of SO_4. a) $Zn_{(T)}$ /Fe =0.000305, b) $Zn_{(T)}$ /Fe =0.00169. c) $Zn_{(T)}$ /Fe =0.00773. Modelled adsorption used all the adsorption parameters of Dzombak and Morel (1990) and the weighted average constant in Table 3.3.

3.3c Ternary Complexes formation

To successfully model the effect of SO_4 on metal adsorption requires an accurate description of the following;

1. solution complexation between SO_4 and metal, which would decrease metal adsorption,
2. competition for surface sites, which would decrease metal adsorption,
3. decreasing surface charge due to SO_4 adsorption, which would increase metal adsorption,
4. any bonding or local electrostatic interaction between the adsorbed SO_4 and metal, which would increase metal adsorption,
5. the precipitation of $MeSO_{4(s)}$, (not applicable here as $CuSO_4$ and $ZnSO_4$ salts are very soluble).

A model using adsorption constants from single sorbate systems should predict the effects of solution complexation, site competition and surface charge changes. Ali and Dzombak (1996a) noted a similar enhancement of Cu adsorption on goethite in the presence of SO_4 which, like the results in this study, was also not predicted by the DLM and intrinsic adsorption constants derived from single sorbate experiments. However, by including a ternary complex; $\equiv FeOHCuSO_4$ with $\log K^{TC} = 9.68$, (Equation 3.1) the effect of SO_4 on Cu adsorption on goethite was accurately predicted for a wide range of conditions (Ali and Dzombak 1996a). Consequently, the potential formation of ternary Me-SO_4-ferrihydrite complexes was investigated by deriving $\log K^{TC}$ for their formation from the experimental adsorption data. If ternary complexes are a plausible explanation for observed adsorption behaviour, values for the $\log K^{TC}$'s derived from each set of data should be close in value and not vary systematically with different Me/Fe ratios and SO_4 concentrations.

$$[\equiv Fe_{(x)}OHCuSO_4] = [\equiv Fe_{(x)}OH^0][Cu^{2+}][SO_4^{2-}]\,\gamma_{Me}\gamma_{SO4}\,K_x^{TC} \qquad \text{Eq. 3.1}$$

One complication when dealing with a ferrihydrite system, rather than goethite, is site heterogeneity. Two surface site types are considered to be necessary in order to model Cu and Zn adsorption on ferrihydrite (Dzombak and Morel 1990), while for the conditions used by Ali and Dzombak (1996a) Cu adsorption onto goethite can be modelled with only one surface site type. Several model options were considered when fitting the data from this study, including the formation of ternary complexes on either type-1 sites or type-2 sites, or on both sites.

Ternary complexes of Cu

Model testing was initially performed on the Cu data because there were more data sets. The stoichiometry $\equiv FeOHCuSO_4$ suggested by Ali and Dzombak (1996a) was tested, then other options were trialed. The results from modelling the various options are described below:

1) Ternary complexes at type-1 sites only. All low Cu/Fe data could be reasonably well fitted by including a ternary complex at the type-1 sites. The $\log K_1^{TC}$ derived for $\equiv Fe_{(1)}OHCuSO_4$ for low $Cu_{(T)}$/Fe systems, ranged from 9.10 to 9.41. However, including the $\log K_1^{TC}$ into the model did not significantly increase predicted Cu adsorption in the high $Cu_{(T)}$/Fe systems with SO_4, suggesting a type-2 site ternary complex was also needed to model this data.

2)Ternary complexes at both type-1 and type-2 sites. It was not possible to optimize $\log K^{TC}$ for ternary complex formation at both type-1 and type-2 sites simultaneously from one data set. Therefore, the $\log K_1^{TC}$ for $\equiv Fe_{(1)}OHCuSO_4$ was fixed at the value derived from the low Cu/Fe data and the value for $\equiv Fe_{(2)}OHCuSO_4$ was optimised from the high Cu/Fe data. The $\log K_2^{TC}$ derived for $\equiv Fe_{(2)}OHCuSO_4$ from high $Cu_{(T)}$/Fe data ranged from 7.59 to 8.22. However, when the $\log K_2^{INT}$ was included with $\log K_1^{TC}$ in the model, the effect of SO_4 on Cu adsorption in low Cu/Fe systems was over predicted by up to 20 %. Furthermore, if the $\log K_2^{TC}$ for $\equiv Fe_{(2)}OHCuSO_4$ was fixed at the value derived above, there was no convergence in the optimisation of $\log K_1^{TC}$ for $\equiv Fe_{(1)}OHCuSO_4$ in the low Cu/Fe data suggesting the $\equiv Fe_{(1)}OHCuSO_4$ species was not significant.

3)Ternary complexes at type-2 sites only. Models with ternary complexes only at type-1 sites or at both type-1 and 2 sites could not satisfy both the low and high Cu/Fe data. Therefore the data was modelled assuming ternary complex formation only on the type-2 sites. This approach provided an acceptable fit of both the high and low Cu/Fe data. The $\log K_2^{TC}$ derived for $\equiv Fe_{(2)}OHCuSO_4$ from both low and high $Cu_{(T)}$/Fe data ranged from 7.55 to 8.31 and the weighted average and uncertainty at the 95 % confidence level was 7.83 ± 0.06. There was no systematic variation in the $\log K_2^{TC}$ with increasing SO_4 concentration or with $Cu_{(T)}$/Fe ratio (Table 3.2) suggesting that this is a reasonable model to fit all the data. Predicted adsorption using this model is shown with the experimental data in Figures 3.2 and 3.3.

Adsorption of SO_4

The ferrihydrite adsorption of anions such as SO_4 can be modelled with only type-2 sites (Dzombak and Morel, 1990). It is possible that SO_4 also adsorbs on type-1 sites (with the same $\log K^{INT}$) but, because the ratio of type-1 to type-2 sites is small (0.025), this would only be evident from the effect of this site competition on cation adsorption. The ternary complex modelling discussed above assumed SO_4 adsorption only at the type-2 sites. When SO_4 adsorption on type-1 sites was included

in option 3 above, the $logK_2^{TC}$ for $\equiv Fe_{(2)}OHCuSO_4$ was 8.00±0.06. This was a little larger than the value with no SO_4 adsorption at type-1 sites due to added site competition. However, the value of $logK_2^{TC}$ decreased systematically for each Cu/Fe set of data as SO_4 concentration increased and were higher in the high Cu/Fe than the low Cu/Fe experiments (model data not shown). The weakness of this option was also evident in the comparison between experimental and modelled adsorption using the *weighted average* $logK_2^{TC}$. For example, when SO_4 adsorption at type-1 sites is included, all the high [SO_4] and low Cu/Fe results were over predicted by up to 15%. Modelling assuming no SO_4 adsorption at type-1 sites was a better option, although there was some over-prediction of Cu adsorption in the high [SO_4] and low Cu/Fe results at less than 20 % adsorption (Figures 3.2 and 3.3). None of the other model options or stoichiometries trialed were improved by including SO_4 adsorption at type-1 sites.

Table 3.2. Intrinsic adsorption constants (and standard deviations in parentheses) optimised from experimental data for the formation of $\equiv Fe_{(2)}OHCuSO_4$ ferrihydrite ternary complexes. The weighted average equilibrium constant is also shown, with the 95% uncertainty level (in italics in parentheses).

Cu/Fe	Cu $\mu mol\ kg^{-1}$	Fe $mmol\ kg^{-1}$	SO_4 $mmol\ kg^{-1}$	$LogK_2^{TC}$	WSOS/ DF
Low $Cu_{(T)}$/Fe					
0.00167	24.4	14.6	1.04	7.92 (0.080)	1.43
0.00167	24.4	14.6	10.4	7.71 (0.024)	7.40
0.00167	24.4	14.6	20.8	7.70 (0.027)	9.41
0.00344	16.5	4.80	1.06	7.60 (0.13)	1.45
0.00344	16.5	4.80	2.10	7.69 (0.039)	1.62
0.00344	16.5	4.80	10.4	7.55 (0.079)	4.53
High $Cu_{(T)}$/Fe					
0.00900	8.37	0.930	2.08	8.31 (0.044)	1.31
0.00900	8.37	0.930	10.4	8.14 (0.033)	2.98
0.0264	24.7	0.935	0.208	7.68 (0.15[a])	1.50
0.0264	24.7	0.935	1.04	7.71 (0.095)	0.72
		Weighted Average		**7.83** *(7.78,7.89)*	

[a] Fixed at this value by convention when the actual value is >0.15 (Dzombak and Morel 1990).

Other ternary complex stoichiometries

Model fits were attempted for other ternary complex stoichiometries, including species with 2 adsorption sites ($\equiv Fe_{(2)}OCuSO_4Fe_2\equiv$) and species with varying charge (eg. $\equiv Fe_{(2)}OCuSO_4^-$ and $\equiv Fe_{(2)}SO_4Cu^+$). However, no stoichiometry other than $\equiv Fe_{(2)}OHCuSO_4$ could fit the data without $logK^{TC}$ showing large variations between different sets of data, or non-convergence for some data sets. For example, for the data with Cu/Fe ratio of 0.00167, the $logK_2^{TC}$ for formation of $\equiv Fe_{(2)}OCuSO_4^-$ ranged from 12.14 to 7.19 as the SO_4 concentration increased from 1.04×10^{-3} to 2.08×10^{-2} mol kg^{-1}. Therefore the best possible model to fit the data was the neutral Cu-SO_4 ternary complex formed at the type-2 binding sites.

Ternary complexes for Zn

The stoichiometry and binding site model found to be the most appropriate for Cu, was also found to be the most appropriate for Zn. That is, by including a $\equiv Fe_{(2)}OHZnSO_4$ ternary complex, and allowing SO_4 adsorption only at type-2 sites, all the experimental data could be predicted and there was no systematic variation in the derived $logK_2^{TC}$ with [SO_4] or Zn/Fe ratio (Table 3.3). The values of $logK_2^{TC}$ for $\equiv Fe_{(2)}OHZnSO_4$ ranged from 6.37 to 6.77 and the weighted average and uncertainty at the 95 % confidence level was 6.67±0.06. Modelled Zn adsorption, using the weighted average $logK_2^{TC}$ for ternary complex formation, are shown with the experimental data in Figure 3.4.

Table 3.3 Intrinsic adsorption constants (and standard deviations in parentheses) from experimental data for the formation of $\equiv Fe_{(2)}OHZnSO_4$ ferrihydrite ternary complexes. The weighted average equilibrium constant is also shown, with the 95% uncertainty level (in italics in parentheses).

Zn/Fe	Zn μmol kg^{-1}	Fe mmol kg^{-1}	SO_4 mmol kg^{-1}	$LogK_2^{TC}$	WSOS/ DF
Low $Zn_{(T)}$/Fe					
0.000305	8.24	27.0	1.04	6.46 (0.15[a])	1.42
0.000305	8.24	27.0	5.20	6.77 (0.031)	3.10
0.000305	8.24	27.0	10.4	6.76 (0.025)	1.79
0.00169	24.0	14.2	2.08	6.55 (0.083)	7.36
0.00169	24.0	14.2	10.4	6.65 (0.032)	8.81
High $Zn_{(T)}$/Fe					
0.00772	7.96×10^{-6}	1.03×10^{-3}	2.08×10^{-2}	6.37 (0.084)	20.65
		Weighted Average		**6.67** *(6.61, 6.72)*	

[a] Fixed at this value by convention when the actual value is >0.15 (Dzombak and Morel 1990).

3.3d The relationship between single sorbate and ternary complex adsorption constants.

The weighted average value for the $logK_2^{TC}$ of the Cu-SO_4-ferrihydrite complex obtained in this work (ie. $logK_2^{TC}$ = 7.83) is considerably lower than the value obtained by Ali and Dzombak (1996a) for the analogous goethite complex (ie. $LogK^{TC}$ = 9.68). The difference in these values is close to the difference between the $logK^{TC}$ for Cu adsorption on ferrihydrite type-2 sites (0.6) and on goethite (2.78). The linear relationship between the $logK^{TC}$'s for $\equiv FeOHMeSO_4$ and $\equiv FeOMe^+$ formation on ferrihydrite (this study) and goethite (Ali & Dzombak, 1996a) is shown in Figure 3.5. The clear positive slope of the line suggests that the strength of the ternary complex is influenced by the binding of the cation to an adsorption site. In addition the plot suggests that the mechanism of ternary complex formation on ferrihydrite may be the same on goethite and ferrihydrite.

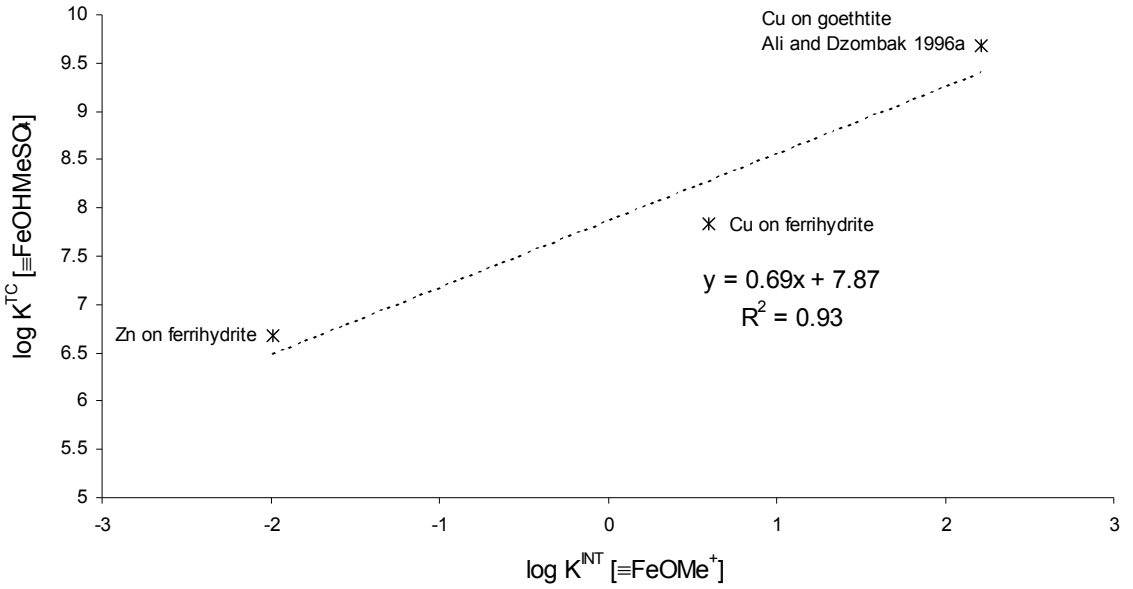

Figure 3.5. Relationship between intrinsic adsorption constants for $\equiv FeOHMeSO_4$ and for $\equiv FeOMe^+$ formation on ferrihydrite (this study) and goethite (Ali and Dzombak, 1996a).

The ternary complex structures supported by the spectroscopic studies of Pb/SO_4/goethite systems by Elzinga et al. (2001) and Ostergren et al. (2000) are given in Figure 3.6. Both structures involve a 1:1 Pb:SO_4 ratio and a bond between the Pb and the iron oxide surface. As discussed in Section 2.3b adsorption reactions were considered to occur on single surface sites despite spectroscopic evidence of edge and corner sharing surface complexes on goethite. This was done to be consistent with the database of Dzombk and Morel (1990) and therefore allow the model results to be widely used. The 1:1 Pb:SO_4 ratio is consistent with the model stoichiometry used and bond between the surface sites and the Pb is consistent with the dependence of $logK^{TC}$'s on the $logK^{INT}$ for the cation. The results of this study would support the structure in Figure 3.6b as presumably that of Figure 3.6a would involve a greater degree of site competition.

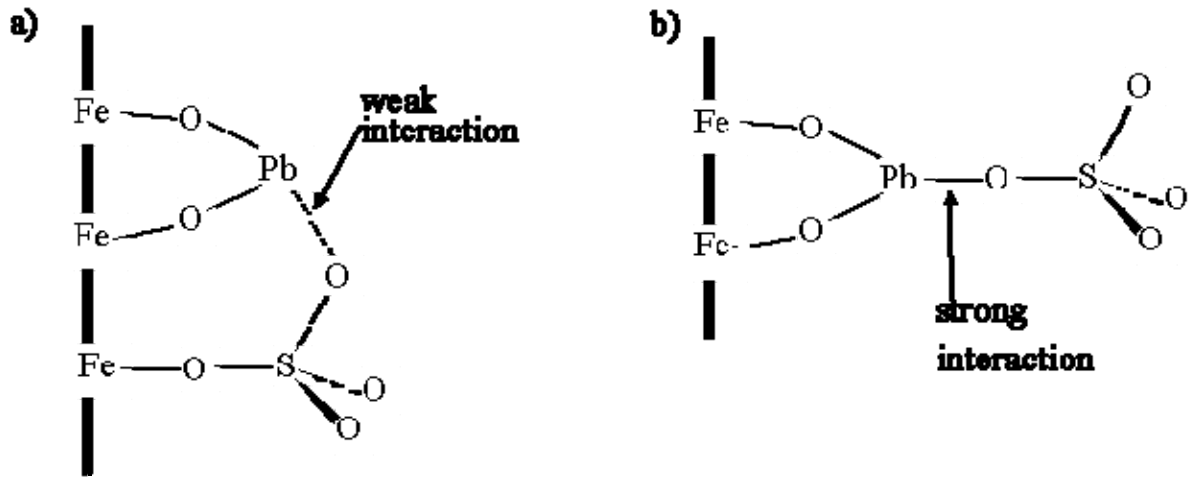

Figure 3.6 Structures of ternary complexes consistent with XAFS and ATR-IR data (Elzinga et al, 2001).

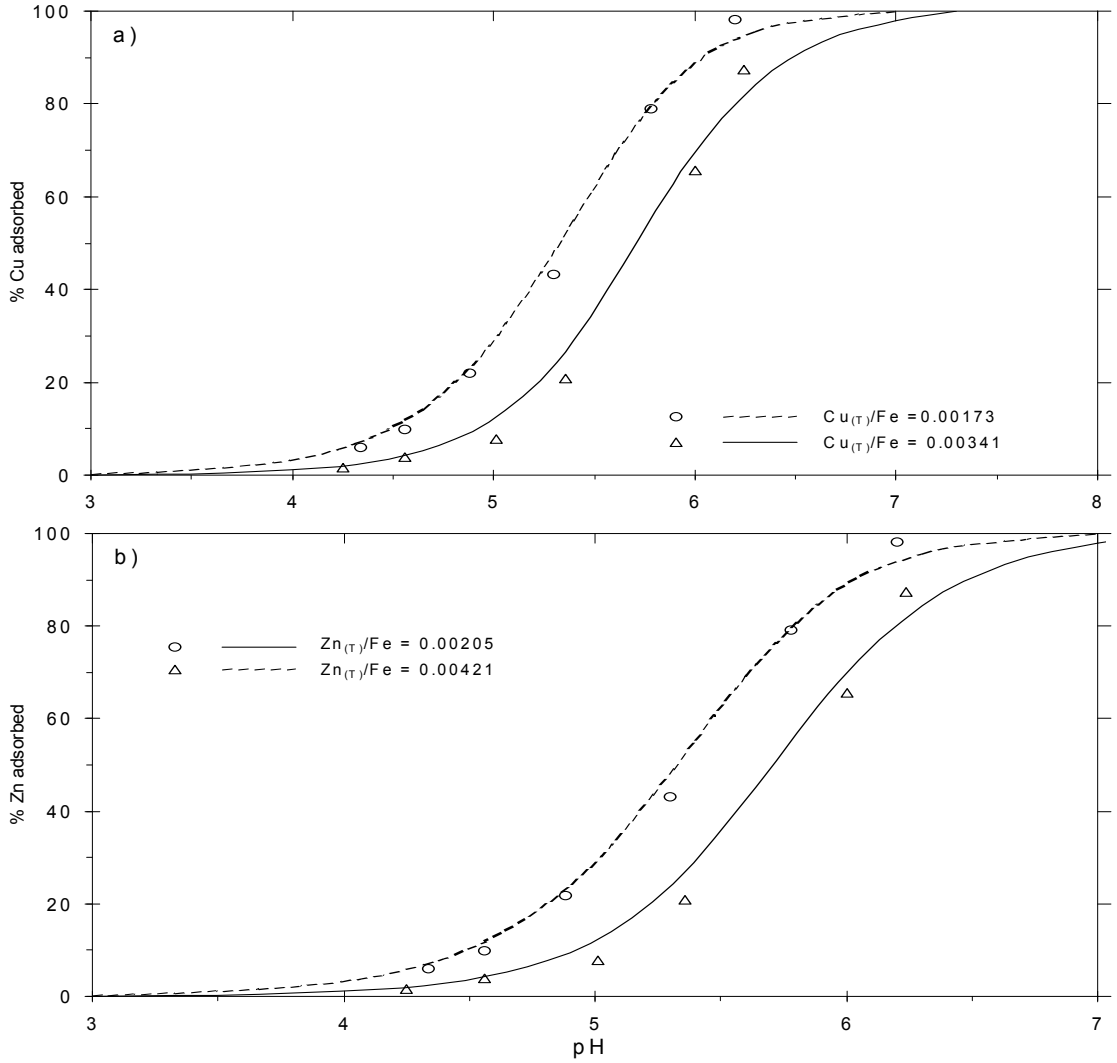

Figure 3.7. Experimental adsorption of Cu and Zn onto schwertmannite. a) 2.53×10^{-5} mol kg^{-1} $Cu_{(T)}$ and 1.46×10^{-2} mol kg^{-1} Fe (o); 1.64×10^{-5} mol kg^{-1} $Cu_{(T)}$ and 4.80×10^{-3} mol kg^{-1} Fe (Δ). b) 3.00×10^{-5} mol kg^{-1} $Zn_{(T)}$ and 1.46×10^{-2} mol kg^{-1} Fe (o), 2.02×10^{-5} mol kg^{-1} $Zn_{(T)}$ and 4.80×10^{-3} mol kg^{-1} Fe (Δ). Modelled curves are for Cu and Zn adsorption onto ferrihydrite in the presence of 0.01 mol kg^{-1} SO_4, using the adsorption constants in Table 3.1 and the weighted average $\log K_2^{TC}$ values in Tables 3.2 and 3.3.

3.3e Metal adsorption on schwertmannite

The schwertmannite adsorption of Cu and Zn for low $Me_{(T)}$/Fe systems (Figure 3.6), is essentially the same as that observed for ferrihydrite in the presence of high solution concentrations of SO_4 (eg. 0.01 mol kg^{-1}). In Figure 3.6, the experimental data for schwertmannite and the modelled adsorption for ferrihydrite in the presence of 0.01 mol kg^{-1} SO_4 are in close agreement. This similarity between Cu and Zn adsorption on schwertmannite, and adsorption on ferrihydrite with high solution SO_4, was observed for Me/Fe ratios from 0.0017 (this work) up to 0.008 (Webster et al., 1998). There might be differences in adsorption at higher Me/Fe ratios, because the measured surface area for schwertmannite in this work was considerably lower than that measured for ferrihydrite, but this has not been studied.

To further the understanding of adsorption onto schwertmannite the site densities and acidity constants would need to be measured, but attempts to determine these values by acid-base titrations were not successful due to the effect of SO_4 adsorption and desorption reactions on the acid-base balance. The results from this work do however support previous assumptions (Webster et al., 1998) that Cu and Zn adsorption on schwertmannite is affected by interaction with SO_4 on the surface, rather than SO_4 in the structure or changes in structure, of the oxide.

3.4 CONCLUSIONS

The ferrihydrite adsorption of Cu, Zn and SO_4 from single sorbate systems was accurately described using the surface area, site densities, surface acidity constants and adsorption constants determined by Dzombak and Morel (1990). However, the enhanced adsorption of Cu and Zn in the presence of SO_4 was not predicted using these parameters. By including a ternary complex with stoichiometry $\equiv Fe_{(2)}OHMeSO_4$ on the type-2 surface sites and only allowing SO_4 adsorption at the type-2 sites the effect of SO_4 on metal adsorption was accurately described for the range of Me, Fe and SO_4 concentrations studied. The value of the adsorption constants for ternary complex formation depended on the adsorption constant for the metal. The adsorption constant for Cu/SO_4 ternary complex formation on goethite (Ali and Dzombak, 1996a) also appeared to fit this relationship. Lastly Cu and Zn adsorption onto schwertmannite at low Me_T:Fe ratios was almost identical to that predicted for ferrihydrite in the presence of 0.01 M SO_4. The ternary complexes derived in this study will improve prediction of Cu and Zn adsorption onto ferrihydrite in SO_4 rich systems and onto the ochreous schwertmannite, which is so commonly precipitated in AMD systems.

CHAPTER FOUR

FERRIHYDRITE ADSORPTION OF CO, PB AND CD: TERNARY COMPLEXES WITH SO_4 AND SITE HETEROGENEITY.

Content published in Applied Geochemistry (Swedlund et al., 2003).

4.1 INTRODUCTION

The capability to model the adsorption of trace metals onto iron oxyhydroxides is an important step in predicting the transport, fate and environmental effects of trace metals in many aquatic systems. One difficulty with any adsorption model is that equilibrium constants derived from single sorbate systems may not be sufficient for modelling adsorption in more chemically complex systems. While competition for surface sites often can be accurately modelled (e.g. Swedlund and Webster, 1999; Christophi and Axe, 2000), surface interactions between different adsorbing species will only become apparent from experimental studies of systems with more than one sorbing species. For example, the experimental observation that SO_4 can enhance trace metal adsorption by the iron oxyhydroxides ferrihydrite and goethite (Swedlund and Webster, 2001; Ali and Dzombak, 1996) is not predicted by the DLM using adsorption constants derived from single sorbate systems.

Spectroscopic studies of goethite/SO_4/trace metal systems have suggested that both electrostatic effects and ternary complex formation may cause SO_4 to enhance trace metal adsorption (Elzinga et al., 2001; Ostergren et al., 2000; Collins et al., 1999). Modelling studies have been able to accurately reproduce the observed effect of SO_4 on goethite adsorption of trace metals by including ternary complexes (Ali and Dzombak, 1996; Hoins et al., 1993). Similarly for ferrihydrite, the effect of SO_4 on the adsorption of Cu and Zn was accurately predicted by including a ternary complex with stoichiometry $\equiv FeOHMeSO_4$ (Swedlund and Webster, 2001; Chapter 3). The purpose of the study described in this chapter was to determine whether the same approach could be used to model the effect of SO_4 on the ferrihydrite adsorption of Co, Pb, and Cd. The metals Pb and Cd were studied because of their environmental significance, while Co was chosen as an additional divalent metal for which Dzombak and Morel (1990) had derived adsorption constants. The 2-site model of Dzombak and Morel (1990) was unable to model Pb adsorption, even in the absence of SO_4, so this chapter also reports a re-assessment of the number of different ferrihydrite sites capable of binding Pb.

4.2 RESULTS AND DISCUSSION

4.2a Ferrihydrite-Co

Adsorption of Co in single sorbate systems was determined as a function of pH for $Co_{(T)}/Fe$ ranging from 0.00017 to 0.0161. These data are shown as adsorption edges, together with model predictions using the constants of Dzombak and Morel (1990), in Figure 4.1a. An isotherm was also measured and is shown, with modelled fit, in Figure 4.1b. Data points interpolated from the adsorption edges in Figure 4.1a have been plotted with the experimental isotherm data in Figure 4.1b. The $logK^{INT}$ values optimised from the adsorption edges and isotherm are given in Table 4.1.

The Co adsorption edges were measured with an Fe concentration of 10.1 mmol kg^{-1}. There was no significant change in the position of the adsorption edge as $Co_{(T)}/Fe$ increased from 0.000170 to 0.00170, but a definite shift to higher pH when $Co_{(T)}/Fe$ increased to 0.0161. This is consistent with the type 1 site density proposed by Dzombak and Morel (1990) which suggests that, with the same Fe concentration and $Me_{(T)}/Fe$ appreciably less than 0.005, adsorption occurs essentially only on the type 1 sites. Therefore the percent of metal adsorbed at a given pH would be independent of the $Me_{(T)}/Fe$ ratio. Conversely, as the $Me_{(T)}/Fe$ ratio approaches and exceeds 0.005, Me adsorption occurs on both the type 1 and 2 sites and the percent of metal adsorbed at a given pH will then continually decrease as the $Me_{(T)}/Fe$ ratio is increased. With a type 1 site density of 0.005, the shape of the Co isotherm, with a slope of 1.04 when $[Co_{aq}] < 10^{-5}$ mol kg^{-1} decreasing to 0.72 at higher $[Co_{aq}]$, was reasonably well modelled.

Adsorption predicted using the Dzombak and Morel (1990) adsorption constants was only slightly lower than measured, for both the isotherm and the adsorption edges. The largest differences were approximately 7 % for the edge with $Co_{(T)}/Fe = 0.0161$ (between pH 7 and 7.5) and 0.14 log unit for the isotherm at Γ_{Co} of -3.28 (where the isotherm changes slope). The values for $logK_1^{INT}$ optimised from the Co data are given in Table 4.1 and are within 0.17 log units of the Dzombak and Morel (1990) value. Note that $logK_2^{INT}$ could not be optimised from data with $Co_{(T)}/Fe << 0.005$. For this data there is a < 0.02 log unit change in the optimised value of $logK_1^{INT}$, regardless of whether $logK_2^{INT}$ is deleted or constrained to the value of Dzombak and Morel (1990). A value for $logK_2^{INT}$ was optimised from the one edge with $Co_{(T)}/Fe > 0.005$, and was 0.34 log units greater than the value from Dzombak and Morel (1990). $LogK_2^{INT}$ was also optimised from the Co isotherm, but had a large uncertainty because the highest Γ_{Co} was only 0.0025 and consequently the type 2 sites were almost insignificant in this isotherm.

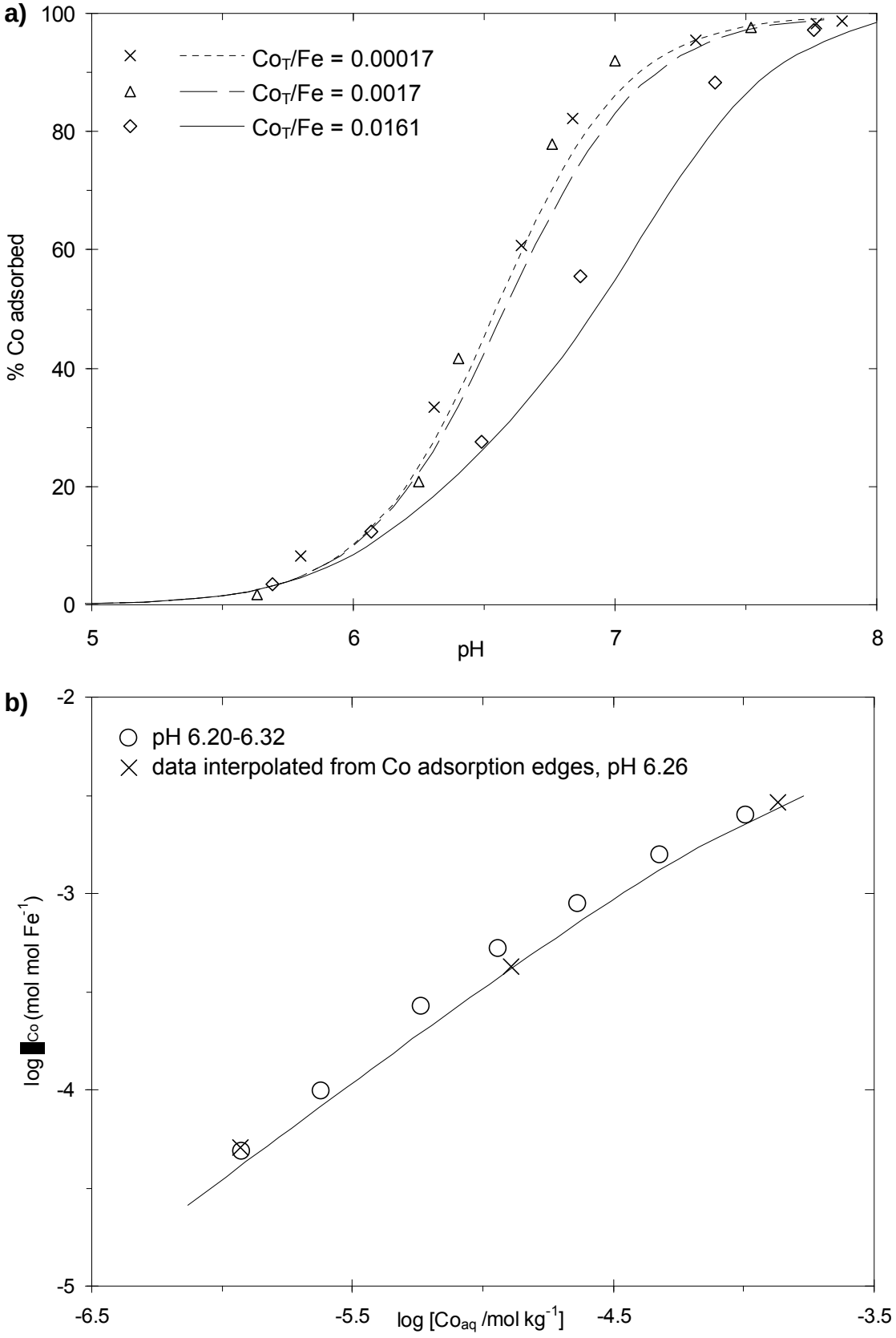

Figure 4.1. Experimental data (symbols) and modelled adsorption (lines) for Co adsorption onto ferrihydrite in single sorbate systems; a) adsorption edges b) adsorption isotherm. The concentrations of Co and Fe, and the adsorption constants from Dzombak and Morel (1990), used for the model fits, are given in Table 4.1.

Table 4.1 Intrinsic adsorption constants (with standard deviations in parentheses) optimised from experimental data for Co adsorption on ferrihydrite for single sorbate systems.

$Co_{(T)}$/Fe	$Co_{(T)}$ μmol kg^{-1}	Fe mmol kg^{-1}	$logK_1^{INT}$	$LogK_2^{INT}$	WSOS/DF
0.000170	1.72	10.1	-0.34	-3.01[a]	1.64
0.00170	17.2	10.1	-0.29	-3.01[a]	6.88
0.0161	163	10.1	-0.58 (0.14)	-2.67	0.60
Isotherm	1.67 to 127	9.83	-0.35	-3.00 (0.71)	2.61
Dzombak and Morel (1990)			-0.46	-3.01	

[a] No convergence of K_2^{INT} for this data so it was fixed at the Dzombak and Morel (1990) value for consistency between results.

In general the Co data from this work were in good agreement with the site densities and adsorption constants proposed by Dzombak and Morel (1990), whose values are therefore used in modelling the effect of SO_4 on Co adsorption (below). Ainsworth et al. (1994) measured ferrihydrite Co adsorption with $Co_{(T)}$/Fe of 0.010 and optimised a $logK_2^{INT}$ value of –1.18 from their data. This is considerably larger than the analogous value from this work or from Dzombak and Morel (1990), and the reason for this is not clear.

4.2b Ferrihydrite-Co-SO_4

The effect of SO_4 on Co adsorption is shown in Figure 4.2. In general Co adsorption increased in the presence of SO_4. A SO_4 concentration of 10.4 mmol kg^{-1} increased Co adsorption by up to 40 %, when $Co_{(T)}$/Fe = 0.000170, and by up to 30 % when $Co_{(T)}$/Fe = 0.00170. The data were modelled using the approach developed in Chapter 3 to model the effect of SO_4 on ferrihydrite adsorption of Cu. This approach assumed the formation of a neutral ternary surface complex on the type-2 sites, involving both Co and SO_4 binding to the oxide surface. The complex was assigned a stoichiometry $\equiv Fe_{(2)}OHMeSO_4$, although this does not imply any specific bonding arrangement but rather a species with that specific combination of the components, $\equiv Fe_{(2)}OH$, SO_4, Me, and a neutral charge. The logK values for ternary complex formation on the type-2 sites ($logK_2^{TC}$) optimised for each data set ranged from 6.20 to 6.49 and are given in Table 4.2. Model fits using the weighted average $logK_2^{TC}$ value from Table 4.2 are shown with the experimental data in Figure 4.2 and generally provide an accurate prediction of the effect of SO_4 on Co adsorption.

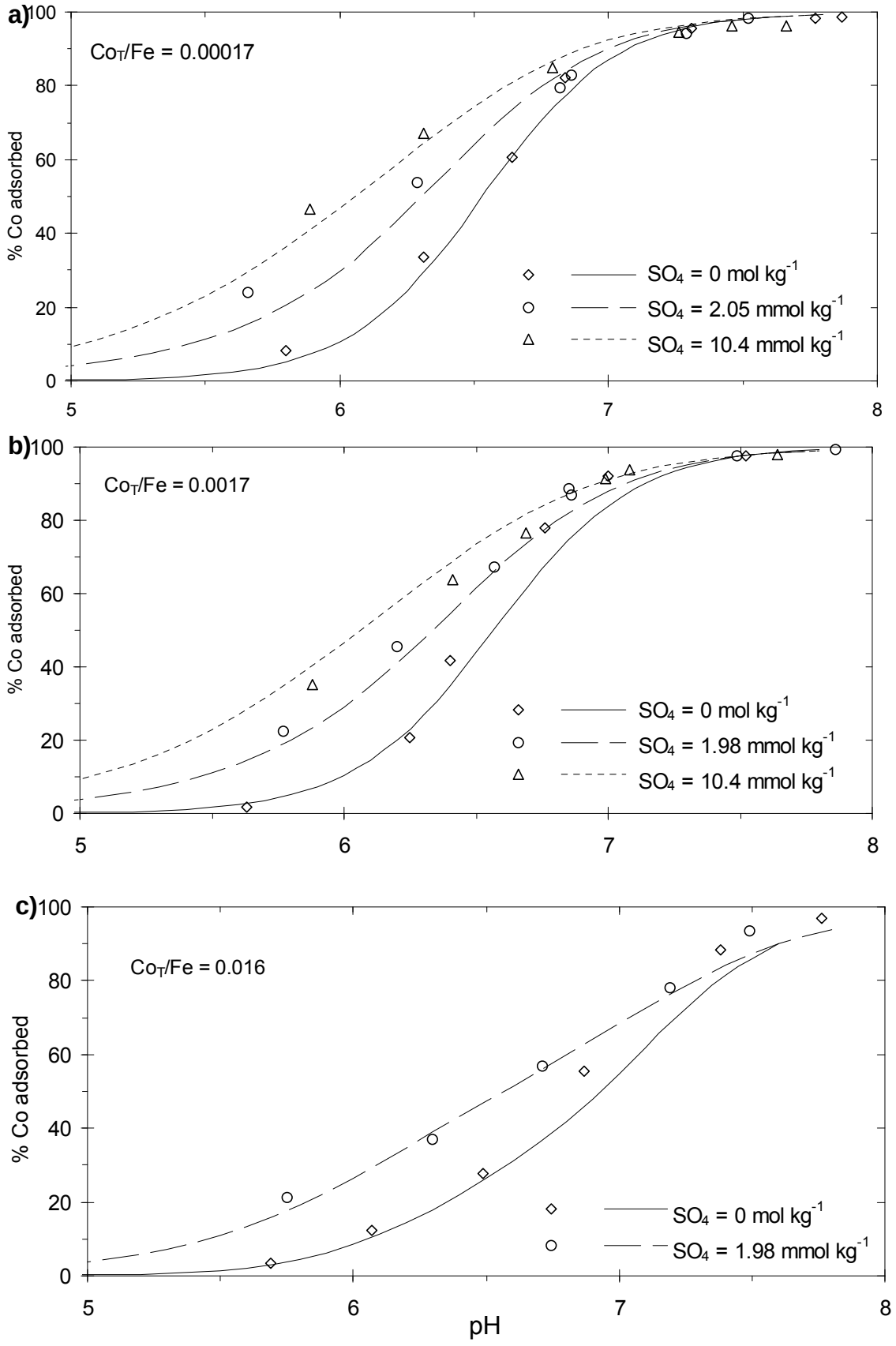

Figure 4.2. Experimental data (symbols) and modelled adsorption (lines) for Co adsorption onto ferrihydrite in the presence of SO_4, for low and high $Co_{(T)}$/Fe ratios. Modelled adsorption used the Dzombak and Morel (1990) adsorption constants in Table 4.1 together with the weighted average $\log K_2^{TC}$ shown in Table 4.2.

Table 4.2. Adsorption constants for the formation of the $\equiv Fe_2OHCoSO_4$ ternary complex (with standard deviations in parentheses) optimised from experimental data for Co adsorption on ferrihydrite in the presence of SO_4. Weighted average equilibrium constants are also shown, with the 95% uncertainty level (in italics in parentheses).

Co/Fe	$Co_{(T)}$ μmol kg^{-1}	Fe mmol kg^{-1}	$SO_{4\,(T)}$ mmol kg^{-1}	$LogK_2^{TC}$	WSOS/ DF
0.000170	1.72	10.1	2.05	6.49 (0.067)	10.30
0.000170	1.72	10.1	10.4	6.44 (0.033)	4.03
0.00170	17.2	10.1	1.98	6.54 (0.039)	4.97
0.00170	17.2	10.1	10.4	6.20 (0.029)	4.69
0.0161	163	10.1	1.98	6.27 (0.043)	12.8
		Weighted Average		**6.38** *(6.31, 6.46)*	

4.2c Ferrihydrite-Pb

At the low pH values required to study Pb adsorption, there was observed to be some finely dispersed particulate Fe passing through even a 0.1 μm membrane filter. The concentration of Fe passing through the membrane decreased as the pH was raised, from 46 μmol kg^{-1} at pH 3.1 to the detection limit of 2 μmol kg^{-1} at pH 3.9, and was independent of the total suspension Fe concentration. The significance of this effect on an individual data point depends on the degree of adsorption occurring and the proportion of total Fe passing through the filter. Because high Pb adsorption at pH < 4 only occurred with high ferrihydrite concentrations, the effect of incomplete phase separation on the results was small. Even assuming that the Γ_{Pb} was twice as large on the highly dispersed < 0.1 μm ferrihydrite than on the bulk ferrihydrite, the maximum error in % adsorption would be less than 1 %.

Adsorption edges with $Pb_{(T)}$/ Fe ranging from 0.000644 to 0.0179 and an isotherm (isotherm A) at pH 3.57-3.60 are shown in Figure 4.3. There was no difference observed in this study in Pb adsorption under N_2 or an air atmosphere, and the results in this study are from experiments under an air atmosphere. The two edges with the lowest $Pb_{(T)}$/ Fe had different Fe concentrations so their relative position can not be used to provide insight into site density or heterogeneity as was the case for Co adsorption previously. Note that the slope for the three isotherm A data points with lowest Γ_{Pb} was 1.18, which is steeper than the theoretical maximum of 1.0. This was probably due to the comparatively high uncertainty in the analysis of these low Pb concentrations. A slope of 1.01 can be achieved by a 10% change in the measured values).

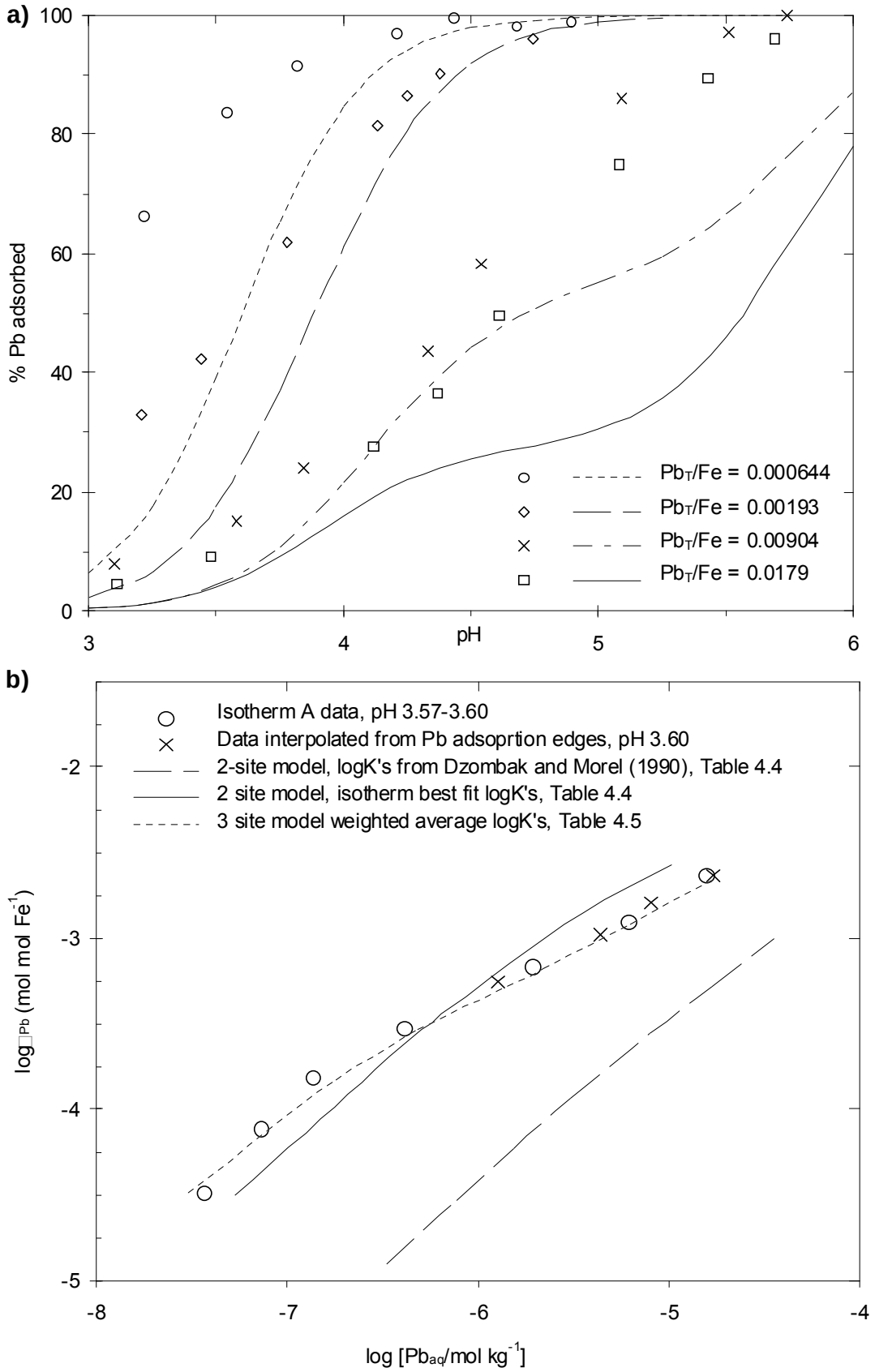

Figure 4.3. Experimental data (symbols) and modelled adsorption (lines) for Pb onto ferrihydrite in single sorbate systems a) adsorption edges b) isotherm A. The concentrations of Pb and Fe are given in Table 4.4. Model fits in Figure 4.3a used the adsorption constants from Dzombak and Morel (1990), which are given in Table 4.4.

Table 4.3. Data for Pb isotherms B and C.

Total Pb μmol kg^{-1}	Pb (aq) μmol kg^{-1}	pH	Total Pb μmol kg^{-1}	Pb (aq) μmol kg^{-1}	pH
0.584	0.0571	3.50	1.21	0.597	3.64
1.17	0.149	3.50	2.41	1.35	3.63
2.32	0.344	3.51	4.64	3.01	3.62
4.87	0.971	3.51	11.8	8.71	3.6
9.61	2.40	3.51	23.6	18.2	3.66
19.2	6.37	3.49	47.4	39.2	3.63
38.0	18.0	3.47			
Isotherm B, Fe=9.83 mmol kg^{-1}			Isotherm C, Fe=1.57 mmol kg^{-1}		

Two other isotherms (B and C) were measured and the data are presented in Table 4.3. Predicted adsorption using the constants of Dzombak and Morel (1990) is shown in Figure 4.3, and significantly underestimates the measured adsorption in all cases. The large discrepancy at high Γ_{Pb} was due to the low value of $\log K_2^{INT}$ for Pb adsorption which Dzombak and Morel (1990) interpolated from the Linear Free Energy Relationships (LFER) between $\log K_2^{INT}$ and metal hydrolysis constant. Dzombak and Morel (1990) acknowledged that this value was probably an underestimate, because the $\log K_1^{INT}$ value optimized from experimental data for Pb adsorption was an outlier, being 1.5 log units higher than the general LFER. The large discrepancy at low Γ_{Pb} was due to the value of $\log K_1^{INT}$ which Dzombak and Morel (1990) optimized from Leckie et al (1980) data with a 4 h equilibration time, which was considered acceptable for data with $Me_{(T)}/Fe < 0.005$. In the course of the present study it was noted that Pb adsorption increased from 56% to 67% between 4 h and 24 h for a $Pb_{(T)}/Fe$ of 0.001. Adsorption is generally slower at higher $Me_{(T)}/Fe$ and the data of Leckie et al (1980), with $Pb_{(T)}/Fe$ between 0.0005 and 0.005, almost certainly underestimated equilibrium adsorption. Previous studies of equilibration times have yielded mixed results. Scheinost et al. (2001) found changes in Pb solution concentration continued for 2 months while Trivedi et al. (2003) found no significant changes in Pb solution concentration after 4 hours.

The $\log K^{INT}$ values optimized from the data of this study are given in Table 4.4. Note that the WSOS/DF were large for the data sets with low Γ_{Pb}. Modelled adsorption using the weighted average $\log K^{INT}$'s from Table 4.4 is shown for the adsorption edges in Figure 4.4a, and the fits are significantly improved, especially for the 2 edges with high $Pb_{(T)}/Fe$. Model fits for the isotherm (Figure 4.3b), even with the $\log K^{INT}$'s optimized from that specific data set, and for the 2 low $Pb_{(T)}/Fe$ edges (Figure 4.4a) were less satisfactory.

Table 4.4. Two-site model intrinsic adsorption constants (with standard deviations in parentheses) optimised from experimental data for Pb adsorption on ferrihydrite for single sorbate systems. Weighted average equilibrium constants are also shown, with the 95% uncertainty level (in italics in parentheses).

$Pb_{(T)}$/Fe	$Pb_{(T)}$ $\mu mol\ kg^{-1}$	Fe $mmol\ kg^{-1}$	$logK_1^{INT}$	$LogK_2^{INT}$	WSOS/DF
Isotherm A	0.518 to 50.5	14.9	5.84 (0.018)	2.03[a]	29.1
Isotherm B	0.584 to 38.0	9.83	5.90 (0.018)	2.03[a]	18.8
Isotherm C	1.21 to 47.4	1.57	5.73 (0.031)	2.03[a]	1.67
0.000644	9.66	15.0	5.72 (0.028)	2.03[a]	20.8
0.00193	9.66	5.00	5.35 (0.031)	2.03[a]	28.3
0.00904	9.86	1.09	5.25 (0.059)	2.01	4.67
0.0179	19.7	1.10	5.49 (0.13)	2.04	2.08
Weighted Average			5.70 (*5.62,5.78*)	2.03 (*1.89,2.16*)	
Dzombak and Morel (1990)			4.65 (*4.51, 4.79*)	0.30[b]	

[a] No convergence of K_2^{INT} for this data so it was fixed at this value for consistency between results
[b] Interpolated from LFER as described in text.

Development of 3-site model

Using the two site densities of Dzombak and Morel (1990) the modelled isotherm can never have the same shape as the measured isotherm. For the measured isotherm shown in Figure 4.3b the slope changed for $\Gamma_{Pb} > 0.00016$ (i.e. $\Gamma_{Pb} > 10^{-3.8}$) whereas the model, using the $logK_1^{INT}$ optimised from the isotherm data, remains linear in this region. Note that the modelled isotherm using the weighted average $logK^{INT}$'s from Table 4.4 was parallel to but lower than the 2-site model with the isotherm best fit $logK^{INT}$'s, shown in Figure 4.3b, intersecting the measured data at log Γ_{Pb} of -3.0.

To accurately model the measured shape of the Pb isotherm the site density for the highest affinity sites would need to be lower. This is also implied by the general trend of decreasing optimised $logK_1^{INT}$ values as the $Pb_{(T)}$/Fe increased (the only exception to this trend was the edge with $Pb_{(T)}$/Fe of 0.0179 where $logK_1^{INT}$ is constrained only by the data at < 25% adsorption and has a high uncertainty). Benjamin and Leckie (1981) found that the isotherm for Pb adsorption onto ferrihydrite differed from that of Cu, Cd and Zn adsorption. The isotherms of Cd, Cu and Zn had a unit slope at low Γ ($10^{-4.5}$ to $10^{-2.3}$). In contrast, the isotherm of Pb had a slope of < 1 (≈0.6) over the range of Γ studied ($10^{-3.5}$ to $10^{-2.1}$). Therefore it is reasonable to suggest that the 2-site model and site densities proposed by Dzombak and Morel (1990) do not accurately reflect site heterogeneity for Pb adsorption.

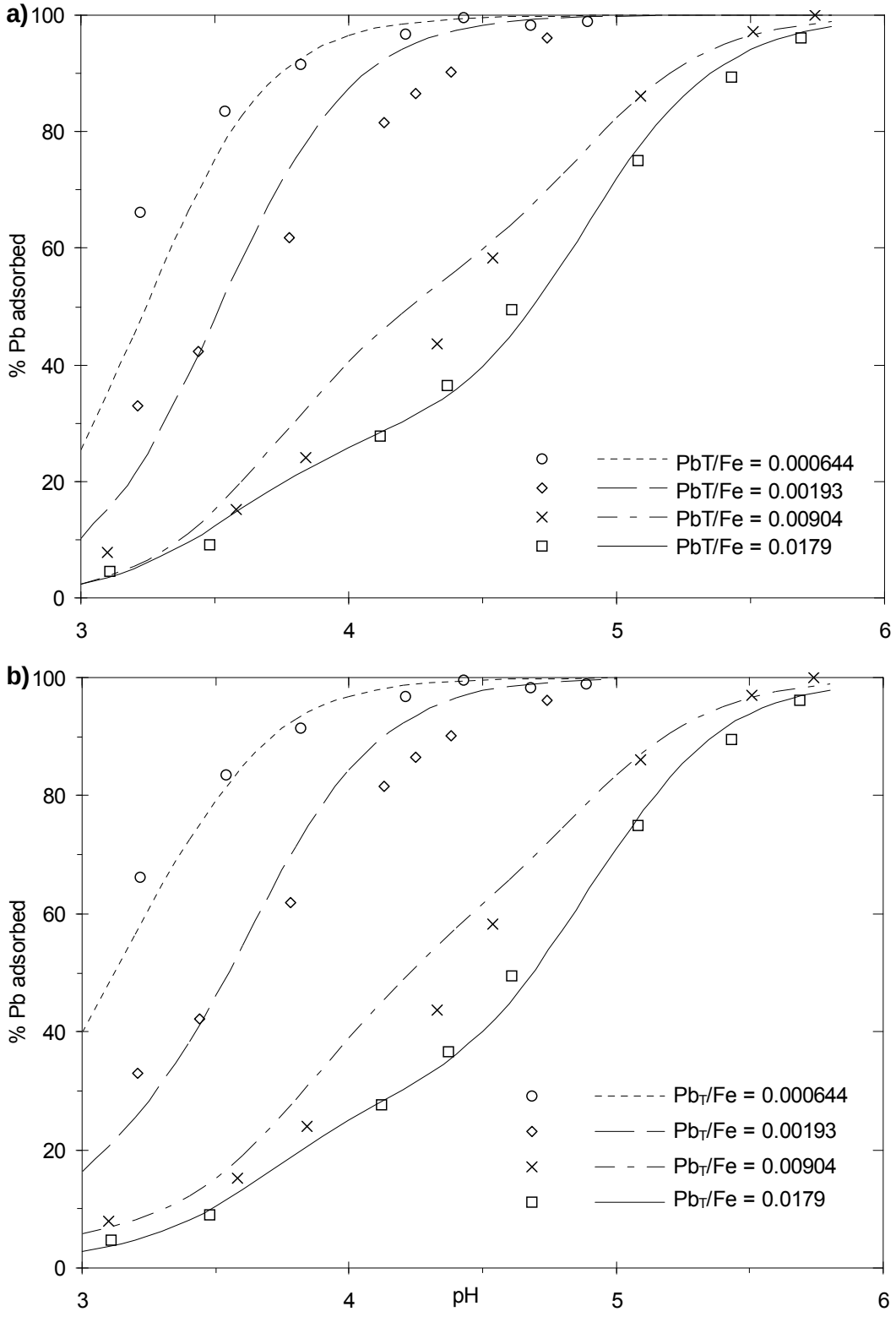

Figure 4.4. Experimental data (symbols) and modelled adsorption (lines) for Pb onto ferrihydrite in single sorbate systems a) 2-site model fit using the weighted average constants in Table 4.4, b) 3-site model fit using the weighted average $\log K^{INT}$ values in Table 4.5.

A third site, referred to here as $\equiv Fe_{(0)}OH$ or type 0 sites, was added to the model and a site density optimized from isotherms A and B. Optimization for type 0 site density values using other data sets would not converge. Because site densities and adsorption constants are intrinsically interdependent, there will tend to be large uncertainties in their optimized values if both are optimized simultaneously, as for isotherms A and B. Furthermore, the initial estimate for the site density needed to be approximately an order of magnitude lower than the site density for the type 1

sites in order to achieve convergence. However, for any initial estimate that fulfilled this criterion, the optimized value for the type 0 site density was the same regardless of the specific initial value.

Table 4.5. Three-site model intrinsic adsorption constants and Type 0 site densities (with standard deviations in parentheses) optimised from experimental data for Pb adsorption on ferrihydrite for single sorbate systems. Weighted average equilibrium constants are also shown, with the 95% uncertainty level (in italics in parentheses).

$Pb_{(T)}/Fe$	$\equiv Fe_0OH$ μmol mol Fe^{-1}	$logK_0^{INT}$	$logK_1^{INT}$	$LogK_2^{INT}$	WSOS/DF
Isotherm A	518 (130)	7.03 (0.13)[a]	5.33	1.99[b]	1.88
Isotherm B	241 (77)	7.44 (0.18)[a]	5.57	1.99[b]	0.69
Isotherm A	350[c]	7.21 (0.040)	5.40 (0.034)	1.99[b]	2.08
Isotherm B	350[c]	7.26 (0.046)	5.49 (0.036)	1.99[b]	0.73
Isotherm C	350[c]	7.00 (0.20)[d]	5.52 (0.045)	1.99[b]	1.09
0.000644	350[c]	7.20[b]	5.34 (0.038)	1.99[b]	10.6
0.00193	350[c]	7.20[b]	5.11 (0.034)	1.99[b]	11.0
0.00904	350[c]	7.20[b]	5.04 (0.070)	1.98 (0.053)	2.24
0.0179	350[c]	7.20[b]	5.32 (0.17)[d]	2.00 (0.038)	1.21
Weighted Average		**7.20** (*7.06,7.35*)	**5.33** (*5.27,5.39*)	**1.99** (*1.90,2.08*)	

[a] Initial iteration, value not included in weighted average.
[b] No convergence of this value so it was fixed to achieve consistency between results.
[c] Weighted average site density from isotherms A and B.
[d] By convention, standard deviation was set to 0.15 for the weighted average calculation.

The results for parameter optimization with a 3-site model are given in Table 4.5. The process is somewhat iterative. Initially the density of the type 0 sites was derived from isotherms A and B, then this site density was fixed to the weighted average value of 0.00035, slightly more than an order of magnitude lower than the type 1 site density of 0.005. The $logK^{INT}$'s were optimized starting with the lowest Γ_{Pb} data. None of the edge data sets converged if $logK_0^{INT}$ was simultaneously optimized, therefore the value was fixed at the weighted average of 7.20 (from the 3 isotherms). The value of $logK_2^{INT}$ only converged for the 2 edges with $Pb_{(T)}/Fe > 0.005$. Finally the value of $logK_2^{INT}$ was fixed at the weighted average (1.99) in the data sets for which it had not been constrained. This made a small difference (< 0.05 log units) in the optimized values in these data sets but ensures consistency between all the data.

Predicted adsorption using the 3 sites and the $logK^{INT}$ values from Table 4.5 is shown for the isotherm and edges in Figures 4.3b and 4.4b respectively. The isotherm fit is close, given that the discrepancy between the measured and modelled isotherm slope at low Γ_{Pb} was most likely due to analytical uncertainty as discussed previously. The modelled fit to the low $Pb_{(T)}/Fe$ edges is significantly improved. There remains a (reduced) trend of decreasing $logK_1^{INT}$ values with

increasing $Pb_{(T)}$/Fe. This might suggest further site heterogeneity, however, this is not supported by the isotherm data and the idea has not been further pursued.

In contrast to Benjamin and Leckie (1981) and the current study, Trivedi et al. (2003) measured Pb isotherms on ferrihydrite with slopes up to 0.97 even at Γ as high as 10^{-1} mol mol Fe^{-1}. Figure 4.5a shows the Trivedi et al. (2003) isotherm at pH 5.5 compared to the model predictions based on the parameters developed in this study. The data with $\Gamma > 10^{-2}$ were somewhat underestimated by the model, but at lower adsorption density the Trivedi et al. (2003) data had considerably less adsorption than that predicted from this study.

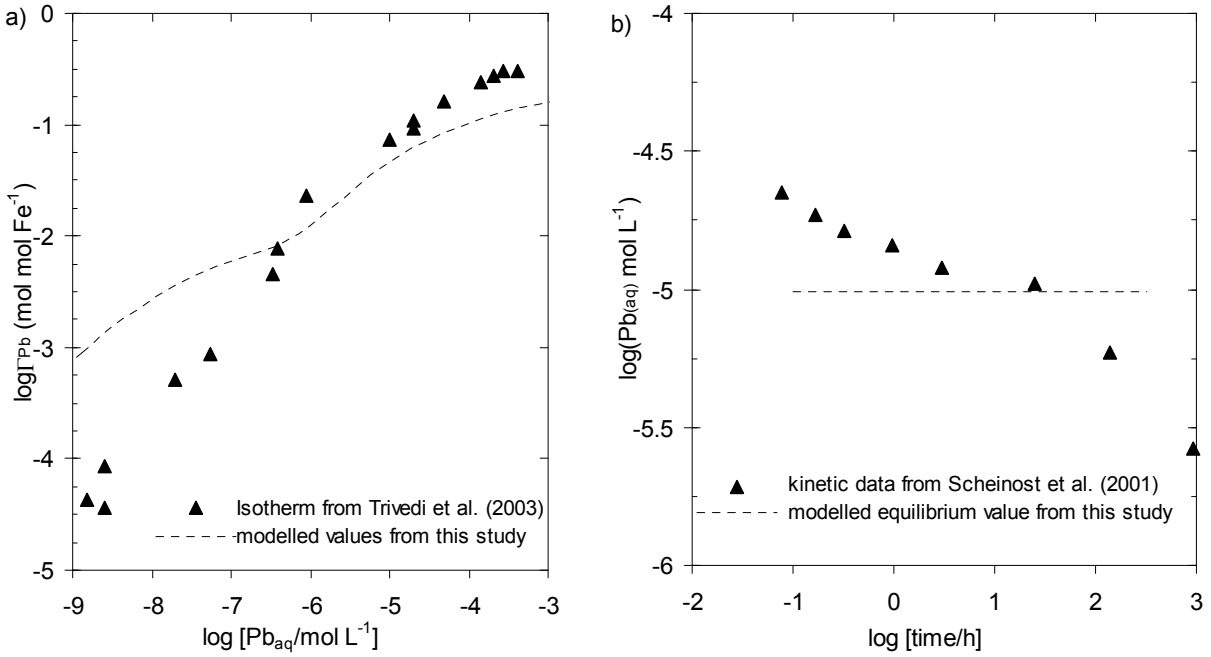

Figure 4.5 Ferrihydrite Pb adsorption compared to model results using parameters from the current study. a) isotherm at pH 5.5, 0.01 M $NaNO_3$ with 1 g L^{-1} ferrihydrite from Trivedi et al. (2003), b) kinetic data from Scheinost et al. (2001) at pH 5.0 with 5 g L^{-1} ferrihydrite, 0.1 M $NaNO_3$ and 1 mM Pb_T.

The possible reasons for the difference between the present study and Trivedi et al. (2003) are not clear. Trivedi et al. (2003) used a lower ionic strength and shorter equilibration time. Ionic strength is not expected to affect cation adsorption to a large extent (Dzombak and Morel, 1990). Trivedi et al. (2003) used an equilibration time of 4 h (as did Benjamin and Leckie (1981)) based on adsorption vs time studies showing no change in adsorption between 2 and 100 h with a Pb_T/Fe of 0.0045. In the course of the present study it was noted that Pb adsorption increased from 56% to 67% between 4 h and 24 h for a $Pb_{(T)}$/Fe of 0.0010. Scheinost et al. (2001) also observed increased Pb adsorption between 4 h and 100 h and even between 100 and 1,000 h (Figure 4.5b) with a $Pb_{(T)}$/Fe of 0.018. There is no systematic trend in these results of increasing equilibration time with increasing Pb_T/Fe. In conclusion the low slope of the isotherms in this work are consistent with Benjamin and Leckie (1981) but not with Trivedi et al. (2003). The extent of adsorption measured

in this work was consistent with Scheinost et al. (2002) after 48 h equilibration, but generally greater than that of Benjamin and Leckie (1981) and the low adsorption density data of Trivedi et al. (2003) after 4 h equilibration. The data do not reveal possible reasons for the different behaviour of Pb adsorption onto ferrihydrite. Two mechanisms could be invoked. The ferrihydrite is more dispersed at the low pH of Pb adsorption and this may present higher affinity sites not available at the higher pH of adsorption of other cations. Alternatively, there may be particularly stable surface co-ordination sites that are available to Pb on account of its ionic radius, which are not available to other cations.

4.2d Ferrihydrite-Pb-SO_4

Data for Pb adsorption in the presence of SO_4 are shown in Figures 4.6 and 4.7 for low and high $Pb_{(T)}$/Fe respectively. In all cases the solutions were well below saturation with respect to anglesite ($PbSO_4$). Using the solubility product of Allison et al. (1991), the highest anglesite saturation index (S.I.) was log S.I.=-0.74 (not allowing for removal of Pb and SO_4 by adsorption) indicating that the SO_4 or Pb concentration could increase by a factor of at least 5 before the solution would approach saturation. While this is under saturated with respect to a bulk $PbSO_4$ phase, the possibility of forming a surface precipitate needs to be kept in mind although there was no evidence for this in this study. As with other metals studied, the largest increase in Pb adsorption attributed to SO_4 was observed in the lower $Me_{(T)}$/Fe systems. This trend was less evident in the Pb adsorption data because at the lowest $Pb_{(T)}$/Fe (0.000644) adsorption of Pb was already high (66 %) even at pH 3.1 (Figure 4.6a).

The initial approach taken to modelling the effect of SO_4 on Pb adsorption was the same as that taken for the ferrihydrite-Cu-SO_4 system developed in Chapter 3 (Swedlund and Webster, 2001), i.e. a ternary complex with stoichiometry $\equiv Fe_{(2)}OHPbSO_4$ was added to the model. However, while the range of $logK_2^{TC}$ values calculated showed similar variability to those for Cu, the Pb $logK_2^{TC}$ values showed a consistent trend of decreasing $logK_2^{TC}$ with increasing $Pb_{(T)}$/Fe. Also, while the WSOS/DF for each data set was acceptable (between 2.84 to 12.5) the data were not well modelled by the weighted average $logK_2^{TC}$ value. The most significant discrepancy was for data with high $Pb_{(T)}$/Fe where the effect of SO_4 on Pb adsorption was overestimated, especially in the region of >50 % adsorption (this model not shown).

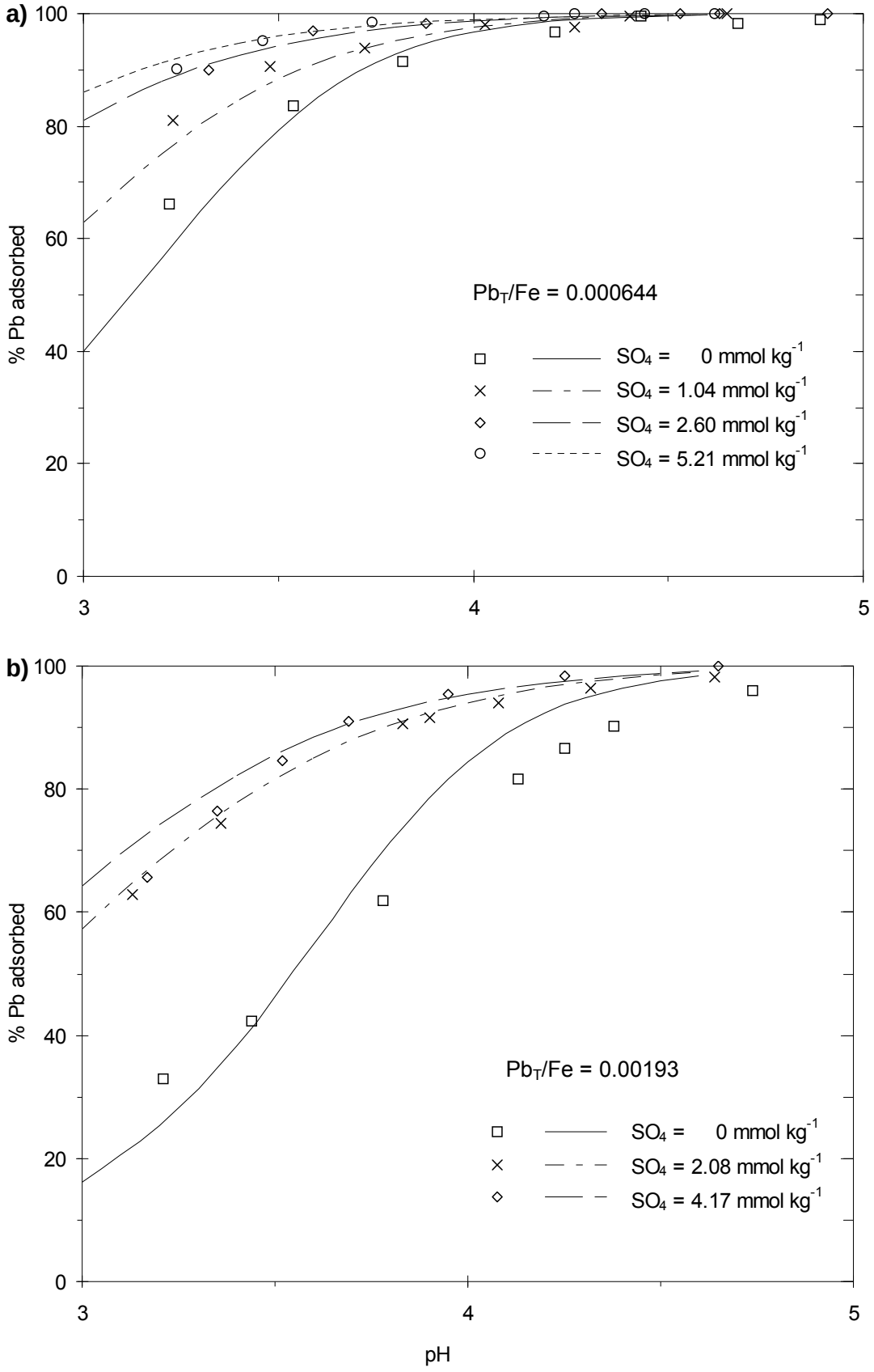

Figure 4.6. Experimental data (symbols) and modelled adsorption (lines) for Pb onto ferrihydrite in the presence of SO_4 for low $Pb_{(T)}$/Fe. Modelled curves shown use the weighted average adsorption constants in Tables 4.5 and 4.6 for a 3-site model.

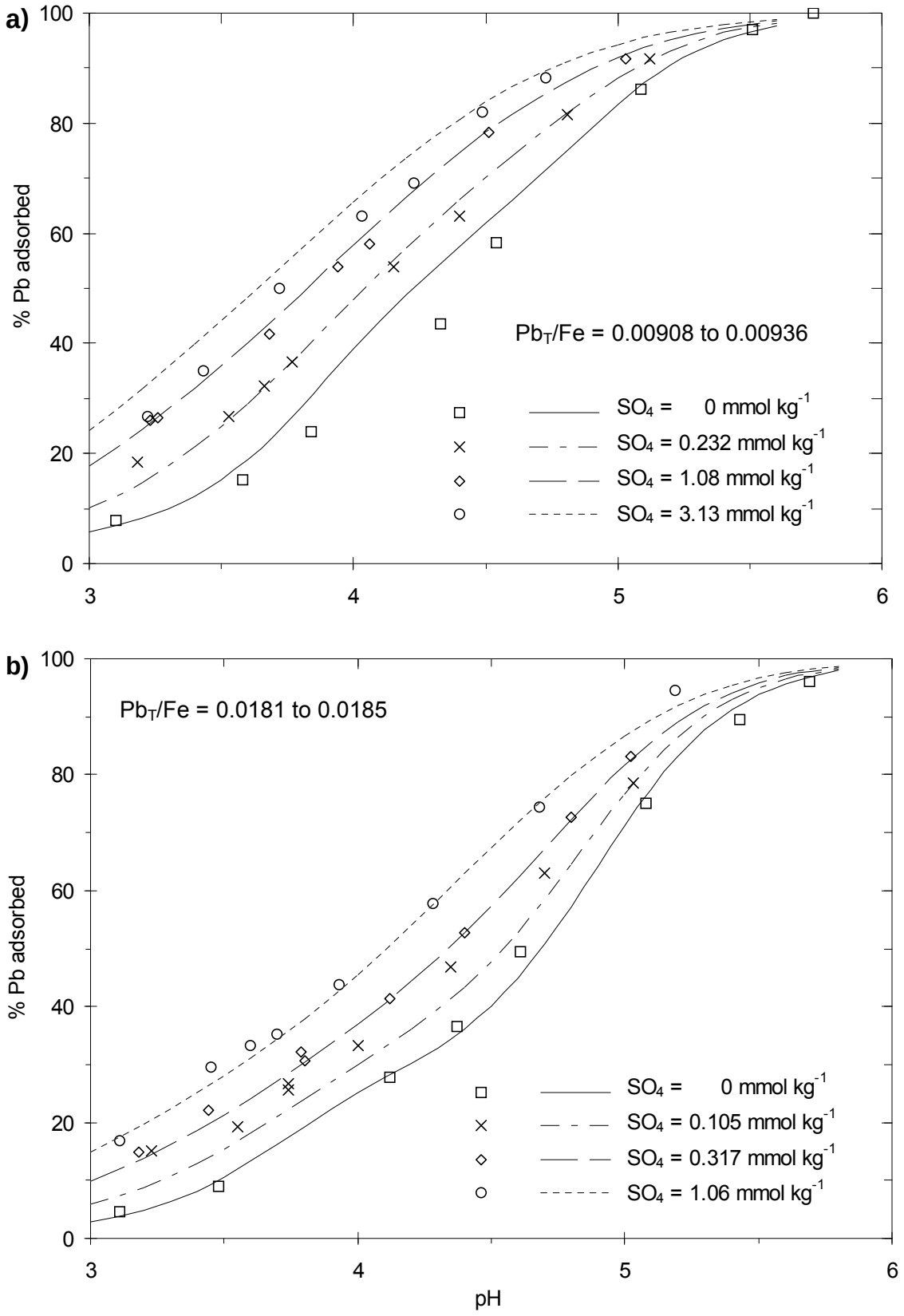

Figure 4.7. Experimental data (symbols) and modelled adsorption (lines) for Pb onto ferrihydrite in the presence of SO_4 for high $Pb_{(T)}$/Fe. Modelled curves shown use the weighted average adsorption constants in Tables 4.5 and 4.6 for a 3-site model.

For these reasons, a second ternary complex using the type 1 sites ($\equiv Fe_{(1)}OHPbSO_4$) was added to the model. The values for $logK_1^{TC}$ and $logK_2^{TC}$ optimised from the data are given in Table 4.6. The value for $logK_2^{TC}$ could not be optimised for the low $Pb_{(T)}$/Fe data, but both $logK_1^{TC}$ and $logK_2^{TC}$ were optimised simultaneously from the high $Pb_{(T)}$/Fe data. Note that, when $logK_2^{TC}$ was fixed at the weighted average (9.48), the $logK_1^{TC}$ value optimised from the low $Pb_{(T)}$/Fe data changed by less than 0.15 log units. This behaviour was quite distinct from that of the Cu-ferrihydrite-SO_4 system. In the case of Cu, it was not possible to optimize $logK_1^{TC}$ from high $Cu_{(T)}$/Fe data, and if the value for $logK_2^{TC}$ (optimized from high $Cu_{(T)}$/Fe data with $logK_1^{TC}$ fixed) was fixed at the weighted average then $logK_1^{TC}$ did not converge for low $Cu_{(T)}$/Fe data (Swedlund and Webster, 2001). In fact the $logK_1^{TC}$ was unnecessary as $logK_2^{TC}$ accounted for the effect of SO_4 on Cu adsorption.

Table 4.6. Three-site model adsorption constants (with standard deviations in parentheses) for the formation of Pb-SO_4-ferrihydrite ternary complexes on type 1 and type 2 sites. Values optimised from experimental data using the weighted average values in Table 4.5 for Pb adsorption. Weighted average equilibrium constants are also shown, with the 95% uncertainty level (in italics in parentheses).

Pb/Fe	Pb μmol kg^{-1}	Fe mmol kg^{-1}	SO_4 mmol kg^{-1}	$LogK_1^{TC}$ 3-site model	$LogK_2^{TC}$ 3-site model	WSOS/DF
0.00064	9.66	15.0	1.04	11.73 (0.056)	9.48[a]	3.61
0.00064	9.66	15.0	2.60	11.64 (0.039)	9.48[a]	8.55
0.00064	9.66	15.0	5.21	11.54 (0.035)	9.48[a]	10.2
0.00193	9.66	5.00	2.08	11.41 (0.038)	9.48[a]	1.91
0.00193	9.66	5.00	4.17	11.42 (0.035)	9.48[a]	2.21
0.00908	9.90	1.09	0.232	11.71 (0.088)	9.36 (0.081)	0.55
0.00936	10.2	1.09	1.08	11.56 (0.072)	9.44 (0.049)	0.35
0.00913	9.95	1.09	3.13	11.36 (0.074)	9.38 (0.039)	0.82
0.0185	20.4	1.10	0.105	12.03 (0.16[b])	9.69 (0.052)	0.62
0.0181	19.9	1.10	0.317	11.75 (0.15)	9.50 (0.035)	0.14
0.0185	20.3	1.10	1.06	11.71 (0.13)	9.47 (0.030)	0.40
Weighted Averages				**11.57** *(11.53,11.60)*	**9.48** (*9.43,9.52*)	

[a] No convergence of $logK_2^{TC}$ so it was fixed at this value to achieve consistency between results.
[b] By convention, standard deviation was set to 0.15 for the weighted average calculation.

Therefore the results suggest that Pb adsorption, both in the absence of SO_4 and for ternary complex formation with Pb and SO_4, requires an additional level of site heterogeneity to be considered when compared to Cu, Zn or Co adsorption. Modelled adsorption using the 3-site model with weighted

average logK values from Tables 4.5 and 4.6 is shown with the experimental data in Figures 4.6 and 4.7. The modelled fits accurately described the effect of SO_4 on Pb adsorption over the range of the data.

Note that some common geochemical speciation models (e.g. MINTEQA2) only accommodate 2 site types on a given surface. For this reason $\log K_1^{TC}$ and $\log K_2^{TC}$ were also optimized using the site densities of Dzombak and Morel (1990) and the weighted average $\log K^{INT}$'s from Table 4.4. The new values optimized from each data set followed similar trends to those optimized from the 3-site model. The new weighted average values (and 95 % confidence intervals) for $\log K_1^{TC}$ and $\log K_2^{TC}$ were 11.66 (11.62, 11.70) and 9.49 (9.44, 9.53) respectively. These values were very close to those optimized using the 3-site model (Table 4.6). Even for low $Pb_{(T)}$/Fe data, Pb adsorption in the presence of SO_4 predicted by the 2-site model was very similar to that predicted by the 3-site model. The reason for this became clear when the distribution of adsorbed Pb species predicted using the 3-site model was plotted. This is shown in Figure 4.8 for systems with $Pb_{(T)}$/Fe = 0.000644 and either 0 or 5.21 mmol kg^{-1} SO_4. At pH 3, for example, 71 % of the adsorbed Pb was present as $\equiv Fe_0OPb^+$ in the absence of SO_4, while this value decreased to 11 % in the presence of 5.21 mmol kg^{-1} SO_4. This was because 86 % of the adsorbed Pb was present as ternary complexes on the type 1 and 2 sites. Therefore, provided there is sufficient SO_4 present (e.g. ≥ 1 mmol kg^{-1}), Pb adsorption can be modelled with the 2-site model.

4.2e Ferrihydrite-Cd

Adsorption edges for $Cd_{(T)}$/Fe ranging from 0.0000921 to 0.0104, and an isotherm at pH 7.58 to 7.68 are shown in Figure 4.9. A data point interpolated from the single Cd edge with data in the pH range of the isotherm is also plotted on the isotherm. Adsorption constants derived from these data are given in Table 4.7. The cited weighted average $\log K_1^{INT}$ value (0.43) is the MINTEQA2 value (Allison et al., 1991). This is obtained from the 19 data sets of Dzombak and Morel (1990) after those involving Cd adsorption in a NaCl electrolyte had been excluded. Including the results from the present work would change this weighted average $\log K_1^{INT}$ value by less than 0.01 log units. Dzombak and Morel's (1990) value for $\log K_2^{INT}$ was derived from just one data set, with $Cd_{(T)}$/Fe > 0.005, and was therefore combined with the results from this work to give a weighted average and confidence interval (Table 4.7). The model fits shown in Figure 4.9 use the weighted average $\log K^{INT}$ values from Table 4.7.

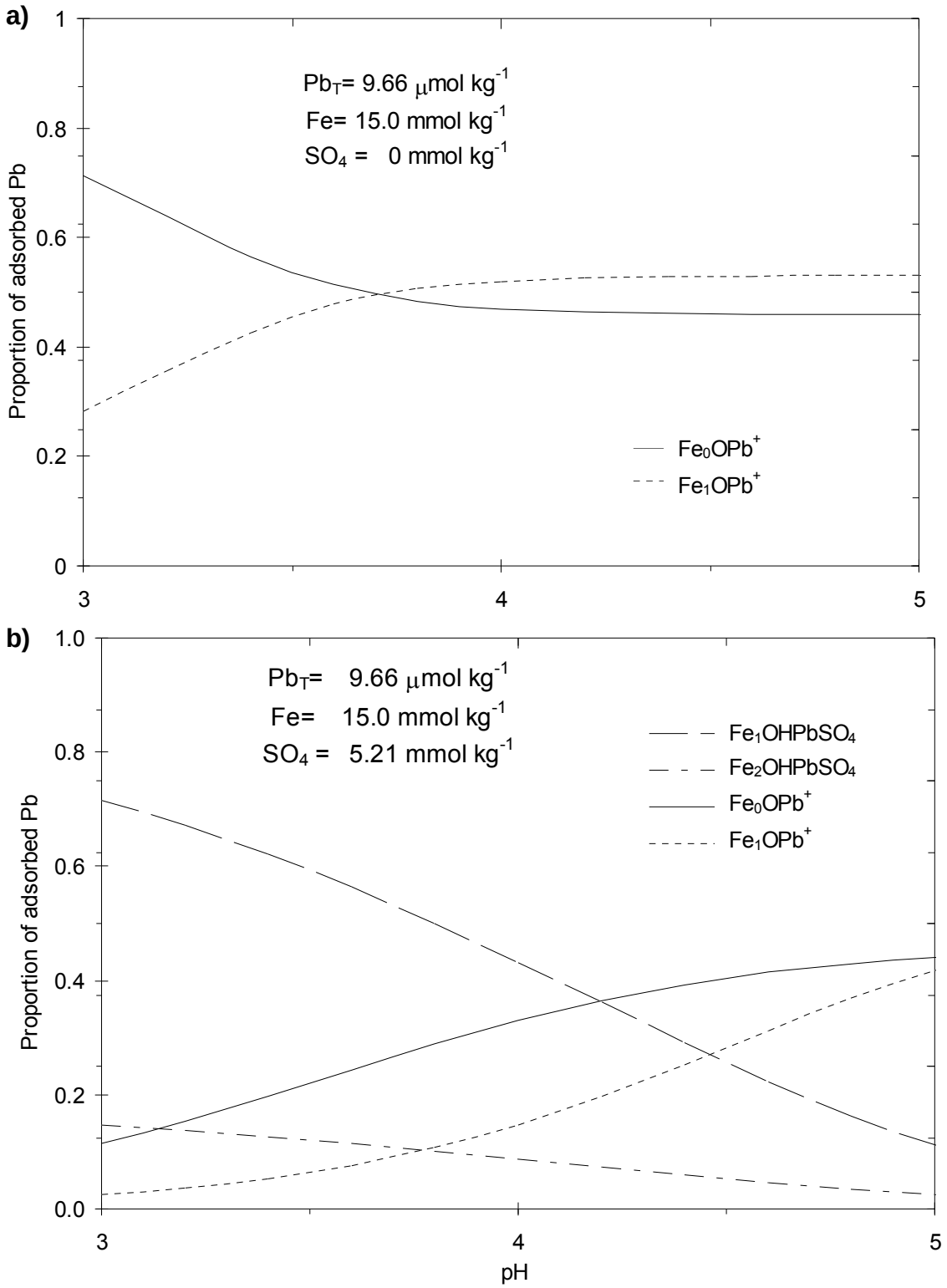

Figure 4.8 Modelled speciation of Pb adsorbed onto ferrihydrite using the weighted average adsorption constants in Tables 4.5 and 4.6 for the 3-site model, a) without SO_4 ; b) SO_4 = 5.21 mmol kg^{-1}.

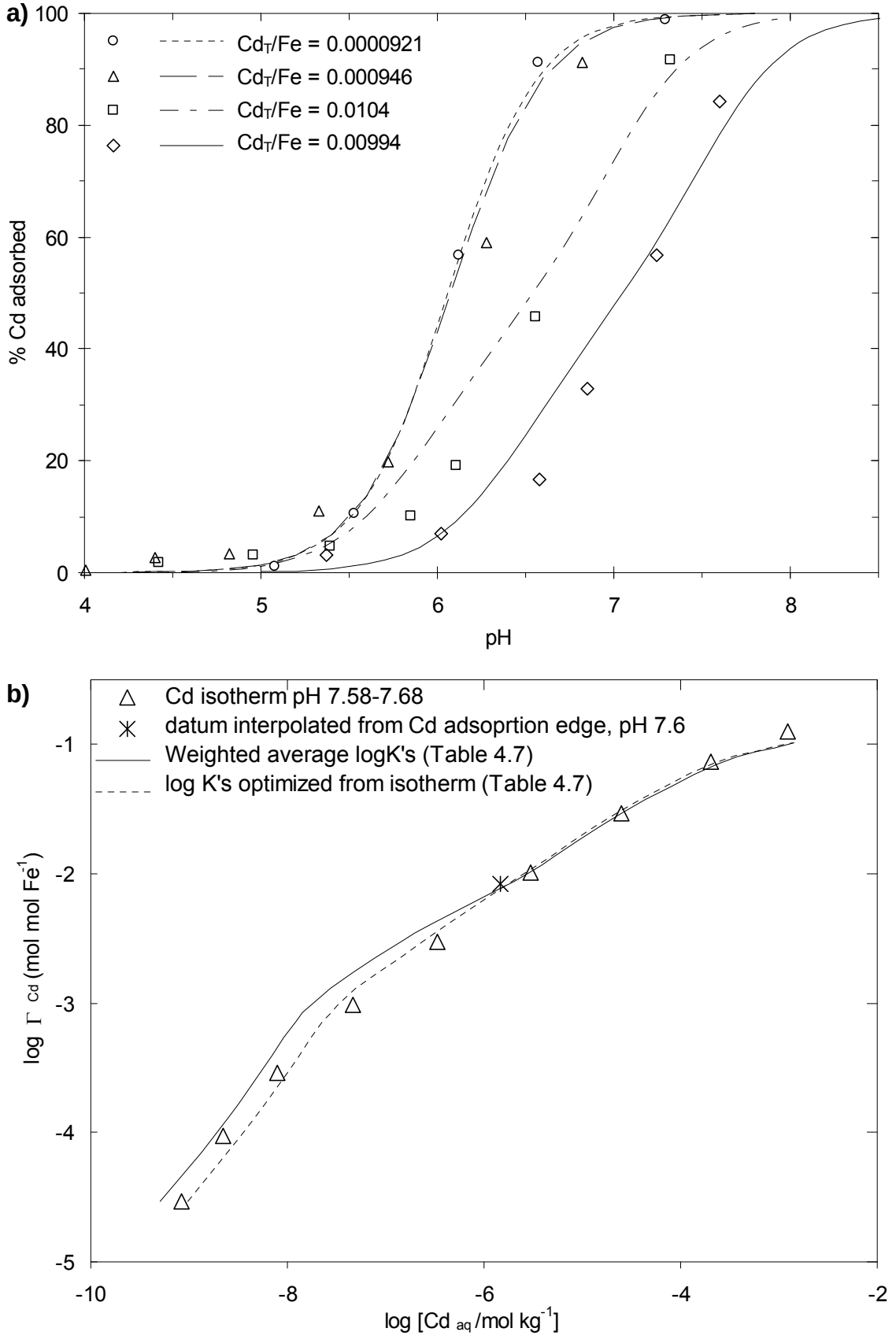

Figure 4.9. Experimental data (symbols) and modelled adsorption (lines) of Cd onto ferrihydrite in single sorbate systems a) adsorption edges, b) adsorption isotherm. The concentrations of Cd and Fe, and the weighted average adsorption constants used for the model fits, are given in Table 4.7.

Table 4.7. Two-site model intrinsic adsorption constants (with standard deviations in parentheses) optimised from experimental data for Cd adsorption on ferrihydrite for single sorbate systems.

$Cd_{(T)}$/Fe	Cd μmol kg^{-1}	Fe mmol kg^{-1}	$\log K_1^{INT}$	$\log K_2^{INT}$	WSOS*I*DF
0.0000921	0.949	10.3	0.49 (0.027)	[a]-2.69	1.68
0.000946	9.93	10.5	0.36 (0.055)	[a]-2.69	7.87
[b]0.00116	9.53	8.25	0.39 (0.031)	[a]-2.69	1.62
0.00994	9.37	0.943	-0.08 (0.026)	-2.40 (0.053)	2.23
0.0104	93.4	9.00	-0.14 (0.023)	-2.50 (0.049)	0.92
Isotherm	0.230 to 2210	7.78	0.14 (0.021)	-2.63 (0.026)	11.4
Dzombak and Morel (1990)			0.47 (*0.45, 0.50*)	-2.90 (0.042)	
Weighted average			[c]**0.43** *(0.39, 0.46)*	[d]**-2.69** *(-2.82, -2.56)*	

a No convergence of K_2^{INT} for this data so it was fixed at this value for consistency between results.
b Replicate of experiment with 10.5 mmol kg^{-1}, data not shown in Figure 4.8.
c Allison et al (1991) value used as described in text
d Weighted value from data in this work and Dzombak and Morel (1990), as described in text.

A feature of the Cd adsorption edges was that the adsorption edge for $Cd_{(T)}$/Fe of 0.00994 is at higher pH than the edge with the slightly higher $Cd_{(T)}$/Fe of 0.0104 but an Fe concentration which is ≈10 times lower (Figure 4.9a). In general, for data with the same $Me_{(T)}$/Fe, the adsorption edge will shift to higher pH as the Fe and Me concentrations decrease and can, as in this case, cause adsorption at higher pH for data with a lower $Me_{(T)}$/Fe. While this may be somewhat counter-intuitive, it is consistent with the isotherm having a positive slope. For the isotherm, at low Γ_{Cd} there was 99.6 % Cd adsorption and adsorption only fell below 90% for the 2 data points at highest Γ_{Cd}. The three data points with $\log(\Gamma_{Cd})$ below –3.53 had a slope of 1.01, while the data at higher Γ_{Cd} had a slope of 0.49 (R^2 of 0.99). Predicted adsorption using the weighted average constants from Table 4.7 slightly overestimated adsorption at low Γ_{Cd}, but converged for the high Γ_{Cd} data. Unlike the Pb isotherm, the shape of the Cd isotherm could be accurately fitted using the 2-site model with a $\log K_1^{INT}$ value of 0.14, which was optimized from the isotherm (shown in Figure 4.9b). The variability in the optimized values of $\log K_1^{INT}$ in Table 4.7 is discussed in a subsequent section.

4.2f Ferrihydrite-Cd-SO_4

The effect of SO_4 on the adsorption of Cd is shown in Figure 4.10. Cadmium adsorption was increased by up to 20 % in the presence of SO_4, which was a less significant effect than observed for Co or Pb adsorption. A ternary complex ($\equiv Fe_{(2)}OHCdSO_4$) was invoked and the $\log K_2^{TC}$ values,

which ranged from 5.96 to 6.51, are given in Table 4.8. The $logK_2^{TC}$ value of 5.96 was not included in the weighted average as discussed below. Modelled fits using the weighted average $logK^{INT}$'s from Tables 4.7 and 4.8 are shown with the experimental data in Figure 4.10. The model was close to the experimental data for $Cd_{(T)}/Fe \approx 0.000093$ (Figure 4.10a). For $Cd_{(T)}/Fe \approx 0.0009$ (Figure 4.10b), adsorption tended to be slightly underestimated when the % Cd adsorbed was < 50%, and slightly overestimated at > 50 % adsorption, both in the presence and absence of SO_4 . This deficiency occurs in the modelling of Cd in the absence of SO_4, and the effect of SO_4 appears to be accurately modelled. This also applied to modelling the data with $Cd_{(T)}/Fe \approx 0.0096$ (Figure 4.10c), however, in this case the effect of SO_4 was less significant and over estimation of Cd adsorption in the absence of SO_4 caused difficulty in the optimization of a value for $logK_2^{TC}$. The value for $logK_2^{TC}$ could not be optimized from the data for 2.20 mmol kg^{-1} SO_4, and the $logK_2^{TC}$ value for 10.9 mmol kg^{-1} SO_4 was low with high uncertainty. However, when the values for $logK_1^{INT}$ and $logK_2^{INT}$ were set at –0.08 and –2.40 (from Table 4.7), the optimised values for the $logK_2^{TC}$ were 6.60 and 6.42 for the data with 2.20 and 10.9 mmol kg^{-1} SO_4 respectively. These values are consistent with the $logK_2^{INT}$ values from the data sets with lower Cd_T/Fe showing that the non-convergence and low $logK_2^{INT}$ value were a result of deficiencies in modelling Cd adsorption in the absence of SO_4. Notwithstanding these problems, the effect of SO_4 on Cd adsorption was reasonably well predicted using the weighted average $logK_2^{TC}$ value from Table 4.8.

Site heterogeneity for Cd adsorption

While the Cd isotherm could be fitted using the 2-site model of Dzombak and Morel (1990), there was some evidence that this model may not accurately reflect site heterogeneity for Cd adsorption. For example, there was a measurable decrease in the percent of Cd adsorbed when the $Cd_{(T)}/Fe$ increased from 0.0000921 to 0.000946, with a constant Fe concentration of 10.3 (± 0.1) mmol kg^{-1}. This decrease exceeded the small modelled decrease in % adsorption and could suggest that site heterogeneity is important even at this low $Cd_{(T)}/Fe$. There was also a consistent trend in the optimised values for $logK_1^{INT}$, which decreased as the $Cd_{(T)}/Fe$ increased, which is another indicator of more complex heterogeneity. While the $logK_1^{INT}$ values optimised from the data with low $Cd_{(T)}/Fe$ were within 0.11 log units of the Dzombak and Morel (1990) value, the $logK_1^{INT}$ values optimised from the data at high $Cd_{(T)}/Fe$ were lower. Therefore the addition of a third site to the Cd model was investigated.

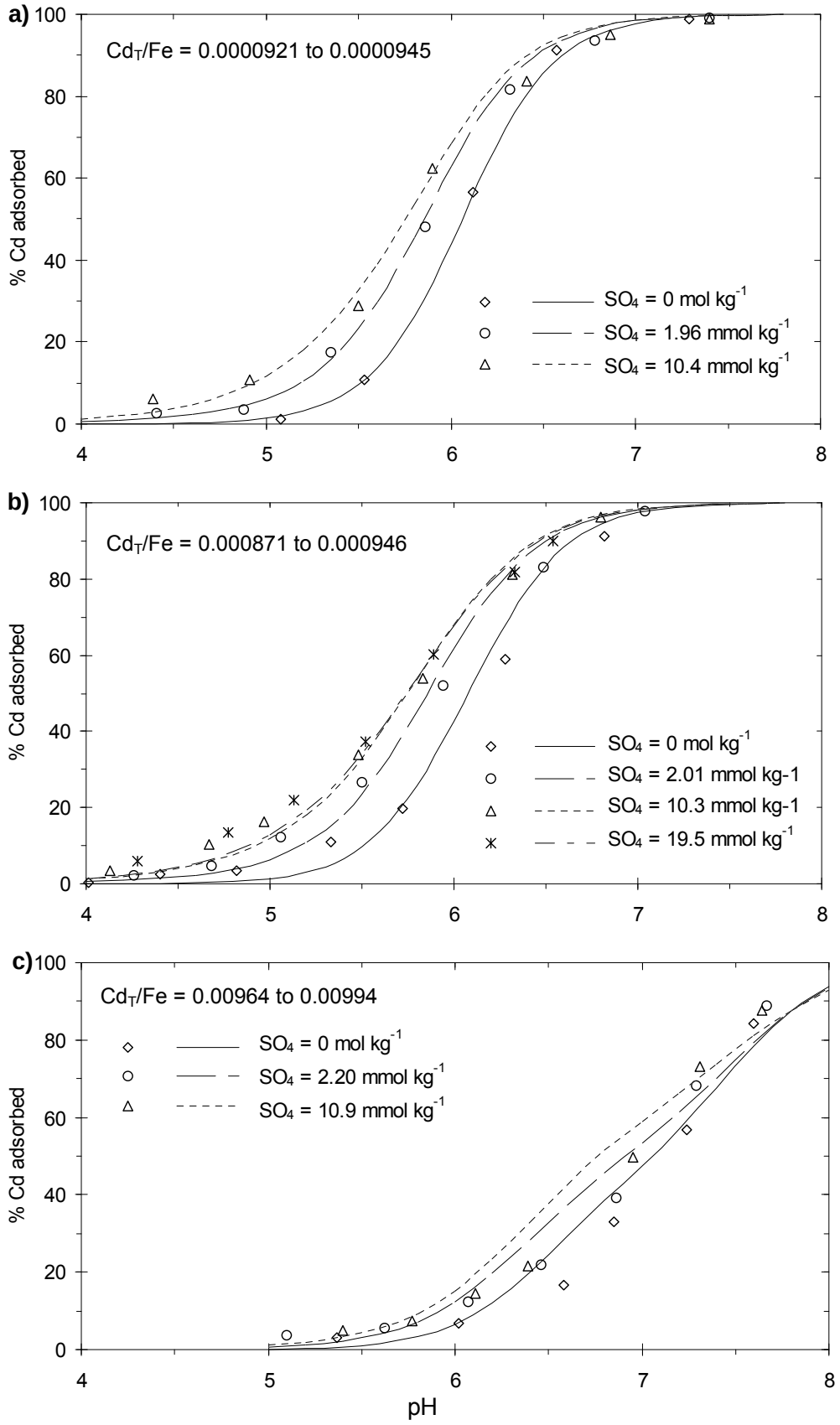

Figure 4.10. Experimental data (symbols) and modelled adsorption (lines) of Cd onto ferrihydrite in the presence of SO_4, for low and high $Cd_{(T)}$/Fe. The concentrations of Cd and Fe, and the weighted average adsorption constants used for the model fits, are given in Tables 4.7 and 4.8.

Table 4.8. Two-site model adsorption constants (with standard deviations in parentheses) for the formation of ≡FeOHCdSO_4 ternary complex on type 2 sites. Values have been optimised from experimental data using the weighted average values in Table 4.7 for Cd adsorption. Weighted average equilibrium constants are also shown, with the 95% uncertainty level (in italics in parentheses).

Cd/Fe	$Cd_{(T)}$ μmol kg^{-1}	Fe mmol kg^{-1}	$SO_{4\,(T)}$ mmol kg^{-1}	$LogK_2^{TC}$	WSOS/ DF
0.0000945	0.973	10.3	1.96	6.39 (0.12)	1.82
0.0000929	0.957	10.3	10.4	6.30 (0.057)	14.2
0.000921	9.67	10.5	2.01	6.51 (0.080)	18.4
0.000916	9.62	10.5	10.3	6.50 (0.036)	8.24
0.000871	9.15	10.5	19.5	6.50 (0.030)	5.45
[a]0.00115	9.53	8.25	2.06	6.50 (0.081)	14.9
[a]0.00115	9.53	8.25	10.2	6.44 (0.047)	24.2
0.00969	9.14	0.943	2.20	[b]n.c.	
0.00969	9.09	0.943	10.9	[c]5.96(0.17)	6.02
		Weighted Average		**6.46** *(6.43,6.48)*	

[a] Replicate of experiment with 10 mmol kg^{-1}, data not shown in Figure 4.10
[b] No convergence of $logK_2^{TC}$, as described in text.
[c] This value was not included in the weighted average as described in text

Table 4.9. Adsorption constants (with standard deviations in parentheses) optimised from experimental data for a 3-site model for Cd adsorption on ferrihydrite using the type 0 site density of 0.00035 mol molFe^{-1} from the Pb isotherms. Weighted average equilibrium constants are also shown, with the 95% uncertainty level (in italics in parentheses).

$Cd_{(T)}$/Fe	$logK_0^{INT}$	$logK_1^{INT}$	$logK_2^{INT}$	WSOS/DF
0.0000921	1.55(0.038)	-0.17[a]	-2.53[a]	2.44
0.000946	1.92(0.11)	-0.17(0.075)	-2.53[a]	4.32
0.00116	1.53(0.19[b])	0.08 (0.081)	-2.53[a]	0.80
0.00994	1.52[a]	-0.23 (0.10)	-2.40(0.061)	1.44
0.0104	1.52[a]	-0.30 (0.090)	-2.50 (0.055)	0.40
Isotherm	1.30(0.052)	-0.21(0.041)	-2.60 (0.024)	15.5
Weighted Average This study only	**1.52** *(1.31, 1.74)*	**-0.17** *(-0.24,-0.09)*	**-2.53** *(-2.68, -2.39)*	
[b]Weighted Average (combined)	**1.78** *(1.76, 1.81)*	**-0.16** *(-0.18,-0.14)*	[c]	

[a] No convergence of this value so it was fixed at this value to achieve consistency between results.
[b] Combined data from this study and the edges from Dzombak and Morel (1990) as described in text.
[c] No Cd adsorption edges in Dzombak and Morel (1990) with $Cd_{(T)}$/Fe > 0.005, see text.

Because the Cd isotherm could be fitted with the 2-site model, the density of a third higher affinity site could not be optimized from these data. However, if the type 0 site density optimized from the Pb isotherm was included in a model for Cd adsorption, it was possible to derive adsorption constants for a 3-site model, as shown in Table 4.9. The second weighted average value given in Table 4.9 is for a combination of the data from this study and from Dzombak and Morel (1990). The values for $\log K_0^{INT}$ optimized from data in this study were slightly lower than those optimized from the data from Dzombak and Morel (1990), but the respective values of $\log K_1^{INT}$ were very close. The 3-site model, with the combined weighted average $\log K^{INT}$ values accurately reproduced the data in Figure 4.9 (not shown) with the only deficiencies (resulting from the higher value of $\log K_0^{INT}$) being that the edge with lowest $Cd_{(T)}$/Fe was shifted approximately 0.1 pH unit to lower pH and adsorption was over predicted by 0.1 to 0.4 log units for the 3 data points with lowest Γ on the isotherm.

Site heterogeneity for Cd ternary complex formation remained inconclusive. Values for $\log K_1^{TC}$ and $\log K_2^{INT}$ could not be simultaneously optimized from the data with $Cd_{(T)}$/Fe > 0.005 (unlike the Pb-SO_4 data). However, the $\log K_2^{INT}$ value optimized from data with $Cd_{(T)}$/Fe > 0.005 did not render the $\log K_1^{TC}$ value redundant for the data with $Cd_{(T)}$/Fe < 0.005 as it did for the analogous Cu-SO_4 data (Swedlund and Webster, 2001). There was no significant benefit in including ternary complexes on both type 1 and 2 sites for the Cd-SO_4 data.

4.2g The relationship between single sorbate and ternary complex adsorption constants.

The results of this study are consistent with the previously identified relationship between the $\log K^{TC}$ and $\log K^{INT}$ values for Cu and Zn (Chapter 3), which is shown in Figure 4.11. The linear relationship between the $\log K^{TC}$ value for a specific cation and site and the $\log K^{INT}$ for cation adsorption covers over 8 orders of magnitude in the $\log K^{INT}$ values. The intercept of this line was $\log K^{TC} = 8.03$ and the slope of the line was 0.63. This relationship implies that, for both ferrihydrite and goethite, an estimate of ternary complex intrinsic adsorption constants for divalent metals could be made in the absence of experimental data for mixed sorbate systems.

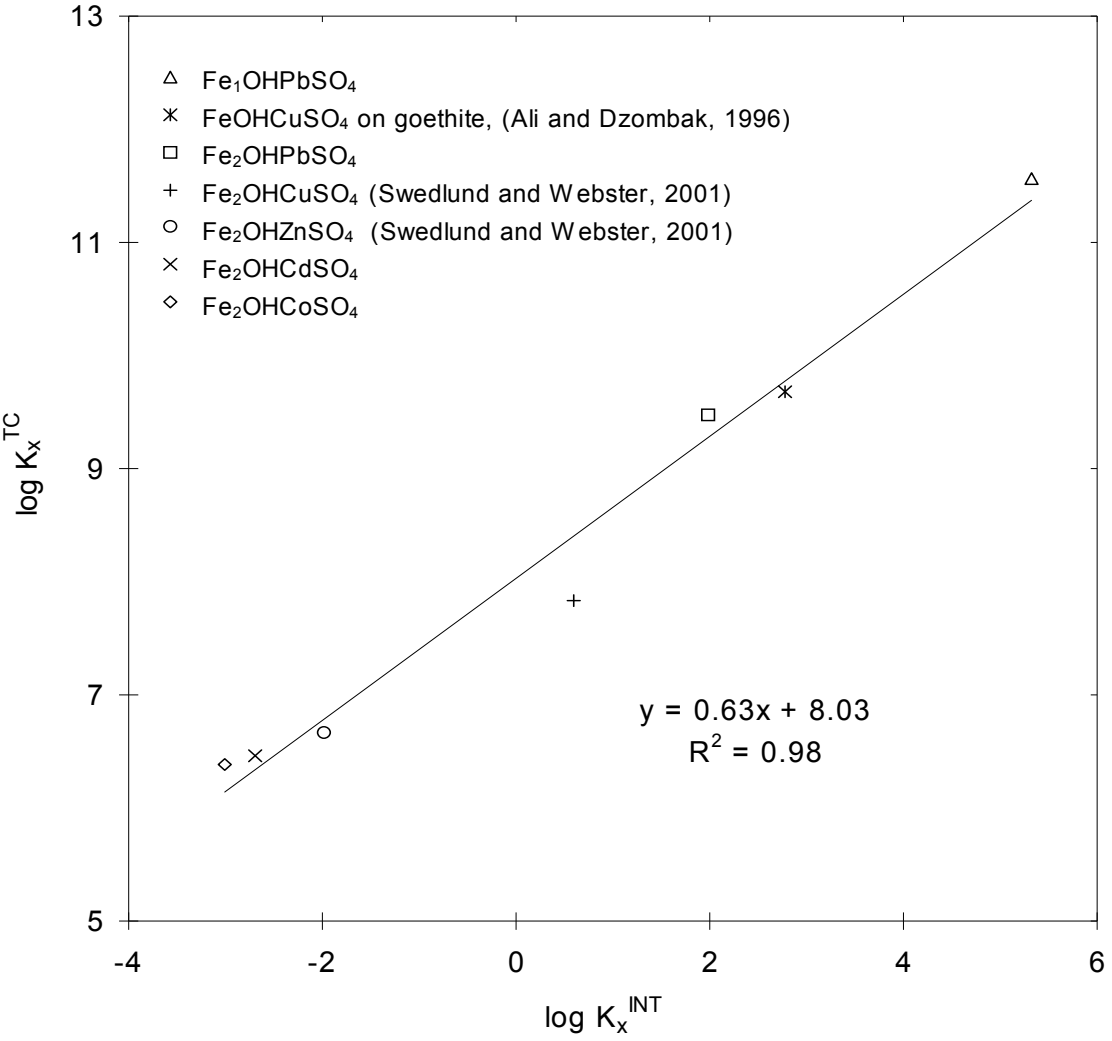

Figure 4.11. The relationship between intrinsic adsorption constants for ≡FeOHMeSO$_4$ and the logK^{INT} for metal adsorption. The data from this study were taken from Dzombak and Morel (1990), and the weighted averages from Tables 4.2, 4.5, 4.6, 4.7, and 4.8.

4.3 CONCLUSIONS

From the results in this work it can be seen that SO_4 will enhance the ferrihydrite adsorption of Co, Pb and Cd. This effect will tend to limit the mobility of metals released especially in acid mine drainage systems where Fe and SO_4 concentrations are typically high. The degree to which SO_4 enhances cation adsorption will depend on the cation, the pH and the concentration of cation, Fe and SO_4. In the absence of SO_4, Co adsorption could be modelled using the 2-site model of Dzombak and Morel (1990) while Pb adsorption required a third higher affinity site with a site density of 0.00035 mol molFe^{-1}. Cadmium adsorption showed some indications of 3-site behaviour but model predictions were only slightly improved by including a third site. The effect of SO_4 on cation adsorption could be modelled by including a neutral ternary complex on the type 2 sites in the case of Co and Cd, and on both the type 1 and type 2 sites in the case of Pb. Predictions of cation mobility in acid mine drainage systems will be enhanced by including these reactions.

However, goethite is also a major component of AMD oxides, particularly SO_4-rich poorly-crystalline goethites which can include up to 11% SO_4. Experimental adsorption studies demonstrated that adsorption of Cu and Zn is significantly enhanced on SO_4-rich goethite, relative to schwertmannite, ferrihydrite or pure goethite (Webster et al., 1998). Even allowing for the formation of ternary Cu-SO_4-goethite complexes (Ali and Dzombak, 1996a), predictions based on experimentally determined synthetic goethite adsorption of Cu (eg. Balistrieri & Murray, 1982) can still not account for the significantly higher adsorption of Cu by natural SO_4-rich goethites. Consequently predictions of metal adsorption in AMD where the SO_4-rich goethite is a significant component of the oxide "blanket", may consistently underestimate the degree of Cu and Zn removal from solution. This has certainly occurred in attempts to model Cu and Zn behaviour downstream of the old Tui Mine tailings dam in New Zealand (Webster et al., 1998). In the proceeding chapters adsorption onto a pure goethite and a SO_4-rich goethite are studied.

CHAPTER FIVE
PURE GOETHITE ADSORPTION OF CU, CD, PB AND ZN: TERNARY COMPLEX FORMATION WITH SO_4

5.1 INTRODUCTION

Goethite is prevalent in many AMD systems. It can be formed *de novo,* for example from the *Thiobacillus ferrooxidans* oxidation of $FeSO_4$ between pH 3.3 to 3.6 (Bigham et al., 1996), or as the transformation product of the metastable phase schwertmannite (Bigham et al., 1996a). Metal adsorption onto goethite formed in AMD systems has been found to differ considerably from that of ferrihydrite (Webster et al., 1998). Therefore applying the ferrihydrite model of Dzombak and Morel (1990) to AMD systems could produce erroneous results where goethite is a significant phase. Unlike ferrihydrite, there are no generally accepted parameters for goethite which can be used to model metal adsorption. This may be in part due to the many different goethite morphologies that are possible depending on the synthetic conditions (Cornell and Schwertmann, 1996). Most goethite adsorption data pertains to an acicular morphology formed by the dissolution/reprecipitation transformation of ferrihydrite at high pH and high temperature in the absence of sorbing ions. In contrast the AMD goethite studied by Webster et al. (1998), termed SO_4-rich goethite, was composed of highly aggregated spherical particles and contained approximately 10 % SO_4.

The experiments described in this chapter were designed to develop parameters to model adsorption onto the well-characterized pure acicular goethite as precipitated at pH 12 and 60 °C. The synthesis and characterization of the pure goethite was discussed in Chapter 2. The synthetic method used produces small needles with a surface area of 80 m^2g^{-1} and was based on the method used by Ali and Dzombak (1996b). The aim is to be able to describe metal adsorption onto a well-characterized pure goethite in SO_4-rich environments, such as those found in AMD systems. In the following chapter (Chapter 6) the applicability of these parameters to a SO_4-rich goethite formed under conditions mimicking the geochemistry of AMD will be tested.

5.2 RESULTS AND DISCUSSION

5.2a Acid-Base Surface Chemistry and Site Densities

A measure of the total density of available adsorption sites (N_s) is the first model parameter required to describe adsorption reactions. A value for N_s can be determined from the model-

based extrapolation of acid-base titration data. Titration data for the goethite used in this work are shown in Figure 5.1 as surface charge σ (Cm^{-2}) versus pH where surface charge was calculated using Equation 1.

$$\sigma = \frac{F}{AS}\{C_A - C_B - [H^+] + [OH^-]\} \qquad \text{Eq. 5.1}$$

F= Faraday's constant (C mol^{-1})
A= specific surface area $m^2\,g^{-1}$
S= solid concentration g L^{-1}
C_A and C_B are the total concentrations of added H^+ or OH^-
[X] is the measured solution concentration of X

The pristine point of zero charge (PPZC) was determined to be at pH = 8.96 ± 0.05 from the intercepts of titration curves at the three ionic strengths. The titration data were modelled using the Diffuse Layer Model (DLM) and the surface acid-base reactions in Equations 5.2 and 5.3. There are three adjustable parameters; two acidity constants and the site density. Note that for minerals like goethite with a well-defined surface area it is customary to express site densities per unit of surface area, as either mol m^{-2} or sites nm^{-2}. Initially all parameters were optimized simultaneously and then the site density was fixed to the weighted average value for the three data sets, and the acidity constants were optimized for this site density. In this way the best consistent set of model parameters to describe all the titration data were obtained

$$[\equiv FeOH_2^+] = [\equiv FeOH^0][H^+]\exp(-F\Psi/RT)\,\gamma_H(K_{A1}^{INT})^{-1} \qquad \text{Eq. 5.2}$$

$$[\equiv FeO^-] = [\equiv FeOH^0][H^+]^{-1}\exp(F\Psi/RT)\,(\gamma_H)^{-1}K_{A2}^{INT} \qquad \text{Eq. 5.3}$$

The values of the three model parameters simultaneously optimized from the data are given in Table 5.1. The weighted average value of N_s was 0.94 nm^{-2}. When the site density was fixed at this value the weighted average $\log K_A^{INT}$ values were 8.17 and –9.93 and these values have been used for the model fits shown in Figure 5.1. At pH < PZC the DLM titration fits provided a reasonably accurate description of the change in surface charge with ionic strength. However, at pH > PZC there was a general underestimation of surface charge. This is a reflection of the fact that, as the pH approaches 11, the difference between (C_A-C_B) and ($[H^+]$-$[OH^-]$), from which the surface charge is calculated, becomes increasingly small compared to (C_A-C_B). Therefore the uncertainty in this data becomes considerably larger as the pH approaches 11. FITEQL3.2 weights data based on the uncertainty and this high pH data will have less influence in FITEQL3.2 than data at lower pH.

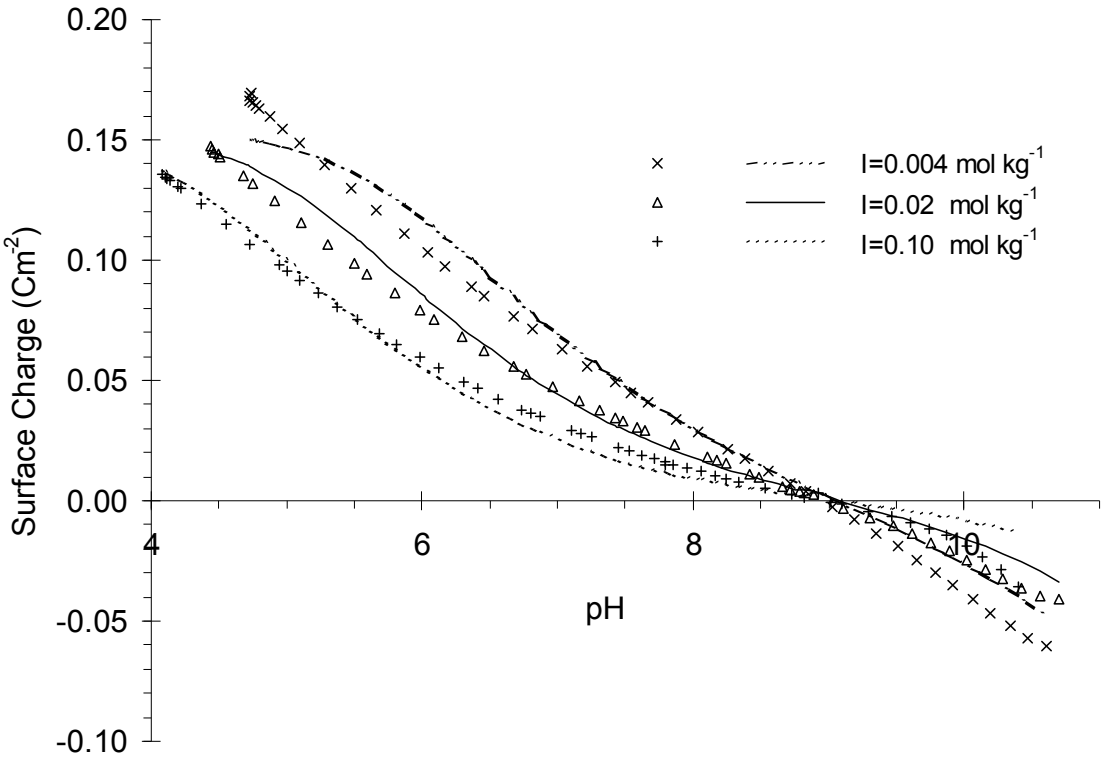

Figure 5.1 Experimental data (symbols) and modelled acid base titration data (lines) for goethite. Model parameters were the weighted average values from Table 5.1.

Table 5.1. Model fits to titration data. $\log K_A^{INT}$ values are given for I = 0 (with standard deviations in parentheses). Weighted average equilibrium constants are also shown, with the 95% uncertainty level (in italics in parentheses). (A = 80 $m^2 g^{-1}$, S = 6.2 g kg^{-1})

I (mol kg^{-1})	$\log K_{A1}^{INT}$	$\log K_{A2}^{INT}$	N_s (nm^{-2})	WSOS/DF
0.004	-8.40 (0.013)	-9.99 (0.025)	0.840(0.006)	29.0
0.020	-8.18 (0.011)	-9.87 (0.023)	0.907(0.005)	18.4
0.100	-7.95(0.097)	-9.89 (0.019)	1.044(0.005)	15.2
Weighted Average	**-8.17[a]**	**-9.93[a]**	**0.94**	
	(-8.30,-8.04)	*(-10.23, -9.64)*	*(0.79,1.09)*	

[a] weighted average $\log K_A^{INT}$ values determined with N_s fixed at 0.94 nm^{-2} as discussed in the text.

Comparison to Previous Studies

The titration data from this work with I=0.1 mol kg^{-1} are shown with results from other studies in Figure 5.2. The PPZC from this work (8.96) was comparable to the PPZC value of Robertson and Leckie (1998) of 8.9. The PPZC is significant because the average value of pK_{A1}^{INT} and pK_{A2}^{INT} will be approximately equal to the PPZC. Lower PPZC's, such as 8.0 obtained by Ali (1994), are attributed to the influence of CO_2 (Van Riemsdijk and Hiemstra, 1993). The PPZC derived in this work provides evidence that the attempts to eliminate CO_2 from the experiments were at least as successful as those of Robertson and Leckie (1998).

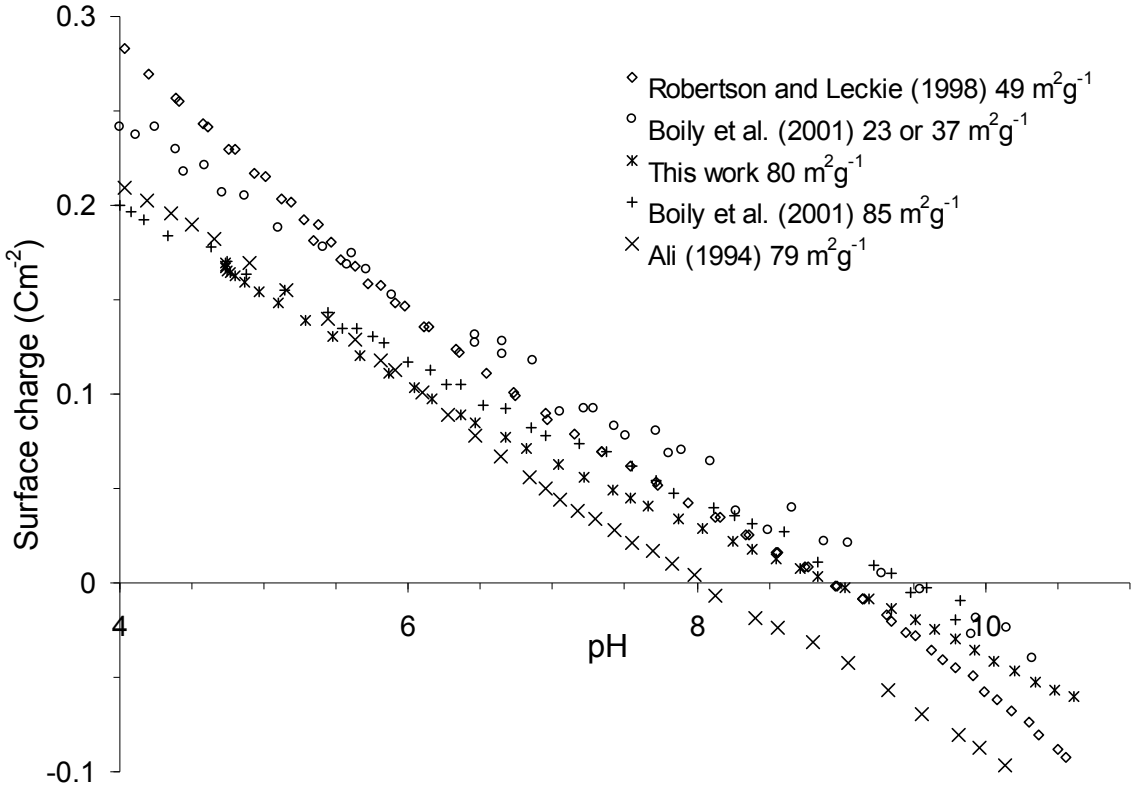

Figure 5.2 Goethite titration data at I = 0.1 mol kg^{-1}, for this study and for previous studies using goethites with surface areas as shown.

The slope of titration data will strongly influence the derived N_s, with steeper slopes corresponding to higher N_s values. The slope of the data in this work was close to that of the 85 m^2g^{-1} goethite of Boily et al. (2001) but lower than that for the low surface area goethites and the 79 m^2g^{-1} goethite of Ali (1994). The titration data of Boily et al. (2000) support an inverse relationship between N_s (expressed per unit surface area) and surface area. To model the effect of CO_3^{2-} on goethite adsorption of Pb^{2+}, CrO_4^{2-} and UO_2^{2+} Villalobos et al. (2001) used site densities of 2.3 and 10 nm^{-2} for goethites with BET surface areas of 94 and 45 m^2g^{-1} respectively, while Boily (1999) found that Cd^{II} and benzenecarboxylate adsorption, per gram of goethite, was identical on both 37 and 90 m^2g^{-1} goethites.

Table 5.2 gives some measured and theoretical N_s values. The theoretical value of 16.8 nm^{-2} was calculated from the structure of the predominant crystallographic planes (Yates, 1975), and gives site densities for singly, doubly and triply coordinated surface oxygen, $\equiv Fe_nOH$. Venema et al. (1996b) have argued that only the $\equiv FeOH$ and one third of the $\equiv Fe_3OH$ sites participate in acid-base reactions over a "normal" pH range which brings the theoretical N_s down to 6.3 nm^{-2} and closer to the larger measured values.

Table 5.2. Measured and theoretical goethite surface site densities.

N_s (nm^{-2})	Method	References
1.4	H^+/OH^- titration	Ali (1994) DLM constrained[a] fit
0.94	H^+/OH^- titration	This work, DLM
1.5, 8.4	H^+/OH^- titration	Robertson and Leckie (1998) DLM and TLM respectively
7.3	F^- adsorption	Sigg and Stumm (1981)
2.9[b]	PO_4^{3-} adsorption	Torrent et al. (1990)
16.8	Theoretical total	Yates (1975)
6.3	Theoretical reactive N_s	Venema et al. (1996a)

[a] determined by visual inspection of model fits with fixed site densities.
[b] based on 2 ≡FeOH groups per phosphate.

The variance in measured site densities is due to differences both in the methods and samples used. For example there is evidence that PO_4 adsorption involves 2 adjacent singly coordinated OH groups and the site density of Torrent et al. (1990), which was obtained for PO_4 adsorption on 31 synthetic goethites with different crystal morphologies, is consistent with the theoretical ≡FeOH site density for the dominant {110} plane. By comparison, the F^- adsorption results of Sigg and Stumm (1981) are more consistent with the total reactive site densities proposed by Venema et al. (1996b), so it would seem that F^- adsorption is not constrained to the ≡FeOH sites.

Site densities optimized from DLM fits to goethite acid-base titration data are generally the lower values. For example, the Robertson and Leckie (1998) DLM fit of titration data gave a site density of 1.4 nm^{-2}, inconsistent with their highest measured Cu adsorption density (Γ_{Cu}) of 3 nm^{-2}, while Triple Layer Model (TLM) fits to the same titration data gave a site density of 8.4 nm^{-2}. This TLM value is reasonably close to the total reactive site densities proposed by Venema et al. (1996b). The DLM considers electrolyte ions as point charges whereas the TLM implicitly accounts for a finite electrolyte ion size by including weak electrostatic complexes between electrolyte ions and charged surface sites. Therefore at high charge densities, such as those involved in extrapolating to site saturation, the DLM will have unrealistic surface potentials.

Selection of N_s and $\log K_A^{INT}$'s for pure goethite

The N_2 BET surface area of the goethite used in this study was 80 ± 1 m^2g^{-1}. The N_s value optimized from this work (0.94 nm^{-2}) was lower than that from the DLM fits of Robertson and Leckie (1998) and Ali (1994). This is to be expected given the lower slope of the titration

data. The difference between the data from this work and that of Robertson and Leckie (1998) is consistent with the inverse relationship between N_s (expressed per unit surface area) and surface area which was apparent in Boily et al. (2000). The difference between the data from this work and that of Ali (1994) may reflect the influence of CO_2 if the PPZC is lowered but the surface charge at low pH is not. It may be significant that, unlike this study and Robertson and Leckie (1998), Ali (1994) could not simultaneously optimize acidity constants and N_s values from his data. However, despite the differences in surface charge behaviour, the adsorption of Cu measured in this work, discussed in Section 5.3a, was very similar (per nm^2) to that of Robertson and Leckie (1998) and Ali (1994).

Except for the titrations, the adsorption experiments in this study were not specifically designed to assess the total site densities. However the highest measured Γ were 0.56 (Zn), 0.98 (Pb), 1.06 (SO_4), 1.06 (H^+), 1.24 (Cu) and 1.34 (Cd) nm^{-2} (Sections 5.2 a, b and c). The selection of a value for N_s should be consistent with the observed highest Γ. However, the ability of the model to fit titration data deteriorates as N_s is increased above 0.94 nm^{-2}. This is illustrated in Figure 5.3 and demonstrates that there is a compromise between an N_s value which is consistent with the higher Γ observed (e.g. the Γ_{Cu} of 3 nm^{-2} from by Robertson and Leckie (1998)), and a realistic description of the acid-base behavior of the goethite, especially in the low pH environments characteristic of AMD. There is also evidence that cation adsorption on goethite can involve two surface hydroxyl groups (e.g. Ostergren et al., 2000 and Elzinga et al., 2001). Therefore N_s values greater than the highest cation Γ could be proposed in conjunction with metal surface complex stoichiometries with two surface sites. This may be reasonable with the TLM where optimized N_s > metal Γ, but for the DLM it is clearly preferable to use a lower N_s and assume metal adsorption on one surface site.

Robertson and Leckie (1998) observed $\Gamma_{Cu} > 1.4$ nm^{-2} at high pH (pH 6.07) and with a total [Cu] > 1 mM. Therefore in terms of the application to realistic aquatic environments an N_s value ≥ 1.4 nm^{-2} would be acceptable. A value of 2.3 nm^{-2} has been used in several studies of adsorption onto goethite (Villalobos et al., 2001; Robertson and Leckie, 1998; Davis and Kent, 1990). For the above reasons a site density of 2.3 nm^{-2} was chosen for the total number of sites. Values for $\log K_A^{INT}$'s optimized from the titration data of this study with $N_s = 2.3$ nm^{-2} are given in Table 5.3. Model fits to the I=0.1 mol kg^{-1} titration data with $N_s = 2.3$ nm^{-2} are shown in Figure 5.3.

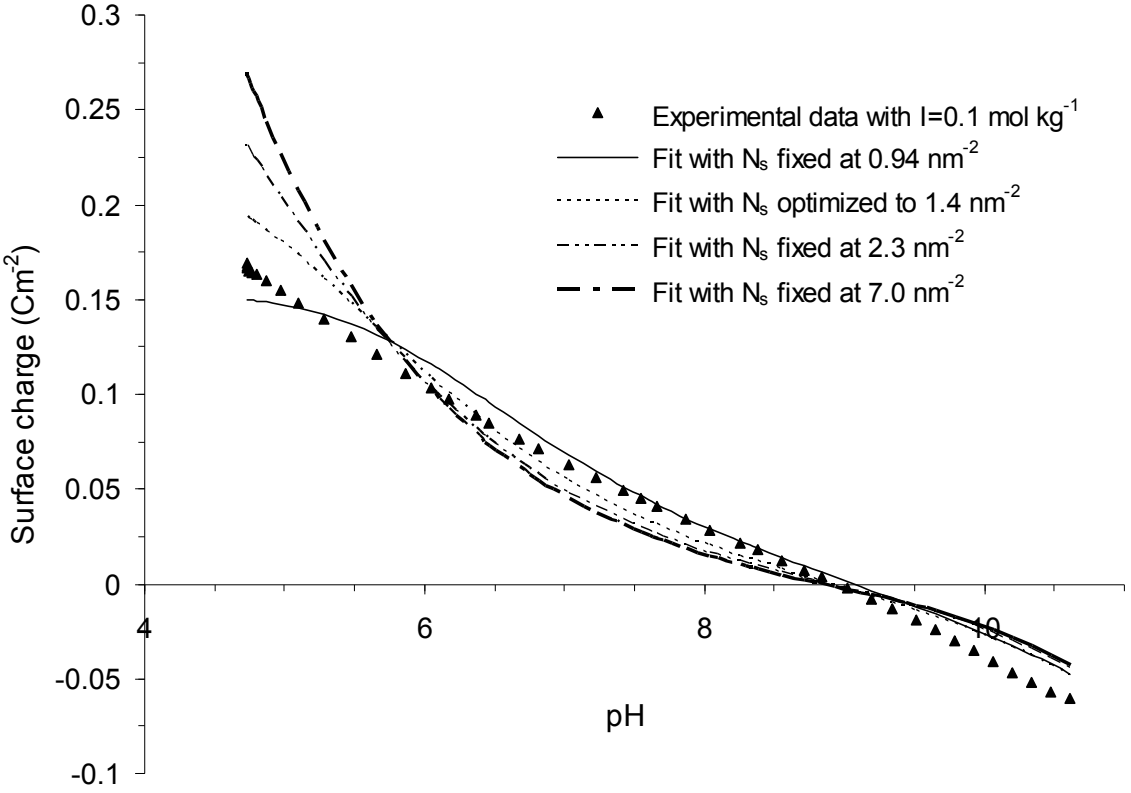

Figure 5.3 Experimental (symbols) and modelled (lines) acid base titration data for goethite at I = 0.10 mol kg^{-1}. Model parameters used varying N_s values, as shown, with weighted average $logK_{A1}^{INT}$ and $logK_{A2}^{INT}$ optimized for that N_s value.

Table 5.3 Model fits to titration data with N_s fixed to 2.3 nm^{-2}. $logK_A^{INT}$ values are given for I = 0 (with standard deviations in parentheses). Weighted average equilibrium constants are also shown, with the 95% uncertainty level (in italics in parentheses).

I (mol kg^{-1})	$logK_{A1}^{INT}$	$logK_{A2}^{INT}$	WSOS/DF
0.004	-7.60 (0.005)	-10.94 (0.026)	107.6
0.020	-7.38 (0.005)	-10.76 (0.023)	129.9
0.100	-7.16 (0.005)	-10.60 (0.017)	171.4
Weighted Average	**-7.38** *(-7.06,-7.70)*	**-10.74** *(-10.99,-10.50)*	

Site heterogeneity for metal adsorption on goethite

There is evidence that metal adsorption on goethite cannot be described with a model where all adsorption sites are equivalent (Robertson and Leckie, 1998; Venema et al., 1996b). Therefore after assigning a value for N_s (2.3 nm^{-2}) the next step for modelling metal adsorption is to determine the significance of site heterogeneity, which will be apparent from

the shape of the isotherm data. Adsorption isotherms were measured in single sorbate systems for Cu, Zn, Cd, Pb and the results are shown, with model fits as discussed below, in Figure 5.4. The isotherm data were modelled using the Diffuse Layer Model (DLM), $\log K_A^{INT}$ values from Table 5.3 and the metal adsorption reactions in Equations 5.4 and 5.5. As discussed in Chapter 2 it was assumed that the $\log K_A^{INT}$ values for both the high and low affinity sites were the same (as given in Table 5.3) and that the concentration of low affinity sites was equivalent to the total site density determined from titrations, i.e. $N_{s2}=N_s$.

$$[\equiv Fe_{(1)}OMe^{+}] = [\equiv Fe_{(1)}OH^{0}][H^{+}]^{-1}[Me^{2+}]\exp(-F\Psi/RT)(\gamma_H)^{-1}\gamma_{Me}\, K_1^{INT} \quad \text{Eq. 5.4}$$

$$[\equiv Fe_{(2)}OMe^{+}] = [\equiv Fe_{(2)}OH^{0}][H^{+}]^{-1}[Me^{2+}]\exp(-F\Psi/RT)(\gamma_H)^{-1}\gamma_{Me}\, K_2^{INT} \quad \text{Eq. 5.5}$$

There are three adjustable parameters including the two adsorption constants and the site density of the high affinity sites (N_{s1}). Initially all parameters were, where possible, optimized simultaneously and these values are given in Table 5.4. The N_{s1} values optimized from the Cu, Pb and Cd isotherms ranged between 0.0078 and 0.055 nm^{-2} with a weighted average of 0.024 nm^{-2}. In contrast the N_{s1} values optimized from the four Zn isotherms ranged between 0.083 and 0.27 nm^{-2} with a weighted average of 0.13 nm^{-2}. Table 5.4 also gives the $\log K^{INT}$ values optimized simultaneously with the N_{s1} values. This demonstrates the interdependence of the parameters in so far as lower N_s values are associated with higher $\log K_1^{INT}$ values.

Comparison to Previous Studies

Robertson and Leckie (1998) measured Cu isotherms at pH 4.07, 5.07 and 6.07 covering 6 orders of magnitude in solution Cu activity. The shape of these isotherms was not consistent with a model where all Cu adsorption sites were equivalent and required a high affinity site with a site density between 0.01 and 0.02 nm^{-2}, which implies that less than 1 % of the surface consists of these types of sites. In contrast, Ali and Dzombak (1996b) used just the one site type, with a site density of 1.4 nm^{-2} to model Cu adsorption edges in their work. Data points interpolated from the adsorption edges of Ali and Dzombak (1996b) are plotted with isotherms of this work and Robertson and Leckie (1998) in Figure 5.5. The data from this work are reasonably consistent with that of Robertson and Leckie (1998) demonstrating the necessity of a 2-site model. The data of Ali and Dzombak (1996b) are also consistent with that of Robertson and Leckie (1998), but could be modelled using only one site type because the comparatively high Cu:Fe ratios meant that the high affinity sites were not significant.

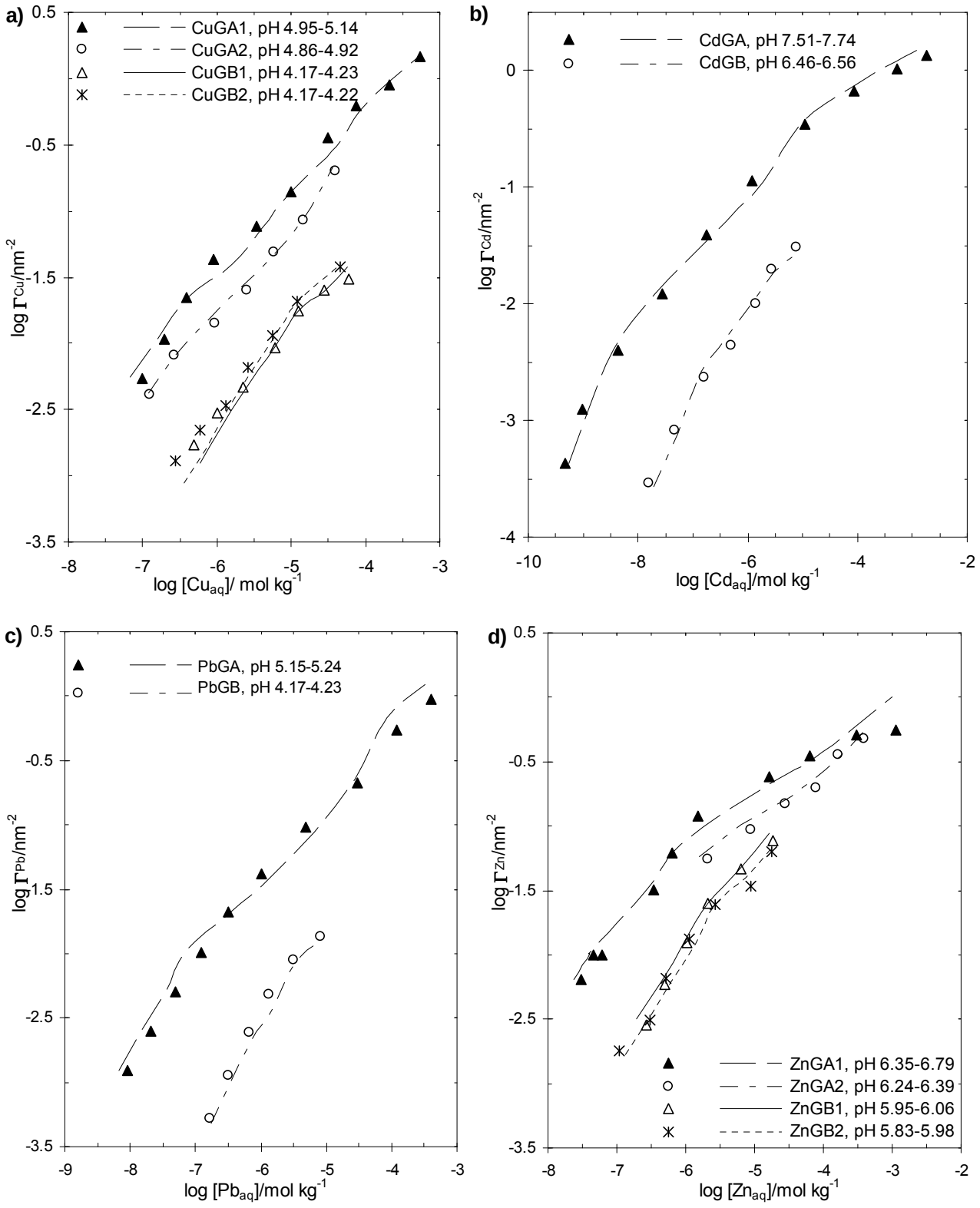

Figure 5.4 Experimental (symbols) and modelled (lines) adsorption isotherms for Cu, Cd, Pb and Zn onto goethite in single sorbate systems. Model fits used N_{s1} of 0.024 for Cu, Pb and Cd and N_{s1} of 0.13 for Zn. Concentrations for each isotherm are given in Table 5.4. Adsorption constants used are the weighted average values in Table 5.5. a) Cu, b) Cd, c) Pb and d) Zn.

Table 5.4 Optimization of the parameter N_{s1} from isotherm data in Figure 5.4 with N_{s2}= 2.3 nm^{-2}. The $logK^{INT}$ values are given for I = 0 (with standard deviations in parentheses). The weighted average N_{s1} values are also shown, with the 95% uncertainty level (in italics in parentheses).

Isotherm	$Me_{(T)}$ $\mu mol\ kg^{-1}$	α-FeOOH $g\ kg^{-1}$	$logK_1^{INT}$	$logK_2^{INT}$	N_{s1} nm^{-2}	WSOS/DF
CuGA1	1.10 to 817	1.39	3.87 (0.10)	1.75[a]	0.045 (0.007)	4.62
CuGA2	1.04 to 83.3	1.42	4.59 (0.12)	1.69 (0.037)	0.017 (0.003)	1.96
CuGB1	0.524 to 52.5	1.66	4.96 (0.11)	1.75[a]	0.013 (0.003)	1.42
CuGB2	0.874 to 65.7	1.70	5.16 (0.22)	1.95 (0.12)	0.0078 (0.0032)	0.84
CdGA	0.0793 to 204	1.38	1.17 (0.047)	-1.83 (0.026)	0.030 (0.003)	11.2
CdGB	0.785 to 14.2	1.65	1.23 (0.063)	-1.83[a]	0.026 (0.003)	6.42
PbGA	0.293 to 61.7	1.73	4.16 (0.047)	1.33 (0.033)	0.055 (0.004)	8.01
PbGB	0.282 to 11.2	1.66	4.92 (0.11)	1.33[a]	0.023 (0.005)	0.79
ZnGA1	1.64 to 126	1.89	0.89 (0.04)	-1.58 (0.11)	0.27 (0.02)	3.51
ZnGA2	16.3 to 50.2	1.91	1.33 (0.15)	-1.17 (0.066)	0.097 (0.015)	2.15
ZnGB1	0.900 to 35.7	1.66	1.27 (0.11)	-1.16 (0.26)	0.12 (0.03)	4.34
ZnGB2	0.523 to 32.3	1.74	1.58 (0.062)	-1.29[a]	0.083 (0.01)	4.32
Weighted average (Cu, Cd, Pb) *(95 % confidence interval)*					**0.024** *(0.020, 0.029)*	
Weighted average (Zn) *(95 % confidence interval)*					**0.13** *(0.05, 0.20)*	

[a] No convergence of this value so it was fixed at this value for consistency between results

There is also spectroscopic evidence supporting site heterogeneity for metal adsorption on goethite. Spadini et al. (1994) detected two different Cd-Fe distances for Cd adsorbed onto goethite and these were attributed to edge and corner linkages. The relative abundance of edge linkages decreased as the Cd surface coverage increased which implies that the edge linkages are high affinity sites. Venema et al. (1996b) have tried to rationalize these results by postulating edge linkages on the {021} face and corner linkages on the {110} face. However, there was no difference in Cd adsorption behavior for a goethite with a {021} face comprising either approximately 10 or 20 % of the surface area. The goethite with approximately 20 % surface area as {021} had shorter needles. Identical Cd adsorption behavior on the two goethites was attributed to the presence of imperfections on the {110} plane.

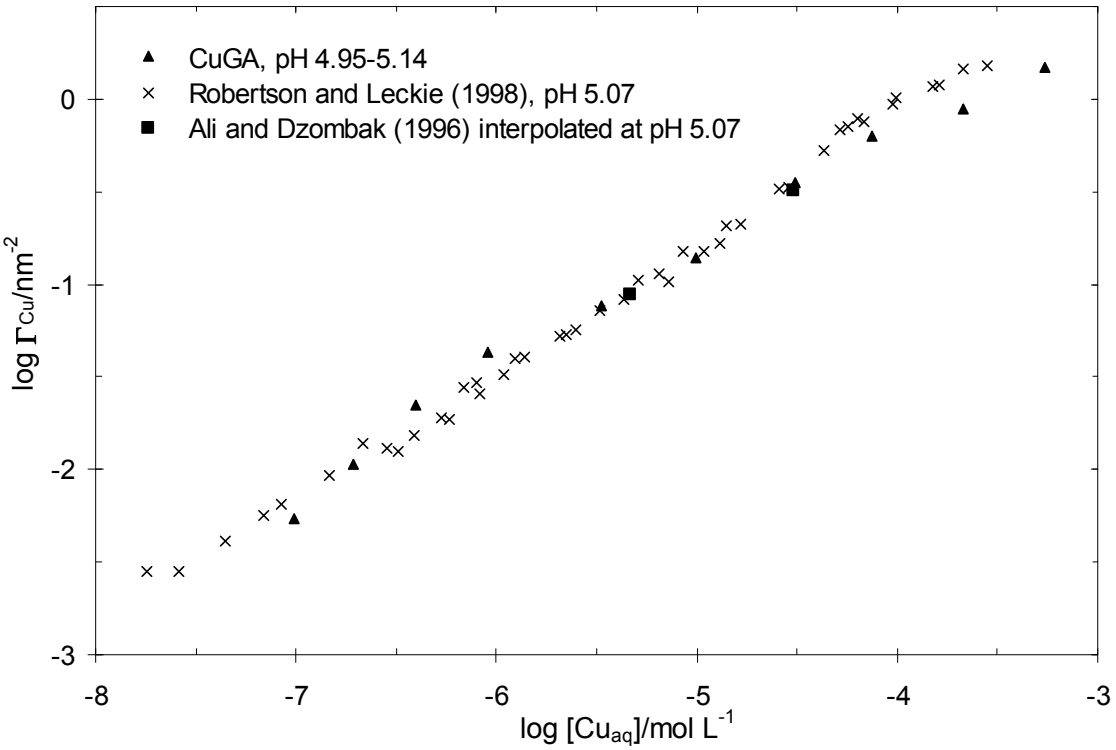

Figure 5.5 Goethite Cu isotherm data from this work compared to that of other studies.

The weighted average N_{s1} value for the Cu, Pb and Cd isotherms in this study was 0.024 nm^{-2}, which is comparable to the 0.01 to 0.02 nm^{-2} range suggested for Cu by Robertson and Leckie (1998). In contrast the weighted average N_{s1} value for Zn isotherms was 0.13 nm^{-2}. The Zn data could suggest that there were high affinity sites that were available to Zn but not Cu, Cd or Pb. This premise could be tested by experiments with pairs of metals competing for adsorption sites

Palmqvist et al. (1999) measured goethite adsorption edges with Cu-Zn and Pb-Zn metal ion combinations. The model used by Palmqvist et al. (1999) involved only one site type but five different possible stoichiometries for adsorbed metal species. The total metal ion to surface area ratios studied were 0.0033, 0.25 and 1.60 nm^{-2}, of which only the 0.25 nm^{-2} data could be expected to show the presence or absence of competition for the high affinity sites. For this data there would be just a 0.2 pH unit shift in the Zn adsorption edge between the 2 extremes of full competition (i.e. all high affinity sites available to all metals) and no competition (i.e. Zn high affinity sites only available for Zn). The authors claim that the effect of competition was well modelled using single ion adsorption data, but unfortunately data for Zn adsorption in the absence of Cu or Pb were not presented and it was not possible to see the magnitude of the effect. As a full determination of adsorption in systems with competing metals is beyond the scope of this work, for the purposes of modelling adsorption where there is only one adsorbing metal present in any experiment in this study, it has been assumed that the high affinity site densities for Cu, Cd and Pb are the same (weighted average of 0.024 nm^{-2}) while

the weighted average N_{s1} for Zn is 0.13 nm^{-2}. It is hard to speculate why the N_{s1} for Zn should be so much larger than the other cations. This discrepancy would certainly warrant further study.

5.2b Equilibrium constants for single sorbate adsorption

Metal adsorption

Having assigned values for the density of the high and low affinity adsorption sites the adsorption constants can be optimized for cation adsorption from the isotherm data in Figure 5.4 and the adsorption edge data in Figure 5.6. The values optimized from each data set are given in Table 5.5. All model fits shown in Figures 5.4 and 5.6 use the weighted average adsorption constants from Table 5.5 with low and high affinity site densities of 2.3 and 0.024 nm^{-2} for Cu, Cd and Pb and 2.3 and 0.13 nm^{-2} for Zn. The model fits are generally in good agreement with the data. Adsorption in the Zn edge with low $[Zn_T]/Fe$ was underestimated, indicating some inconsistency between the data for the isotherms and the edges. The highest Γ_{Zn} point on the isotherm ZGA1 had only 11 % adsorption therefore a high uncertainty in Γ_{Zn}. Adjusting the measured $[Zn_{aq}]$ by 5 % would bring the experimental data point up to the modelled value.

From the $\log K^{INT}$ values for the different metals it can be seen that the strength of adsorption is in the order Cu ≈Pb >>Zn>Cd. Note that while the Pb $\log K_1^{INT}$ was slightly larger than that of Cu, the reverse was true of $\log K_2^{INT}$. This may explain why some studies have found Pb adsorbing onto goethite at a slightly lower pH than Cu, while others have found the reverse (Cornell and Schwertmann, 1996). The goethite order of adsorption contrasts with that of ferrihydrite where Pb>>Cu (i.e $\log K_1^{INT}$ for Pb and Cu were 5.01 and 2.89 respectively and $\log K_2^{INT}$ for Pb and Cu were 1.77 and 0.60 respectively). The reason for the different order on the two oxyhydroxides is the anomalously high adsorption of Pb on ferrihydrite (refer Chapter 4). The $\log K_1^{INT}$ value for Pb adsorption on ferrihydrite was an approximately 1.5 log units higher than expected based on the LFER between $\log K_1^{INT}$ and the first metal hydrolysis constant (Dzombak and Morel, 1990). In addition, ferrihydrite adsorption of Pb at low Γ required a third site with even higher affinity and lower density than the $\equiv Fe_1OH$ sites. In contrast the $\log K^{INT}$ values for goethite adsorption of Pb were close to those for Cu, which is more consistent with the similarity between the Pb and Cu first hydrolysis constants ($\log K_{MOH}$) of 6.3 and 6.5 respectively (Smith and Martell, 1976).

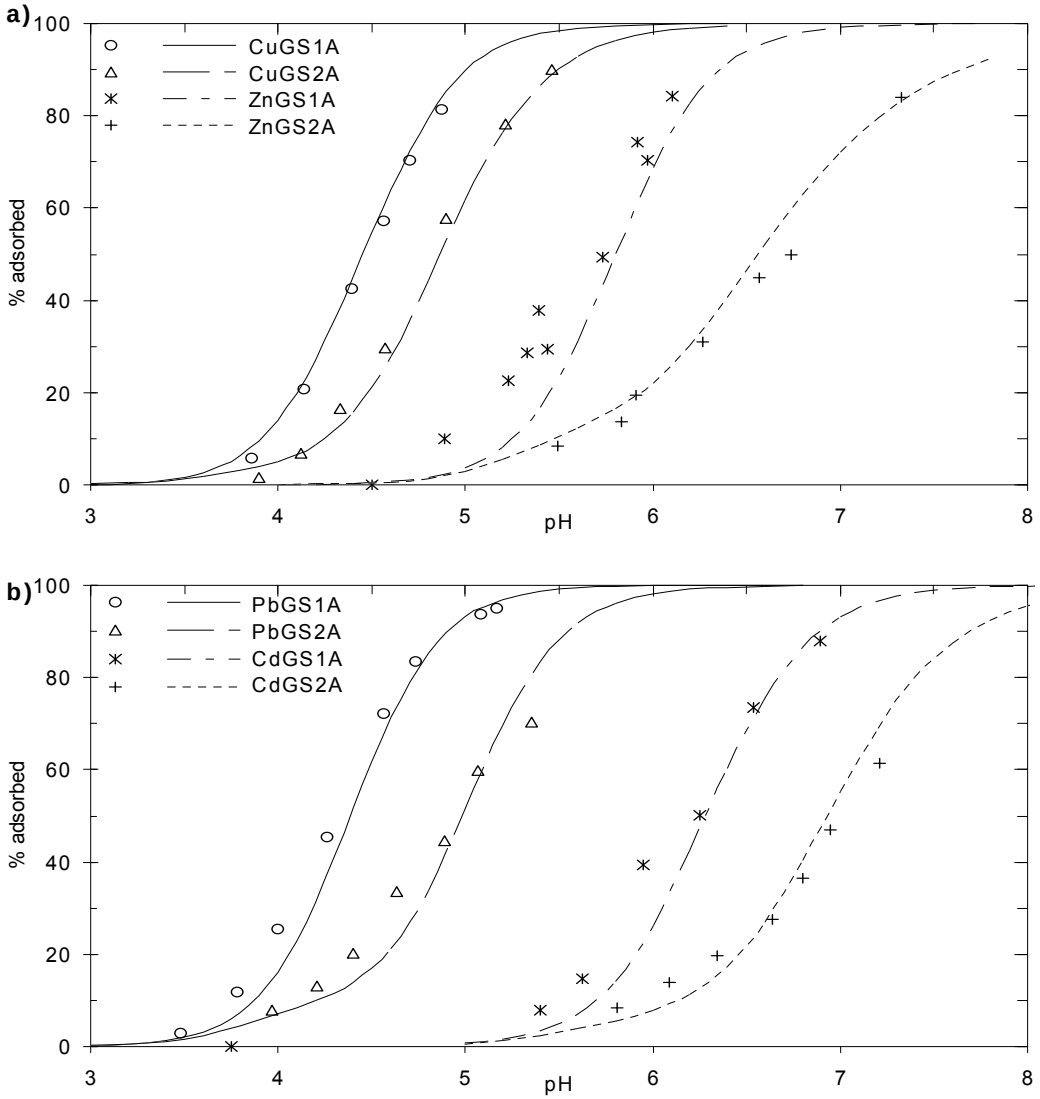

Figure 5.6 Experimental data (symbols) and modelled adsorption edges (lines) for Cu, Cd, Pb and Zn onto goethite in single sorbate systems. Model fits used N_{s1} of 0.024 for Cu, Pb and Cd and N_{s1} of 0.13 for Zn. Adsorption constants used are the weighted average values in Table 5.5.

This differential adsorption of Pb onto goethite and ferrihydrite explains one of the enigmas raised by the work of Webster et al. (1998), where Cu, Zn, Cd and Pb adsorption onto an AMD goethite was compared to that on ferrihydrite. They found that at low $[Me_T]/[Fe]$ the adsorption of Cu and Zn on the AMD goethite occurred at a significantly lower pH than onto ferrihydrite, whereas Pb adsorption was at a slightly higher pH on the AMD oxide. This is therefore explained not by anomalous behavior of the AMD goethite, but by anomalous Pb adsorption by ferrihydrite. In fact the Pb and Cu adsorption on the AMD goethite occurred at very similar pH which, from the adsorption constants for pure goethite in Table 5.5, should be expected.

Table 5.5 Optimization of $logK_1^{INT}$ and $logK_2^{NT}$ for metal adsorption for N_{s2} of 2.3 nm^{-2} and N_{s1} of 0.024 nm^{-2} (Cu, Pb and Cd) or 0.13 nm^{-2} (Zn) . Data sets given in Figures 5.4 and 5.6. The $logK^{INT}$ values are given for I = 0 (with standard deviations in parentheses). Weighted average equilibrium constants are also shown, with the 95% uncertainty level (in italics in parentheses).

Data	$Me_{(T)}$ $\mu mol\ kg^{-1}$	α-FeOOH $g\ kg^{-1}$	$logK_1^{INT}$	$LogK_2^{INT}$	WSOS DF
CuGA1	1.10 to 817	1.39	4.21 (0.048)	1.81 (0.020)	6.00
CuGA2	1.04 to 83.3	1.42	4.37 (0.038)	1.63 (0.027)	2.30
CuGB1	0.524 to 52.5	1.66	4.64 (0.039)	1.31 (0.34[b])	2.18
CuGB2	0.874 to 65.7	1.70	4.62 (0.042)	1.31 (0.29[b])	1.39
CuGS1A	3.37	1.51	4.29 (0.16[b])	1.74 (0.29[b])	0.13
CuGS1A2[c]	4.32	1.57	4.23 (0.038)	1.68[a]	2.28
CuGS2A	165	1.57	4.41[a]	1.73 (0.030)	0.36
CuGS2A2[c]	172	1.57	4.41[a]	1.63 (0.034)	0.48
Weighted average for Cu *(95 % confidence interval)*			**4.41** *(4.33, 4.50)*	**1.68** *(1.63, 1.73)*	
CdGA	0.0793 to 204	1.38	1.28 (0.022)	-1.80 (0.020)	10.12
CdGB	0.785 to 14.2	1.65	1.25 (0.032)	-1.68 (0.10)	6.10
CdGS1A	1.65	1.34	1.33 (0.027)	-1.83[a]	8.58
CdGS2A	67.4	1.44	1.29[a]	-1.93 (0.030)	1.20
Weighted average for Cd *(95 % confidence interval)*			**1.29** *(1.23, 1.34)*	**-1.83** *(-1.97, -1.69)*	
PbGA	0.293 to 61.7	1.73	4.61 (0.023)	1.52 (0.022)	14.11
PbGB	0.282 to 11.2	1.66	4.89 (0.025)	1.52[a]	0.66
PbGS1A	0.888	1.36	4.86 (0.027)	1.52[a]	0.59
PbGS2A	44.0	1.42	4.78[a]	1.51 (0.028)	6.81
Weighted average for Pb *(95 % confidence interval)*			**4.78** *(4.55, 5.08)*	**1.52** *(1.47, 1.56)*	
ZnGA1	1.64 to 126	1.89	1.21 (0.021)	-1.06 (0.030)	9.63
ZnGA2	16.3 to 50.2	1.91	1.08 (0.045)	-1.28 (0.045)	2.30
ZnGB1	0.900 to 35.7	1.66	1.22(0.025)	-1.28 (0.16[b])	3.50
ZnGB2	0.523 to 32.3	1.74	1.34 (0.018)	-1.21[a]	5.12
ZnGS1A	2.89	1.42	1.49 (0.019)	-1.21 [a]	6.40
ZnGS2A	152	1.36	1.30 [a]	-1.29 (0.026)	4.45
Weighted average for Zn *(95 % confidence interval)*			**1.30** *(1.22, 1.38)*	**-1.21** *(-1.33, -1.09)*	

[a] No convergence of this value so it was fixed at this value to ensure consistency between results
[b] By convention fixed at 0.15 for weighted average calculation
[c] Replicate experiments, data not shown in Figure 5.6

Sulfate Adsorption

A SO_4 adsorption isotherm and three adsorption edges were measured and the data are presented in Figure 5.7. The adsorption behavior of the SO_4 anion was quite distinct from that of the cations. For example, the adsorption edge covered a wide pH range and increasing the sorbate/sorbent ratio resulted in a decrease in the slope of the adsorption edge. In contrast the cation adsorption edges occurred over 1-2 pH units and increasing the sorbate/sorbent ratio resulted in an horizontal shift of the adsorption edge. This difference in behavior between cations and anions is typical of adsorption onto iron oxyhydroxides (Dzombak and Morel, 1990). Anion isotherms are often described as having a Langmuirian shape with slope of 1 at low adsorption density (Γ). However, this was not evident in this study because the isotherm pH (pH≈4.1) was low, such that the Γ was high even when the solution concentration was close to the SO_4 detection limit.

Comparison to Previous Studies

As with ferrihydrite, anion adsorption on goethite can be modelled with one site type. ATR-IR studies (Peak et al., 1999, Elzinga et al., 2001) suggest monodentate adsorption with either H bonding from an adjacent site or monodentate adsorption of a bisulfate species. In addition at pH > 6, where SO_4 adsorption densities were low, a weak ion-pair (e.g. $\equiv FeOH_2^+$---SO_4^{2-}) was the principal mode of association. While this sort of species is an integral part of the TLM it is not possible to include it in the DLM, where all charge resides on a single plane. However goethite SO_4 adsorption data can be successfully modelled with just 1 site type (Ali and Dzombak, 1996a; Geelhoed et al., 1997). Ali and Dzombak (1996a) have modelled SO_4 adsorption by goethite using three surface species, varying in degree of protonation, on one site. This is analogous to the approach of Dzombak and Morel (1990) for modelling adsorption of anions onto ferrihydrite.

Using all the surface species from Ali and Dzombak (1996a); $\equiv FeHSO_4$, $\equiv FeSO_4^-$, and $\equiv FeOSO_4^{3-}$, adsorption constants were derived from the data and are given in Table 5.6. Note that the high uncertainty in the weighted average $\log K_4^{INT}$ for the $\equiv FeOSO_4^{3-}$ species is because this species will only be significant at a Γ_{SO4} that is lower than those measured. Data points interpolated from the edges of Ali and Dzombak (1996a) are plotted on the isotherm (Figure 5.7a) and modelled adsorption using constants derived from the data of Ali and Dzombak (1996b) are plotted for one of the edges in Figure 5.7b. The degree of adsorption

shown in this work was greater than that shown by Ali and Dzombak (1996b), with the adsorption edge displaced by up to 15 %. One possible reason for this, despite the agreement noted for Cu adsorption, could be the presence of CO_2 which was evident from Ali and Dzombak's (1996b) lower PPZC (at pH 8.0). Villalobos et al. (2001) demonstrated that CO_2 inhibited anion adsorption (specifically CrO_4^{2-}) on goethite, but not that of cations (specifically Pb^{2+}).

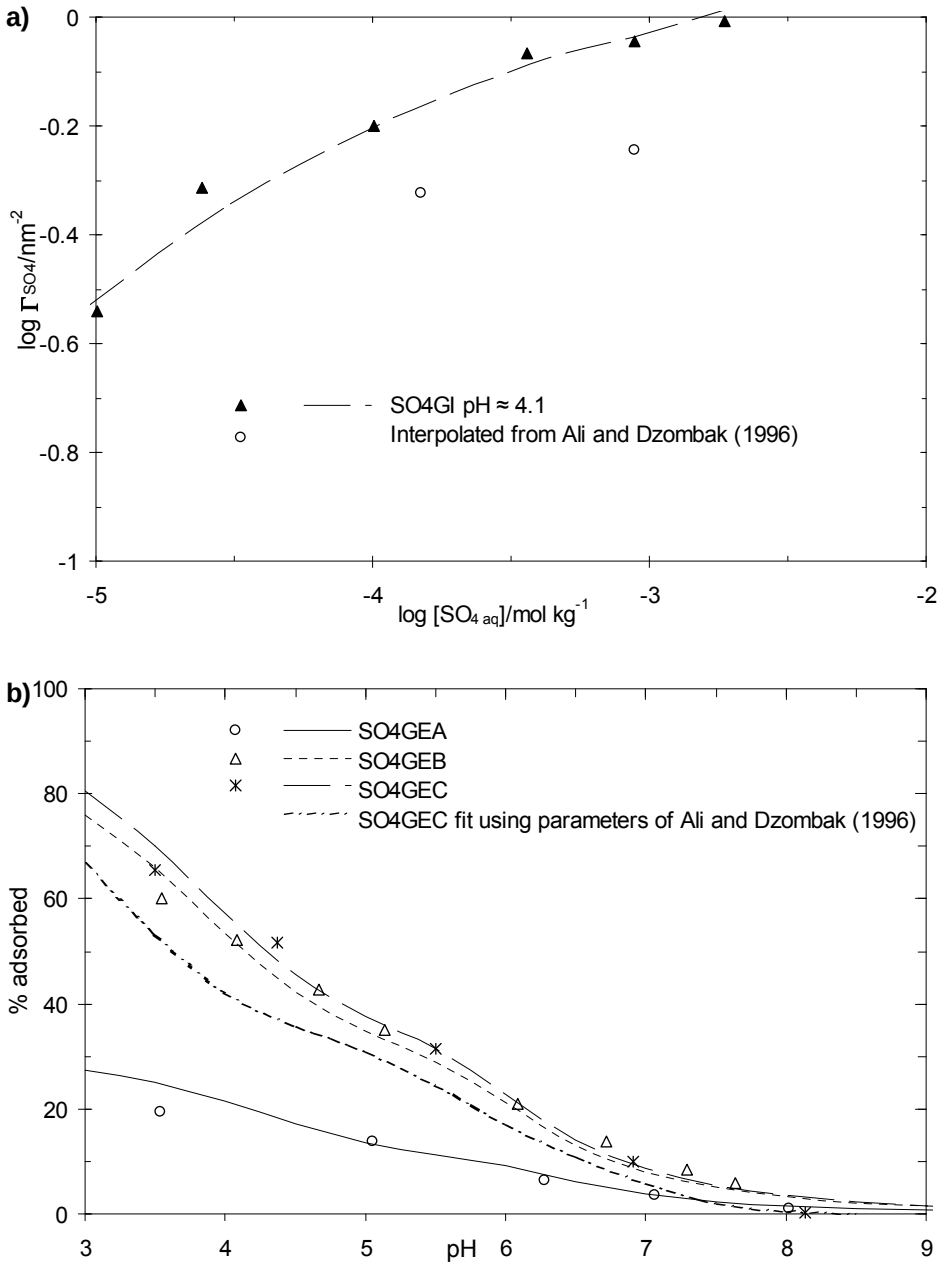

Figure 5.7 Experimental data (symbols) and modelled adsorption isotherms (lines) for SO_4 onto goethite in single sorbate systems. Model fits used the weighted average adsorption constants Table 5.6. a) isotherm, including data interpolated from Ali and Dzombak (1996b), b) edges including a model fit using the adsorption constants derived from Ali and Dzombak (1996b).

Table 5.6 Optimization of adsorption constants for SO_4 from data sets shown in Figure 5.7. The $logK^{INT}$ values are given for I = 0 (with standard deviations in parentheses). Weighted average equilibrium constants are also shown, with the 95% uncertainty level (in italics in parentheses).

Data	$SO_{4\ (T)}$ mmol kg^{-1}	α-FeOOH g kg^{-1}	$LogK_1^{INT}$ $\equiv FeHSO_4^{(0)}$	$LogK_2^{INT}$ $\equiv FeSO_4^{(-)}$	$LogK_4^{INT}$ $\equiv FeOSO_4^{(3-)}$	WSOS DF
SO4GI	1.10 to 817	1.39	13.29(0.093)	7.68 (0.052)	-6.32[a]	4.38
SO4GEA	0.776	1.31	12.08 (0.82[b])	7.56 (0.43[b])	-6.49 (1.1[b])	0.02
SO4GEB	0.206	1.22	12.86 (0.13)	7.73 (0.091)	-5.99 (0.26[b])	0.10
SO4GEC	0.202	1.31	12.88 (0.11)	7.74 (0.10)	-6.48 (0.42[b])	0.95
Weighted average for SO_4 *(95 % confidence interval)*			**12.85** *(12.39, 13.31)*	**7.69** *(7.62, 7.75)*	**-6.32** *(-6.73, -5.91)*	

[a] No convergence of this value so it was fixed at this value for consistency between results
[b] By convention fixed at 0.15 for weighted average calculation

5.2c Adsorption in Ternary Systems

Ali and Dzombak (1996b) modelled the enhanced Cu adsorption on goethite in the presence of SO_4 by including a ternary complex with stoichiometry $\equiv FeOHCuSO_4$. As discussed earlier, the work of Ali and Dzombak (1996b) had a high Cu_T/α-FeOOH and only one site type was used to describe cation, anion and proton adsorption. In this work two Me_T/α-FeOOH ratios were studied for each metal. The low Me_T/α-FeOOH ratios were (on a surface area basis) between 0.005 and 0.017 nm^{-2}, less than the N_{s1} of 0.13 nm^{-2} for Zn and 0.024 nm^{-2} for Cu, Cd and Pb. The high Me_T/α-FeOOH ratios were between 0.23 and 0.83 nm^{-2}, compared to the N_{s2} of 2.3 nm^{-2}. In this way the significance of ternary complexes on both the high and low affinity sites could be assessed.

The effect of SO_4 on the goethite adsorption of Cu, Cd, Pb and Zn is shown in Figures 5.8 and 5.9 with model fits as discussed below. As was the case with ferrihydrite, for all metals adsorption was enhanced in the presence of SO_4. This effect was greatest for Cu and Pb, which adsorb at lower pH, and greatest for data with lower $[Me_T]$/Fe. Compared to the data for ferrihydrite there was generally a larger increase in adsorption at low $[SO_4]$ (e.g. 2 mmol kg^{-1}) but a smaller increase at higher $[SO_4]$. As was the case for ferrihydrite, in general the adsorption constants from single sorbate systems predicted that metal adsorption would increase by no more than 5 % due to the presence of sulfate. The adsorption of Zn in the high $[Me_T]$/Fe experiments was an exception which is discussed below.

The formation constants for ternary complexes on the type-1 and type-2 sites, $\log K_1^{TC}$ and $\log K_2^{TC}$ respectively, are given in Table 5.7. For Cu both $\log K_1^{TC}$ and $\log K_2^{TC}$ could be optimized from the data with low Cu_T/α-FeOOH, however the $\log K_2^{TC}$ values had high standard deviations and were higher than the $\log K_2^{TC}$ values optimized from the high Cu_T/α-FeOOH data. Therefore, for consistency, $\log K_1^{TC}$ was optimized with $\log K_2^{TC}$ fixed to the weighted average value determined from the high Cu_T/α-FeOOH data. A value for $\log K_1^{TC}$ could be optimized from the data with low Me_T/α-FeOOH when the weighted average $\log K_2^{TC}$ determined from the data with high Me_T/α-FeOOH was included. This is in contrast to the data with Cu-ferrihydrite-SO_4, where including the weighted average $\log K_2^{TC}$ determined from the data with high Me_T/α-FeOOH rendered $\log K_1^{TC}$ redundant when fitting the low Me_T/α-FeOOH data.

For Cd and Pb it was not possible to optimize both $\log K_1^{TC}$ and $\log K_2^{TC}$ from the same data set. Compared to Cu, the low Me_T/α-FeOOH data for Cd and Pb data had a lower Me_T/α-FeOOH, which is consistent with non-convergence of $\log K_2^{TC}$ for these data. A value for $\log K_1^{TC}$ could be optimized from the data with low Me_T/α-FeOOH and a value for $\log K_2^{TC}$ could be optimized from the data with high Me_T/α-FeOOH. As with Cu-goethite-SO_4 a value for $\log K_1^{TC}$ could be optimized from the data with low Me_T/α-FeOOH when the weighted average $\log K_2^{TC}$ determined from the data with high Me_T/α-FeOOH was included. A value for $\log K_2^{TC}$ was not constrained by the low Zn_T/α-FeOOH data, which is reasonable given the greater significance of the type-1 sites for Zn.

Where $\log K_1^{TC}$ was not constrained it was fixed at the weighted average from the low Me_T/α-FeOOH data to ensure consistency between results. There was generally only little change in $\log K_2^{TC}$ (< 0.2 log units) when $\log K_1^{TC}$ was either deleted or fixed to the weighted average. The significance of ternary complex formation on both site types was quite distinct from that observed for Cu- and Zn-ferrihydrite-SO_4 systems where modelling over all the concentrations studied could only be achieved if ternary complex formation only occurred on the low affinity sites. Therefore, unlike the Cu- and Zn-ferrihydrite-SO_4 systems, ternary complex formation at both adsorption sites is required to describe the effect of SO_4 on metal adsorption on goethite.

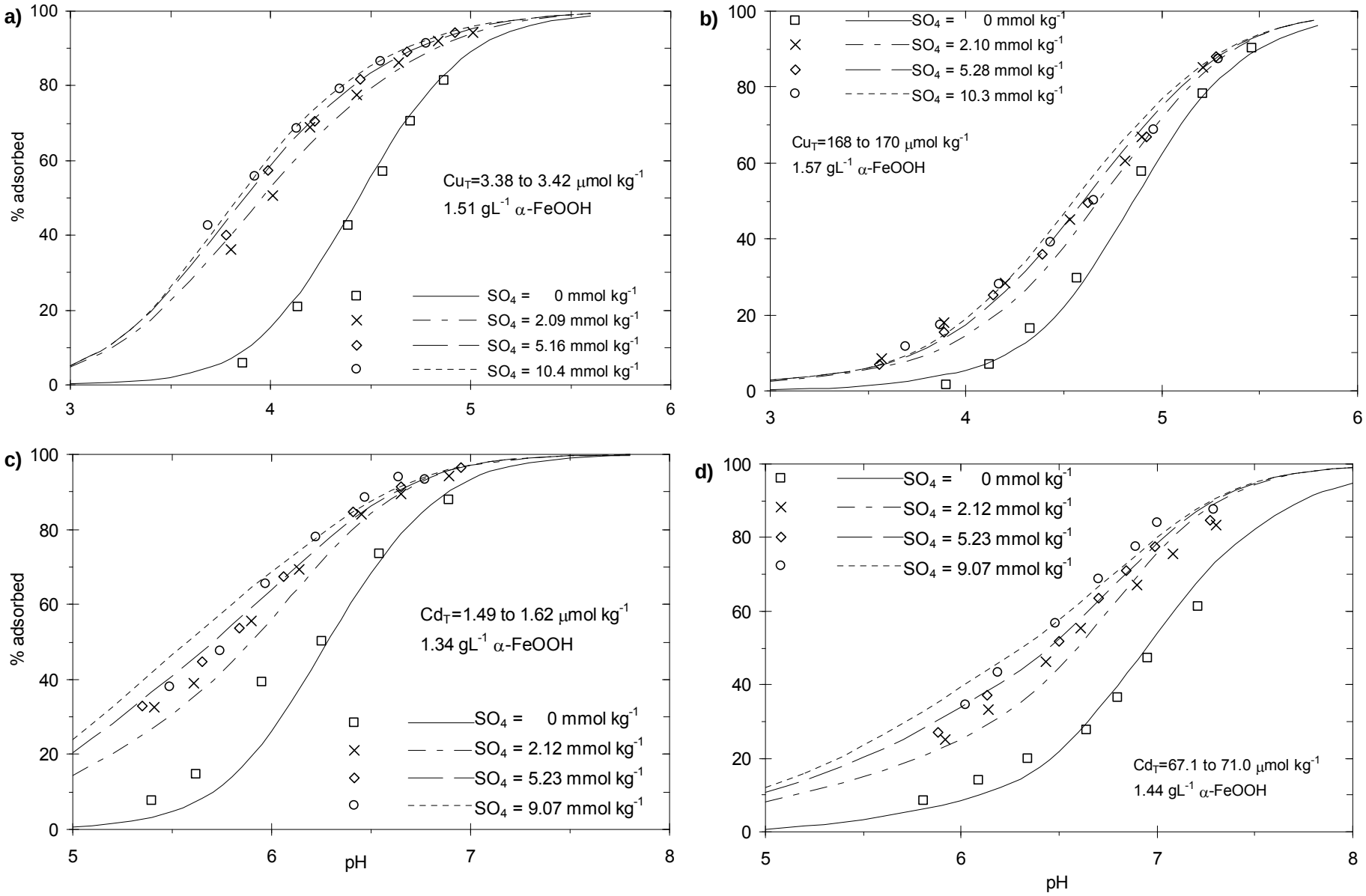

Figure 5.8 Experimental data (symbols) and modelled adsorption edges (lines) for Cu and Cd onto goethite in the presence of SO_4. Concentrations are given in Table 5.7. Model fits used 0.024 nm^{-2} (N_{s1}), 2.3 nm^{-2} (N_{s2}) and the weighted average logK's from Tables 5.5, 5.6 and 5.7.

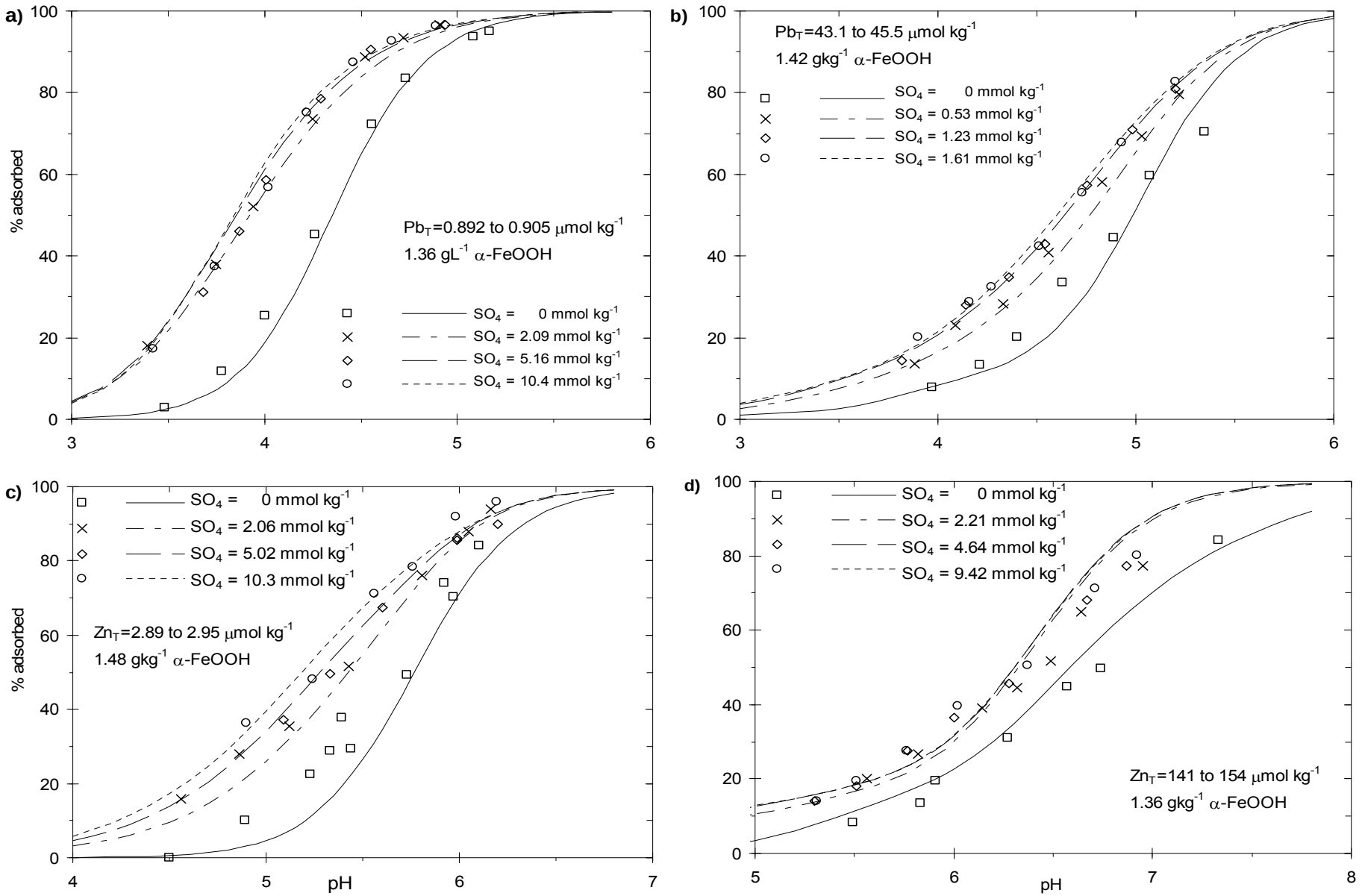

Figure 5.9 Experimental data (symbols) and modelled adsorption edges (lines) for Pb and Zn onto goethite in the presence of SO_4. Concentrations are given in Table 5.7. Model fits used N_{s1} = 0.024 nm^{-2} (Pb) or 0.14 nm^{-2} (Zn), 2.3 nm^{-2} (N_{s2}) and the weighted average logK's from Tables 5.5, 5.6 and 5.7.

Table 5.7 Optimization of $\log K_1^{TC}$ and $\log K_2^{TC}$ for ternary complex formation on goethite, from data sets given in Figures 5.8 and 5.9. The $\log K^{TC}$ values are given for I = 0 (with standard deviations in parentheses). Weighted average equilibrium constants are also shown, with the 95% uncertainty level (in italics in parentheses). N_{s2} = 2.3 nm^{-2} and N_{s1} = 0.024 nm^{-2} (Cu, Cd and Pb) or 0.13 nm^{-2} (Zn).

Data	$Me_{(T)}$ $\mu mol\ kg^{-1}$	SO_4^{2-} $mmol\ kg^{-1}$	α-FeOOH $g\ kg^{-1}$	$\log K_1^{TC}$	$\log K_2^{TC}$	WSOS/DF
CuGS1B	3.38	2.09	1.51	11.52 (0.029)[a]	9.17 (0.20)[b]	3.06[a]
CuGS1C	3.39	5.16	1.51	11.45 (0.029)[a]	8.85 (0.30)[b]	0.59[a]
CuGS1D	3.42	10.4	1.51	11.47 (0.026)[a]	8.88 (0.97)[b]	0.48[a]
CuGS2B	168	2.1	1.57	11.48[c]	8.57 (0.033)	0.92
CuGS2C	170	5.28	1.57	11.48[c]	8.42 (0.023)	1.45
CuGS2D	168	10.3	1.57	11.48[c]	8.33 (0.031)	1.83
Weighted average for Cu *(95 % confidence interval)*				**11.48** *(11.45, 11.53)*	**8.44** *(8.28, 8.60)*	
CdGS1B	1.62	2.12	1.34	9.65 (0.035)	7.00[c]	1.15
CdGS1C	1.61	5.23	1.34	9.44 (0.035)	7.00[c]	2.08
CdGS1D	1.49	9.07	1.34	9.35 (0.035)	7.00[c]	6.91
CdGS2B	69.3	2.12	1.44	9.48[c]	7.07 (0.042)	11.56
CdGS2C	71.0	5.23	1.44	9.48[c]	6.96 (0.032)	4.87
CdGS2D	67.1	9.07	1.44	9.48[c]	7.00 (0.024)	6.63
Weighted average for Cd *(95 % confidence interval)*				**9.48** *(9.26, 9.70)*	**7.00** *(6.93, 7.08)*	
PbGS1B	0.892	2.09	1.36	11.70 (0.024)	8.84[c]	3.21
PbGS1C	0.897	5.16	1.36	11.60 (0.023)	8.84[c]	5.41
PbGS1D	0.905	10.4	1.36	11.56 (0.024)	8.84[c]	2.75
PbGS2B	43.4	0.530	1.42	11.62[c]	8.91 (0.089)	0.039
PbGS2C	43.1	1.23	1.42	11.62[c]	8.84 (0.069)	0.040
PbGS2D	45.5	1.61	1.42	11.62[c]	8.80 (0.065)	0.040
Weighted average for Pb *(95 % confidence interval)*				**11.62** *(11.52, 11.72)*	**8.84** *(8.77, 8.92)*	
ZnGS1B	2.89	2.06	1.48	9.16(0.030)	6.12[c]	1.24
ZnGS1C	2.95	5.02	1.48	9.02 (0.028)	6.12[c]	0.17
ZnGS1D	2.93	10.3	1.48	9.05 (0.023)	6.12[c]	2.04
ZnGS2B	149	2.21	1.36	9.07[c]	no convergence	
ZnGS2C	141	4.64	1.36	9.07[c]	6.00 (0.33[d])	12.16
ZnGS2D	154	9.42	1.36	9.07[c]	6.23 (0.14)	11.19
Weighted average for Zn *(95 % confidence interval)*				**8.77** *(8.68, 8.86)*	**6.12** *(5.09, 7.15)*	

[a] With $\log K_2^{TC}$ fixed at 8.44 as discussed in the text
[b] Not included in weighted average as discussed in the text
[c] No convergence of this value so it was fixed at this value for consistency between results
[d] By convention fixed at 0.15 for weighted average calculation

Model fits are shown with the data in Figures 5.8 and 5.9. Given the complexity of the interaction between Me, SO_4 and the goethite surface (including site competition, electrostatic effects, ternary complex formation and solution complex formation) the model provides a relatively accurate description of the effect of SO_4 on metal adsorption. Deviations between the model and experimental data are minor and comparable in magnitude to the differences between modelled and measured adsorption in the absence of SO_4. In some cases (e.g. high Cu_T/Fe data and high Cd_T/Fe data with low [SO_4]) there was a tendency to slightly underestimate the effect of SO_4 at low % Me adsorption and to overestimate the effect of SO_4 at higher Me adsorption. In other cases (e.g. all Cd data with high [SO_4]) there was a tendency to do the reverse.

From Table 5.7 it can be seen that for the high Zn_T/Fe data a value of $\log K_2^{TC}$ was not constrained with the 2.21 mmol kg^{-1} [SO_4] dataset and had high uncertainty for the two data sets with higher [SO_4]. In addition the model fit to this data had an unusual shape, with SO_4 having a greater modelled effect on Zn adsorption where Zn adsorption was > 50 %. The reason for this aberration was the effect of the trivalent adsorbed SO_4 species ($\equiv FeOSO_4^{3-}$) on the surface charge. Even without ternary complexes modelled Zn adsorption in the presence of SO_4 increased significantly, compared to that in the absence of SO_4, in this pH region.

From Table 5.6 it can be seen that the value for $\log K_4^{INT}$ was poorly constrained and this species was only included to be consistent with the work of Ali and Dzombak (1996a). When the $\equiv FeOSO_4^{(3-)}$ species is removed from the model $\log K_1^{INT}$ and $\log K_2^{INT}$ for SO_4 adsorption (with no metal) increase slightly to 13.02 and 7.77 respectively. The $\log K^{TC}$ values optimized from Zn adsorption in the presence of SO_4 when fitted using just $\log K_1^{INT}$ and $\log K_3^{INT}$ for SO_4 adsorption are given in Table 5.8 and Figure 5.10 shows Zn adsorption in the presence of SO_4 when modelled using these values. The fit to Zn adsorption is considerably improved when the $\equiv FeOSO_4^{3-}$ species is removed. While there is almost no change for the low Zn_T/Fe experiments there is a dramatic change in the model fit for the high Zn_T/Fe experiments. This is consistent with the significance of surface charge effects being greater at higher adsorption densities.

Table 5.8 Optimization of $logK_1^{TC}$ and $logK_2^{TC}$ for Zn ternary complex formation on goethite, from data sets given in Figure 5.9. Model excludes $\equiv FeOSO_4^{3-}$ species. The $logK^{TC}$ values are given for I = 0 (with standard deviations in parentheses). Weighted average equilibrium constants are also shown, with the 95% uncertainty level (in italics in parentheses). N_{s2} = 2.3 nm^{-2} and N_{s1} = 0.13 nm^{-2}.

Data	$Me_{(T)}$ μmol kg^{-1}	SO_4^{2-} mmol kg^{-1}	α-FeOOH g kg^{-1}	$logK_1^{TC}$	$LogK_2^{TC}$	WSOS/DF
ZnGS1B	2.89	2.06	1.48	9.16(0.027)	6.52 [a]	2.12
ZnGS1C	2.95	5.02	1.48	9.00 (0.027)	6.52[a]	0.16
ZnGS1D	2.93	10.3	1.48	9.05 (0.023)	6.52 [a]	2.11
ZnGS2B	149	2.21	1.36	9.06[a]	6.54 (0.090)	1.25
ZnGS2C	141	4.64	1.36	9.06[a]	6.52 (0.080)	1.14
ZnGS2D	154	9.42	1.36	9.06[a]	6.52 (0.051)	2.04
Weighted average for Zn *(95 % confidence interval)*				**9.06** *(8.94, 9.18)*	**6.52** *(6.51, 6.54)*	

[a] No convergence of this value so it was fixed at this value for consistency between results

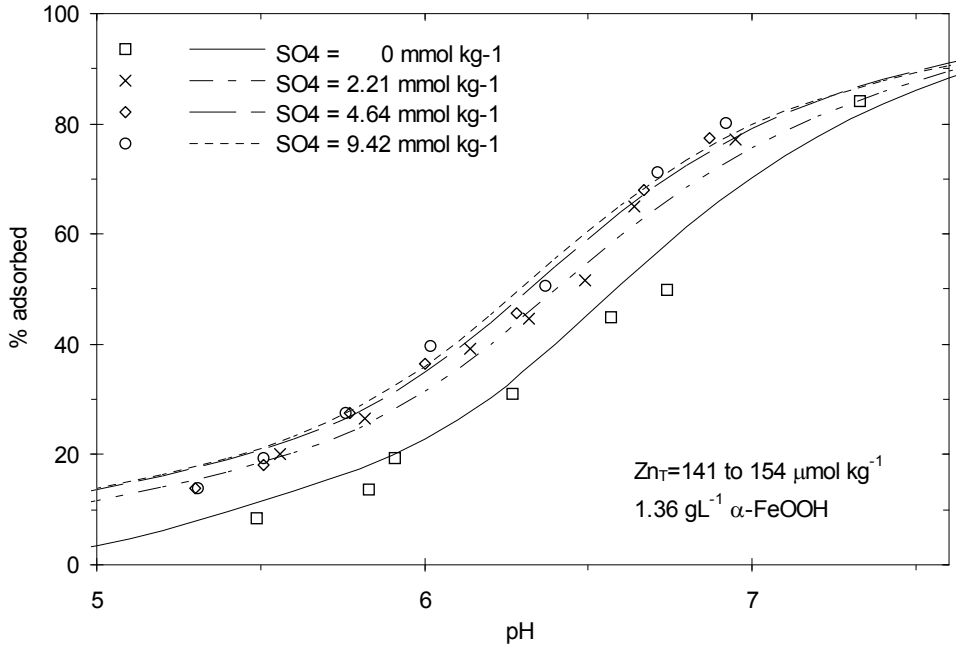

Figure 5.10 Experimental data (symbols) and modelled adsorption edges (lines) for Zn onto goethite in the presence of SO_4. Concentrations and model adsorption constants are given in Table 5.10. Model fits used N_{s1} = 0.14 nm^{-2} (Zn), 2.3 nm^{-2} (N_{s2}) and the weighted average logK's from Tables 5.10.

As discussed in Section 5.2b ATR-FTIR studies (Peak et al., 1999, Elzinga et al., 2001) suggest that at pH > 6, where SO_4 adsorption densities were low, a weak ion-pair (e.g. $\equiv FeOH_2^+$---SO_4^{2-}) was the principal mode of association. It is not possible to include this sort of species in the DLM, where all charge resides on a single plane. Furthermore when modelling adsorption the higher charged anion surface species are most significant at higher pH. Therefore it seems reasonable that the $\equiv FeOSO_4^{(3-)}$ species required by Ali and Dzombak

(1996a) to model SO_4 adsorption might be accounting for the SO_4 adsorbed by ion pair formation. Therefore it might be expected that the effect of SO_4 on surface charge at high pH would be overestimated. There was almost no change in $\log K^{TC}$ values optimized for Pb and Cu adsorption when $\equiv FeOSO_4^{(3-)}$ was deleted because Cu and Pb adsorb at a lower pH than Zn. For Cd there was only a small change in the optimized $\log K^{TC}$ values when $\equiv FeOSO_4^{(3-)}$ was deleted (maximum change was 0.09). In this case it is because the Cd_T/Fe ratios was considerably lower than that of Zn, so surface charge effects are less significant. Therefore for modeling systems with Zn and SO_4 the $\equiv FeOSO_4^{(3-)}$ species were excluded.

Sulfate adsorption on the type-1 sites

When modelling the effect of SO_4 on the ferrihydrite adsorption of Cu it was found that the best model fits were obtained when both ternary complex formation and SO_4 adsorption only occurred on the type-2 sites. For goethite, ternary complex formation was required at both the type-1 and type-2 sites to describe the effect of SO_4 on Me adsorption at low and high Me_T/Fe ratios. The above modelling for ternary complex formation on goethite includes SO_4 adsorption on the type-1 and type-2 sites. If SO_4 adsorption is only allowed on the type-2 sites the most significant effect is on the adsorption of Cu and Pb at low Me_T/Fe ratios, where the type-1 sites are more significant because of the low pH. When SO_4 adsorption is restricted to the type-2 sites the weighted average $\log K_1^{TC}$ decrease slightly, to 11.11 and 11.23 for Cu and Pb respectively. The weighted average $\log K_2^{TC}$ was unaffected for Cu and increased from 8.84 to 8.86 for Pb. The effect that removing SO_4 adsorption on the type-1 sites has on modelled Cu and Pb adsorption on goethite is shown in Figure 5.11. With competition from SO_4 for the type-1 sites metal adsorption decreases more steeply as the pH decreases. While the differences are not great there is a fairly definitive preference for including SO_4 adsorption on the type-1 sites, especially from the Pb data where there is more data at low metal adsorption compared to Cu.

Site Densities Revisited

The only model parameter that was not derived from the experimental data was the site density of the low affinity sites (N_{s2}). Therefore other options for N_{s2} values were investigated to see how the model results were affected by the value of this parameter. Modelling was attempted with site densities of 1.4 and 3.0 nm^{-2}. A site density of 1.4 nm^{-2} was used by Ali and Dzombak (1996a) and a site density of 3.0 nm^{-2} is consistent with the highest Γ_{Cu} observed by Robertson and Lecki (1998).

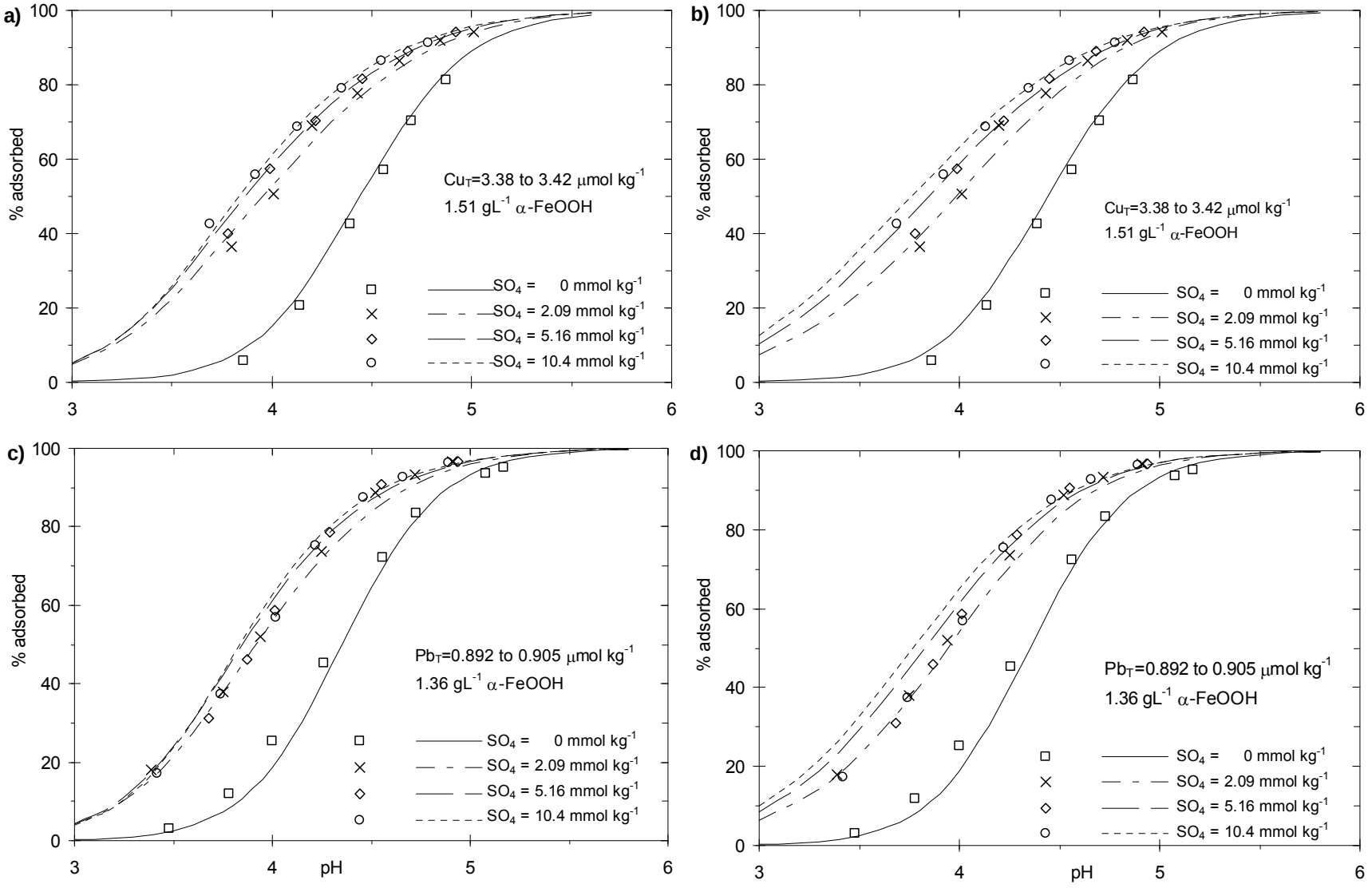

Figure 5.11 Experimental data (symbols) and modelled adsorption edges (lines) for Cu and Pb onto goethite in the presence of SO_4. Model fits using N_{s2} of 2.3 nm^{-2} and N_{s1} of 0.024 nm^{-2} Modelled curves either include or exclude SO_4 adsorption on the type-1 sites. a) Cu with SO_4 adsorption on the type-1 sites b) Cu without SO_4 adsorption on the type-1 sites, c) Pb with SO_4 adsorption on the type-1 sites d) Pb without SO_4 adsorption on the type-1 sites.

All model parameters, including the $\log K_A^{INT}$, N_{1s}, $\log K^{INT}$ and $\log K^{TC}$ values, were re-optimized with these N_{s2} values. Modelling of adsorption in single sorbate systems was not substantially affected by using N_{s2} of 1.4 or 3.0 nm^{-2}. The most significant difference in the model results with different N_{s2} values was for the high Me_T/α-FeOOH systems. The adsorption of Cu and Cd in the high Me_T/α-FeOOH experiments and model fits using N_{s2} of 1.4 and 3 nm^{-2} are shown in Figure 5.12. The adsorption of Cu in the high Me_T/α-FeOOH experiments with SO_4 was well modelled with N_{s2} of 2.3 or 3.0 nm^{-2}, however, with N_{s2} of 1.4 nm^{-2} Cu adsorption was underestimated at low pH in the presence of SO_4. At these comparatively low pH's, SO_4 adsorption will be greatest and site competition will be most significant. From the SO_4 isotherm (Figure 5.7a) at pH ≈ 4.1 the measured Γ_{SO4} was 0.98 nm^{-2} at a total [SO_4] of 2.1 mmol kg^{-1}. This represents a significant reduction in surface sites. The adsorption of Pb occurs at a similar pH range to that of Cu and, when modelled with N_{s2} of 1.4 nm^{-2}, was also underestimated at low pH in the presence of SO_4. This underestimation of Pb adsorption was less significant than that of Cu because the total [Pb] was approximately four times lower than the [Cu_T] in the high Me_T/α-FeOOH experiments.

With N_{s2} of 1.4 nm^{-2} the adsorption of Cd in the high Me_T/α-FeOOH experiments with SO_4 was accurately predicted but with N_{s2} of 3.0 nm^{-2} adsorption was overestimated. This might suggest that the N_{s2} for Cd may be lower than that of Cu and Pb, but a full investigation of this would require further study. This sensitivity analysis has shown that a N_{s2} of 2.3 nm^{-2} provides the best prediction of the results for the experimental conditions used in this work.

Overall modelling suggests that the effect of SO_4 on metal adsorption can be well described by including ternary complexes on both the type-1 and type-2 sites. As has been shown in Chapter 4 there is a linear free energy relationship between the $\log K^{TC}$ and $\log K^{INT}$ values for ferrihydrite. The data from goethite also show the same relationship, as shown in Figure 5.13. This would suggest that the mechanism for the enhancement of metal adsorption on both ferrihydrite and goethite is the same.

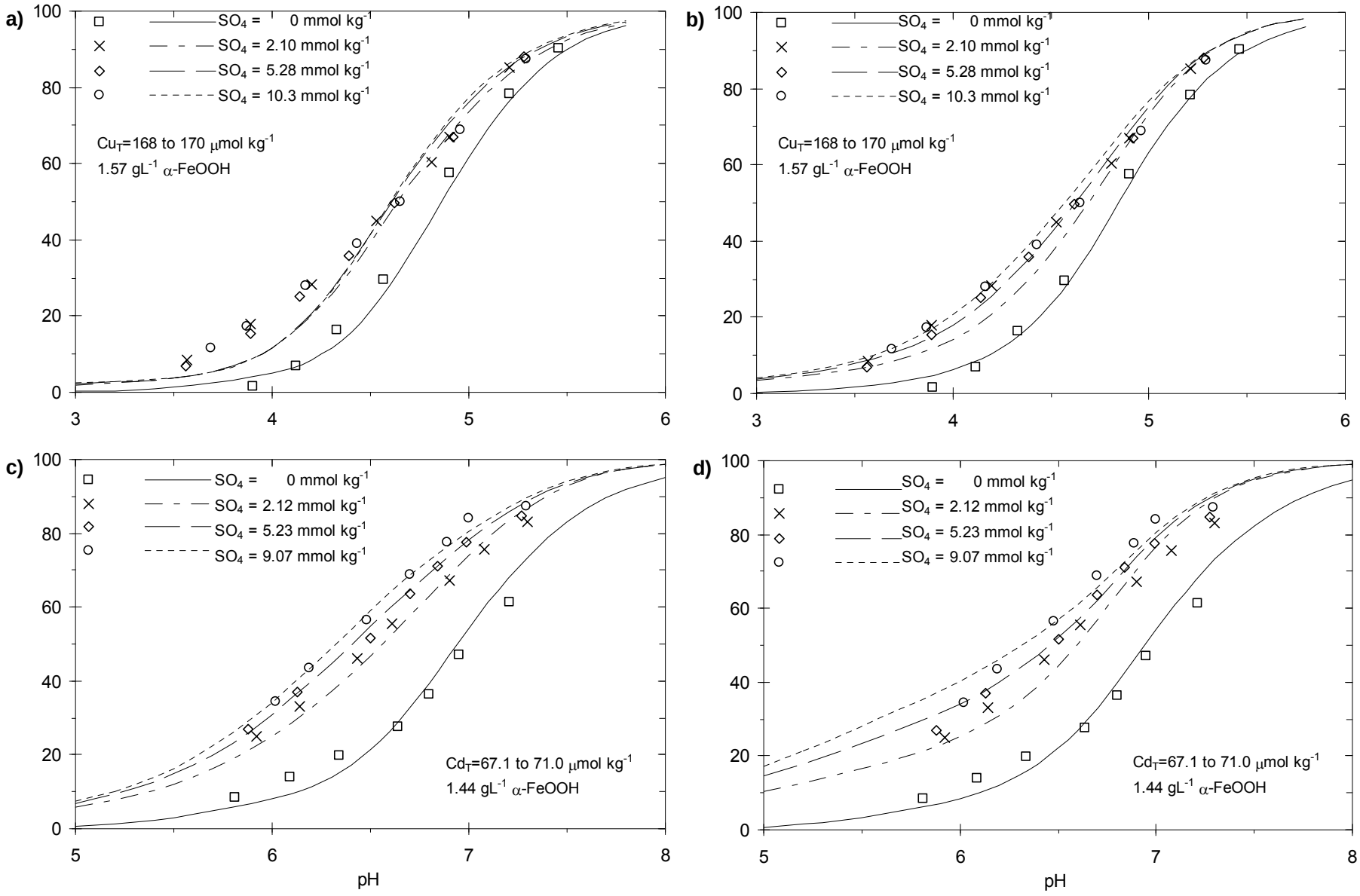

Figure 5.12 Experimental data (symbols) and modelled adsorption edges (lines) for Cu and Cd onto goethite in the presence of SO_4. Model fits using N_{s2} of 1.4 and 3.0 nm^{-2}. a) Cu and 1.4 nm^{-2}, b) Cu and 3.0 nm^{-2}, c) Cd and 1.4 nm^{-2}, d) Cd and 3.0 nm^{-2}.

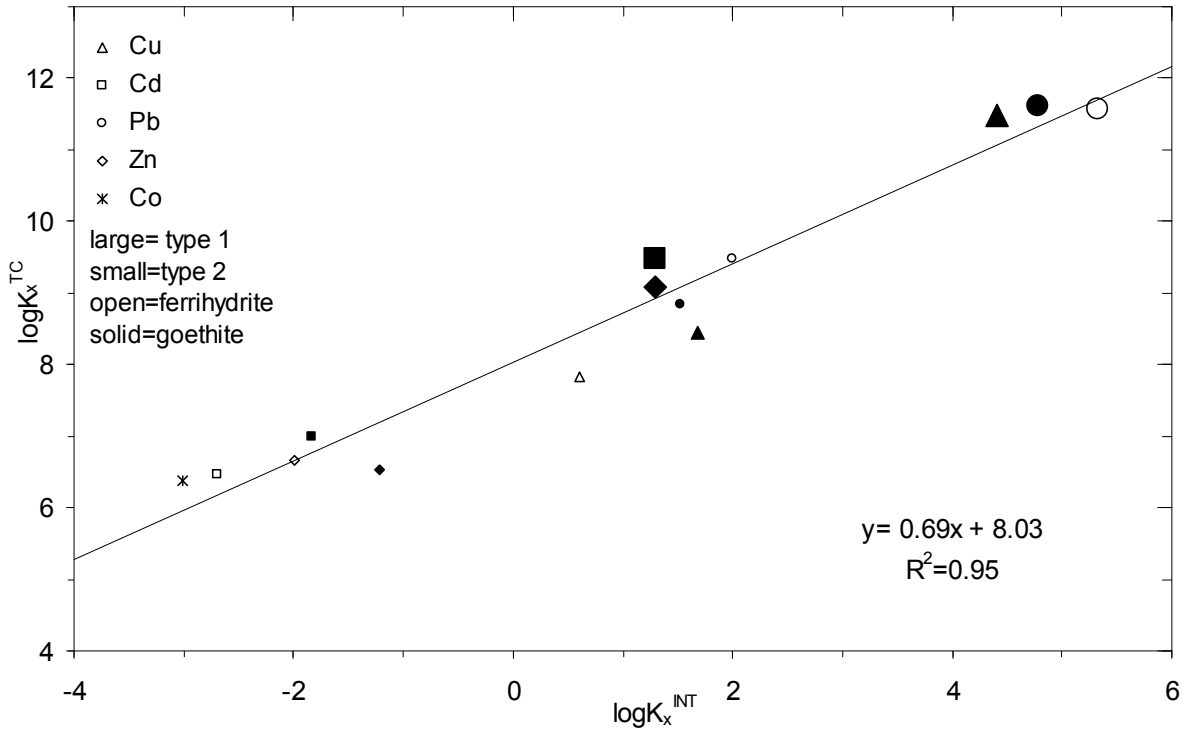

Figure 5.13 The relationship between intrinsic adsorption constants for ≡FeOHMeSO$_4$ formation (logK^{TC}) and the logK^{INT} for metal adsorption. The goethite data were taken from Tables 5.5 and 5.7 and the ferrihydrite data were from Chapters 3 and 4.

Comparison to Previous Studies

As earlier discussed, the Cu adsorption data of Ali and Dzombak (1996a) were consistent with the results of this study. Using a 2.3 nm^{-2} site density and the acidity constants from Table 5.3 the weighted average logK_2^{INT} values optimized from the Cu adsorption data of Ali and Dzombak (1996b) was 1.72, compared to logK_2^{INT} of 1.68 optimized from the data of this study. Because of the comparatively high Cu_T/Fe (Figure 5.5), there was no convergence for a value of logK_1^{INT} for the data of Ali and Dzombak (1996b). Using the single sorbate adsorption constants from Tables 5.5 and 5.6, the weighted average logK_2^{TC} value optimized from the Ali and Dzombak (1996b) Cu adsorption data with 0.25 and 1.00 mM SO_4 was 8.92, which is somewhat larger than the value from the data from this study (8.44 ± 0.16).

It has been noted that SO_4 adsorption reported in Ali and Dzombak (1996b) was less than that observed in this study. Using the site density of 2.3 nm^{-2} and acidity constants from Table 5.3 the weighted average logK^{INT} optimized from the SO_4 adsorption data of Ali and Dzombak (1996b) were 11.56, 7.06 and –7.16 for formation of ≡$Fe_{(2)}HSO_4$, ≡$Fe_{(2)}SO_4^-$ and ≡$Fe_{(2)}OSO_4^{3-}$ respectively. These values are all between 0.5 and 1.5 log units lower than the results from this study. Using these logK^{INT} values for SO_4 adsorption, derived from Ali and Dzombak

(1996b), the weighted average $logK_2^{TC}$ value optimized from the Ali and Dzombak (1996b) Cu adsorption data (with 0.25 and 1.00 mM SO_4) was 8.50, which is within experimental error of the value from this study. The optimized $logK_2^{TC}$ decreases with decreasing $logK^{INT}$ for SO_4, because SO_4 adsorption would compete with ternary complex formation. Therefore accurate modelling of SO_4 adsorption is important in obtaining consistent ternary complex formation constants.

Ternary Complex Structure

There have been several recent spectroscopic studies of the goethite-Me-SO_4 ternary system. Collins et al. (1999) state that "the enhancement of Cd^{2+} adsorption in the presence of SO_4 and PO_4 is solely by electrostatic interaction" based on XAFS studies. In contrast, Ostergren et al. (2000) used ATR-FTIR and XAFS spectroscopies to describe a Pb-SO_4 adsorbed ternary complex that was bound to the surface through the Pb and had a stoichiometry of $(\equiv Fe—O)_2—Pb—OSO_3$. Most recently Elzinga et al. (2001) proposed two ternary complex structures that would be consistent with their ATR-IR and XAFS data (Figure 5.14) and also supported the importance of electrostatic effects enhancing SO_4 adsorption, particularly at low Γ_{Pb} and high pH. The results from the present study show that $logK^{TC}$ (which reflects the strength of ternary complex formation) increases as $logK^{INT}$ for metal adsorption increases. This supports a ternary complex structure with the metal attached to the goethite surface, as is the case for both structures proposed by Elzinga et al. (2001).

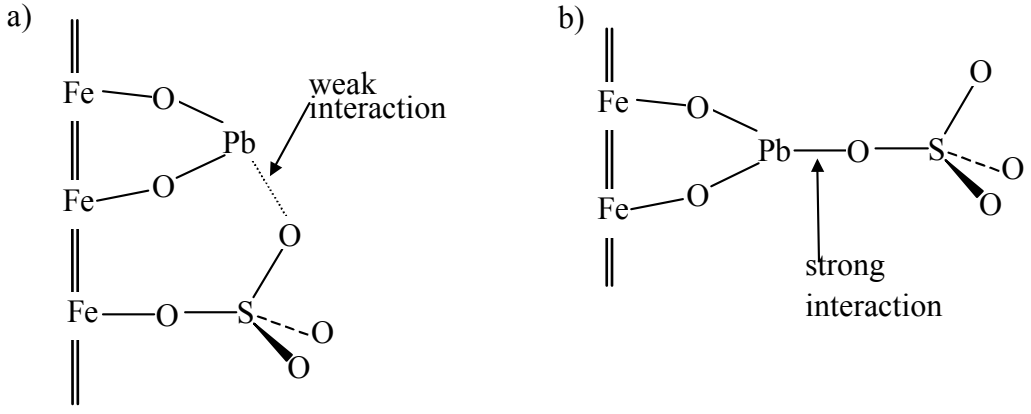

Figure 5.14 Structures of ternary complexes consistent with XAFS and ATR-IR data (Elzinga et al, 2001).

5.3 CONCLUSIONS

Metal adsorption onto a pure acicular goethite in SO_4-rich waters, such as those found in AMD systems, was accurately described by the DLM. The major deficiency was the DLM's poor prediction of the acid-base behaviour of the goethite surface when the total site density is set to a value consistent with maximum adsorption densities. The site density optimised from the acid-base titration data was 0.94 nm^{-2} and model fits with this N_s value were reasonably close to the measured titration data. This value should be compared to the highest measured adsorption density in this work (1.34 nm^{-2} for Cd) and the site density that provided the best fit to all the experimental data was 2.3 nm^{-2}.

All metal adsorption data could be modelled using a two-site model. The site densities of the high affinity sites optimized from the Cu, Pb and Cd data were reasonably consistent and a weighted average value of 0.024 nm^{-2} was used for these metals. The site density of the high affinity sites optimized from the Zn data were considerably higher and a weighted average value of 0.13 nm^{-2} was used for Zn. The increased adsorption of metals in the presence of SO_4 was accurately predicted by including ternary complex formation at both the high and low affinity adsorption sites.

The site density that provided the best fit to all the experimental data was 2.3 nm^{-2}. The main model discrepancy modelling with a site density of 1.4 nm^{-2} was at high Cu and Pb concentration where site competition from SO_4 appeared to be overestimated. The main model discrepancy modelling with a site density of 3.0 nm^{-2} was at high Cd concentration where site competition from SO_4 appeared to be underestimated. The difference between Cd and Cu or Pb could suggest that Cd has a lower site density than Cu and Pb on acicular goethite, but this would require more study to substantiate.

CHAPTER SIX

SULFATE-RICH GOETHITE ADSORPTION OF CU, ZN, CD AND PB.

6.1 INTRODUCTION

The preceding chapters have considered the effect of solution heterogeneity on trace metal adsorption onto pure synthetic ferrihydrite and goethite, specifically the effect of pH, [metal] and [SO_4]. In this chapter the parameters developed to model metal adsorption onto the pure acicular goethite (Chapter 5) are applied to a goethite synthesized under conditions simulating the geochemistry of AMD systems, i.e. $FeSO_4$ oxidation by oxygen at pH 3.0. The iron oxyhydroxide formed under these conditions is a goethite with between 5 and 10 % w/w SO_4 content, termed SO_4-rich goethite.

Webster et al. (1998) found that, under the range of conditions studied, Cu and Pb adsorption onto a SO_4-rich goethite formed in this way was essentially identical to adsorption onto a naturally occurring AMD goethite collected from the stream below the Tui mine tailings impoundment near Te Aroha, New Zealand. For this reason the synthetic SO_4-rich goethite is used as an analogue for the natural AMD goethite. The synthesis and characterization of the SO_4-rich goethite was described in Chapter 2. Using a synthetic analogue, compared to the natural oxide, avoids the potential added complexities of organic material, the range of anions and cations that may be incorporated in the natural oxide when it is precipitated, and other solid phases that might be present, such as clays or silicates. In Chapter 7 adsorption of Cu, Zn, Pb and Cd onto the natural SO_4-rich goethite is compared to model predictions based on the synthetic SO_4 rich goethite.

6.2 RESULTS AND DISCUSSION

6.2a Acid-Base Surface Chemistry and Site Densities

Prior to acid-base titrations being performed, SO_4 needed to be removed from the SO_4-rich goethite. This was because SO_4 adsorption and desorption in response to pH changes would consume and release protons respectively, which would interfere with the titration results. Sulfate was completely desorbed at pH 10.0 (Section 6.2c), and desorption was rapid, occurring in approximately 10 min. After 30 min at pH 10 at least 92 % of this desorbed SO_4 was re-adsorbed when the pH was lowered to 3.0 (i.e. desorption was 92 % reversible). Therefore suspensions used for titrations were taken to pH 10.0 for 30 min and, after two

rinses in 0.1 M $NaNO_3$ at pH 10.0, the solid was resuspended in MilliQ water and the ionic strength adjusted as necessary. The results from titrations performed at 0.004, 0.02 and 0.1 mol kg^1 $NaNO_3$ are shown in Figure 6.1 as plots of TOTH vs pH, where $TOTH=C_A-C_B$.

The PPZC of the sulfate-rich goethite, determined from the intersection of titration curves at the three ionic strengths, was pH 8.90 ± 0.1. This is equivalent, within experimental error, to the PPZC determined for pure goethite (Section 5.2). The significant difference between the two goethites was the amount of NaOH required to titrate the SO_4-rich goethite compared to the pure goethite. Titration data for the two goethites at I=0.1 are shown as plots of TOTH vs pH in Figure 6.2 with the blank data. To lower the pH from the PPZC to pH ≈ 4.7, for example, the SO_4-rich goethite required approximately 3 times more HNO_3 (per gram of goethite) than the pure goethite.

The N_2 BET surface area of the sulfate-rich goethite was 47 m^2g^{-1} compared to 80 m^2g^{-1} for the pure goethite. As discussed in Chapter 2 this value was considered to be artificially low. The sulfate-rich goethite was clumpy, even after drying for 24 h at 110 °C under N_2. From the SEM images (Figure 2.2) the surface area of sulfate-rich goethite would be expected to be larger than that of the pure goethite. If the measured surface area was correct, then the sulfate-rich goethite would have to have a surface charge up to five times greater than that of the pure goethite. This is contrary to evidence that, when normalized for differences in PPZC, the surface charging curves of minerals coincide within a tight band. For example, Wieland et al. (1988) have compared the surface charge due to protonation for a range of minerals, including goethite. When plotted as a function of pH the data for the different minerals were widely spread over the pH range. However, when plotted as a function of pH normalized for the PPZC (i.e. pH-PPZC) the data for all minerals formed a tight band. This has been justified by considering surface charging as involving both chemical interaction and electrostatic interaction. The PPZC was considered to reflect the chemical interaction, specific for that mineral, while the process of charge formation was independent of the mineral and determined by the solution side of the interface (Stumm, 1992).

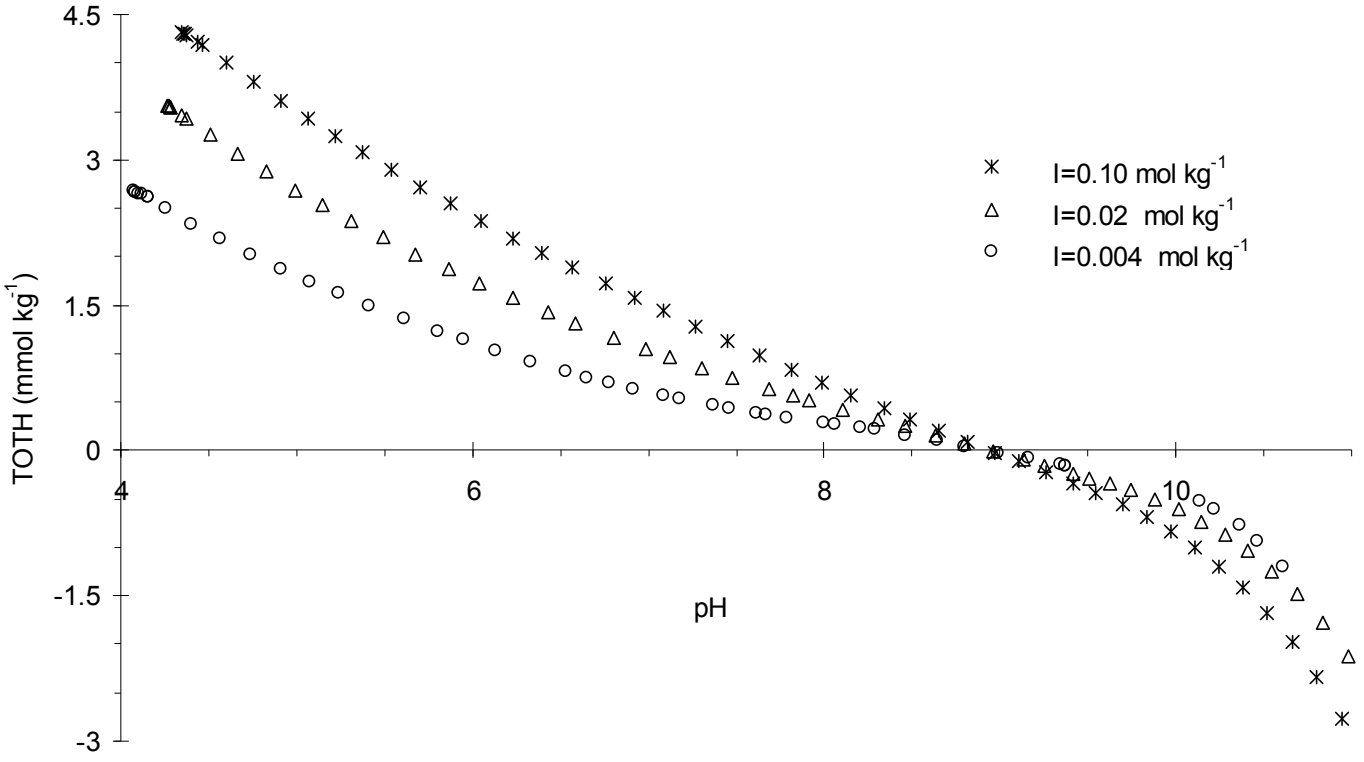

Figure 6.1 Experimental (symbols) acid base titration data for sulfate-rich goethite.

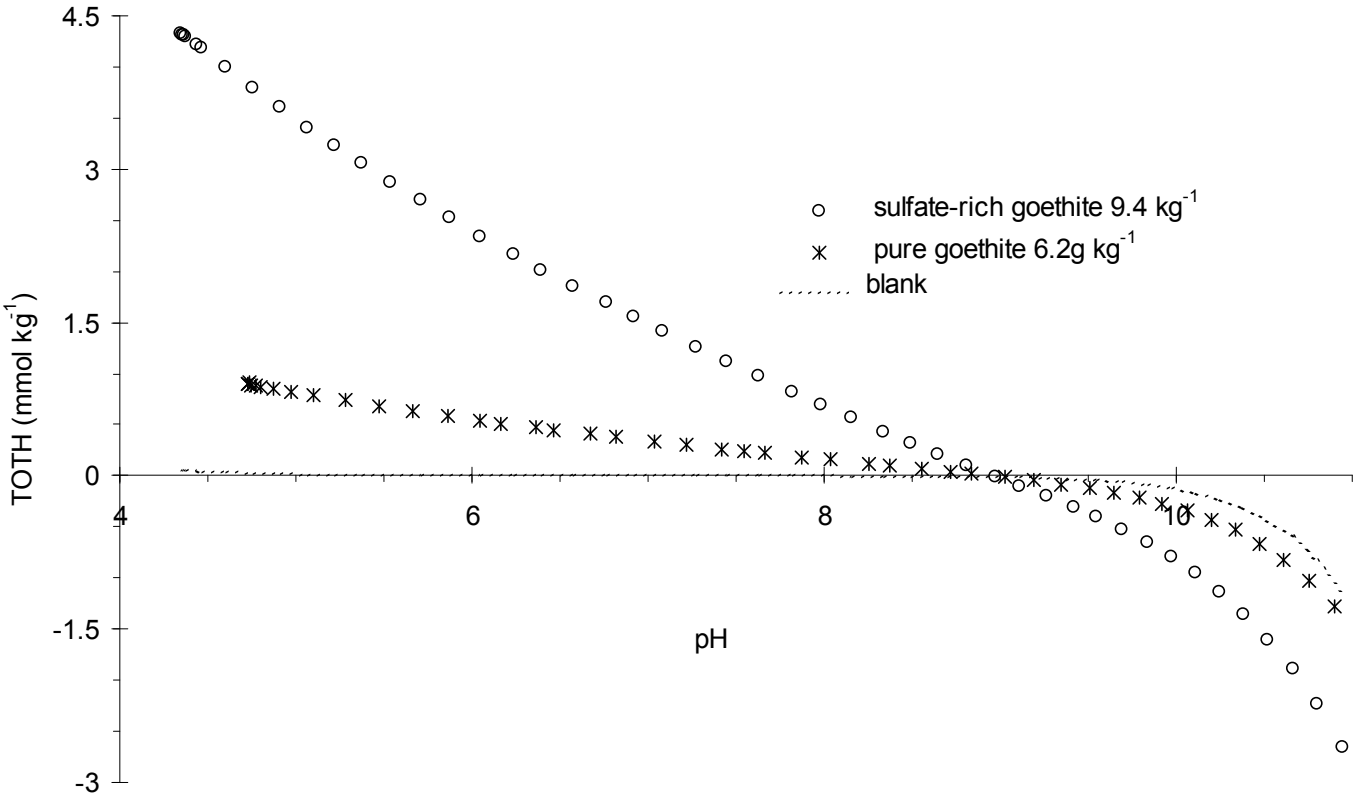

Figure 6.2 Experimental (symbols) acid base titration data at I = 0.1 mol kg^{-1} for pure goethite, sulfate-rich goethite and blank (no oxide present).

As discussed in Chapter 5, Boily et al (2001) have demonstrated that the surface charges were lower on a 85 m^2g^{-1} goethite compared with a 23 or 37 m^2g^{-1} goethite. For example at a pH of 4.0, the 85 m^2g^{-1} goethite had a surface charge of 0.20 Cm^{-2} compared with 0.24 Cm^{-2} for the 23 or 37 m^2g^{-1} goethite. This 20 % difference in surface charge would fit within the band of data described by Wieland et al. (1988). Therefore, based on these arguments the initial approach taken to modelling the titration data was to find a suitable estimate of the surface area for the sulfate-rich goethite, such that the surface charge densities calculated from the titration data would be as close as possible to those determined for the pure goethite.

Comparisons of the surface charge calculated from the titration data for the pure and sulfate-rich goethite at the three ionic strengths are shown in Figure 6.3. The figure shows the calculated surface charge for a range of surface areas for the sulfate-rich goethite. At ionic strengths of 0.1, 0.02 and 0.004 mol kg^{-1} the best fits were obtained with surface areas of approximately 235, 230 and 190 m^2g^{-1} respectively. The average surface area determined by this method was 220 m^2g^{-1} with a standard deviation of 20 m^2g^{-1}. From the work of Boily et al (2001) it could be expected that the higher sulfate-rich goethite site density would correspond to a somewhat lower surface charge than that of the pure goethite. However, without a reliable measurement of the SO_4-rich goethite surface area, it is not possible to support this.

Using the surface area of 220 m^2g^{-1} the titration data were modeled using the DLM and the surface acid-base reactions in Equations 5.2 and 5.3. As with the pure goethite, initially all three parameters were optimized simultaneously, and then the site density was fixed to the weighted average value for the three data sets, and the acidity constants were optimized for this site density. In this way the best consistent set of model parameters to describe all the titration data were obtained. The values of the three model parameters simultaneously optimized from the data are given in Table 6.1. The weighted average value of N_s was 0.97 nm^{-2} and, when the site density was fixed at this value, the weighted average $\log K_A^{INT}$ values were -8.14 and –9.82. The three parameters optimized from the SO_4-rich goethite data are all within experimental error of those of the pure goethite.

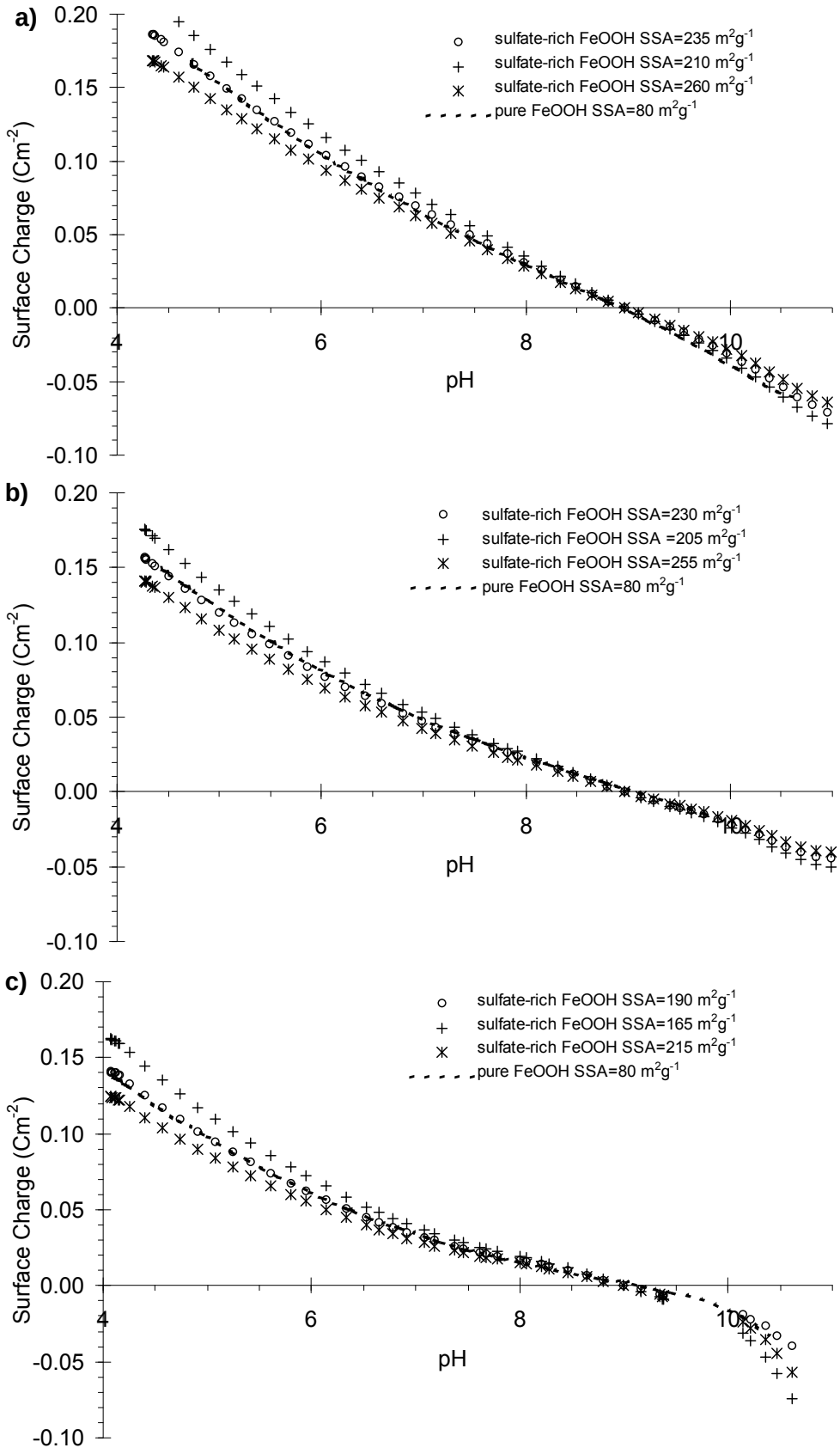

Figure 6.3. Calculated surface charge for titration data of sulfate-rich goethite, compared to pure goethite data. For a) I=0.10 mol kg^{-1}, b) I=0.02 mol kg^{-1}, and c) I=0.004 mol kg^{-1}.

When the input SSA was varied from 100 to 300 m^2g^{-1} there was very little change in optimized site densities on a concentration basis, i.e. mol (kg suspension)$^{-1}$, which corresponded to a steady decrease in site density (on a nm^{-2} basis) as the SSA was increased. The effect of lowering the input SSA was to decrease the ΔpK_A^{INT} (i.e. pK_{A2}^{INT}- pK_{A1}^{INT}) which compensates for the increase in modeled surface charge with a lower SSA.

Table 6.1. Model fits to SO_4-rich goethite titration data. $logK_A^{INT}$ values are given for I = 0 mol kg^{-1} (with standard deviations in parentheses). Weighted average equilibrium constants are also shown, with the 95% uncertainty level (in italics in parentheses). SSA = 220 m^2g^{-1}

I (mol kg^{-1})	$logK_{A1}^{INT}$	$logK_{A2}^{INT}$	N_s (nm^{-2})	WSOS/DF
0.004	-8.28 (0.012)	-9.83 (0.022)	0.76 (0.008)	80.3
0.020	-8.14 (0.011)	-9.68 (0.017)	1.00 (0.005)	34.2
0.100	-7.83(0.009)	-9.80 (0.012)	1.18 (0.005)	23.3
Weighted Average	**-8.14[a]**	**-9.82[a]**	**0.97**	
SO_4-rich goethite	*(-8.31,-7.97)*	*(-10.21, -9.43)*	*(0.65,1.28)*	
Weighted Average	**-8.17[a]**	**-9.93[a]**	**0.94**	
pure goethite (Chapter 5)	*(-8.30,-8.04)*	*(-10.23, -9.64)*	*(0.79,1.09)*	

[a] weighted average $logK_A^{INT}$ values determined with N_s fixed at 0.97 nm^{-2} (SO_4-rich goethite) or 0.94 nm^{-2} (pure goethite).

Figure 6.4 shows the sulfate-rich goethite titration data as surface charge vs pH, using a surface area of 220 m^2g^{-1} and modeled fits using the parameters optimized for pure goethite, i.e. Ns=0.94 nm^{-2}, $logK_{A1}^{INT}$=-8.17 and $logK_{A2}^{INT}$=-9.93. The model does provide a reasonable fit to the sulfate-rich goethite titration data, especially given that the only parameter varied from the pure goethite was the surface area. The surface charge was underestimated at pH>PPZC and overestimated at pH<PPZC until site saturation became significant in the model when the surface charge approached 0.15 Cm^{-2}. This occurred with the data at I of 0.02 and 0.1 $molkg^{-1}$ and caused a significant underestimation of the surface charge at for the data with pH < 5 and I = 0.1 mol kg^{-1}.

6.2b Site density derived from metal adsorption and sulfate desorption

The fact that the acidity constants for both pure and SO_4-rich goethite are the same , within experimental error, is important. Because the surface acid-base reactions compete with metal and ligand adsorption, the adsorption constants for metals and ligands will directly depend on the values of $logK_{A2}^{INT}$ and $logK_{A1}^{INT}$. The logK values are also dependent on the choice of

site density. Based on the results of modelling metal adsorption in the presence of SO_4 the best N_{s2} value for pure goethite was taken as 2.3 nm^{-2}, while N_{s1} was optimized from the data. In this section metal and ligand adsorption onto the sulfate-rich goethite is modeled assuming the $logK^{INT}$ values for adsorption are the same as those for adsorption on the pure acicular goethite, but the density of the type 1 and type 2 sites will be optimized to fit the data.

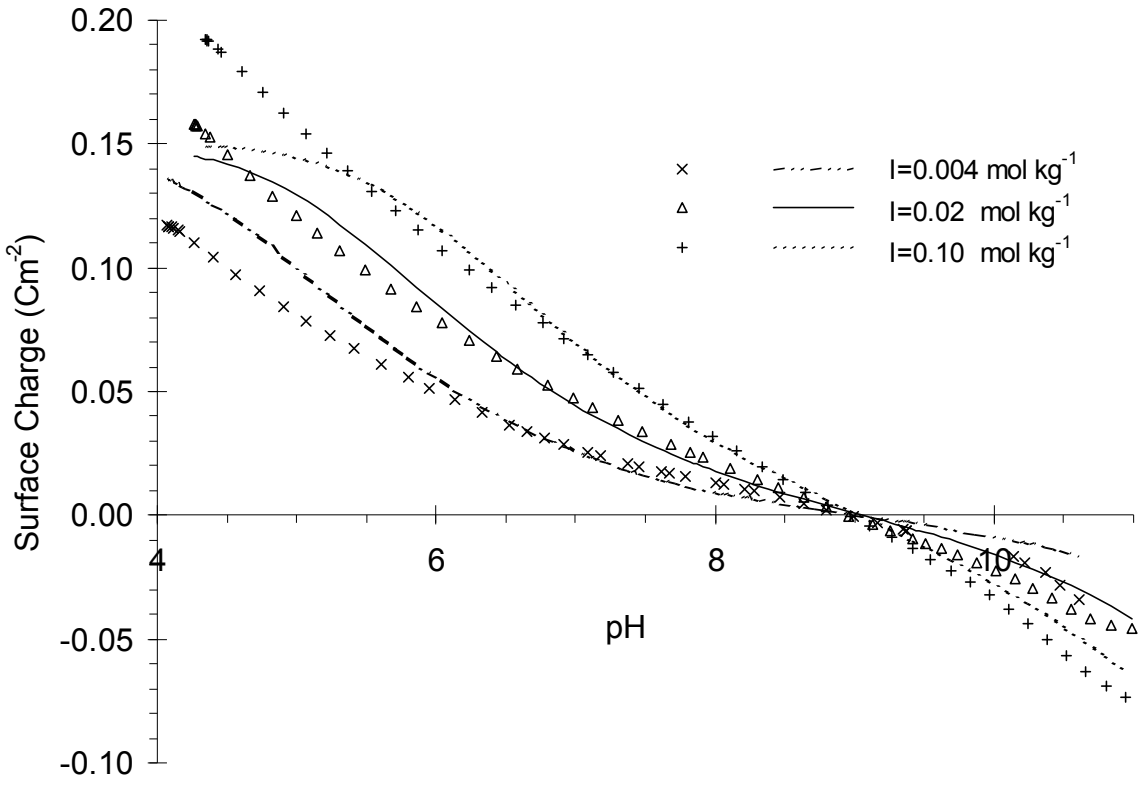

Figure 6.4 Experimental data (symbols) and modeled acid base titrations (lines) for goethite. Model fits used the parameters optimized for the pure goethite, i.e. Ns=0.94 nm^{-2}, $logK_{A1}^{INT}$=-8.17 and $logK_{A2}^{INT}$=-9.93.

Sulfate Desorption

The desorption of sulfate from the sulfate-rich goethite was measured as a function of pH and is shown in Figure 6.5. Sulfate was removed from the sulfate-rich goethite as suspension pH was raised until all the SO_4 was in the solution phase (pH 10). Even though SO_4 was present during goethite precipitation, and may be incorporated throughout the mineral, desorption at pH 10 was rapid, occurring within 10 min. The desorption data in Figure 6.5 are for samples after 3 days equilibration at the desired pH. After this length of time at high pH there was a decrease in the reversibility of SO_4 desorption. For example, after 3 days at pH 10.5 when the pH was returned to 3 only 60 % SO_4 was re-adsorbed, even 28 days after the pH hab been

lowered. This was significantly lower than in the original suspension (kept at pH 3) where 87 % of the sulfate was adsorbed at pH 3. This was not a kinetic effect as there was < 1 % change in adsorption between 1 day and 28 days after the pH was lowered to pH 3. Furthermore, SO_4 desorption was 92 % reversible after 30 min at pH 10. This would suggest that there might be some irreversible structural changes occurring in the goethite over time at high pH, which causes a decrease in its ability to re-adsorb SO_4.

To model the data the surface area was set initially to 220 m^2g^{-1} and the logK values for all adsorption reactions were fixed at the values determined for the pure acicular goethite using N_{s2} of 2.3 nm^{-2} as discussed in Chapter 5. The desorption data were then fitted by optimizing the N_{s2} site density. The optimized site density (given in Table 6.2) was 3.18 nm^{-2}. The model fit to the SO_4 data shown in Figure 6.5 used the weighted average site density determined for SO_4 and metal adsorption on SO_4-rich goethite as described below (Table 6.2).

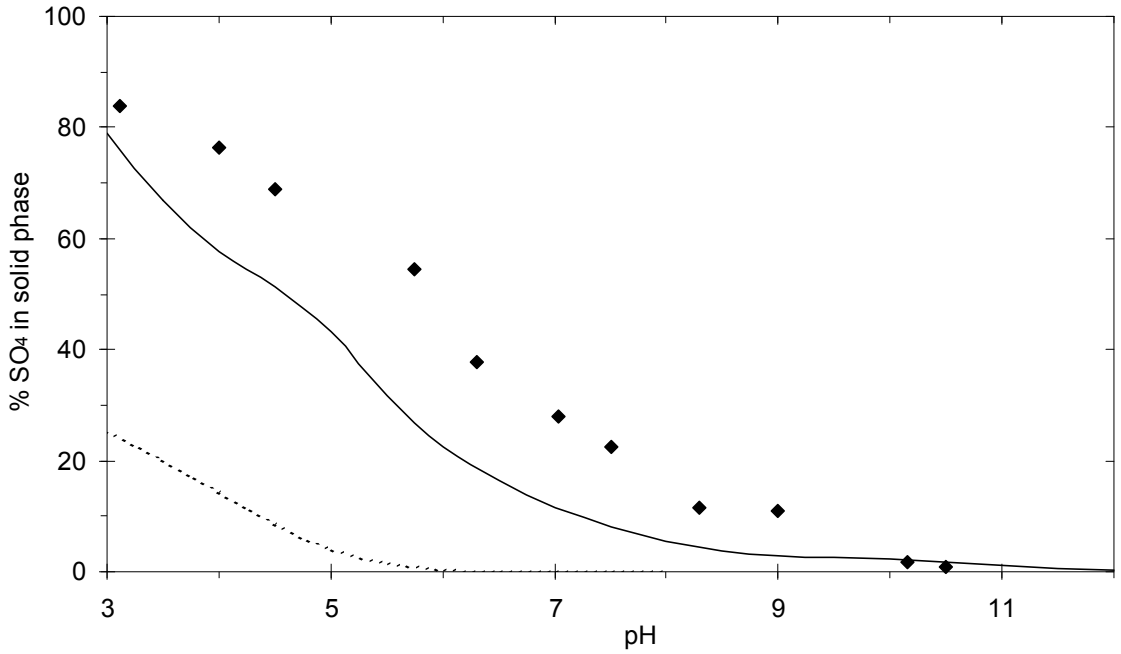

Figure 6.5 Sulfate desorption from sulfate-rich goethite as a function of pH. Showing experimental data (♦), and model fits using the adsorption parameters for pure goethite with N_{s2}=2.3 nm^{-2} and SSA of 270 m^2g^{-1} (———) or 80 m^2g^{-1} (-------).

Metal Adsorption

Isotherms for Cu, Pb, Zn and Cd adsorption onto sulfate-rich goethite were measured and the results are shown in Figure 6.6, with modeled fits as discussed below. Sulfate was not removed from the goethite prior to these adsorption experiments. For site density optimization, the surface area was initially set to 220 m^2g^{-1} and the logK for all adsorption

reactions were set to the values determined for the pure acicular goethite using N_{s2} of 2.3 nm^{-2} and N_{s1} of 0.024 nm^{-2} for Cd, Cu and Pb or 0.13 nm^{-2} for Zn. Optimizing the site densities for the high and low affinity sites then derived the best fit to the isotherm data. The optimized site densities from each isotherm are given in Table 6.2.

a) Low Affinity Sites

Based on the SSA estimate of 220 m^2g^{-1} for the sulfate-rich goethite, the N_{s2} values optimized from the metal isotherms ranged from 1.98 to 3.65 nm^{-2} with a weighted average of 2.8 nm^{-2}. This is 22 % larger than the N_{s2} from the pure acicular goethite. When the input SSA was varied from 200 to 300 m^2g^{-1} there was very little change in optimized site densities, on a moles of sites present in suspension basis. This corresponded to a steady decrease in site density (on a nm^{-2} basis) as the SSA was increased. A weighted average N_{s2} value of 2.3 nm^{-2} was obtained when the surface area was fixed at 270 m^2g^{-1}. Therefore, when compared to the pure goethite, the sulfate-rich goethite adsorption of metals and SO_4 was, on average, greater than expected from the titration data. However, because of the difficulties of measuring a surface area for this highly aggregated material, it is uncertain whether the SO_4-rich goethite deviates from the pure goethite in the titrations or in the N_{s2} derived from the adsorption experiments.

Consequently it could either be assumed that the site densities of the two goethites were the same and use a SSA of 270 m^2g^{-1} for the SO_4-rich goethite (in which case the titrations for the two goethites as shown in Figure 6.3 would differ) or use a SSA of 220 m^2g^{-1} for the SO_4-rich goethite in conjunction with a higher N_{s2} site density for metal and SO_4 adsorption (2.8 nm^{-2}). In Chapter 5 it was noted that the pure goethite surface acid-base titration curves from this study, Robertson and Leckie (1998) and Ali (1994) were quite different yet the Cu adsorption data, plotted on a nm^{-2} basis, were very similar. In addition, the process of removing the SO_4 from the SO_4-rich goethite prior to titrations involved 30 minutes at pH 10. After this time SO_4 adsorption was only 92 % reversible, so the SSA derived from fitting the titration data might be lower because of changes to the oxide in this time. For these reasons it seems more reasonable to use the higher SSA for the sulfate-rich goethite, having metal adsorption as close as possible to that expected from the pure goethite (on a nm^{-2} basis), and have the surface charging during acid-base titrations lower than the pure goethite. The modeled fits shown in Figures 6.5 and 6.6 therefore use a SSA of 270 m^2g^{-1}, N_{s2} site density of 2.3 nm^{-2} and the adsorption constants for pure goethite. In general the model is in agreement with the

shape and position of the metal isotherms (Figure 6.6). The greatest difference was underestimating the amount of SO_4 adsorbed as a function of pH (Figure 6.5), which may partly reflect the fact that the SO_4 data were for desorption rather than adsorption.

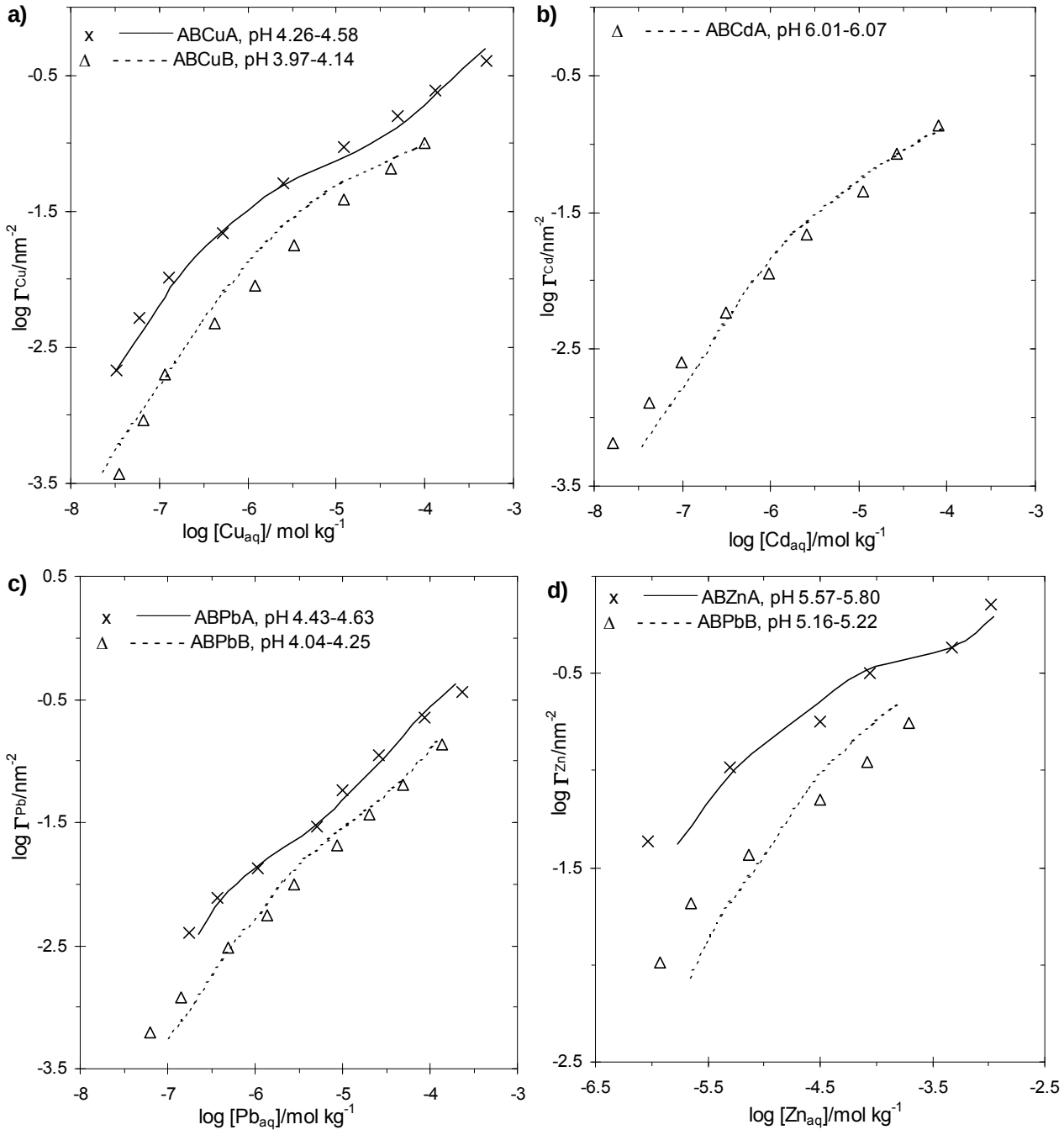

Figure 6.6 Experimental data (symbols) and modeled adsorption isotherms (lines) for Cu, Cd, Pb and Zn onto sulfate-rich goethite. Model fits used weighted average adsorption constants values in Table 5.5, as well as a SSA of 270 m^2g^{-1}, N_{s2} of 2.3 nm^{-2} and N_{s1} values as given in Table 6.2.

Table 6.2 Optimization of site densities for sulfate-rich goethite using adsorption constants derived from pure goethite with N_{s2}=2.3 nm^{-2}. Site densities were optimized for each data set using a SSA of 220 m^2g^{-1} and are given with standard deviations in parentheses. The weighted average values are also shown, with the 95% uncertainty level (in italics in parentheses) for SSA of 220 and 270 m^2g^{-1}.

Data	$Me_{(T)}$ $\mu mol\ kg^{-1}$	α-FeOOH $g\ kg^{-1}$	N_{s1} nm^{-2}	N_{s2} nm^{-2}	
ABCuA	1.75 to 830	1.80	0.051 (0.003)	3.31 (0.25)	8.35
ABCuB	0.325 to 17.7	1.72	0.081 (0.003)	3.65 (0.27)	6.61
ABCd	0.459 to 17.3	1.52	0.070 (0.002)	2.36 (0.25)	29.1
ABPbA	2.61 to 45.3	1.37	0.0303 (0.0008)	2.46 (0.12)	9.89
ABPbB	0.481 to 23.1	1.51	0.0248 (0.0006)	1.98 (0.12)	17.20
ABZnA	30.8 to 153	1.54	0.326 (0.007)	2.10 (0.36)	12.20
ABZnB	7.77 to 30.7	1.44	0.356 (0.011)	2.8[a]	50.5
ABS	$[SO_4]$=750	1.20	n.a.	3.18 (0.04)	14.3
Weighted average N_s 220 m^2g^{-1}				**2.8**	
(95 % confidence interval)				*(2.6, 3.0)*	
Weighted average N_s 270 m^2g^{-1}				**2.3**	
(95 % confidence interval)				*(2.1, 2.5)*	
Weighted average N_{s2} 220 m^2g^{-1} (Cu, Cd, Pb)			**0.049**		
(95 % confidence interval)			*(0.034, 0.064)*		
Weighted average N_{s2} 270 m^2g^{-1} (Cu, Cd, Pb)			**0.041**		
(95 % confidence interval)			*(0.029, 0.054)*		
Weighted average N_{s2} 220 m^2g^{-1} (Cu, Cd)			**0.083**		
(95 % confidence interval)			*(0.058, 0.11)*		
Weighted average N_{s2} 270 m^2g^{-1} (Cu, Cd)			**0.068**		
(95 % confidence interval)			*(0.048, 0.088)*		
Weighted average N_{s2} 220 m^2g^{-1} (Pb)			**0.033**		
(95 % confidence interval)			*(0.004, 0.063)*		
Weighted average N_{s2} 270 m^2g^{-1} (Pb)			**0.027**		
(95 % confidence interval)			*(0.003, 0.051)*		
Weighted average N_{s2} 220 m^2g^{-1} (Zn)			**0.42**		
(95 % confidence interval)			*(0.23, 0.60)*		
Weighted average N_{s2} 270 m^2g^{-1} (Zn)			**0.34**		
(95 % confidence interval)			*(0.20, 0.47)*		

[a] No convergence of this value so it was fixed at this value for consistency between results.

b) High Affinity Sites

The values for the high affinity sites using the SSA of 270 m^2g^{-1} are given in Table 6.2. The N_{s1} values were higher for the sulfate-rich goethite than the pure goethite (0.024 nm^{-2} for Cu, Cd and Pb and 0.13 nm^{-2} for Zn). This would suggest that the ratio of high to low affinity sites is higher for the sulfate-rich goethite. This could be considered to relate to the smaller particle

size of the sulfate-rich goethite. The average ratio of N_{s1} (for Cu, Cd and Pb) to N_{s2} sites for ferrihydrite, sulfate-rich goethite and pure goethite are 0.025, 0.017 and 0.010 nm^{-2} respectively, with the ratio for the sulfate-rich goethite intermediate between ferrihydrite and pure goethite. These values show a relationship with the surface areas used for the oxides of 600, 270 and 80 m^2g^{-1} respectively, with the higher surface area corresponding to higher N_{s1}/N_{s2}.

Venema et al. (1996b) have postulated that high affinity edge linkages occur on the goethite {021} face, and low affinity corner linkages occur on the {110} face. However, there was no difference in Cd adsorption behaviour for a goethite with a {021} face comprising either approximately 10 or 20 % of the surface area. The goethite with approximately 20 % surface area as {021} had shorter needles. The identical Cd adsorption behaviour on the two goethites was attributed to the presence of imperfections on the {110} plane. The SSA of the 20 % {021} face goethite used by Venema et al. (1996b) was not stated but presumably the difference in surface area for the two samples of Venema et al. (1996b) was considerably less than that of the two samples in this study.

The N_{s1} values for Pb adsorption onto SO_4-rich goethite are lower than those for Cu and Cd adsorption. Although there was a small overlap in the 95 % confidence intervals for the weighted averages determined for Pb compared to Cu and Cd, in the absence of more data sets it is assumed that the difference is real and therefore the N_{s1} values used were 0.027 nm^{-2} for Pb and 0.068 nm^{-2} for Cu or Cd. The isotherms plotted using the surface area of 270 m^2g^{-1} had a similar shape to those of the pure goethite, and the position of the isotherms were also similar. For example, both the pure goethite Pb isotherm at pH 4.17 to 4.23 and the sulfate rich goethite Pb isotherm at pH 4.04 to 4.25 had a data point at approximately $[Pb_{aq}] \approx 10^{-5}$ and $\Gamma_{Pb} \approx 10^{-1.7}$ nm^{-2}. This similarity belies the fact that the surface area of the sulfate-rich goethite used to calculate adsorption density was approximately 3 times larger than that of the pure goethite. Therefore in the above example, with $[Pb_{aq}] \approx 10^{-5}$ mol kg^{-1}, the sulfate-rich goethite would have approximately 3 times as much Pb adsorbed per mol of Fe than the pure acicular goethite.

The Effect of Sulfate on Metal Adsorption

It is important to quantify the effect of sulfate on metal adsorption to the sulfate-rich goethite. Webster et al. (1998) found that removing the SO_4 from the Tui mine sulfate-rich goethite shifted the Cu adsorption edge by 0.2 pH units to a higher pH. Based on the above approach to modelling, the measured SO_4 content and the ternary complexes for pure goethite, the anticipated shift in pH edge would only be approximately 0.03 pH units. To shift the Cu adsorption edge by 0.2 pH units would require approximately 5×10^{-3} mol kg^{-1} $SO_{4(T)}$, compared to the measured value of approximately 1×10^{-4} mol kg^{-1}. There are two explanations for this difference in the measured and modelled effect of SO_4. Either the effect of SO_4 is greater in the SO_4-rich goethite than solution SO_4 with pure goethite, or the high pH required to remove SO_4 (Webster et al. 1998) has in fact changed the oxide surface to lower the absorbance. It had been noted that after 30 minutes at pH 10 adsorption of SO_4 was only 92 % reversible, and after 3 days at pH 10, SO_4 adsorption was only 70 % reversible. Webster et al. (1998) removed the SO_4 by keeping the oxide at pH 10 overnight, so there may have been changes to the oxide that may have decreased the extent of Cu adsorption, in addition to the removal of SO_4.

To distinguish between these two options, Cu adsorption edges onto SO_4-rich goethite were measured with and without added solution SO_4 to see how additional SO_4 shifted the adsorption edge. The pH of 50 % adsorption (pH_{50}) was calculated by fitting the Boltzman sigmoidal equation to the data and had between 0.02 and 0.03 standard error. Addition of 1×10^{-3} mol kg^{-1} SO_4 and 1×10^{-2} mol kg^{-1} SO_4 to the oxide shifted the curve to lower pH by 0.05 and 0.11 pH units respectively. Because of the high Cu_T/Fe of these edges, the effect of SO_4 is fairly small so the differences in pH_{50} are not great. From modelling, this shift in adsorption edges corresponds to an initial SO_4 concentration of approximately 3×10^{-4} mol kg^{-1} SO_4. This was closer to the measured SO_4 concentration than the value of 5×10^{-3} mol kg^{-1} SO_4, which was estimated from the effect on the Cu adsorption edge of removing SO_4. For modelling real systems it is desirable to use the measured concentration of components and, given the small shifts in pH_{50} due to addition or removal of SO_4, it seems reasonable to use the measured SO_4 concentration even though this may somewhat underestimate the effect of SO_4 in these systems.

6.3 CONCLUSIONS

Compared to adsorption onto pure goethite described in Chapter 5, the sulfate-rich goethite had a considerably higher site density per mol of oxide. The sulfate-rich goethite titration data (after removal of SO_4) could be modelled reasonably accurately using the parameters developed to model the pure goethite titrations (including the same site density per unit area) but with a surface area of 220 m^2g^{-1}, compared to 80 m^2g^{-1} for the pure goethite. In contrast, the average surface area required to model metal adsorption and SO_4 desorption using the pure goethite parameters was somewhat larger, at 270 m^2g^{-1}. The sulfate-rich goethite also appeared to have a higher ratio of high affinity metal adsorption sites to low affinity sites, compared to pure goethite. For sulfate-rich goethite, the site density of high affinity sites for Pb was less than for Cu and Cd. In general, therefore, the parameters developed for pure goethite are apparently similar to those for the sulfate-rich goethite, but are not directly transferable. The difficulty in measuring the surface area of the highly aggregated sulfate-rich goethite makes a definitive comparison between the adsorptive behaviour of the two goethites more difficult.

CHAPTER SEVEN
DISCUSSION AND APPLICATIONS

7.1 INTRODUCTION

The overall aim of this study was to provide insight into trace metal adsorption onto the various iron oxyhydroxides that are typically present in AMD systems. Rather than an empirical study of adsorption onto a naturally occurring sorbate, this study has aimed to incrementally increase the complexity of the experimental adsorption systems to approach the simulation of adsorption occurring in AMD environments. Chapters 3, 4 and 5 have considered the effect of solution heterogeneity on trace metal adsorption onto pure synthetic ferrihydrite, goethite and, to a lesser extent, schwertmannite. Specifically the effect of pH, [metal] and [SO_4] were considered. In Chapter 6 the parameters developed to model metal adsorption onto pure acicular goethite were applied to a SO_4-rich goethite synthesized from the $FeSO_4$ oxidation at pH 3.0.

In this chapter modelled metal adsorption onto ferrihydrite and goethite are compared. Ferrihydrite adsorption is modelled without SO_4 and with 0.01 mol kg^{-1} SO_4. The ferrihydrite model with 0.01 mol kg^{-1} SO_4 was considered to be a reasonable estimate of Cu and Zn adsorption onto schwertmannite at low Me_T/Fe. Goethite adsorption is modelled both on the pure acicular and SO_4-rich goethites. The modelling parameters developed in this work are then applied to the data from Webster et al. (1998). The emphasis is on comparing the modelled and experimental adsorption onto the SO_4-rich goethite, which was collected from the stream below the Tui mine tailings impoundment near Te Aroha, New Zealand. The model parameters from this work were also applied to Tonkin et al. (2002) data from experiments mixing AMD waters with neutral drainage. Lastly the conclusions drawn from this work are presented.

7.2 COMPARISON BETWEEN THE OXIDES

The parameters required for modelling adsorption are surface area, site densities, acidity constants, and adsorption constants. When comparing metal adsorption on different oxides it is important to bear in mind that these parameters are strongly interdependent and one cannot simply compare adsorption constants. Furthermore, with the exception of the surface area of the acicular goethite, these parameters cannot be measured directly or independently of assumptions relating to other parameters and experimental design. For example, optimised

acidity constants will be not only dependent on the surface area and site density used but also on the efficiency of CO_2 exclusion in the experimental design. Finally the value of the adsorption constant (e.g. Equation 7.1) will be dependent on all the other parameters. The site density will directly affect the number of available surface sites ([≡FeOH]), the acidity constants will affect the proportion of the total sites ($\equiv FeOH_T$) that are available for adsorption (i.e. present as ≡FeOH) and the surface area will affect the surface potential. Values for the parameters used to model adsorption in this work are given in Table 7.1.

$$[\equiv FeOMe^{+}] = [\equiv FeOH^{0}][H^{+}]^{-1}[Me^{2+}]\exp(-F\Psi/RT)(\gamma_H)^{-1}\gamma_{Me}K^{INT} \quad \text{Eq. 7.1}$$

Table 7.1 A summary of the recommended parameters which can be used to model adsorption onto ferrihydrite, pure goethite and SO_4-rich goethite.

Parameter	ferrihydrite	acicular goethite	SO_4-rich goethite
surface area (m^2g^{-1})	600	80	270 [a]
N_{s2} (nm^{-2})	2.3	2.3	2.3[a]
N_{s1} (nm^{-2})	0.056	0.024[b], 0.13[c]	0.068[d], 0.028[e], 0.34[c]
N_{s0} (nm^{-2})	0.0039[e]	n.a.	n.a.
N_{s2} (mol Fe)$^{-1}$	0.20	0.027	0.092
N_{s1} (mol Fe)$^{-1}$	0.005	0.00028[b], 0.0015[c]	0.0027[d], 0.0011[e], 0.014[c]
N_{s0} (mol Fe)$^{-1}$	0.00035[e]	n.a.	n.a.
$\log K_{A1}^{INT}$	-7.29	-7.38	-7.38[a]
$\log K_{A2}^{INT}$	-8.93	-10.74	-10.74[a]
$\log K_{1Cu}^{INT}$	2.85	4.41	4.41[a]
$\log K_{2Cu}^{INT}$	0.60	1.68	1.68[a]
$\log K_{0Pb}^{INT}$	7.20	n.a.	n.a.
$\log K_{1Pb}^{INT}$	5.33	4.78	4.78[a]
$\log K_{2Pb}^{INT}$	1.99	1.52	1.52[a]
$\log K_{1Cd}^{INT}$	0.43	1.29	1.29[a]
$\log K_{2Cd}^{INT}$	-2.69	-1.83	-1.83[a]
$\log K_{1Zn}^{INT}$	0.97	1.30	1.30[a]
$\log K_{2Zn}^{INT}$	-1.99	-1.21	-1.21[a]
$\log K_{1Cu}^{TC}$	n.a.	11.48	11.48[a]
$\log K_{2Cu}^{TC}$	7.83	8.44	8.44[a]
$\log K_{1Pb}^{TC}$	11.57	11.62	11.62[a]
$\log K_{2Pb}^{TC}$	9.48	8.84	8.84[a]
$\log K_{1Cd}^{TC}$	n.a.	9.48	9.48[a]
$\log K_{2Cd}^{TC}$	6.46	7.00	7.00[a]
$\log K_{1Zn}^{TC}$	n.a.	9.28	9.28[a]
$\log K_{2Zn}^{TC}$	6.67	6.52	6.52[a]

[a] fixed at this value for consistency with acicular goethite
[b] Cu, Cd and Pb
[c] Zn
[d] Cu and Cd
[e] Pb

The density of the low affinity adsorption sites (N_{s2}) that best described all the goethite data was equivalent (on a nm^{-2} basis) to the value used for ferrihydrite by Dzombak and Morel (1990). However, because of its much higher surface area ferrihydrite has 7.5 times (i.e. 600/80) more sites per gram (or per mole) than the pure acicular goethite used in this study. Also, the $\log K_{A1}^{INT}$ values for ferrihydrite and goethite were similar, although the goethite $\log K_{A2}^{INT}$ was considerably lower than that of ferrihydrite, reflecting the higher goethite PPZC. As a consequence of the similarity in low affinity site density (per nm^2) and $\log K_{A1}^{INT}$, both the surface charge and the proportion of surface sites that are available for adsorption in acidic conditions (i.e. not protonated) will be similar for the two oxides.

This allows a comparison to be made of metal adsorption at low adsorption densities for the two oxides under acid conditions, by simply considering the site densities and adsorption constants. Note that acid-base reactions at the low affinity sites will dominate the surface potential (Ψ) at low metal adsorption densities, therefore the difference in the ferrihydrite and goethite high affinity site densities will not significantly affect Ψ. From Equation 7.1, the ratio $[\equiv Fe_1OMe^+]/[Me^{2+}]$ at constant pH and Ψ will be proportional to $[\equiv Fe_1OH] \times K_{1Me}^{INT}$. As discussed above, because N_{s2} and $\log K_{A1}^{INT}$ for ferrihydrite and goethite are almost identical, the proportion of total sites available for adsorption (i.e. $[\equiv Fe_1OH]/[\equiv Fe_1OH]_T$) at a given pH will be almost identical for ferrihydrite and goethite. Therefore $N_{s1} \times K_{1Me}^{INT}$ can be used to compare the relative extent of adsorption of metals at low adsorption density on the two oxides. Table 7.2 gives $N_{s1} \times K_{1Me}^{INT}$ values for Cu, Pb, Cd and Zn on ferrihydrite, pure goethite and SO_4-rich goethite. Note that the above argument does not consider the effect of SO_4 and will therefore tend to underestimate metal adsorption onto the SO_4-rich goethite. Figure 7.1 shows the adsorption isotherms for Cu and Pb at pH 4, and for Zn and Cd at pH 6 using the parameters from Table 7.1. Isotherms are plotted with adsorption density as mol (mol Fe)$^{-1}$.

Metal	ferrihydrite	acicular goethite	SO_4-rich goethite
Cu	3.54	7.20	69.4
Pb	1069	16.9	66.3
Cd	0.0135	0.00546	0.0526
Zn	0.0467	0.0299	0.279

.

Table 7.2. Values for $N_{s1} \times K_{1Me}^{INT}$ for Cu, Pb, Cd and Zn adsorption onto ferrihydrite, pure goethite and SO_4-rich goethite. N_{s1} values are expressed as mol (mol Fe)$^{-1}$.

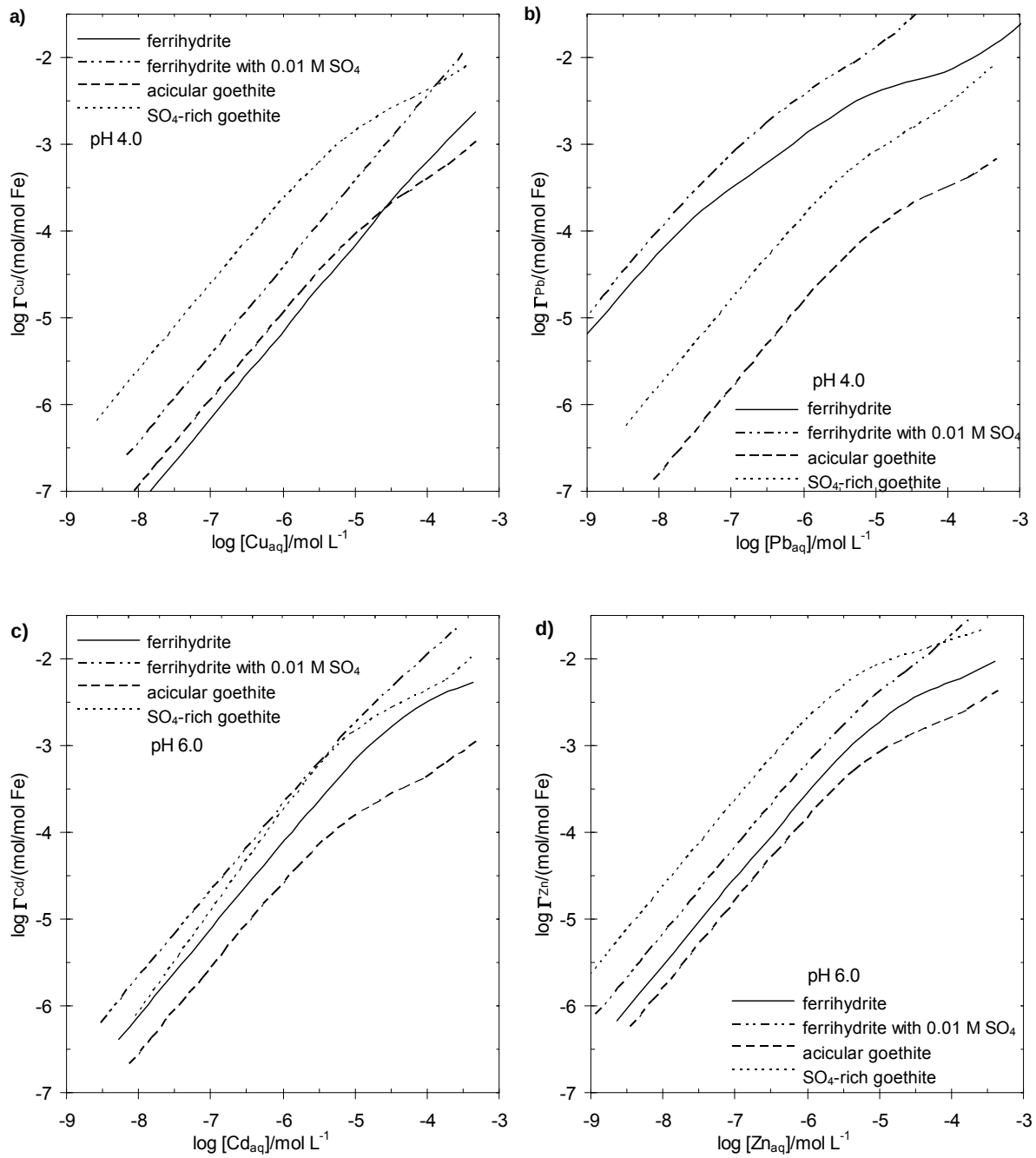

Figure 7.1 Model adsorption onto ferrihydrite (with and without 0.01 mol kg^{-1} SO_4) acicular goethite and SO_4-rich goethite. a) Cu, b) Pb, c) Cd, d) Zn. Model used the parameters from Table 7.1.

In the region of low adsorption density in Figure 7.1, the order of adsorption onto the oxides does, in general, follow the trend of the $N_{s1} \times K_{1Me}^{INT}$ values, with higher $N_{s1} \times K_{1Me}^{INT}$ corresponding to higher adsorption densities. For example, Cu adsorption is in the order SO_4-rich goethite>>acicular goethite>ferrihydrite. However, at higher site coverage, the lower site density of acicular goethite causes a reverse in the order of ferrihydrite and goethite. In contrast, Pb adsorption was in the order ferrihydrite>>SO_4-rich goethite> acicular goethite. At

low adsorption density, Zn and Cd adsorption are in the order SO_4-rich goethite>ferrihydrite>acicular goethite.

Compared to the Pb isotherms, the Cu, Cd and Zn isotherms on acicular goethite and ferrihydrite are fairly similar. This is due to the larger $\log K^{INT}$ values of goethite compensating for the lower site densities. The differences between the goethite and ferrihydrite $\log K_1^{INT}$ values were 0.33, 0.86 and 1.56 for Zn, Cd and Cu. The low difference for Zn is a reflection of the higher type-one site density for Zn adsorption on goethite. The differences between the goethite and ferrihydrite $\log K_2^{INT}$ values were 0.78, 0.86 and 1.08 for Zn, Cd and Cu. These values can be compared to the ratio of goethite to ferrihydrite site densities, i.e. $10^{-0.87}$ for N_{s2}, $10^{-1.3}$ for N_{s1} (for Cu and Cd) and $10^{-0.52}$ for N_{s1} (for Zn). These site density ratios are expressed as exponents so that they can be directly compared to the differences in logK values for metal adsorption onto the two oxides. Therefore the larger goethite adsorption constants are approximately balanced by the lower site density which explains why, for Cu, Cd and Zn, the ferrihydrite and acicular goethite adsorption isotherms are fairly close. Copper, Zn and Cd adsorption onto the SO_4-rich goethite exceeds that onto ferrihydrite because these same relatively high adsorption constants for goethite are combined with the considerably higher site densities of the SO_4-rich goethite (compared to the acicular goethite).

In the case of Pb, both the site densities and the adsorption constants are larger on ferrihydrite than goethite. Therefore the adsorption of Pb on ferrihydrite is much greater than onto goethite. For Pb adsorption, the higher site densities of the SO_4-rich goethite compared to the acicular goethite do not compensate for the low $\log K^{INT}$ values of Pb adsorption on goethite. Therefore SO_4-rich goethite adsorption of Pb is lower than that of ferrihydrite.

7.3 COMPARISON TO PREVIOUS STUDIES

The impetus for the current study was the work of Webster et al. (1998), which compared Cu, Zn, Cd and Pb adsorption onto synthetic ferrihydrite, synthetic schwertmannite and a natural SO_4-rich goethite collected from the drainage of the Tui mine tailings impoundment near Te Aroha, New Zealand. Before comparing the experimental data of Webster et al. (1998) to model fits based on the parameters from the current study, differences in the methods used in the two studies need to be considered. The three main differences are that the Webster et al. (1998) study used a SO_4-rich goethite that had not been dried, used a shorter equilibration

time for adsorption experiments and also conducted experiments under an air atmosphere, as opposed to Ar or N_2 atmospheres as used in the current study.

Effect of freeze-drying

In the current study goethite samples were freeze-dried. Drying samples allowed comparison with Ali and Dzombak (1996a) and, in general, enables long-term studies on field samples of metastable phases such as ferrihydrite and schwertmannite. Lane (2001) compared the adsorption of Cu onto freeze-dried SO_4-rich oxide from the Tui mine drainage system and freeze-dried synthetic SO_4-rich goethite prepared from the abiotic oxidation of $FeSO_4$ at pH 3.0. Figure 7.2 shows the comparison of Cu adsorption on the dried (Lane, 2001) and un-dried (Webster et al., 1998) SO_4-rich goethites. The adsorption data of Lane (2001) are from experiments with 2.0 mM freeze-dried α-FeOOH and demonstrated that the adsorption edges for the synthetic and natural (Tui mine) SO_4-rich goethites were essentially identical. In addition, these edges were generally reasonably well predicted by the model for SO_4-rich goethite described in Chapter 6, apart from a degree of underestimation of adsorption where adsorption was > 50 %.

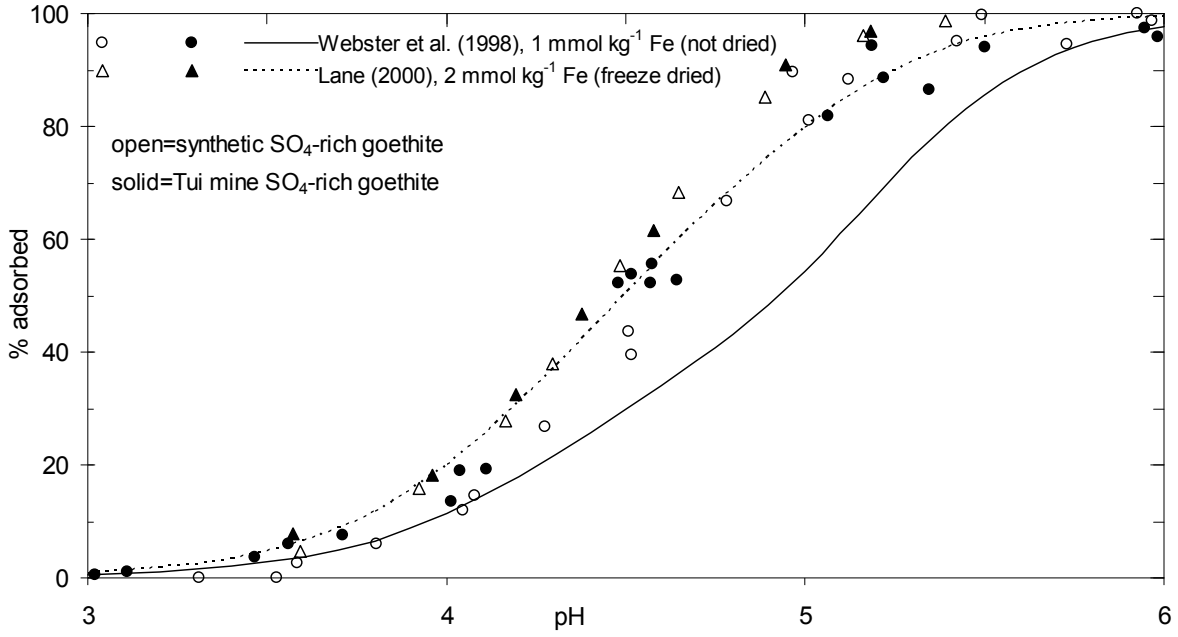

Figure 7.2 Adsorption of Cu (7.87 x 10^{-6} mol kg^{-1}) onto synthetic and natural (Tui mine) samples of SO_4-rich goethite.

The adsorption data of Webster et al. (1998) are from experiments with 1.0 mM α-FeOOH that were not dried and the adsorption edges for the synthetic and Tui mine SO_4-rich goethites

were also essentially identical. However, modelled adsorption of these edges was generally poor, with under estimation by up to 30 % where adsorption was > 10 %. This suggests that freeze-drying the SO_4-rich goethites may have decreased its ability to adsorb Cu. This is further demonstrated in Figure 7.3 where the SO_4-rich goethite data interpolated from Webster et al. (1998) is plotted with the isotherms from the current study. In general the data from Webster et al. (1998) have higher adsorption densities that the data from the current study using a dried SO_4-rich goethite. This was especially true for the Cu and Zn data with lower Me_T and the data at higher pH. This is consistent with the effect of drying the oxide evident in Figure 7.2 and suggests that the decrease in adsorption on the dried oxide is due to a decrease in the number of available surface sites. Note that both the current study and Webster et al. (1998) used ferrihydrite and schwertmannite that had not been dried.

Effect of equilibration time

Webster et al. (1998) used an equilibration time up to 2 h, compared with 24-48 h in the current study. In Chapter 4 it was noted that ferrihydrite adsorption of Pb increased from 56% to 67% between 4 h and 24 h. Therefore the difference in equilibration times may be significant when comparing the data from this work and that of Webster et al. (1998).

Effect of using an air or inert atmosphere

Differences in Cu, Cd, Zn or Pb adsorption under air compared to N_2 or Ar would be due to the presence of CO_2. Villalobos et al. (2001) found that CO_2 did not affect Pb adsorption by goethite. However, CO_2 dissolving into a solution will change the solution pH and could influence adsorption data if the pH changes after sample equilibration, as in the case of the pH being measured in an open vessel after equilibration in a closed vessel.

Model fits to Webster et al. (1998) data

The data from Webster et al. (1998) are shown in Figure 7.4 and 7.5 with model predictions using the parameters developed in this study. For some scenarios the model predicted that metals would be oversaturated with respect to their oxides or hydroxides and this precipitation was included with the predicted adsorption as discussed below. Model predictions for Cu, Zn and Cd adsorption onto schwertmannite were based on ferrihydrite adsorption with 0.01 mol kg^{-1} SO_4.

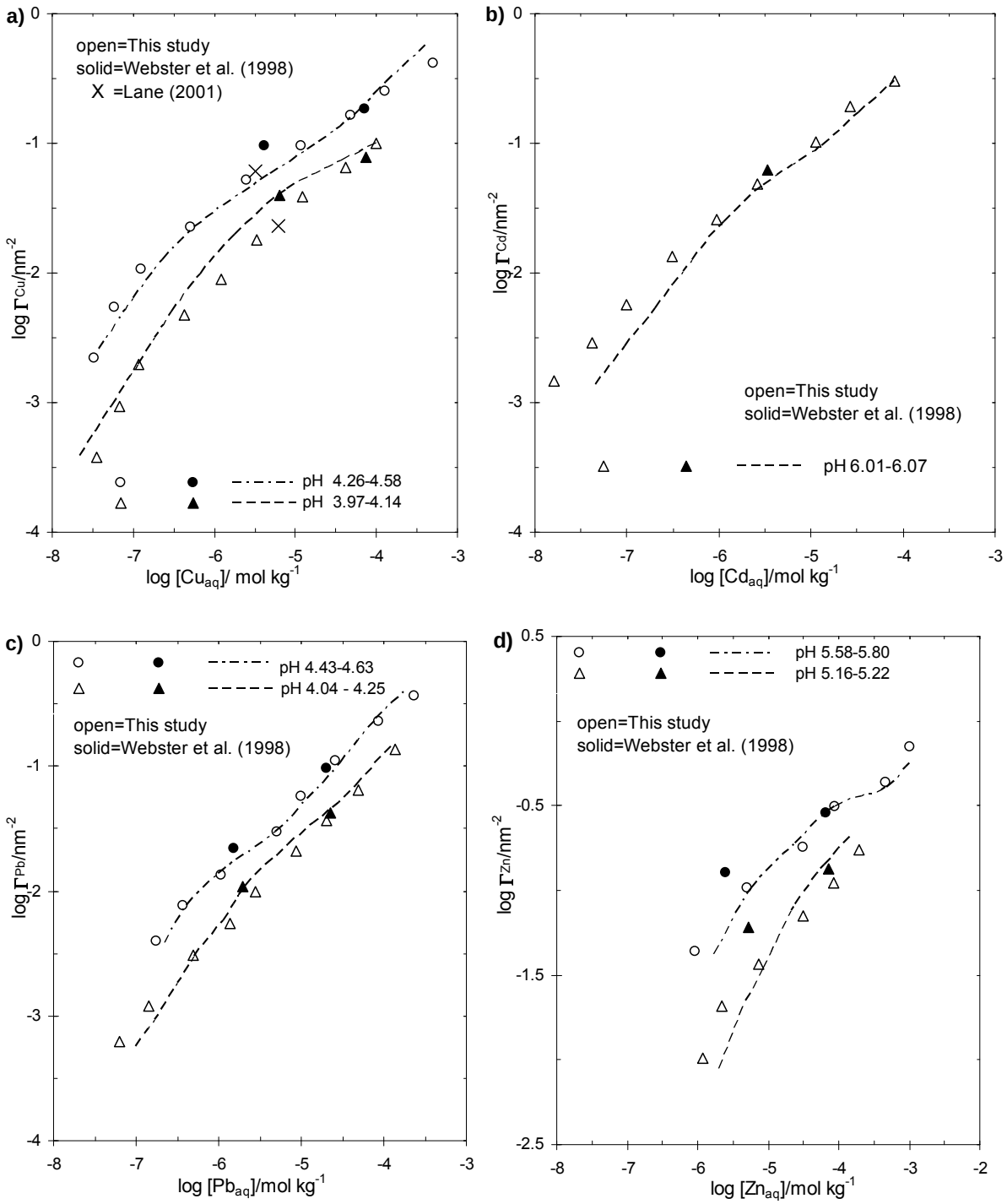

Figure 7.3 Adsorption isotherms for freeze-dried synthetic SO_4-rich goethite (o, △) with data points interpolated from adsorption edges for the natural SO_4-rich goethite that had either been freeze dried, x (Lane, 2001) or not dried (▲,●)(Webster et al., 1998). a) Cu, b) Cd, c) Pb, d) Zn.

Schwertmannite predictions are not shown for Pb adsorption, because the anomalously high adsorption of Pb onto ferrihydrite meant that the ferrihydrite adsorption of Pb occurred at a lower pH than schwertmannite, even though SO_4 enhanced the ferrihydrite adsorption of Pb. Removing adsorbed SO_4 from schwertmannite further increased the pH of the schwertmannite

adsorption edge (Webster et al. 1998), demonstrating that SO_4 does enhance the schwertmannite adsorption of Pb. Consequently the adsorption of Pb onto schwertmannite could not be modelled using ferrihydrite and 0.01 mol kg^{-1} SO_4. This decreased adsorption of Pb on schwertmannite compared to ferrihydrite was similar to the decreased adsorption of Pb on goethite compared to ferrihydrite, but occurred to a lesser extent. On goethite the Pb and Cu adsorption edges were very similar, however on schwertmannite Pb adsorption still occurred at a lower pH than Cu, but the difference was less than that between Cu and Pb adsorption on ferrihydrite (Figure 7.4, Webster et al. 1998).

Copper

The modelled ferrihydrite adsorption edge with Cu_T of 7.87 μmol kg^{-1} (Figure 7.4a) is slightly steeper than the experimental edge. The model agrees with the experimental data where adsorption is < 10 % but is at lower pH, by up to 0.3 pH units, where adsorption is >10 %. In the current study (Chapter 3) Cu adsorption on ferrihydrite was measured for a range of the Cu_T/Fe which covered the Cu_T/Fe in Figure 7.4a and there was no significant difference between the modelled and measured adsorption. This would suggest that the difference in Figure 7.4a) is due to differences in the experimental methods, possibly the shorter equilibration time of Webster et al. (1998).

The modelled schwertmannite adsorption edge with 7.87 μmol kg^{-1} Cu_T (Figure 7.4a) is generally in good agreement with the experimental edge, being displaced by no more than 0.1 pH units. This is consistent with the observation that the adsorption edges for schwertmannite and ferrihydrite with 0.01 mol kg^{-1} SO_4 were essentially identical at this Cu_T/Fe ratio. The reason why adsorption onto ferrihydrite was over-predicted but not adsorption onto schwertmannite is not clear.

In contrast the modelled SO_4-rich goethite edge with 7.87 μmol kg^{-1} Cu_T (Figure 7.4a) agreed with the experimental data where adsorption was < 20 % but then is shifted to higher pH, by up to 0.5 pH units, where adsorption is >20 %. This underestimation of adsorption onto the natural SO_4-rich goethite, as discussed above, is likely to be due to the effect of freeze-drying the goethite. The adsorption edge measured with freeze-dried SO_4-rich goethite (Figure 7.2) was accurately predicted using the model parameters developed in this study.

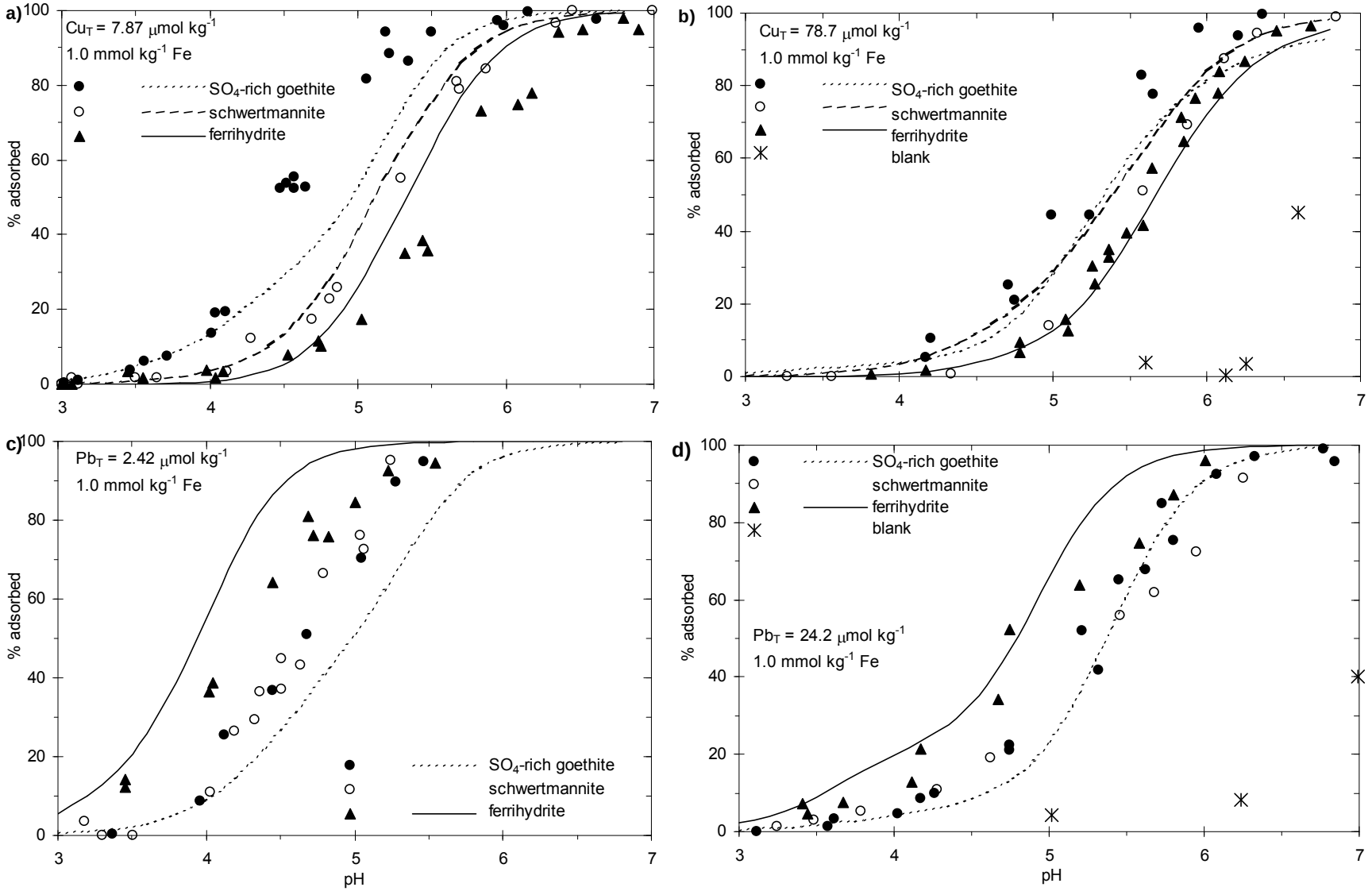

Figure 7.4 Adsorption data of Webster et al. (1998) modelled using the parameters from this study. Modelled adsorption for schwertmannite (where shown) used the parameters for ferrihydrite in the presence of 0.01 mol kg^{-1} SO_4. Blank data show precipitation for experiments with no iron oxyhydroxide. Modelled adsorption includes predicted bulk phase precipitation as discussed in the text, but does not include surface precipitation.

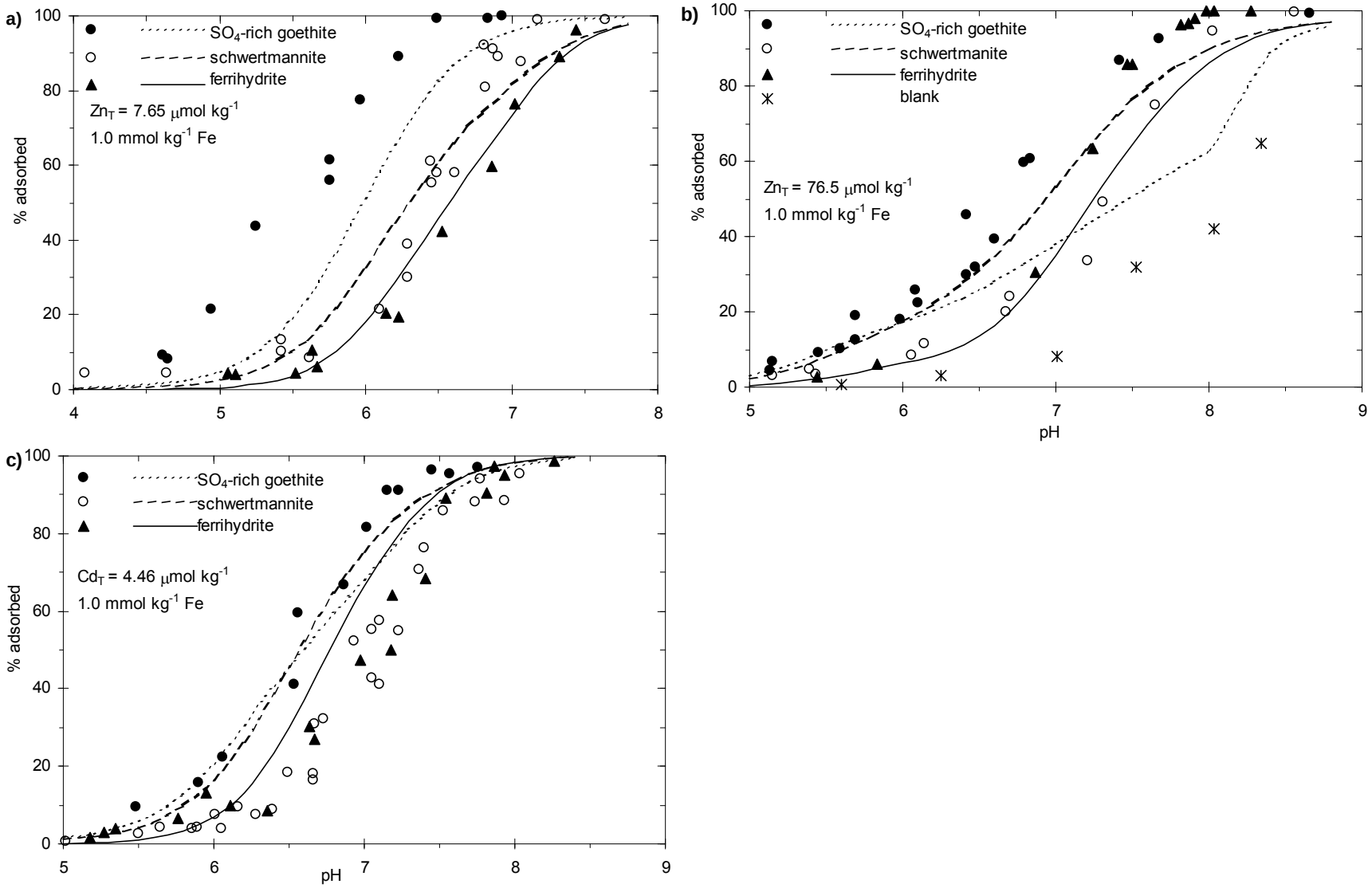

Figure 7.5 Adsorption data of Webster et al. (1998) modelled using the parameters from this study. Modelled adsorption for schwertmannite (where shown) used the parameters for ferrihydrite in the presence of 0.01 mol kg^{-1} SO_4. Blank data show precipitation for experiments with no iron oxyhydroxide. Modelled adsorption includes predicted bulk phase precipitation as discussed in the text, but does not include surface precipitation.

For the data with 78.7 μmol kg^{-1} Cu_T (Figure 7.4b) the modelled and experimental ferrihydrite adsorption edges are generally in good agreement, with the model being approximately 0.1 pH units higher where adsorption is > 50%. The experimental schwertmannite edge is essentially the same as the ferrihydrite edge, whereas the model with ferrihydrite and 0.01 mol kg^{-1} SO_4 shifts the adsorption edge to lower pH by up to 0.4 pH units. The effect of SO_4 on the ferrihydrite adsorption of Cu was not measured for a Cu_T/Fe as high as that of this data (0.0787). Therefore it remains uncertain whether the difference between the model and the data reflects a true difference in the adsorption of Cu onto schwertmannite, or a difference in the effect of SO_4 on Cu adsorption by ferrihydrite at this high Cu_T/Fe ratio.

The modelled SO_4-rich goethite adsorption edge with 78.7 μmol kg^{-1} Cu_T is at higher pH than the measured, by up to 0.2 pH units. Where adsorption is > 80 % there is evidence of the effects of limited site availability at the high Cu/Fe as the modelled SO_4-rich goethite edge plateaus and crosses below that of ferrihydrite. With a site density of 2.3 nm^{-2} and a surface area of 270 m^2g^{-1} the number of moles of sites available would be 92 μmol kg^{-1}, which is close to the Cu_T of 78.7 μmol kg^{-1}. The modelled adsorption onto SO_4-rich goethite includes 4.6 % bulk phase precipitation of copper hydroxide at pH 6.8. It is possible that surface precipitation occurs at pH < 6.8 and, in addition to the effect of drying on adsorption by the SO_4-rich goethite, could account for the differences between the modelled and experimental data. Surface precipitation is discussed in relation to the Zn data of Webster et al. (1998).

Lead

The adsorption data with 2.42 μmol kg^{-1} Pb_T (Figure 7.4c) show a similar pattern to the Cu data in Figure 7.4a. The modelled ferrihydrite Pb adsorption edge is slightly steeper than the experimental edge, and is at lower pH than the experimental data, by up to 0.4 pH units. In the current study (Chapter 4) Pb adsorption on ferrihydrite was measured for a Pb_T/Fe of 1.93 x 10^{-3}, which is similar to the Pb_T/Fe in Figure 7.4c. For the data of this study (Figure 4.4b) the model edge was again steeper than the experimental edge, but the modelled and measured pH of 50 % adsorption were within ± 0.1 pH unit. This would suggest that the difference in the ferrihydrite data in Figure 7.4c) is due to differences in the experimental method, presumably the shorter equilibration time of Webster et al. (1998). This is consistent with the kinetics of Pb adsorption on ferrihydrite as discussed in Chapter 4.

The modelled ferrihydrite adsorption edge with 24.2 μmol kg^{-1} Pb_T (Figure 7.4d) is also slightly steeper than the experimental edge, and at lower pH than the experimental data by up to 0.3 pH units. The modelled SO_4-rich goethite adsorption edge with 24.2 μmol kg^{-1} Pb_T is only slightly steeper than the experimental edge but the modelled and measured pH of 50 % adsorption were within ± 0.1 pH unit. Because of the lower Me_T/Fe (compared to the experiments with Cu) there is no evidence of site saturation or bulk phase precipitation in the modelled adsorption.

Zinc

The ferrihydrite and schwertmannite adsorption edges with 7.65 μmol kg^{-1} Zn_T (Figure 7.5a) were generally well modelled using the parameters from this study and from Dzombak and Morel (1990). However, the modelled SO_4-rich goethite Zn adsorption edge is up to 0.5 pH units higher than the experimental data, leading to an underestimation of adsorption. There has been no experimental comparison between synthetic and natural SO_4-rich goethite adsorption of Zn. Therefore it is possible that the observed difference between the model and experimental data could be caused by a decrease in adsorption due to drying and/or another difference between the synthetic and natural SO_4-rich goethites.

The ferrihydrite adsorption edge with 76.5 μmol kg^{-1} Zn (Figure 7.5b) was generally well modelled using the parameters from Dzombak and Morel (1990) where adsorption was less than 30 %. At higher adsorption the experimental data rises more steeply than the model, and is up to 0.5 pH units lower than the model prediction. In fact the measured adsorption onto ferrihydrite is greater than onto schwertmannite in this pH region. Although the model solution remains undersaturated with respect to bulk phase precipitation of $Zn(OH)_2$, the least soluble Zn mineral under these conditions, surface precipitation may still be occurring. Surface precipitation is considered to be the formation of a Fe and Zn oxyhydroxide solid solution, where the activity of each solid species is equal to the mole fraction of that species in the solid solution (Dzombak and Morel, 1990). Therefore surface precipitation can occur at lower pH, or lower [Zn], than bulk phase precipitation.

Dzombak and Morel (1990) modelled the effect of surface precipitation for Zn adsorption onto ferrihydrite at high Zn_T/Fe ratios using $K_{sp} = 10^{-3.16}$ and $10^{-11.92}$ for the precipitation of $Fe(OH)_3$ and $Zn(OH)_2$ respectively at an ionic strength of 0.1 mol kg^{-1}. Using these surface

precipitation parameters for the ferrihydrite adsorption edge with 76.5 μmol kg^{-1} Zn causes adsorption to increase by up to 10 % (Figure 7.6), which brings the modelled curve closer to the experimental data. The speciation for the solid phase Zn shows that $Zn(OH)_2$ accounts for up to 40 % of the total Zn, but because precipitation and adsorption are competitive the net change in solid phase Zn is no more than 10%..

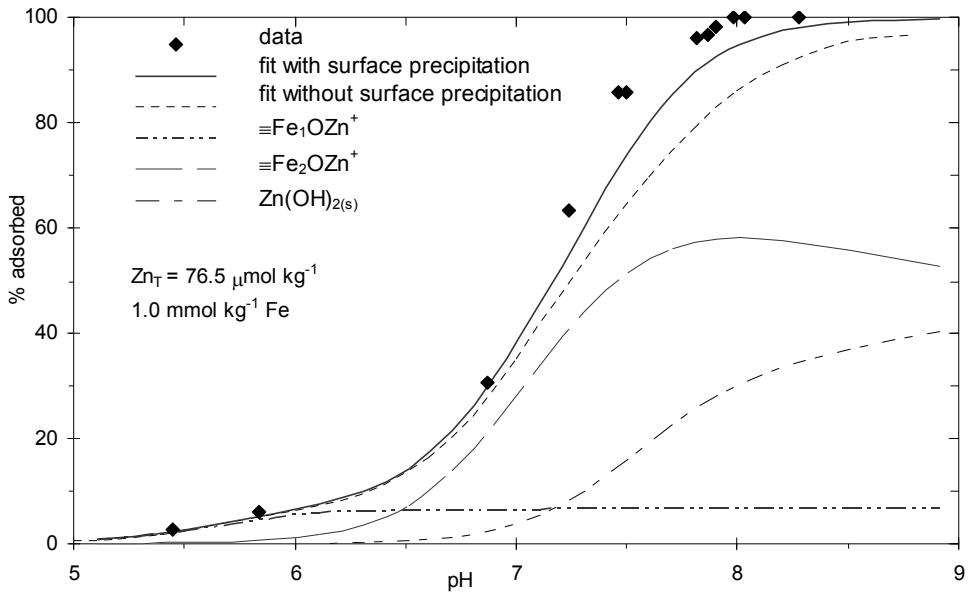

Figure 7.6 Modelled adsorption on ferrihydrite for 76.5 μmol kg^{-1} Zn_T; the effect of surface precipitation. Speciation is shown for the model fit including surface precipitation.

The experimental schwertmannite edge with 76.5 μmol kg^{-1} Zn_T (Figure 7.5b) is essentially the same as the ferrihydrite edge where adsorption was less than 20 %, and then adsorption falls below that of ferrihydrite. The modelled edge for ferrihydrite with 0.01 mol kg^{-1} SO_4 shows the usual effect of SO_4 enhancing metal adsorption and a good fit to the experimental data. As with Cu (Figure 7.4b) the effect of SO_4 on the ferrihydrite adsorption of Zn was not measured for a Zn_T/Fe as high as that of this data (0.0765) therefore it is not known whether the slight difference between the model and the experimental data reflects a difference in the adsorption onto schwertmannite or a difference in the effect of SO_4 on Zn adsorption by ferrihydrite at this high Zn_T/Fe ratio.

The experimental SO_4-rich goethite adsorption edge with 76.5 μmol kg^{-1} Zn_T (Figure 7.5b) was well modelled where adsorption was less than 10 % with pH < 6. Between pH 6 and 8 the modelled edge rises less steeply and then, at pH > 8, bulk phase precipitation is predicted to occur, accounting for 0 % of Zn_T at pH 8 to 45% of Zn_T at pH 8.8. Therefore the results were

modelled including surface precipitation and this is shown in Figure 7.7. Note that the effect of SO_4 on modelled Zn adsorption was small, only increasing adsorption by a maximum of 3 % and SO_4 was not included in the model with surface precipitation.

Surface precipitation was more significant on the SO_4-rich goethite compared to ferrihydrite because of the lower availability of surface sites. Adding surface precipitation decreases the large difference between the experimental and modelled Zn adsorption, however, there is still some underestimation of adsorption, which may be due to the effects of drying the SO_4-rich goethite in the current study.

Surface precipitation is described as being a continuum between adsorption and bulk phase precipitation (Dzombak and Morel, 1990) and including surface precipitation in the model smoothes out the transition between adsorption and precipitation evident when comparing Figures 7.5b and 7.7. The K_{sp} for the formation of goethite will be $10^{-1.16}$ compared to $10^{-3.16}$ for ferrihydrite. Changing the K_{sp} for oxyhydroxide formation from $10^{-1.16}$ (for goethite) to $10^{-3.16}$ (for ferrihydrite) makes less than 1 % change in the effect of surface precipitation. For SO_4-rich goethite and 7.65 μmol kg^{-1} Zn_T almost all the adsorbed Zn was on the high affinity sites and surface precipitation was predicted to be almost insignificant (< 1.5 % Zn_T).

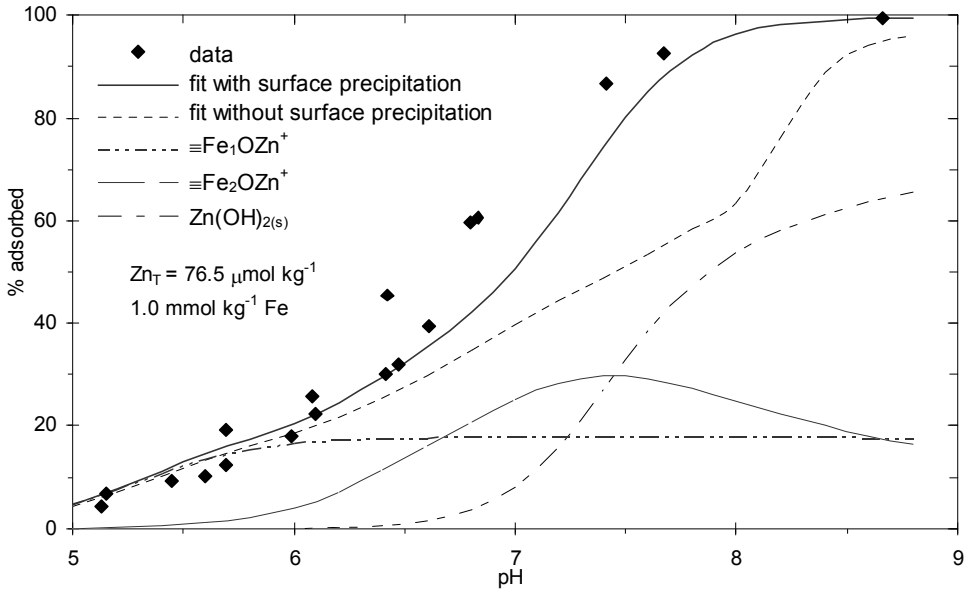

Figure 7.7 Modelled adsorption on SO_4-rich goethite for 76.5 μmol kg^{-1} Zn; the effect of surface precipitation. Speciation is shown for the model fit including surface precipitation.

Cadmium

The modelled ferrihydrite adsorption edge with 4.46 μmol kg^{-1} Cd (Figure 7.5c) was at lower pH than the experimental data, by up to 0.2 pH units. Furthermore, there was a 0.2 pH unit shift in the ferrihydrite adsorption edge in the presence of 0.01 mol kg^{-1} SO_4, although there was no difference between the experimental ferrihydrite and schwertmannite edges. Cadmium adsorption onto schwertmannite was not measured in this study, nor was the effect of SO_4 on the ferrihydrite adsorption of Cd measured in the study of Webster et al. (1998). Therefore it cannot be determined whether the difference between the modelled Cd adsorption on ferrihydrite with 0.01 mol kg^{-1} and adsorption on schwertmannite was due to experimental differences between the studies or differences between adsorption in the ferrihydrite/SO_4 and schwertmannite systems. The modelled SO_4-rich goethite adsorption edge with 4.46 μmol kg^{-1} Cd (Figure 7.5c) was reasonably close to the experimental data.

Comparison to experimental systems simulating mixing in AMD systems

Tonkin et al. (2002) measured the partitioning of trace metals onto the predominantly iron oxide solid phases formed during the mixing of AMD waters with near neutral surface waters. The mix ratios produced final pH values ranging from 2.9 to 6.6 and the mineralogy of the dominant iron oxide phase included schwertmannite (for final pH 2.9 to 3.1), goethite (for final pH 3.1 to 3.8) and amorphous (for final pH 6.0 to 6.5). Under these conditions Cu and Pb exhibited nonconservative behaviour, i.e. the dissolved metal concentration was less than the total acid soluble metal concentration. This is a considerably more complex system than that of Webster et al. (1998) and includes the effects of competition between adsorbing species, other than SO_4, and iron oxide precipitation in the presence of the metals. High concentrations of Zn were present in the AMD water (160 mg L^{-1}) but the difference between the total acid soluble and dissolved Zn in the mixing experiments was less than the experimental error. The main other sorbing species present was SO_4 (930 mg L^{-1}) and trace sorbing species included arsenate, molybdate and antimonate (up to 50 μg L^{-1}).

The model parameters determined from this work were applied to the Cu and Pb adsorption data of Tonkin et al. (2002). Modelling was based on the total concentrations of Fe^{III}, Pb, Cu and SO_4, the calculated ionic strength and measured pH. The model fits are shown in Figure 7.8. Calculations were done for ferrihydrite over the entire pH range and for goethite over the pH range where goethite was the predominant iron oxide based on XRD.

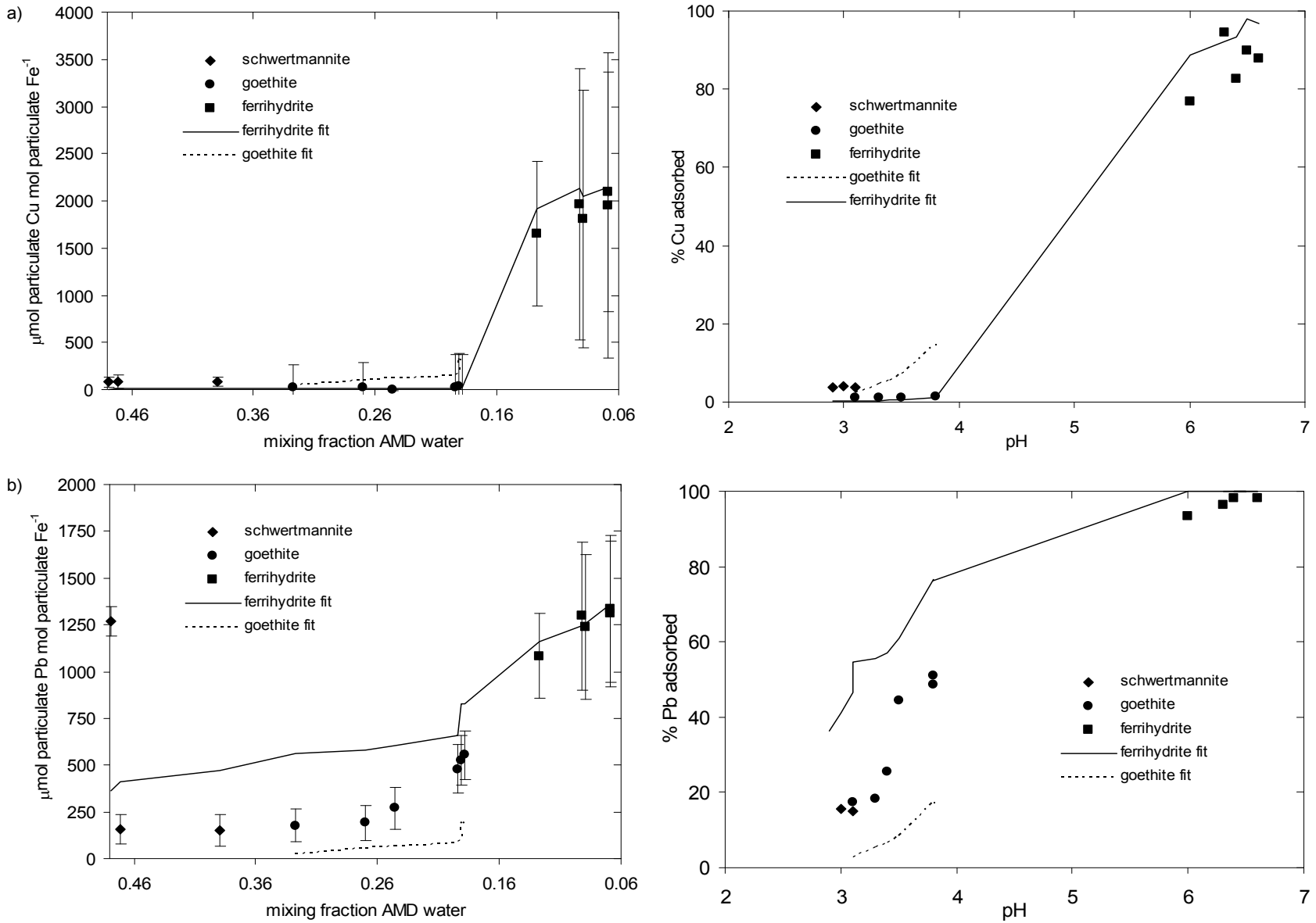

Figure 7.8 Model fits to Tonkin et al. (2002) mixing experiments. The same data are shown as a function of mix ratio and as a function of pH. a) Cu b) Pb.

In Figure 7.8 the Fe^{III} concentration decreases from 54 mg L^{-1} to 7 mg L^{-1} across the range of mix fractions while the Cu/Fe and Pb/Fe are fairly constant at 0.002 and 0.001 mol mol^{-1} respectively. These Cu/Fe and Pb/Fe ratios are in the low Me/Fe region for both ferrihydrite and goethite where the high affinity sites are most significant. Discontinuities (e.g. Pb adsorption at pH 3.1) are a reflection of the fact that the measured pH was used for modelling. There were two mix ratios that had a measured pH of 3.1, but had different Fe^{III} concentrations, i.e. 51 and 43 mg L^{-1}. In addition, based on the results of the current study (Chapter 3), at this Cu/Fe ratio the adsorption of Cu onto schwertmannite should be almost identical to that onto ferrihydrite in the presence of SO_4.

Because of the large jump in pH from 3.8 to 6.0 between the mix ratios of 0.182 and 0.12 respectively, the data for Cu involves adsorption that is either <10 % or ≥ 90 %. At pH 3.1 the Cu adsorption onto schwertmannite was greater than onto goethite, which is contrary to the results of Webster et al. (1998) and the results of this study where Cu adsorption onto SO_4-rich goethite was significantly greater than onto schwertmannite. From the model results in Figure 7.8a it is apparent that the reversal in order of adsorption is due to both a greater than predicted adsorption onto the schwertmannite and a less than predicted adsorption onto the goethite. The measured schwertmannite Cu adsorption was ≈ 4% compared to modelled adsorption (based on the ferriydrite adsorption parameters) of 0.2 %. This enhanced schwertmannite adsorption of Cu, when compared to the results from Chapter 3 from this study, could be due to Tonkin et al. (2002) precipitating schwertmannite in the presence of the Cu, or differences in the precipitation conditions such as pH, [SO_4] and the rate of pH change.

In contrast to schwertmannite the adsorption of Cu onto goethite in Tonkin et al. (2002) was less than predicted based on the parameters for SO_4-rich goethite in this study. From Figure 7.2 it might be expected that the model would underpredict adsorption because the goethite in Tonkin et al. (2002) was not dried. This lower measured adsorption could be due to the different formation conditions for the Tonkin et al. (2002) goethite. The SO_4 content of the goethite was not reported but it was precipitated in the presence of 2 to 3 mmol L^{-1} SO_4 compared to 100 mmol L^{-1} in the current study. In addition the Tonkin et al. (2002) goethite was formed over 2 h starting from Fe^{III} in the mixing solutions compared to being formed over several weeks from Fe initially present as Fe^{II} in the current study. While conditions of SO_4-rich goethite formation would be expected to affect adsorption it should be noted that Lane (2001) showed that natural and synthetic (prepared as in this study) SO_4-rich goethites

had equivalent Cu adsorption. The natural SO_4-rich goethite of Lane (2001) was collected from waters with a pH of 2.8 and a SO_4 content of 17 mmol L^{-1}.

The adsorption of Cu by ferrihydrite was fairly well predicted, although experimental data in the pH region between 10 and 90 % adsorption would provide a more exacting test for the model.

The high particulate Pb at a mix ratio of 0.48 (Figure 7.8b) was attributed by Tonkin et al. (2002) to the possible formation of lead jarosite, which was supersaturated for systems where schwertmannite was the major iron oxide phase. The Tonkin et al. (2002) adsorption of Pb onto schwertmannite was similar to that onto goethite (at pH 3.1) but less than that predicted using the ferrihydrite model parameters. This is consistent with Webster et al. (1998) and the results of this study. Unlike Cu and Zn, the adsorption of Pb by schwertmannite could not be modelled using the ferrihydrite parameters, because despite the fact that SO_4 enhanced ferrihydrite adsorption of Pb, adsorption on schwertmannite was less than that on ferrihydrite.

However, the model underestimated SO_4-rich goethite adsorption of Pb, unlike the Cu:goethite case discussed above. If the lower than predicted Cu adsorption by goethite was due to morphological differences in the goethite of Tonkin et al. (2002) then it would be expected that Pb adsorption would also be less than predicted. One possible explanation for this higher adsorption of Pb and lower adsorption of Cu on the Tonkin et al. (2002) goethite could be the presence of an amorphous phase, occurring with the goethite, which would not be evident from the XRD. For both Pb and Cu the measured adsorption was, in general, in between that predicted for SO_4-rich goethite and ferrihydrite. The ferrihydrite model parameters predict the ferrihydrite Pb adsorption reasonably accurately.

Summary

The results from this thesis have significantly improved the ability of the DLM to predict trace metal adsorption in AMD systems, compared to using ferrihydrite as a proxy for all iron oxyhydroxides and adsorption data derived only from single sorbate systems. In terms of the application of the model parameters derived in this thesis to real oxides from AMD systems the main discrepancies with the data from Webster et al. (1998) was the underestimate of Cu, Zn and Pb adsorption onto the SO_4-rich goethite for the low Me/Fe data. The model parameters did accurately predict Cu adsorption on to a freeze dried SO_4-rich goethite at low

Cu/Fe and it is most likely that the cause of the discrepancy with Webster et al. (1998) was the drying. Therefore it would be useful to measure some cation adsorption isotherms for un-dried SO_4-rich goethite and, using the approach derived in this work, optimise an effective specific surface area for this material.

The main discrepancies between the model parameters derived in this thesis and the data from Tonkin et al. (2002) involved the the AMD goethite. The adsorption of Cu was the over-predicted while that of Pb was under-predicted. As discussed one possible reason for both these discrepancies could be the presence of ferrihydrite as a minor phase. This would not be evident from XRD but could be determined from the dissolution of Fe in 0.2 mol/L ammonium oxalate/oxalic acid at pH 3.0. If there was significant Fe dissolution using this test the soluble phase could be ferrihydrite or schwertmannite and could be identified by difference XRD. The schwertmannite adsorption of Pb has not been modelled in this study and, unlike that of CU and Zn, it is identical to adsorption by ferrihydrite in the presence of SO_4. Therefore it would be useful to develop the parameters required to model Pb adsorption on schwertmannite although the presence of SO_4 precludes titrations to determine total site densities.

CHAPTER EIGHT
CONCLUSIONS

8.1 FERRIHYDRITE

The ferrihydrite adsorption of Cu, Zn and SO_4 from single sorbate systems was accurately described by the DLM using the two-site model, surface area, site densities, surface acidity constants and adsorption constants determined by Dzombak and Morel (1990). However, the enhanced adsorption of Cu and Zn in the presence of SO_4 was not predicted using these parameters. By including a ternary complex with stoichiometry $\equiv Fe_{(2)}OHMeSO_4$ on the low affinity surface sites, and allowing SO_4 adsorption only at these sites, the effect of SO_4 on metal adsorption was accurately described for the range of Me, Fe and SO_4 concentrations studied. The adsorption of Cu and Zn onto schwertmannite at low Me_T:Fe ratios was almost identical to that predicted for ferrihydrite in the presence of 0.01 mol kg^{-1} SO_4.

In the absence of SO_4, Co adsorption could also be modelled using the two-site model of Dzombak and Morel (1990), while Pb adsorption required a third higher affinity site with a site density of 0.00035 mol $molFe^{-1}$. Cadmium adsorption showed some indications of 3-site behavior but model predictions were only slightly improved over a two-site model. The effect of SO_4 on cation adsorption could be modelled by including a neutral ternary complex on the low affinity sites in the case of Co and Cd, and on both the high and low affinity sites in the case of Pb.

The issue of site heterogeneity and the unusually high $logK^{INT}$ for Pb adsorption was the main peculiarity identified from all the ferrihydrite data of this thesis. As discussed site heterogeneity could either be related to changes in the ferrihydrite surface at the low pH of Pb adsorption, or may relate to the presence of adsorption sites with limits on ionic radii. The fact that Cd, which adsorbs at high pH, exhibited some evidence of additional site heterogeneity would support the latter hypothesis. This question would best be answered by spectroscopic studies, such as XAFS, of the ferrihydrite/Pb system.

8.2 SCHWERTMANNITE

For the conditions studied in this work the schwertmannite adsorption of Cu and Zn was essentially the same as that of ferrihydrite with high SO_4 solution concentrations (e.g. 0.01 mol L^{-1}). In contrast, Pb adsorption onto schwertmannite was less than that onto ferrihydrite, despite the fact that SO_4 enhanced Pb adsorption onto ferrihydrite (Webster et al., 1998). This difference was considered to be another reflection of the unusually and unexplained high efficiency of Pb adsorption onto ferrihydrite. Because of the integral presence of SO_4 it was not possible to perform acid-base titrations of schwertmannite to estimate the total site density, therefore a full study of schwertmannite adsorption was not undertaken.

8.3 GOETHITE

Metal adsorption onto a pure acicular goethite could be accurately described by the DLM. The major deficiency was an inconsistency between the total site density derived from the DLM's prediction of the acid-base behaviour of the goethite surface and the total site density required to accurately model metal adsorption. The site density optimised from the titration data was 0.94 nm^{-2}, whereas the highest measured metal adsorption density in this work was 1.34 nm^{-2} (for Cd), and the site density which was the optimum for fitting the metal adsorption data in the presence of SO_4 (2.3 nm^{-2}).

All metal adsorption data could be modelled using a two-site model. The site densities of the high affinity sites optimised from the Cu, Pb and Cd data were reasonably consistent and a weighted average value of 0.024 nm^{-2} was used for these metals. The site densities of the high affinity sites optimised from the Zn data were considerably higher and a weighted average value of 0.13 nm^{-2} was used for Zn. The issue of type-1 site density for Zn adsorption on both pure and SO_4-rich goethite was the main peculiarity identified from all of the goethite data of this thesis. As discussed it is hard to envisage a mechanism that may cause the Zn type-1 density to be so much larger than that of the other cations studied. This question would be answered by studies of Zn adsorption by goethite in competitive with other cations. Also, as for Pb on ferrihydrite, spectroscopic studies, such as XAFS, may help to understand the reason for this difference.

In all cases studied the presence of SO_4 caused an increase in the extent of metal adsorption. This effect was accurately predicted by including ternary complex formation at both the high and low affinity adsorption sites. The low affinity site density that provided the best fit to all the experimental data was 2.7 nm^{-2}. The main model discrepancy modelling with a site density of 1.4 nm^{-2} was at high Cu and Pb concentration where site competition from SO_4 appeared to be overestimated. The main model discrepancy modelling with a 3.0 nm^{-2} site density was at high Cd concentration where site competition from SO_4 appeared to be underestimated. The difference between these site densities could suggest that Cd may have a lower site density than Cu (and Pb) on acicular goethite, but this would require more study to substantiate.

The value of the adsorption constants for ternary complex formation showed a positive, linear relationship with the adsorption constant for metal adsorption, evident from a plot of $\log K_{xMe}^{TC}$ as a function of $\log K_{xMe}^{INT}$ for all metals. This showed a clear linear relationship (r^2=0.95) with slope of 0.69 and intercept of 8.03. The data for both ferrihydrite and goethite fit this relationship, which suggests that the enhancement of metal adsorption due to SO_4 on both oxyhydroxides occurs by the same process.

Compared to pure acicular goethite, SO_4-rich goethite had a considerably higher low affinity site density per mole of oxide. The SO_4-rich goethite acid-base titration data (after removal of SO_4) could be modelled reasonably accurately using the parameters developed to model the pure goethite titrations (including the same site density per unit area) but with a surface area of 220 m^2g^{-1}, compared to 80 m^2g^{-1} for the pure goethite. In contrast, the average surface area required to model metal and SO_4 adsorption onto SO_4-rich goethite, using the pure goethite parameters, was somewhat larger at 270 m^2g^{-1}. In addition, for Cu, Cd and Zn adsorption the SO_4-rich goethite required a higher ratio of high affinity metal adsorption sites to low affinity sites, compared to that of pure goethite. For SO_4-rich goethite, the high affinity site density was less for Pb than for Cu and Cd. In general, therefore, the parameters developed for pure goethite are apparently similar to those for the sulfate-rich goethite, but are not directly transferable. The difficulty in reliably measuring the surface area of the highly aggregated sulfate-rich goethite makes comparison between the two goethites more difficult.
Direct comparisons between the data from this work and the natural SO_4-rich goethite data of Webster et al. (1998) are somewhat compounded by differences in the methods between the two studies, in particular the fact that goethite samples were freeze-dried for this work but not

in Webster et al. (1998). In general, however, it can be concluded that the reason why Cu, Zn and Cd adsorption onto the natural SO_4-rich goethite exceeded that of ferrihydrite in Webster et al. (1998) is because the same higher adsorption constants of goethite are combined with the considerably higher site densities of the SO_4-rich goethite compared to the acicular goethite. In contrast, for Pb, the higher site densities of the SO_4-rich goethite do not compensate for the lower $\log K^{INT}$ values for Pb adsorption on goethite compared to ferrihydrite. Therefore SO_4-rich goethite adsorption of Pb is lower than that of ferrihydrite.

Therefore the aim of this study; to provide an improved understanding of metal adsorption processes pertinent to AMD systems, has been met. Many of the characteristics of metal adsorption in this system, which had appeared to be difficult to explain, are now explicable. Modelling of metal speciation in AMD systems using the parameters and adsorption constants from this study will lead to more reliable predictions than those based on metal adsorption onto synthetic ferrihydrite, as have been commonly used in the past.

LITERATURE CITED

Ainsworth, C.C., Pilon, J.L., Gassman, P.L. and Van Der Sluys, W.G., 1994. Cobalt, cadmium and lead sorption to hydrous iron oxide: resident time effect. Soil Sci. Soc. Am. J. 58, 1615-1623.

Ali, M.A., 1994, The influence of simple organic acids on sorption of inorganic ions at the goethite/water interface. PhD Thesis, Carnegie Melon University, Pittsburgh

Ali, M.A. and Dzombak, D.A., 1996a. Competitive sorption of simple organic acids and sulfate on goethite. Environ. Sci. Technol. 30**,** 1061-1071.

Ali, M.A. and Dzombak, D.A., 1996b. Interactions of copper, organic acids, and sulfate in goethite suspensions. Geochim. Cosmochim. Acta 60**,** 5045-5053.

Atkinson, R.J., Posner, A.M. and Quirk, J.P., 1968, Crystal nucleation in Fe(III) solutions and hydroxide gels. J. Inorg. Nucl. Chem. 30, 2371-2381.

Allison, J.D., Brown, D.S. and Novo-Gradac, K. J., 1991. MINTEQA2/PRODEFA2, A Geochemical Assessment Model for Environmental Systems: Version 3.0 User's Manual, USEPA Report No. EPA/600/3-91/021, Athens, Georgia.

Avontis, P. V., 1975, Adsorption and Coprecipitation Studies of Mercury on Hydrous Iron Oxide, PhD Thesis, Stanford University, California, cited in Dzombak & Morel, 1990.

Balistrieri, L.S. and Murray, J.W., 1982. The adsorption of Cu, Pb, Zn, and Cd on goethite from major ion seawater. Geochim. Cosmochim. Acta 46**,** 1253-1265.

Ball, J.W., Runkel, R.L. and Nordstrom, D.K., 2001. Reactive transport modeling at high flow-Wightman Fork/Alamosa River, USA. Proceedings of the 10th International Symposium on Water Rock Interaction, Cidu, R. (Ed), Swets and Zeitlinger, Lisse.

Bard, Y., 1974, Nonlinear parameter estimation, Academic Press, New York. (cited in Dzombak and Morel, 1990)

Benjamin, M.M. and Leckie, J.O., 1981, Multiple site adsorption of Cd, Cu, Zn and Pb on amorphous iron oxyhydroxides. J. Colloid Interface Sci 79, 209-221.

Bigham, J.M., Carlson, R.M. and Murad, E., 1994. Schwertmannite, a new iron oxyhydroxy-sulphate from Pyhäsalmi, Finland, and other localities. Min. Mag. 58, 641-648.

Bigham, J.M., Schwertmann, U., Carlson, L., Muran, E., 1990. A poorly crystallized oxyhydroxysulfate of iron formed by bacterial oxidation of Fe(II) in acid mine waters. Geochim. Cosmochim. Acta 54, 2743-2758.

Bigham, J.M., Schwertmann, U. and Pfab, G. 1996, Influence of pH on mineral speciation in a bioreactor simulating acid mine drainage. Applied Geochemistry, 11, 845-849.

Bigham, J.M., Schwertmann, U., TRania, S.J., WInland, R.L. and Wolf, M. (1996a) Schwertmannite and goethite solubilities and the chemical modeling of iron in acid sulfate waters. Geochim. Cosmochim. Acta 60, 2111-2121.

Boily, J.F., 1999, The surface complexation of ions at the goethite (α-FeOOH)-water interface. A multi-site complexation approach. PhD thesis, Umeå University, Sweden. Cited in Boily et al. (2001).

Boily, J.F., Lützenkirchen, J., Balmes, O., Beattie, J. and Sjöberg, S., 2001, Modeling proton binding at the goethite (α-FeOOH)-water interface. Colloids and surfaces A. Physicochemical and Engineering Aspects, 179. 11-27.

Christophi, C.A. and Axe, L., 2000. Competition of Cd, Cu and Pb adsorption on goethite. J. Environ. Engin. 2000, 66-74.

Collins English Dictionary, 1990, Patrick Hanks (Ed)

Collins, C.R., Ragnarsdottir, K.V. and Sherman, D.M., 1999. Effect of inorganic and organic ligands on the mechanism of cadmium sorption to goethite. Geochim. Cosmochim. Acta 63, 2989-3002.

Cornell R.M. and Schwertmann, U., 1996, The iron oxides structure, properties, reactions, occurrence and uses. VCH, Weinheim.

Cotton, F. A. & G. Wilkinson, 1980, Advanced Inorganic Chemistry: A Comprehensive Text, 4th Ed, John Wiley & Sons, Brisbane.

Davis, J. A., 1977, Adsorption of Trace Metals and Complexing Ligands at the Oxide/Water Interface, Ph.D. Thesis, Stanford University, Stanford, Calif., cited in Dzombak & Morel, 1980.

Davis, J.A. and Kent, D.B., 1990, Surface complexation modeling in aqueous geochemistry. Reviews in Mineralogy; Hochella, M.F. and White, A.A., Eds.; Mineralogical Society of America, Wahington D.C., Vol. 23, Chapter 5.

Davis, J. A. & J. O. Leckie, 1978, 'Surface Ionization and Complexation at the Oxide/Water Interface. II. Surface Properties of Amorphous Iron Oxyhydroxide and Adsorption of Metal Ions', J. Colloid Interface Sci., (67), pp. 90 - 107.

Doyle, F., 199, Acid mine drainage from sulfide ore deposits. In Sulphide deposits : their origin and processing. P.M.J. Gray, Ed. The Institution of Mining and Metallurgy, London, England.

Dyer, J. A.; Trivedi, P.; Scrivner, N.; Sparks, D. L., 2003, Lead sorption onto ferrihydritr.2. Surface complexation modeling. Env. Sci. and Technology, 37, 915-922.

Dzombak, D.A. and Morel F.M.M., 1990. Surface Complexation Modeling: Hydrous Ferric Oxide. John Wiley & Sons, New York.

Elzinga, E.J., Peak, D. and Sparks, D.L., 2001, Spectroscopic studies of Pb(II)-sulfate interactions at the goethite-water interface. Geochim. Cosmochim. Acta 65, 2219-2230.

Evangelou, V.P. and Zhang, Y.L., 1995, A review: Pyrite oxidation mechanisms and acid mine drainage prevention. Crit. Rev. Env. Sci. and Technology, 25, 141-199.

Gans, P., 1976, Numerical Methods for dtat-fitting problems. Coord. Chem Review, 19, 99-124.

Geelhoed, J.S., Hiemstra, T. and Van Riemsdijk, W.H., 1997, Phosphate and sulfate adsorption on goethite: Single anion and competitive adsorption. Geochim. Cosmochim. Acta, 61, 2389-2396.

Goodman, B.A. and Lewis, D.G., 1981, Mossbaur spectra of aluminous goethites (α-FeOOH). J. SOil Sci., 32, 351-363.

Hayes, K.F., Redden, G., Ela, W. and Leckie, J.O., 1990, Surface complexation modles: An evaluation of model parameter estimation using FITEQL and oxide mineral titration data., J. Colloid Interface Sci., 142, 448-469.

Herbelin, A.L. and Westall, J.C., 1996. FITEQL: A computer program for determination of chemical equilibrium constants from experimental data. Report 96-01; Chemistry Department, Oregon State University: Corvallis, OR.

Hoins, U., Charlet, L. and Sticher, H., 1993. Ligand effect on the adsorption of heavy metals: the sulfate-cadmium-goethite case. Water air and soil pollution, 68, 241-255.

Johnson, C.A., 1986, The regulation of trace element concentrations in river and estuarine waters contaminated with acid mine drainage: The adsorption of Cu and Zn on amorphous Fe oxyhydroxides. Geochim. Cosmochim. Acta, 50, 2433-2438.

Johnson, D.B. 1995, Selective solid media for isolating and enumerating acidophilic bacteria. Journal of microbiological media, 23, 205-218.

Kleinmann, R.L.P., Crerar, D.A. and Pacelli, R.R., 1981, Biogeochemistry of acid mine drainage and a method to control acid formation. Min. Eng., 33, 300-306.

Lane, V. 2000. Characterisation of selected natural iron oxide precipitates and their ability to remove copper and arsenic from the water column. MSc Thesis, University of Auckland, Auckland.

Leckie, J.O., Benjamin, M., Hayes, K., Kaufman, G. and Altman, S., 1980. Adsorption/co-precipitation of trace elements from water with iron oxyhydroxide. Final Report, EPRI RP-910, Electric Power Research Institute, Palo Alto, Calif.

Lee, G., Bigham, J.M. and Faure, G., 2002, Removal of trace metals by coprecipitation with Fe, Al and Mn from natural waters contaminated with acid mine drainage in the Ducktown mining dsitrict, Tennessee. Applied Geochem., 17, 569-581.

Manceau, A. Nagy, K.L., Spandini, L. and Ragnarsdottir, K.V., 2000, Influence of anionic layer structure of Fe-oxyhydroxides on the structure of Cd surface complexes. J. Colloid Interface Sci., 228, 306-316.

Martycak, K., Zeman, J. and Vacek-Vesely, M., 1994, Supergene processes on ore deposits-a sorce of heavy metals. Env. Geology, 23, 156-165.

Murphy, P. J., A. M. Posner, & J. P. Quirk, 1976, 'Characterization of Partially Neutralized Ferric Nitrate Solutions', J. Colloid Interface Sci., (52), pp. 270 - 283. cited in Dzombak & Morel, 1990.

Nordstrom, D.K. and Alpers, C.N., 1997, Geochemistry of acid mine water, in Reviews in Economic Geology Volume 7A, The environmental geochemistry of mineral deposits, Part A: Processes, techniques, and health issues, Eds. Plumless, G.S. and Logsdon, M.J. Society of Economic Geologists.

Nordstrom, D.K., Alpers,C.N. and Ball, J.W., 1991, Measurement of negative pH and extremely high metal concentrations in acid mine water from Iron Mountain, California, Geological Society of America Annual Meeting, 23, A383, cited in Nordstrom and Alpers (1997).

Ostergren, J.D., Brown, G.E. Jr., Parks, G.A. and Persson, P., 2000. Inorganic ligand effects on Pb(II) sorption to goethite (alpha-FeOOH)-II. Sulfate. J. Colloid Interface Sci. 225, 483-493.

Palmqvist, U.,Ahlberg, E., Lovgren, L. and Sjoberg, S., 1999, Competitive metal ion adsorption in goethite systems using in situ voltammetric methods and potentiometry. J. Colloid Interface Sci., 218, 388-396.

Paulson, A.J. and Balistrieri, L., 1999, Modeling removal of Cd, Cu, Pb and Zn in acidic groundwater during neutralization by ambient surface waters and groundwaters, Environ. Sci Technol., 33, 3850-3856.

Peak, D., Ford,R.G. and Sparks, D.L., 1999, An in situ ATR-FTIR investigation of sulfate bonding mechanisms on goethite. J. Colloid Interface Sci. 218, 289-299.

Robertson A.L. and Leckie, J.O. 1998, Acid/base, copper binding and Cu^{2+}/H^{+} exchange properties of goethite, an experimental and modeling study. Environ. Sci. Technol. 32, 2519-2530.

Scheinost, A. C., Abend, S., Pandya, K. I., Sparks, D. L., 2001, Kinetic controls on Cu and Pb sorption by ferrihydrite. Environ. Sci. Technol. *35*, 1090-1096.

Schindler, P.W. and Stumm, W., 1987. The surface chemistry of oxides, hydroxides and oxide minerals. In: Stumm, W. (Ed.) Aquatic surface chemistry. John Wiley, New York.

Schwertmann, U. and Cornell, R.M., 1991. Iron oxides in the laboratory: Preparation and characterization. Weinheim, New York.

Scheinost AC, Abend S, Pandya KI, and Sparks DL, 2001, Kinetic controls on Cu and Pb sorption by ferrihydrite. Environmental Science & Technology, 35, 1090-1096.

Sigg, L. and Stumm, W. 1981, The interaction of anions and weak acids with the hydrous goethite (α-FeOOH) surface. Colloids and Surfaces, 2, 101-117.

Smith, R.M. and Martell, A.E., 1976. Critical stability constants, Vol. 4, Inorganic Complexes, Plenum Press. New York.

Spandini, L., Manceau, A., Schindler, P.W. and Charlet, L. 1994, Structure and stability of Cd^{2+} surface complexes on ferric oxides 1. Results from EXAFS spectroscopy. J. Colloid Interface Sci 168, 73-86

Stahl, R.S., Fawning, D.S. and James, B.R., 1993, Goethite and jarosite precipitation from ferrous sulfate solutions. Soil Sci. Soc. Am. J., 57, 280-282.

Stumm, W. 1992, Chemistry of the solid-water interface: Processes at the mineral-water and pareticle-water interface in natural systems. John Wiley and Sons Inc. NY.

Swedlund, P.J. and Webster, J.G., 1999, Adsorption and polymerization of silicic acid on ferrihydrite, and its effect on arsenic adsorption. Water Research, 33, 3413-3422.

Swedlund, P.J. and Webster, J.G., 2001. Cu and Zn ternary surface complex formation with SO_4 on ferrihydrite and schwertmannite. Applied Geochem, 16, 503-511.

Swedlund, P.J., Webster J.W., and Miskelly, G.M., 2003, The effect of SO_4 on the ferrihydrite adsorption of Co, Pb and Cd: Ternary complexes and site heterogeneity. Applied Geochemistry, 18, 1671-1689.

Taylor, R.M., 1984, Influence of chloride on the formation of iron oxides from Fe(II) chloride. Effect of (Cl) on the formation of lepidocrocite and its crytallinity. Clays and Clay Minerals, 32, 175-180.

Tonkin, J.W., Balistieri, L.S. and Murray, J.W., 2002, Modeling metal removal onto natural particles formed during mixing of acid rock drainage with ambient surface water. Environ. Sci. Technol. 36, 484-492.

Torrent, J., Barrón, V. and Schwertmann, U., 1990, Phosphate adsorption and desorption by goethites differing in crystal morphology. Soil Sci. Soc. Am. J., 54, 1007-1012.

Van Riemsdijk, W.H and Hiemstra, T., 1993, Adsorption to heterogeneous surfaces. In Metals in Groundwater, Allen, H.E., Perdue, A.E. and Brown, D.S. Eds. Lewis Publishers, Chelsea.

Venema, P., Hiemstra, T. and van Riemsdijk, W.H., 1996a, Comparison of different site binding models for cation sorption: Description of pH dependency, salt dependency, and cation-proton exchange. J. Colloid Interface Sci., 181, 45-59.

Venema, P., Hiemstra, T. and van Riemsdijk, W.H., 1996b, Multisite adsorption of cadmium on goethite. J. Colloid Interface Sci., 183, 515-527.

Villalobos, M.Trotz, M.A. and Leckie, J.O., 2001, Surface complexation modeling of carbonate effects on the adsorption of Cr(VI), Pb(II) and U(IV) on goethite. Environ. Sci. Technol. 35, 3849-3856.

Vogel A. I., 1981, Textbook of Quantitative Inorganic Analysis, 4th ed., Longman, London.

Webster, J. and Brown, K., 2001, Results of West Coast ARD Sampling. GEOKEM Client Report (West Coast Regional Concil, NZ), 40pp.

Webster, J., Lane, V., Howarth, R., Swedlund, P. and Saul, D., 2000, Factors influencing the precipitation of sulfate-rich iron oxides and their ability to adsorb trace metals, Goldschmidt, Journal of Conference Abstracts, 5, 1073.

Webster, J.G., Swedlund, P.J., Webster, K.S., 1998. Trace metal adsorption onto an acid mine drainage iron(III) oxy hydroxy sulfate. Environ. Sci. Technol. 32**,** 1361-1368.

Wieland, W., Wehrli, B. and Stumm, W., 1988, The co-ordination chemistry of weathering: III. A generalization on the dissolution rates of minerals. Geochim. Cosmochim acta, 52, 1969-1981.

Yates, D.E., 1975, The structure of the oxide/aqueous electrolyte interface. Ph.D. Thesis, Univ. Melbourne, Australia, Cited in Cornell and Schwertmann (1996).

Appendix

Tables in the Appendix are numbered according to the figure they refer to.

Table A2 Thermodynamic data for solution species used in this study.

Reaction			log K (I=0)
H_2O	⇔	$H^+ + OH^-$	-14.00
$Cu^{2+} + H_2O$	⇔	$Cu(OH)^+ + H^+$	-8
$Cu^{2+} + 2H_2O$	⇔	$Cu(OH)_2 + 2H^+$	-13.68
$Cu^{2+} + 3H_2O$	⇔	$Cu(OH)_3^- + 3H^+$	-26.899
$Cu^{2+} + 4H_2O$	⇔	$Cu(OH)_4^{2-} + 4H^+$	-39.6
$2Cu^{2+} + 2H_2O$	⇔	$Cu_2(OH)_2^{2+} + 2H^+$	-10.359
$Cu^{2+} + SO_4^{2-}$	⇔	$CuSO_{4(aq)}^{(0)}$	2.31
$Zn^{2+} + H_2O$	⇔	$Zn(OH)^+ + H^+$	-8.96
$Zn^{2+} + 2H_2O$	⇔	$Zn(OH)_2 + 2H^+$	-16.899
$Zn^{2+} + 3H_2O$	⇔	$Zn(OH)_3^- + 3H^+$	-28.399
$Zn^{2+} + 4H_2O$	⇔	$Zn(OH)_4^{2-} + 4H^+$	-41.199
$Zn^{2+} + SO_4^{2-}$	⇔	$ZnSO_{4(aq)}^{(0)}$	2.37
$Zn^{2+} + 2SO_4^{2-}$	⇔	$Zn(SO_4)_{2(aq)}^{(2-)}$	3.28
$Cd^{2+} + H_2O$	⇔	$Cd(OH)^+ + H^+$	-10.08
$Cd^{2+} + 2H_2O$	⇔	$Cd(OH)_2 + 2H^+$	-20.35
$Cd^{2+} + 3H_2O$	⇔	$Cd(OH)_3^- + 3H^+$	-33.3
$Cd^{2+} + 4H_2O$	⇔	$Cd(OH)_4^{2-} + 4H^+$	-47.35
$2Cd^{2+} + H_2O$	⇔	$Cd_2OH^{3+} + H^+$	-9.39
$Cd^{2+} + SO_4^{2-}$	⇔	$CdSO_{4(aq)}^{(0)}$	2.46
$Cd^{2+} + 2SO_4^{2-}$	⇔	$Cd(SO_4)_{2(aq)}^{(2-)}$	3.5
$Pb^{2+} + H_2O$	⇔	$Pb(OH)^+ + H^+$	-7.71
$Pb^{2+} + 2H_2O$	⇔	$Pb(OH)_2 + 2H^+$	-17.12
$Pb^{2+} + 3H_2O$	⇔	$Pb(OH)_3^- + 3H^+$	-28.06
$Pb^{2+} + 4H_2O$	⇔	$Pb(OH)_4^{2-} + 4H^+$	-39.699
$2Pb^{2+} + 3H_2O$	⇔	$Pb_2(OH)_3^+ + 3H^+$	-6.36
$3Pb^{2+} + 4H_2O$	⇔	$Pb_3(OH)_4^{2+} + 4H^+$	-23.88
$Pb^{2+} + SO_4^{2-}$	⇔	$PbSO_{4(aq)}^{(0)}$	2.75
$Pb^{2+} + 2SO_4^{2-}$	⇔	$Pb(SO_4)_{2(aq)}^{(2-)}$	3.47
$Co^{2+} + H_2O$	⇔	$Co(OH)^+ + H^+$	-9.7
$Co^{2+} + 2H_2O$	⇔	$Co(OH)_2 + 2H^+$	-15.5
$Co^{2+} + 3H_2O$	⇔	$Co(OH)_3^- + 3H^+$	-32.3
$Co^{2+} + 4H_2O$	⇔	$Co(OH)_4^{2-} + 4H^+$	-45.8
$2Co^{2+} + 3H_2O$	⇔	Co_2OH^{3+}	-11.3
$3Co^{2+} + 4H_2O$	⇔	$Co_4(OH)_4^{4+}$	-30.4
$Co^{2+} + SO_4^{2-}$		$CoSO_{4(aq)}$	2.36
$SO_4^{2-} + H^+$	⇔	HSO_4^-	0.44
$SO_4^{2-} + Na^+$	⇔	$NaSO_4^-$	0.11
$Cd^{2+} + NO_3^-$	⇔	$Cd(NO_3)^+$	0.399
$Pb^{2+} + NO_3^-$	⇔	$Pb(NO_3)^+$	1.17
$Co^{2+} + NO_3^-$		$Co(NO_3)^+$	0.2

Table A3.1a

Expt. Conditions [Fe]= 14.7 mmol kg^{-1} [Cu]= 24.4 μmol kg^{-1}		Expt. Conditions [Fe]= 4.80 mmol kg^{-1} [Cu]= 16.5 μmol kg^{-1}		Expt. Conditions [Fe]= 0.930 mmol kg^{-1} [Cu]= 8.37 μmol kg^{-1}		Expt. Conditions [Fe]= 0.935 mmol kg^{-1} [Cu]= 24.7 μmol kg^{-1}	
pH	% Cu sorbed	pH	% Cu sorbed	pH	% Cu sorbed	pH	% Cu sorbed
3.17	-0.06	3.92	1.62	4.65	9.86	3.98	0.00
3.83	5.55	4.13	10.02	4.80	14.87	4.04	4.46
4.25	22.65	4.40	17.69	5.13	33.18	4.53	3.18
4.49	37.55	4.48	18.67	5.21	39.43	4.62	8.28
4.85	67.35	4.60	25.37	5.35	44.00	4.85	12.74
5.16	87.55	4.84	40.57	5.52	56.67	5.26	31.08
5.63	97.55	5.01	56.97	5.71	79.50	5.28	32.48
		5.03	59.87	5.74	76.20	5.74	71.29
		5.15	65.95	5.93	85.49	5.78	74.65
		5.26	78.06	5.96	91.11	6.31	95.48
		5.32	75.14	6.22	91.96	6.31	95.29
		5.51	92.07	6.29	92.00	6.50	94.52
		5.52	88.48	6.56	94.31	6.84	98.73
		6.27	92.47	6.64	94.80		
		6.53	94.16	6.69	100.00		
		6.77	97.74	6.89	100.00		

Table A3.1b

Expt. Conditions [Fe]= 27.0 mmol kg^{-1} [Zn]= 8.24 μmol kg^{-1}		Expt. Conditions [Fe]= 14.2 mmol kg^{-1} [Zn]= 24.0 μmol kg^{-1}		Expt. Conditions [Fe]= 1.03 mmol kg^{-1} [Zn]= 7.96 μmol kg^{-1}	
pH	% Zn sorbed	pH	% Zn sorbed	pH	% Zn sorbed
4.53	0.00	3.60	-0.25	4.01	4.00
5.06	12.14	4.21	0.64	5.05	4.00
5.33	33.93	4.80	2.42	5.62	9.99
5.62	59.46	5.38	21.66	6.10	19.99
5.81	75.89	6.08	77.07	6.50	41.97
6.03	91.07	6.59	96.75	7.00	75.95
6.65	99.46	6.64	98.34	7.43	95.94

Table A3.2a.

Expt. Conditions [Fe] = 14.6 mmol kg^{-1} [Cu]= 24.4 μmol kg^{-1} [SO_4]= 1.04 mmol kg^{-1}		Expt. Conditions [[Fe] = 14.6 mmol kg^{-1} [Cu]= 24.4 μmol kg^{-1} [SO_4] =10.4 mmol kg^{-1}		Expt. Conditions [Fe] = 14.6 mmol kg^{-1} [Cu]= 24.4 μmol kg^{-1} [SO_4]= 20.8 mmol kg^{-1}	
pH	% Cu sorbed	pH	% Cu sorbed	pH	% Cu sorbed
3.53	1.81	3.35	2.71	3.19	-0.06
3.98	15.87	3.75	17.87	3.71	19.81
4.33	39.42	4.02	34.65	4.12	44.90
4.58	61.48	4.39	61.16	4.54	74.00
4.87	80.90	4.41	63.55	5.05	92.45
5.18	94.45	4.59	73.35	5.49	98.45
5.64	97.94	4.74	81.42		
		4.96	89.16		
		5.05	92.06		
		5.29	95.81		
		5.59	99.16		

Table A3.2b.

Expt. Conditions [Fe] = 4.80 mmol kg^{-1} [Cu]= 16.5 μmol kg^{-1} [SO_4]= 1.06 mmol kg^{-1}		Expt. Conditions [Fe] = 4.80 mmol kg^{-1} [Cu]= 16.5 μmol kg^{-1} [SO_4] =2.10 mmol kg^{-1}		Expt. Conditions [Fe] = 4.80 mmol kg^{-1} [Cu]= 16.5 μmol kg^{-1} [SO_4]= 10.4 mmol kg^{-1}	
pH	% Cu sorbed	pH	% Cu sorbed	pH	% Cu sorbed
3.92	5.93	4.26	20.03	3.92	13.14
4.54	31.62	4.48	30.70	4.36	30.76
4.94	64.76	4.71	44.63	4.76	57.90
5.35	88.48	4.89	58.88	5.09	79.71
5.46	91.71	5.23	82.31	5.35	90.02
5.57	95.14	5.33	87.16	5.82	98.76
6.05	100.00	5.57	93.93	6.11	99.90

Table A3.3

Expt. Conditions [Fe] = 0.930 mol kg^{-1} [Cu] = 8.37 μmol kg^{-1} [SO_4]=2.08 mmol kg^{-1}		Expt. Conditions [Fe] = 0.930 mol kg^{-1} [Cu] = 8.37 μmol kg^{-1} [SO_4]= 10.4 mmol kg^{-1}		Expt. Conditions [Fe] =0.935 mmol g^{-1} [Cu]= 24.7 μmol kg^{-1} [SO_4]= 0.208 mmol kg^{-1}		Expt. Conditions [Fe] =0.935 mmol g^{-1} [Cu]= 24.7 μmol kg^{-1} [SO_4] =1.04 mmol kg^{-1}	
pH	% Cu sorbed	pH	% Cu sorbed	pH	% Cu sorbed	pH	% Cu sorbed
4.38	7.00	3.80	3.33	4.29	3.25	4.36	6.37
4.61	14.59	4.22	7.06	4.88	14.14	4.93	20.06
4.90	26.99	4.88	38.43	5.31	39.49	5.23	37.26
5.10	40.52	5.18	56.27	5.81	78.60	5.58	62.48
5.30	55.40	5.76	89.41	6.24	90.96	6.16	93.38
5.55	74.75	6.42	100.00	6.70	94.13	6.51	97.46
5.74	86.37			5.40	47.01	6.98	98.60

Table A3.4

Expt. Conditions [Fe] = 27.0 mmol kg^{-1} [Zn] = 8.24 μmol kg^{-1} [SO_4] = 1.04 mmol kg^{-1}		Expt. Conditions [Fe] = 27.0 mmol kg^{-1} [Zn] = 8.24 μmol kg^{-1} [SO_4] =5.20 mmol kg^{-1}		Expt. Conditions [Fe] = 27.0 mmol kg^{-1} [Zn] = 8.24 μmol kg^{-1} [SO_4] = 10.4 mmol kg^{-1}	
pH	% Zn sorbed	pH	% Zn sorbed	pH	% Zn sorbed
4.78	11.61	4.47	18.39	4.33	14.11
5.14	31.25	4.85	36.07	4.64	25.18
5.41	54.46	5.22	53.75	5.08	50.89
5.71	77.32	5.41	69.29	5.37	66.96
5.84	83.04	5.73	83.93	5.59	79.11
5.99	92.50	5.74	84.82	5.76	86.79
6.24	97.32	6.27	98.04	5.92	91.96

Expt. Conditions [Fe] = 1.42 mmol kg^{-1} [Zn] = 24.0 μmol kg^{-1} [SO_4] = 2.08 mmol kg^{-1}		Expt. Conditions [Fe] = 1.42 mmol kg^{-1} [Zn] = 24.0 μmol kg^{-1} [SO_4] = 10.4 mmol kg^{-1}		Expt. Conditions [Fe] = 1.03 mmol kg^{-1} [Zn] = 7.96 μmol kg^{-1} [SO_4] = 20.8 mmol kg^{-1}	
pH	% Zn sorbed	pH	% Zn sorbed	pH	% Zn sorbed
4.38	7.00	3.80	3.33	3.13	0.00
4.61	14.59	4.22	7.06	3.96	1.90
4.90	26.99	4.88	38.43	4.89	7.69
5.10	40.52	5.18	56.27	5.38	13.48
5.30	55.40	5.76	89.41	5.98	24.97
5.55	74.75	6.42	100.00	6.41	46.05
5.74	86.37			6.74	67.22
				7.55	96.09

Table A3.6

Expt. Conditions [Fe] = 14.6 mmol kg^{-1} [Cu] = 23.5 μmol kg^{-1}		Expt. Conditions [Fe] = 4.80 mmol kg^{-1} [Cu] = 1.64 μmol kg^{-1}		Expt. Conditions [Fe] = 14.6 mmol kg^{-1} [Zn] = 30.0 μmol kg^{-1}		Expt. Conditions [Fe] = 4.80 mmol kg^{-1} [Zn] = 20.2 μmol kg^{-1}	
pH	% Cu sorbed	pH	% Cu sorbed	pH	% Zn sorbed	pH	% Zn sorbed
4.41	2.74	4.39	6.10	4.26	2.05	4.13	3.50
4.88	3.45	4.91	10.67	4.68	4.79	4.67	10.50
5.35	17.52	5.50	28.74	5.06	12.30	4.97	16.32
5.86	47.98	5.90	62.46	5.50	26.52	5.48	33.98
6.32	81.75	6.41	83.79	5.94	52.13	5.83	53.96
6.78	93.71	6.86	95.13	6.49	83.16	6.32	81.08
7.40	99.16	7.40	98.97	7.04	97.85	6.80	96.36

Table A4.1

Expt. Conditions [Fe]= 10.1 mmol kg^{-1} [Co]= 1.72 μmol kg^{-1}		Expt. Conditions [Fe]= 10.1 mmol kg^{-1} [Co]= 17.2 μmol kg^{-1}		Expt. Conditions [Fe]= 10.1 mmol kg^{-1} [Co]= 163 μmol kg^{-1}		Expt. Conditions [Fe]= 9.83 mmol kg^{-1} [Co]= 1.67 to 127 μmol kg^{-1}		
pH	% Co sorbed	pH	% Co sorbed	pH	% Co sorbed	pH	log $[Co]_{aq}$ mol kg^{-1}	log Γ_{Co} mol (mol Fe^{1})
5.80	8.29	5.63	1.79	5.69	3.38	6.26	-5.93	-4.31
6.31	33.44	6.25	20.85	6.07	12.30	6.23	-5.62	-4.01
6.64	60.75	6.40	41.60	6.49	27.59	6.26	-5.23	-3.58
7.31	95.50	6.76	77.97	6.87	55.64	6.2	-4.94	-3.28
7.87	98.67	7.00	92.06	7.38	88.19	6.32	-4.64	-3.05
7.77	98.20	7.52	97.57	7.76	97.09	6.28	-4.32	-2.81
6.84	82.30	8.06	99.84	8.47	99.37	6.28	-3.99	-2.60

Table A4.2

Expt. Conditions [Fe] = 10.1 mmol kg^{-1} [Co]= 1.72 μmol kg^{-1} $[SO_4]$= 2.05 mmol kg^{-1}		Expt. Conditions [Fe] =10.1 mmol kg^{-1} [Co] =1.72 μmol kg^{-1} $[SO_4]$ =10.4 mmol kg^{-1}		Expt. Conditions [Fe]= 10.1 mmol kg^{-1} [Co] = 17.2 μmol kg^{-1} $[SO_4]$=1.98 mmol kg^{-1}		Expt. Conditions [Fe] = 10.1 mmol kg^{-1} [Co] =17.2 μmol kg^{-1} $[SO_4]$ =10.4 mmol kg^{-1}		Expt. Conditions [Fe] =10.1 mmol kg^{-1} [Co] = 163 μmol kg^{-1} $[SO_4]$ = 1.98 mmol kg^{-1}	
pH	% Co sorbed	pH	% Co sorbed	pH	% Co sorbed	pH	% Co sorbed	pH	% Co sorbed
5.66	24.13	5.89	46.73	5.77	22.33	5.88	35.25	5.75	21.36
6.29	53.90	6.31	66.99	6.20	45.68	6.41	63.62	6.30	36.84
6.86	82.78	6.79	84.87	6.57	67.07	6.69	76.60	6.71	56.88
6.82	79.37	7.26	94.59	6.85	88.62	6.99	91.50	7.19	78.20
7.29	94.04	7.66	96.21	6.86	86.91	7.08	93.75	7.49	93.62
7.52	98.37	8.11	96.99	7.49	97.68	7.64	97.78	8.20	99.02
8.10	99.13	7.46	96.21	7.86	99.38	8.02	98.88	8.36	99.53

Table A4.3

Expt. Conditions [Fe]= 15.0 mmol kg^{-1} [Pb]= 9.66 μmol kg^{-1}		Expt. Conditions [Fe]= 5.00 mmol kg^{-1} [Pb]= 9.66 μmol kg^{-1}		Expt. Conditions [Fe]= 1.09 mmol kg^{-1} [Pb]= 9.86 μmol kg^{-1}		Expt. Conditions [Fe]= 1.10 mmol kg^{-1} [Pb]= 19.7 μmol kg^{-1}		Expt. Conditions [Fe]= 14.9 mmol kg^{-1} [Pb]= 0.518 to 50.5 μmol kg^{-1}		
pH	% Pb sorbed	pH	% Pb sorbed	pH	% Pb sorbed	pH	% Pb sorbed	pH	log $[Pb]_{aq}$ mol kg^{-1}	log Γ_{Pb} mol(mol Fe^{1})
3.22	66.14	3.21	33.00	3.10	7.84	3.11	4.66	3.59	-7.43	-4.49
3.54	83.59	3.44	42.25	3.58	15.20	3.48	9.07	3.59	-7.13	-4.12
3.82	91.50	3.78	61.80	3.84	24.02	4.12	27.70	3.60	-6.86	-3.81
4.21	96.80	4.13	81.55	4.33	43.63	4.37	36.52	3.60	-6.39	-3.53
4.43	99.50	4.25	86.60	4.54	58.28	4.61	49.51	3.58	-5.71	-3.17
4.68	98.20	4.38	90.15	5.09	86.13	5.08	75.00	3.57	-5.21	-2.91
4.89	99.00	4.74	96.05	5.51	97.11	5.43	89.41	3.57	-4.80	-2.63
						5.69	96.05			

Table A4.6

Expt. Conditions [Fe] = 15.0 mmol kg^{-1} [Pb] = 9.66 μmol kg^{-1} [SO_4] = 1.04 mmol kg^{-1}		Expt. Conditions [Fe] =15.0 mmol kg^{-1} [Pb] =9.66 μmol kg^{-1} [SO_4] =2.60 mmol kg^{-1}		Expt. Conditions [Fe] = 15.0 mmol kg^{-1} [Pb] = 9.66 μmol kg^{-1} [SO_4] =5.21 mmol kg^{-1}		Expt. Conditions [Fe] = 5.00 mmol kg^{-1} [Pb] = 9.66 μmol kg^{-1} [SO_4] =2.08 mmol kg^{-1}		Expt. Conditions [Fe] = 5.00 mmol kg^{-1} [Pb] = 9.66 μmol kg^{-1} [SO_4] =4.17 mmol kg^{-1}	
pH	% Pb sorbed	pH	% Pb sorbed	pH	% Pb sorbed	pH	% Pb sorbed	pH	% Pb sorbed
3.23	80.99	3.32	90.02	3.24	90.26	3.13	62.90	3.17	65.65
3.48	90.53	3.59	97.05	3.46	95.30	3.36	74.40	3.35	76.45
3.72	93.86	3.88	98.35	3.74	98.50	3.83	90.65	3.52	84.65
4.03	98.00	4.33	100.00	4.18	99.50	3.90	91.65	3.69	91.10
4.26	97.65	4.53	100.00	4.26	100.00	4.08	94.05	3.95	95.40
4.40	99.60	4.63	100.00	4.44	100.00	4.32	96.50	4.25	98.40
4.65	100.00	4.91	100.00	4.62	100.00	4.64	98.25	4.65	100.00

Table A4.7

Expt. Conditions [Fe] = 1.09 mmol kg^{-1} [Pb] = 9.90 μmol kg^{-1} [SO_4]=0.232mmol kg^{-1}		Expt. Conditions [Fe] =1.09 mmol kg^{-1} [Pb] =10.2 μmol kg^{-1} [SO_4]=1.08 mmol kg^{-1}		Expt. Conditions [Fe] = 1.09 mmol kg^{-1} [Pb] = 9.95 μmol kg^{-1} [SO_4]=3.13 mmol kg^{-1}	
pH	% Pb sorbed	pH	% Pb sorbed	pH	% Pb sorbed
3.23	15.17	3.18	14.84	3.11	16.86
3.55	19.19	3.44	22.14	3.45	29.45
3.74	26.78	3.79	32.12	3.70	35.15
4.00	33.18	4.12	41.36	3.93	43.71
4.35	46.92	4.40	52.80	4.28	57.72
4.70	63.03	4.80	72.75	4.68	74.35
5.03	78.51	5.02	83.26	5.19	94.58
3.74	25.59	3.80	30.66	3.60	33.25

Expt. Conditions [Fe] = 1.10 mmol kg^{-1} [Pb] = 20.4 μmol kg^{-1} [SO_4]=0.105mmol kg^{-1}		Expt. Conditions [Fe] = 1.10 mmol kg^{-1} [Pb] = 19.9 μmol kg^{-1} [SO_4]=0.317mmol kg^{-1}		Expt. Conditions [Fe] = 1.10 mmol kg^{-1} [Pb] = 20.3 μmol kg^{-1} [SO_4]=1.06 mmol kg^{-1}	
pH	% Pb sorbed	pH	% Pb sorbed	pH	% Pb sorbed
3.18	18.34	2.95	16.11	2.97	18.45
3.53	26.83	3.26	26.54	3.22	26.70
3.77	36.54	3.68	41.71	3.43	34.95
4.15	53.90	4.06	58.01	3.72	50.00
4.40	63.22	4.51	78.39	4.03	63.16
4.81	81.66	5.03	91.75	4.23	69.17
5.12	91.66	3.94	53.93	4.49	82.09
3.66	32.20	3.23	26.07	4.73	88.16

Table A4.9

Expt. Conditions [Fe]=10.3 mmol kg^{-1} [Cd]=0.949μmol kg^{-1}		Expt. Conditions [Fe]=10.5mmol kg^{-1} [Cd]=9.93 μmol kg^{-1}		Expt. Conditions [Fe]=0.943mmol kg^{-1} [Cd]= 9.37 μmol kg^{-1}		Expt. Conditions [Fe]= 9.00 mmol kg^{-1} [Cd]= 93.4 μmol kg^{-1}		Expt. Conditions [Fe]= 7.78 mmol kg^{-1} [Cd]= 0.230 to 2210 μmol kg^{-1}		
pH	% Cd sorbed	pH	% Cd sorbed	pH	% Cd sorbed	pH	% Cd sorbed	pH	log [Cd]$_{aq}$ mol kg^{-1}	log Γ_{Cd} mol (mol Fe^{-1})
5.08	1.18	4.01	0.44	5.37	3.13	4.42	1.82	7.62	-9.08	-4.53
5.53	10.68	4.40	2.60	6.02	6.94	4.96	3.14	7.60	-8.65	-4.02
6.12	56.67	4.82	3.42	6.58	16.58	5.39	4.76	7.62	-8.10	-3.54
6.57	91.31	5.33	11.06	6.85	32.90	5.85	10.15	7.66	-7.33	-3.01
7.29	98.85	5.72	19.87	7.24	56.75	6.11	19.17	7.58	-6.48	-2.53
		6.28	59.08	7.60	84.29	6.56	45.66	7.68	-5.53	-1.99
		6.82	91.12			7.32	91.64	7.64	-4.61	-1.53
								7.66	-3.69	-1.13
								7.69	-2.91	-0.89

Expt. Conditions: Replicate experiment, data not shown in Figure 8. [Fe]= 8.25 mmol kg^{-1} [Cd]= 9.53 μmol kg^{-1}							
pH	4.35	5.09	5.56	5.89	6.30	6.85	7.00
% Cd sorbed	0.00	3.39	13.85	25.80	60.41	91.95	97.19

Table A4.10

Expt. Conditions [Fe] =10.3 mmol kg^{-1} [Cd]=0.973 μmol kg^{-1} [SO_4]=1.96 mmol kg^{-1}		Expt. Conditions [Fe]=10.3 mmol kg^{-1} [Cd]=0.957 μmol kg^{-1} [SO_4]=10.4 mmol kg^{-1}		Expt. Conditions [Fe] = 10.5 mmol kg^{-1} [Cd] = 9.67 μmol kg^{-1} [SO_4] =2.01 mmol kg^{-1}		Expt. Conditions [Fe] = 10.5 mmol kg^{-1} [Cd] = 9.62 μmol kg^{-1} [SO_4] =10.3 mmol kg^{-1}		Expt. Conditions [Fe] = 10.5 mmol kg^{-1} [Cd] = 9.15 μmol kg^{-1} [SO_4] = 19.5 mmol kg^{-1}	
pH	% Cd sorbed	pH	% Cd sorbed	pH	% Cd sorbed	pH	% Cd sorbed	pH	% Cd sorbed
4.41	2.74	4.39	6.10	4.26	2.05	4.13	3.50	4.28	5.99
4.88	3.45	4.91	10.67	4.68	4.79	4.67	10.50	4.77	13.34
5.35	17.52	5.50	28.74	5.06	12.30	4.97	16.32	5.13	21.85
5.86	47.98	5.90	62.46	5.50	26.52	5.48	33.98	5.52	37.37
6.32	81.75	6.41	83.79	5.94	52.13	5.83	53.96	5.89	60.05
6.78	93.71	6.86	95.13	6.49	83.16	6.32	81.08	6.33	81.93
7.40	99.16	7.40	98.97	7.04	97.85	6.80	96.36	6.54	90.05

Expt. Conditions [Fe] = 8.25 mmol kg^{-1} [Cd] = 9.53 μmol kg^{-1} [SO_4] = 2.06 mmol kg^{-1} Replicate experiments, data not shown in Figure 9		Expt. Conditions [Fe] = 8.25 mmol kg^{-1} [Cd] = 9.53 μmol kg^{-1} [SO_4] = 10.2 mmol kg^{-1}		Expt. Conditions [Fe] = 0.943 mmol kg^{-1} [Cd] = 9.14 μmol kg^{-1} [SO_4] =2.20 mmol kg^{-1}		Expt. Conditions [Fe] = 0.943 mmol kg^{-1} [Cd] = 9.09 μmol kg^{-1} [SO_4] = 10.9 mmol kg^{-1}	
PH	% Cd sorbed	pH	% Cd sorbed	pH	% Cd sorbed	pH	% Cd sorbed
4.36	4.81	4.87	13.52	5.10	3.79	5.40	4.93
4.91	8.82	5.26	24.16	5.62	5.44	5.77	7.29
5.41	22.02	5.74	41.51	6.07	12.41	6.11	14.37
5.64	29.12	6.25	69.11	6.46	21.87	6.39	21.46
6.16	57.00	6.56	89.03	6.86	39.24	6.95	49.80
6.68	90.77	6.86	97.41	7.29	68.35	7.31	73.17
6.98	96.45			7.67	88.80	7.64	87.58

TABLE A5.1

Expt. Conditions I = 0.10 mol kg^{-1} 6.2 g kg^{-1} α-FeOOH		Expt. Conditions I = 0.020 mol kg^{-1} 6.2 g kg^{-1} α-FeOOH		Expt. Conditions I = 0.0040 mol kg^{-1} 6.2 g kg^{-1} α-FeOOH	
pH	C_A-C_B	pH	C_A-C_B	pH	C_A-C_B
4.737	8.95E-04	4.434	7.99E-04	4.082	7.85E-04
4.727	8.87E-04	4.449	7.92E-04	4.099	7.78E-04
4.729	8.80E-04	4.466	7.85E-04	4.120	7.70E-04
4.745	8.73E-04	4.491	7.77E-04	4.141	7.63E-04
4.770	8.66E-04	4.513	7.70E-04	4.196	7.40E-04
4.797	8.59E-04	4.680	7.20E-04	4.219	7.33E-04
4.871	8.37E-04	4.754	6.98E-04	4.364	6.80E-04
4.970	8.09E-04	4.912	6.55E-04	4.548	6.21E-04
5.098	7.73E-04	5.103	6.04E-04	4.731	5.68E-04
5.283	7.23E-04	5.307	5.53E-04	4.945	5.16E-04
5.472	6.73E-04	5.495	5.10E-04	5.004	5.01E-04
5.663	6.23E-04	5.590	4.88E-04	5.099	4.79E-04
5.864	5.73E-04	5.798	4.45E-04	5.234	4.49E-04
6.045	5.31E-04	5.981	4.09E-04	5.373	4.19E-04
6.168	5.02E-04	6.092	3.87E-04	5.525	3.89E-04
6.365	4.59E-04	6.295	3.51E-04	5.684	3.59E-04
6.462	4.38E-04	6.458	3.22E-04	5.810	3.37E-04
6.674	3.95E-04	6.678	2.86E-04	5.982	3.07E-04
6.818	3.66E-04	6.771	2.72E-04	6.117	2.85E-04
7.035	3.24E-04	6.962	2.43E-04	6.309	2.55E-04
7.222	2.88E-04	7.159	2.14E-04	6.411	2.40E-04
7.421	2.52E-04	7.310	1.92E-04	6.566	2.17E-04
7.541	2.31E-04	7.419	1.78E-04	6.737	1.95E-04
7.664	2.09E-04	7.480	1.71E-04	6.802	1.88E-04
7.870	1.74E-04	7.585	1.56E-04	6.867	1.80E-04
8.036	1.45E-04	7.644	1.49E-04	7.105	1.50E-04
8.251	1.10E-04	7.865	1.20E-04	7.176	1.43E-04
8.377	8.81E-05	8.109	9.11E-05	7.255	1.35E-04
8.550	5.96E-05	8.175	8.38E-05	7.450	1.13E-04
8.714	3.11E-05	8.242	7.66E-05	7.534	1.05E-04
8.834	9.68E-06	8.414	5.50E-05	7.622	9.79E-05
9.023	-2.60E-05	8.481	4.77E-05	7.711	9.04E-05
9.194	-6.16E-05	8.656	2.61E-05	7.791	8.29E-05
9.347	-9.72E-05	8.720	1.89E-05	7.792	7.55E-05
9.511	-1.40E-04	8.781	1.16E-05	7.856	7.55E-05
9.647	-1.83E-04	8.894	2.80E-06	7.960	6.80E-05
9.787	-2.32E-04	9.108	-3.17E-05	8.062	6.05E-05
9.921	-2.89E-04	9.307	-6.05E-05	8.158	5.31E-05
10.061	-3.60E-04	9.474	-8.93E-05	8.247	4.56E-05
10.198	-4.45E-04	9.611	-1.18E-04	8.338	3.81E-05
10.340	-5.50E-04	9.753	-1.54E-04	8.532	2.32E-05
10.474	-6.77E-04	9.891	-1.97E-04	8.731	8.28E-06
10.613	-8.38E-04	10.023	-2.47E-04	8.822	8.21E-07
		10.158	-3.12E-04	8.928	6.63E-06
		10.289	-3.91E-04	9.017	-1.41E-05
		10.420	-4.91E-04	9.094	-2.15E-05
		10.556	-6.19E-04	9.298	-4.39E-05
		10.695	-7.82E-04	9.470	-6.62E-05
				9.604	-8.85E-05
				9.742	-1.18E-04
				9.874	-1.55E-04
				10.014	-2.07E-04
				10.138	-2.67E-04
				10.270	-3.48E-04
				10.399	-4.52E-04

Table A5.4a

Expt. Conditions CuGA1 1.39 kg^{-1} α-FeOOH [Cu] =1.10 to 817 μmol kg^{-1}			Expt. Conditions CuGA2 1.42 g kg^{-1} α-FeOOH [Cu] =1.04 to 83.3 μmol kg^{-1}			Expt. Conditions CuGB1 1.66 g kg^{-1} α-FeOOH [Cu] =0.524 to 52.5 μmol kg^{-1}			Expt. Conditions CuGB2 1.70 g kg^{-1} α-FeOOH [Cu]=0.874 to 65.7μmolkg^{-1}		
pH	log [Me_{aq}] mol kg^{-1}	log Γ_{Me} nm^{-2}	pH	log [Me_{aq}] mol kg^{-1}	log Γ_{Me} nm^{-2}	pH	log [Me_{aq}] mol kg^{-1}	log Γ_{Me} nm^{-2}	pH	log [Me_{aq}] mol kg^{-1}	log Γ_{Me} nm^{-2}
5.09	-7.10	-2.33	4.92	-6.90	-2.32	4.18	-6.56	-2.95	4.18	-6.31	-2.78
5.09	-6.72	-2.04	4.91	-6.58	-2.02	4.17	-6.23	-2.72	4.18	-6.00	-2.53
5.14	-6.41	-1.73	4.89	-6.02	-1.78	4.18	-5.89	-2.53	4.18	-5.64	-2.33
5.05	-6.04	-1.44	4.88	-5.59	-1.53	4.18	-5.59	-2.25	4.18	-5.22	-2.03
5.06	-5.47	-1.19	4.87	-5.23	-1.24	4.19	-5.25	-2.01	4.22	-4.91	-1.76
5.05	-5.01	-0.93	4.86	-4.83	-1.00	4.23	-4.92	-1.75	4.17	-4.56	-1.60
4.95	-4.51	-0.52	4.91	-4.41	-0.63	4.19	-4.34	-1.49	4.18	-4.23	-1.52
4.97	-4.13	-0.28									
4.95	-3.67	-0.13									
5.00	-3.26	0.09									

Table A5.4b and A5.4c

Expt. Conditions CdGA 1.38 kg^{-1} α-FeOOH [Cd]=0.0793 to 204 μmol kg^{-1}			Expt. Conditions CdGB 1.65 g kg^{-1} α-FeOOH [Cd] =0.785 to 14.2 μmol kg^{-1}			Expt. Conditions PbGA 1.73 g kg^{-1} α-FeOOH [Pb] =0.293 to 61.7 μmol kg^{-1}			Expt. Conditions PbGB 1.66 g kg^{-1} α-FeOOH [Pb] =0.282 to 11.2 μmol kg^{-1}		
pH	log [Me_{aq}] mol kg^{-1}	log Γ_{Me} nm^{-2}	pH	log [Me_{aq}] mol kg^{-1}	log Γ_{Me} nm^{-2}	pH	log [Me_{aq}] mol kg^{-1}	log Γ_{Me} nm^{-2}	pH	log [Me_{aq}] mol kg^{-1}	log Γ_{Me} nm^{-2}
7.51	-9.32	-3.37	6.46	-7.81	-3.54	5.18	-8.04	-2.91	4.17	-6.78	-3.28
7.58	-9.00	-2.91	6.48	-7.32	-3.09	5.18	-7.68	-2.60	4.19	-6.50	-2.94
7.66	-8.36	-2.39	6.56	-6.80	-2.63	5.17	-7.30	-2.30	4.20	-6.18	-2.61
7.59	-7.57	-1.91	6.49	-6.30	-2.36	5.23	-6.91	-1.99	4.18	-5.87	-2.32
7.63	-6.76	-1.40	6.45	-5.85	-2.01	5.19	-6.49	-1.68	4.23	-5.49	-2.05
7.55	-5.92	-0.94	6.50	-5.55	-1.71	5.24	-5.99	-1.38	4.18	-5.09	-1.87
7.71	-4.97	-0.46	6.46	-5.12	-1.52	5.19	-5.32	-1.02			
7.66	-4.06	-0.17				5.15	-4.53	-0.67			
7.65	-3.28	0.02				5.24	-3.93	-0.26			
7.74	-2.75	0.13				5.20	-3.40	-0.03			

Table A5.4d

Expt. Conditions ZnGA1 1.839 kg^{-1} α-FeOOH [Zn] =1.64 to 126 μmol kg^{-1}			Expt. Conditions ZnGA2 1.91 g kg^{-1} α-FeOOH [Zn] =16.3 to 50.2 μmol kg^{-1}			Expt. Conditions ZnGB1 1.66 g kg^{-1} α-FeOOH [Zn]=0.900 to 35.7μmol kg^{-1}			Expt. Conditions ZnGB2 1.74 g kg^{-1} α-FeOOH [Zn]=0.523 to 32.3μmol kg^{-1}		
pH	log [Me_{aq}] mol kg^{-1}	log Γ_{Me} nm^{-2}	pH	log [Me_{aq}] mol kg^{-1}	log Γ_{Me} nm^{-2}	pH	log [Me_{aq}] mol kg^{-1}	log Γ_{Me} nm^{-2}	pH	log [Me_{aq}] mol kg^{-1}	log Γ_{Me} nm^{-2}
6.79	-7.51	-2.19	6.39	-5.68	-1.25	6.06	-6.58	-2.54	5.98	-6.97	-2.74
6.77	-7.21	-2.00	6.33	-5.05	-1.03	6.02	-6.30	-2.23	5.95	-6.51	-2.51
6.78	-7.34	-2.00	6.26	-4.56	-0.83	6.02	-5.98	-1.90	5.94	-6.29	-2.18
6.62	-6.47	-1.49	6.24	-4.11	-0.70	6.02	-5.67	-1.60	5.91	-5.95	-1.88
6.65	-6.20	-1.21	6.24	-3.79	-0.44	5.95	-5.20	-1.33	5.95	-5.57	-1.61
6.62	-5.83	-0.92	6.27	-3.42	-0.32	5.99	-4.72	-1.12	5.84	-5.06	-1.47
6.58	-4.78	-0.62							5.83	-4.75	-1.20
6.45	-4.19	-0.46									
6.40	-3.52	-0.29									
6.35	-2.95	-0.25									

Table A5.6a

Expt. Conditions CuGS1A 1.51 g kg^{-1} α-FeOOH [Cu] = 3.37 μmol kg^{-1}		Expt. Conditions CuGS2A 1.57 g kg^{-1} α-FeOOH [Cu] = 165 μmol kg^{-1}		Expt. Conditions ZnGS1A 1.42 g kg^{-1} α-FeOOH [Zn] = 2.89 μmol kg^{-1}		Expt. Conditions ZnGS2A 1.36 g kg^{-1} α-FeOOH [Zn] = 152 μmol kg^{-1}	
pH	% Cu sorbed	pH	% Cu sorbed	pH	% Zn sorbed	pH	% Zn sorbed
3.86	5.88	3.90	1.57	4.50	-0.04	5.49	8.41
4.14	20.72	4.12	6.84	4.89	10.03	5.83	13.54
4.39	42.54	4.33	16.44	5.23	22.57	5.91	19.43
4.56	57.17	4.57	29.56	5.33	28.68	6.27	31.06
4.70	70.45	4.90	57.66	5.39	37.71	6.57	44.81
4.87	81.26	5.21	78.30	5.44	29.41	6.74	49.77
		5.46	90.14	5.73	49.36	7.33	84.09
				5.92	74.15		
				5.97	70.40		
				6.10	84.13		

Table A5.6b

Expt. Conditions PbGS1A 1.36 g kg^{-1} α-FeOOH [Pb] = 0.888 μmol kg^{-1}		Expt. Conditions PbGS2A 1.42 g kg^{-1} α-FeOOH [Pb] = 44.4 μmol kg^{-1}		Expt. Conditions CdGS1A 1.35 g kg^{-1} α-FeOOH [Cd] = 1.65 μmol kg^{-1}		Expt. Conditions CdGS2A 1.44 g kg^{-1} α-FeOOH [Cd] = 62.4 μmol kg^{-1}	
pH	% Pb sorbed	pH	% Pb sorbed	pH	% Cd sorbed	pH	% Cd sorbed
3.48	2.91	3.97	7.96	3.75	0.00	5.81	8.43
3.78	11.87	4.21	13.23	5.40	7.82	6.09	14.03
4.00	25.37	4.40	20.10	5.62	14.75	6.34	19.72
4.26	45.40	4.63	33.59	5.95	39.45	6.64	27.68
4.56	72.28	4.89	44.57	6.25	50.01	6.80	36.51
4.73	83.39	5.07	59.74	6.54	73.36	6.95	47.08
5.08	93.67	5.35	70.46	6.89	87.99	7.21	61.33
5.17	95.00						

Table A5.7

Expt. Conditions SO4GI 1.49 g kg^{-1} α-FeOOH $[SO_4]$ = 0.0671 to 2.06 mmol kg^{-1}			Expt. Conditions GSA 1.31 g kg^{-1} α-FeOOH $[SO_4]$ = 776 μmol kg^{-1}		Expt. Conditions GSB 1.22 g kg^{-1} α-FeOOH $[SO_4]$ = 206 μmol kg^{-1}		Expt. Conditions GSC 1.31 g kg^{-1} α-FeOOH $[SO_4]$ = 202 μmol kg^{-1}	
pH	log $[SO_{4\,aq}]$ mol kg^{-1}	log Γ_{SO_4} nm^{-2}	pH	% SO_4 sorbed	pH	% Pb sorbed	pH	% Pb sorbed
4.15	-4.99	-0.54	3.54	19.33	3.55	60.20	3.50	65.44
4.10	-4.62	-0.31	5.05	13.90	4.08	52.22	4.37	51.71
4.08	-4.00	-0.20	6.28	6.34	4.67	42.79	5.50	31.40
4.10	-3.44	-0.07	7.06	3.51	5.14	35.06	6.91	10.10
4.16	-3.05	-0.04	8.02	1.00	6.09	21.10	8.14	0.16
4.15	-2.73	-0.01	10.30	0.00	6.72	13.85		
					7.29	8.47		
					7.64	5.91		

Table A5.8a and A5.8b

Expt. Conditions 1.51 g kg^{-1} FeOOH SO_4=2.09 mmol kg^{-1} Cu = 3.38 μmol kg^{-1}		Expt. Conditions 1.51 g kg^{-1} FeOOH SO_4 =516 mmol kg^{-1} Cu = 3.39 μmol kg^{-1}		Expt. Conditions 1.31 g kg^{-1} FeOOH SO_4=10.4 mmol kg^{-1} Cu = 3.42 μmol kg^{-1}		Expt. Conditions 1.57 g kg^{-1} FeOOH SO_4 =2.10mmol kg^{-1} Cu = 168 μmol kg^{-1}		Expt. Conditions 1.57 g kg^{-1} FeOOH SO_4=5.28mmol kg^{-1} Cu = 174 μmol kg^{-1}		Expt. Conditions 1.57 g kg^{-1} FeOOH SO_4 =10.3mmol kg^{-1} Cu = 168 μmol kg^{-1}	
pH	% Cu sorbed	pH	% Cu sorbed	pH	% Cu sorbed	pH	% Cu sorbed	pH	% Cu sorbed	pH	% Cu sorbed
3.80	36.35	3.78	39.99	3.69	42.59	3.57	8.50	3.56	6.84	3.69	11.79
4.01	50.71	3.99	57.47	3.92	55.65	3.89	18.05	3.89	15.50	3.87	17.30
4.20	68.94	4.22	70.48	4.13	68.56	4.20	28.25	4.14	25.13	4.17	27.97
4.43	77.62	4.45	81.65	4.35	79.03	4.53	45.11	4.39	35.87	4.43	39.06
4.64	86.34	4.68	89.18	4.55	86.40	4.81	60.42	4.62	49.66	4.65	50.07
4.84	91.89	4.92	94.08	4.78	91.26	4.90	66.87	4.92	67.01	4.96	68.91
5.01	94.23					5.21	85.28	5.28	87.91	5.29	87.33

Table A5.8c and A5.8d

Expt. Conditions 1.34 g kg^{-1} FeOOH SO_4=2.12mmol kg^{-1} Cd= 1.62 μmol kg^{-1}		Expt. Conditions 1.34 g kg^{-1} FeOOH SO_4 =523 mmol kg^{-1} Cd = 1.61 μmol kg^{-1}		Expt. Conditions 1.34 g kg^{-1} FeOOH SO_4=9.07 mmol kg^{-1} Cd = 1.49 μmol kg^{-1}		Expt. Conditions 1.44 g kg^{-1}FeOOH SO_4=2.12mmolkg^{-1} Cd=69.3 μmol kg^{-1}		Expt. Conditions 1.44 g kg^{-1} FeOOH SO_4=5.23mmol kg^{-1} Cd = 71.0 μmol kg^{-1}		Expt. Conditions 1.44 g kg^{-1} FeOOH SO_4=9.07mmol kg^{-1} Cd= 67.1 μmol kg^{-1}	
pH	% Cd sorbed	pH	% Cd sorbed	pH	% Cd sorbed	pH	% Cd sorbed	pH	% Cd sorbed	pH	% Cd sorbed
5.41	32.47	5.35	32.92	5.49	37.95	5.92	24.93	5.88	27.09	6.02	34.46
5.61	38.83	5.65	44.75	5.74	47.57	6.14	33.16	6.13	37.17	6.19	43.38
5.90	55.63	5.84	53.79	5.97	65.61	6.43	46.22	6.50	51.74	6.48	56.58
6.14	69.29	6.06	67.54	6.22	77.88	6.61	55.38	6.70	63.68	6.70	68.68
6.45	83.93	6.41	84.64	6.47	88.60	6.90	67.22	6.84	71.00	6.89	77.69
6.65	89.43	6.65	91.47	6.64	93.89	7.08	75.51	6.99	77.50	7.00	84.01
6.89	94.29	6.95	96.44	6.77	93.33	7.30	83.27	7.27	84.84	7.29	87.49

Table A5.9a and A5.9b

Expt. Conditions 1.36 g kg^{-1} FeOOH SO_4=2.09 mmol kg^{-1} Pb =0.892 μmol kg^{-1}		Expt. Conditions 1.36 g kg^{-1} FeOOH SO_4 =5.16 mol kg^{-1} Pb=0.897 μmol kg^{-1}		Expt. Conditions 1.36 g kg^{-1} FeOOH SO_4=10.4 mmol kg^{-1} Pb=0.905 μmol kg^{-1}		Expt. Conditions 1.42 g kg^{-1} FeOOH SO_4=0.53mmol kg^{-1} Pb =43.4 μmol kg^{-1}		Expt. Conditions 1.42 g kg^{-1} FeOOH SO_4 =1.23mmol kg^{-1} Pb = 43.1 μmol kg^{-1}		Expt. Conditions 1.42 g kg^{-1} FeOOH SO_4 =1.61mmol kg^{-1} Pb = 45.5 μmol kg^{-1}	
pH	% Pb sorbed	pH	% Pb sorbed	pH	% Pb sorbed	pH	% Pb sorbed	pH	% Pb sorbed	pH	% Pb sorbed
3.39	18.02	3.68	31.07	3.42	17.23	3.88	13.49	3.82	14.52	3.9	20.11
3.75	37.93	3.87	46.03	3.74	37.43	4.09	23.13	4.14	28.03	4.16	28.83
3.94	52.08	4.01	58.74	4.02	56.74	4.33	28.38	4.36	34.87	4.27	32.51
4.25	73.69	4.29	78.65	4.22	75.24	4.56	40.83	4.54	43.02	4.51	42.28
4.52	88.64	4.55	90.70	4.46	87.48	4.83	58.02	4.75	57.25	4.73	55.45
4.72	93.38	4.94	96.67	4.66	92.71	5.03	69.29	4.98	70.91	4.93	67.91
4.91	96.63			4.89	96.32	5.22	79.62	5.2	80.99	5.2	82.68

Table A5.9c and A5.9d

Expt. Conditions 1.48 g kg^{-1} FeOOH SO_4=2.06 mmol kg^{-1} Zn = 2.89 μmol kg^{-1}		Expt. Conditions 1.48 g kg^{-1} FeOOH SO_4 =5.02mmol kg^{-1} Zn = 2.95 μmol kg^{-1}		Expt. Conditions 1.48 g kg^{-1} FeOOH SO_4=10.3 mmol kg^{-1} Zn = 2.93μmol kg^{-1}		Expt. Conditions 1.36 g kg^{-1} FeOOH SO_4 =2.21mmol kg^{-1} Zn = 145 μmol kg^{-1}		Expt. Conditions 1.36 g kg^{-1} FeOOH SO_4 =4.64mmol kg^{-1} Zn = 145 μmol kg^{-1}		Expt. Conditions 1.36 g kg^{-1} FeOOH SO_4 =9.42mmol kg^{-1} Zn = 154 μmol kg^{-1}	
pH	% Zn sorbed	pH	% Zn sorbed	pH	% Zn sorbed	pH	% Zn sorbed	pH	% Zn sorbed	pH	% Zn sorbed
4.56	15.71	5.09	37.23	4.90	36.20	5.56	20.04	5.3	13.99	5.31	13.97
4.86	27.87	5.33	49.47	5.24	48.20	5.82	26.66	5.51	18.17	5.51	19.42
5.12	35.50	5.60	67.30	5.56	71.30	6.14	39.17	5.77	27.52	5.76	27.59
5.43	51.51	5.99	85.60	5.76	78.50	6.32	44.68	6	36.52	6.02	39.63
5.81	76.11	5.99	86.30	5.98	91.84	6.49	51.72	6.28	45.77	6.37	50.63
6.05	87.81	6.20	90.00	6.19	95.85	6.64	65.05	6.67	67.97	6.71	71.23
6.16	94.08					6.95	77.19	6.87	77.43	6.92	80.24

Table A6.1

Expt. Conditions I = 0.10 mol kg^{-1} 9.4 g kg^{-1} α-FeOOH		Expt. Conditions I = 0.020 mol kg^{-1} 9.4 g kg^{-1} α-FeOOH		Expt. Conditions I = 0.0040 mol kg^{-1} 9.4 g kg^{-1} α-FeOOH	
pH	C_A-C_B	pH	C_A-C_B	pH	C_A-C_B
4.071	2.68E-03	4.268	3.56E-03	4.348	4.31E-03
4.078	2.67E-03	4.273	3.55E-03	4.353	4.31E-03
4.086	2.66E-03	4.279	3.54E-03	4.361	4.30E-03
4.103	2.66E-03	4.286	3.54E-03	4.369	4.29E-03
4.120	2.65E-03	4.348	3.46E-03	4.436	4.21E-03
4.150	2.62E-03	4.375	3.43E-03	4.462	4.18E-03
4.159	2.61E-03	4.507	3.26E-03	4.603	4.00E-03
4.259	2.50E-03	4.660	3.07E-03	4.753	3.81E-03
4.402	2.34E-03	4.825	2.88E-03	4.911	3.61E-03
4.563	2.18E-03	4.994	2.69E-03	5.068	3.42E-03
4.733	2.02E-03	5.144	2.54E-03	5.218	3.25E-03
4.910	1.87E-03	5.314	2.37E-03	5.371	3.08E-03
5.071	1.75E-03	5.490	2.20E-03	5.535	2.90E-03
5.241	1.62E-03	5.676	2.03E-03	5.706	2.72E-03
5.415	1.49E-03	5.863	1.87E-03	5.871	2.55E-03
5.608	1.36E-03	6.039	1.72E-03	6.046	2.37E-03
5.805	1.23E-03	6.233	1.57E-03	6.234	2.19E-03
5.949	1.14E-03	6.430	1.42E-03	6.394	2.04E-03
6.134	1.03E-03	6.587	1.31E-03	6.568	1.88E-03
6.328	9.17E-04	6.800	1.16E-03	6.760	1.72E-03
6.527	8.12E-04	6.982	1.05E-03	6.919	1.58E-03
6.648	7.53E-04	7.121	9.61E-04	7.082	1.44E-03
6.780	6.93E-04	7.304	8.54E-04	7.269	1.28E-03
6.915	6.33E-04	7.474	7.54E-04	7.449	1.13E-03
7.084	5.66E-04	7.683	6.39E-04	7.629	9.85E-04
7.179	5.29E-04	7.822	5.69E-04	7.815	8.37E-04
7.371	4.61E-04	7.913	5.23E-04	7.985	7.04E-04
7.460	4.32E-04	8.109	4.23E-04	8.154	5.71E-04
7.617	3.87E-04	8.308	3.23E-04	8.341	4.30E-04
7.672	3.72E-04	8.456	2.47E-04	8.487	3.21E-04
7.785	3.42E-04	8.635	1.54E-04	8.648	2.04E-04
8.000	2.90E-04	8.799	7.00E-05	8.812	8.68E-05
8.063	2.75E-04	8.962	-1.45E-05	8.970	-2.25E-05
8.206	2.37E-04	9.132	-9.88E-05	9.107	-1.16E-04
8.284	2.15E-04	9.253	-1.60E-04	9.264	-2.25E-04
8.460	1.63E-04	9.413	-2.37E-04	9.415	-3.34E-04
8.638	1.03E-04	9.505	-2.83E-04	9.546	-4.35E-04
8.799	4.33E-05	9.622	-3.44E-04	9.695	-5.59E-04
8.992	-2.38E-05	9.741	-4.12E-04	9.834	-6.91E-04
9.159	-8.34E-05	9.878	-5.04E-04	9.971	-8.38E-04
9.343	-1.43E-04	10.015	-6.10E-04	10.108	-1.01E-03
9.375	-1.58E-04	10.148	-7.31E-04	10.245	-1.20E-03
9.373	-1.65E-04	10.282	-8.75E-04	10.382	-1.42E-03
10.139	-5.20E-04	10.411	-1.04E-03	10.522	-1.68E-03
10.218	-6.01E-04	10.549	-1.24E-03	10.660	-1.98E-03
10.363	-7.63E-04	10.687	-1.48E-03	10.802	-2.34E-03
10.467	-9.40E-04	10.836	-1.78E-03	10.945	-2.76E-03
10.611	-1.20E-03	10.984	-2.12E-03		

Table A6.5 and A6.6

Expt. Conditions ABCuA 1.80 kg^{-1} α-FeOOH [Cu] =1.75 to 830 μmol kg^{-1}			Expt. Conditions ABCuB 1.72 g kg^{-1} α-FeOOH [Cu] =0.325 to 17.7 μmol kg^{-1}			Expt. Conditions ABCd 1.52 g kg^{-1} α-FeOOH [Cd] =0.459 to 17.3 μmol kg^{-1}			Expt. Conditions ABS 1.20 g kg^{-1} α-FeOOH	
pH	log [Me_{aq}] mol kg^{-1}	log Γ_{Me} nm^{-2}	pH	log [Me_{aq}] mol kg^{-1}	log Γ_{Me} nm^{-2}	pH	log [Me_{aq}] mol kg^{-1}	log Γ_{Me} nm^{-2}	pH	% adsorbed
4.14	-7.48	-2.65	4.58	-7.45	-3.41	6.07	-7.79	-2.83	3.12	83.77
4.14	-7.23	-2.26	4.58	-7.17	-3.01	6.05	-7.38	-2.54	4.00	76.42
4.13	-6.90	-1.97	4.59	-6.93	-2.68	6.04	-7.00	-2.25	4.50	68.97
4.14	-6.29	-1.65	4.56	-6.37	-2.30	6.05	-6.51	-1.88	5.75	54.34
4.12	-5.59	-1.28	4.52	-5.92	-2.03	6.06	-6.02	-1.59	6.30	37.87
4.09	-4.92	-1.01	4.43	-5.48	-1.73	6.05	-5.59	-1.31	7.04	27.85
4.05	-4.31	-0.78	4.35	-4.91	-1.40	6.01	-4.95	-0.99	7.50	22.42
4.01	-3.89	-0.59	4.32	-4.38	-1.17	6.07	-4.57	-0.72	8.30	11.64
3.97	-3.30	-0.38	4.26	-4.00	-0.98	6.04	-4.09	-0.52	9.00	11.06
									10.15	1.74
									10.50	0.79
									11.04	2.99

Expt. Conditions ABPBA 1.37 kg^{-1} α-FeOOH [Pb] =2.61 to 45.3 μmol kg^{-1}			Expt. Conditions ABPbB 1.51 kg^{-1} α-FeOOH [Pb=0.481 to 23.1 μmol kg^{-1}			Expt. Conditions ABZnA 1.54 g kg^{-1} α-FeOOH [Zn] =30.8 to 153 μmol kg^{-1}			Expt. Conditions ABZnB 1.44 g kg^{-1} α-FeOOH [Zn] =7.77 to 30.7 μmol kg^{-1}		
pH	log [Me_{aq}] mol kg^{-1}	log Γ_{Me} nm^{-2}	pH	log [Me_{aq}] mol kg^{-1}	log Γ_{Me} nm^{-2}	pH	log [Me_{aq}] mol kg^{-1}	log Γ_{Me} nm^{-2}	pH	log [Me_{aq}] mol kg^{-1}	log Γ_{Me} nm^{-2}
4.43	-6.76	-2.38	4.04	-7.20	-3.19	5.8	-5.93	-1.97	5.18	-6.03	-1.34
4.49	-6.43	-2.10	4.04	-6.84	-2.90	5.78	-5.65	-1.66	5.22	-5.30	-0.96
4.47	-5.98	-1.85	4.08	-6.31	-2.50	5.68	-5.14	-1.41	5.19	-4.50	-0.72
4.44	-5.29	-1.51	4.06	-5.87	-2.24	5.78	-4.50	-1.13	5.20	-4.05	-0.48
4.56	-5.00	-1.22	4.12	-5.55	-1.99	5.57	-4.08	-0.93	5.16	-3.33	-0.34
4.60	-4.59	-0.94	4.15	-5.06	-1.66	5.65	-3.71	-0.73	5.16	-2.98	-0.13
4.63	-4.06	-0.62	4.19	-4.69	-1.41						
4.59	-3.63	-0.42	4.22	-4.31	-1.17						
			4.25	-3.86	-0.84						